

Expeditions in Siberia in 2003

Edited by Lutz Schirrmeister

Russian-German Cooperation SYSTEM LAPTEV SEA: The Expedition Lena-Anabar 2003

Edited by Lutz Schirrmeister, Mikhail N. Grigoriev,
Lars Kutzbach, Dirk Wagner and Dmitry Yu. Bolshiyarov

The Russian-German TRANSDRIFT IX Expedition of RV "Ivan Kireyev" 2003

Edited by Carolyn Wegner, Jens Hölemann and Vladimir Churun

**Ber. Polarforsch. Meeresforsch. 489 (2004)
ISSN 1618 - 3193**

Contents

Russian-German Cooperation SYSTEM LAPTEV SEA:

The Expedition Lena-Anabar 2003

by the participants of the expedition

edited by Lutz Schirrmeister, Mikhail N. Grigoriev,

Lars Kutzbach, Dirk Wagner and Dmitry Yu. Bolshiyarov

page 1- 210

The Russian-German TRANSDRIFT IX Expedition of RV "Ivan Kireyev" 2003

Edited by Carolyn Wegner, Jens Hölemann

and Vladimir Churun

231

page 210-

Lutz Schirrmeyer, Dirk Wagner and Lars Kutzbach Alfred-Wegener-Institute
for Polar and Marine Research, Research Department Potsdam, PO
Box 60 01 49, D-14401 Potsdam, Germany

Mikhail N. Grigoriev, Permafrost Institute, Russian Academy of Sciences
677018 Yakutsk, Yakutia, Russia

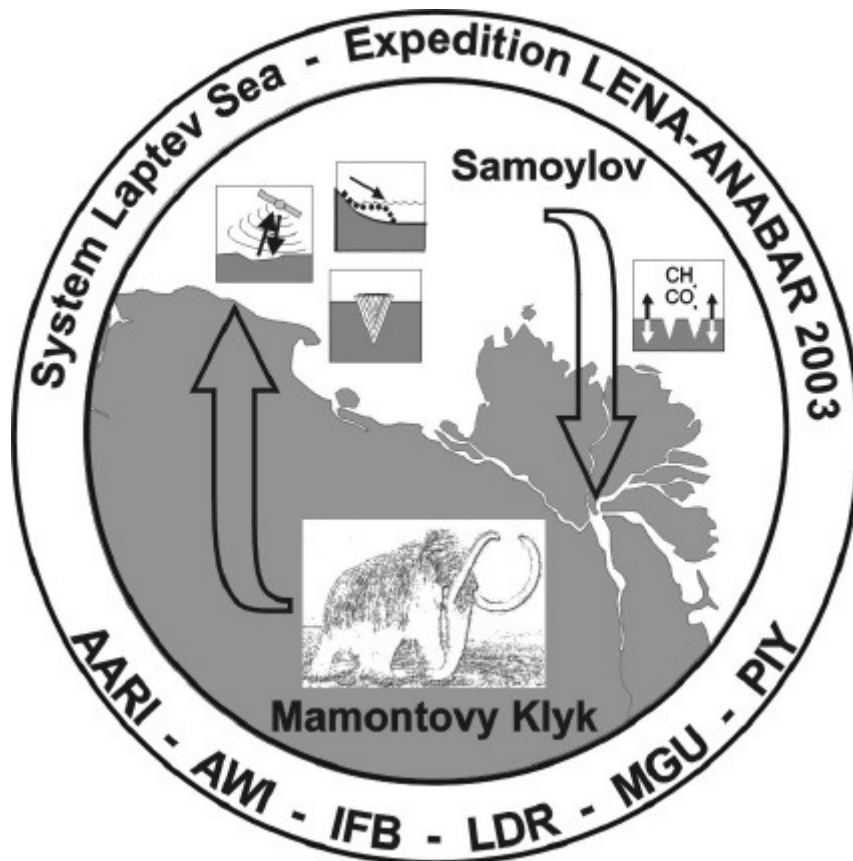
Dmitry Yu. Bolshiyakov, Arctic and Antarctic Research Institute (AARI),
Bering St. 38, 199397 St. Petersburg, Russia

Jens Hölemann, Alfred-Wegener-Institute for Polar and Marine Research
Columbusstrasse, D-27568 Bremerhaven

Russian-German Cooperation SYSTEM LAPTEV SEA: The Expedition Lena-Anabar 2003

by the participants of the expedition

*edited by Lutz Schirrmeister, Mikhail N. Grigoriev, Lars Kutzbach, Dirk Wagner
and Dmitry Yu. Bolshiyarov*



Contents

1	Introduction.....	1
2	Expedition itinerary and general logistics.....	4
3	Ecological studies on permafrost soils and landscapes of the central Lena Delta.....	6
3.1	Aims and study area.....	6
3.2	Energy and water budget of permafrost soils – long time soil survey station on Samoylov Island.....	10
3.3	Micrometeorological measurements of energy, water, and carbon exchange between Arctic tundra and the atmosphere....	12
3.3.1	Introduction.....	12
3.3.2	Experimental set-up.....	12
3.3.3	The observation period 2003.....	15
3.3.3.1	Wind characteristics.....	15
3.3.3.2	Meteorological conditions.....	16
3.3.3.3	Turbulent fluxes.....	17
3.4	Microbial process studies on methane fluxes from permafrost environments.....	20
3.4.1	Introduction.....	20
3.4.2	Methane emission and microbial methane production....	20
3.4.2.1	Methods and field experiments.....	20
3.4.2.2	Preliminary results.....	21
3.4.3	Process studies on methane oxidation.....	26
3.4.3.1	Introduction and objectives.....	26
3.4.3.2	Methods and field experiments.....	26
3.4.3.3	Preliminary results.....	27
3.4.4	Further investigations.....	29
3.5	Studies on recent cryogenesis.....	30
3.6	Seasonal progression of active-layer thickness dependent on microrelief.....	34
3.6.1	Introduction.....	34
3.6.2	Methods.....	34
3.6.3	First results.....	37
3.7	Air photography and surface classification of Samoylov Island.....	39
3.8	Hydrobiological investigations in the Lena Delta in summer 2003.....	41
3.8.1	Objectives.....	41
3.8.2	Research tasks.....	42
3.8.3	Material and methods.....	42
3.8.4	Preliminary results.....	43

3.9	Appendices	
	Appendix 3-1 Collected variables determined by direct measurements within the micrometeorological campaign Samoylov, 2003.....	46
	Appendix 3-2 Variables derived from calculations within the micrometeorological campaign Samoylov, 2003.....	50
	Appendix 3-3 Constants required in calculations.....	54
	Appendix 3-4 List of samples for methane emission and microbial methane production studies.....	55
	Appendix 3-5 List of soil samples for methane oxidation studies.....	56
3.10	References.....	58
4	Periglacial studies around Cape Mamontov Klyk.....	61
4.1	Introduction.....	61
4.2	Geological and geographical background.....	63
4.3	Geomorphologic route along the Urasalakh River.....	67
	4.3.1 Structure of Quaternary deposits along the Urasalakh River valley.....	67
	4.3.2 Geomorphologic structure of the valley.....	69
	4.3.3 Studies of lakes.....	72
4.4	Multi-sensor optical remote sensing of periglacial tundra landscapes	75
	4.4.1 Research aim.....	75
	4.4.2 Satellite data.....	76
	4.4.3 General geomorphology in the Lena-Anabar interfluve....	77
	4.4.4 Geomorphology in the investigation area near Cape Mamontov Klyk.....	79
	4.4.5 Field data.....	80
	4.4.6 Tachymetric survey of periglacial surface features.....	87
	4.4.7 Characterisation in situ surface properties with a soil probe at a typical elevated Edoma plain.....	91
4.5	Methane-related studies on recent tundra soils.....	92
	4.5.1 Introduction and objectives.....	92
	4.5.2 Methods.....	92
	4.5.3 First results.....	94
4.6	The coastal section of Cape Mamontov Klyk.....	98
	4.6.1 General profile	98
	4.6.2 Cryolithological studies of permafrost deposits.....	101
	4.6.2.1 The first composite profile.....	101
	4.6.2.2 The second composite profile.....	106
	4.6.2.3 Additional sampled subprofiles.....	109
	4.6.3 Ice wedges of Cape Mamontov Klyk.....	111
	4.6.3.1 Introduction.....	111
	4.6.3.2 The ice wedges in the lower sands (Unit A) and in the sand-peat-complex (Unit B).....	112
	4.6.3.3 Ice wedges of the Late Pleistocene Ice Complex (Unit C) and of Holocene deposits (Unit D).....	121

	4.6.3.4 Ground ice of unknown origin.....	130
	4.6.3.5 Ice wedge section west of the Nuchcha Dzhiele River mouth.....	130
	4.6.3.6 General interpretation of the sampled profile.....	132
	4.6.4 Geomicrobiological studies.....	133
	4.6.4.1 Introduction and objectives.....	133
	4.6.4.2 Methods.....	133
	4.6.4.3 First results: Methane content of permafrost samples.....	134
	4.6.5 Paleontological studies	136
4.7	Studies of coastal dynamics and sub sea permafrost.....	139
	4.7.1 Preliminary results of sub-sea permafrost drilling in the near-shore zone (spring 2003).....	139
	4.7.1.1 Introduction and background.....	139
	4.7.1.2 Methods and preliminary results.....	141
	4.7.1.3 Further investigations.....	141
	4.7.2 Measurements of the coast relief in the area of Cape Mamontov Klyk and ice and sediment sampling.....	143
	4.7.2.1 Introduction.....	143
	4.7.2.2 Methods.....	143
	4.7.2.3 Preliminary results.....	145
	4.7.2.4 Further investigations.....	147
	4.7.3 Shore face profiles in the area of Cape Mamontov Klyk: echo sounding, seawater and sea bottom deposits sampling.....	148
	4.7.3.1 Introduction.....	148
	4.7.3.2 Methods.....	148
	4.7.3.3 Preliminary results.....	148
	4.7.3.4 Further investigations.....	150
4.8	References.....	151
4.9	Appendices.....	154
	Appendix 4-1. Surface parameters for the studied geolocated sites around Cape Mamontov Klyk	155
	Appendix 4-2. Active layer data of the geo-located sites.....	170
	Appendix 4-3. List of soil samples (active layer); collected in the coastal lowland.....	171
	Appendix 4-4. List of permafrost sediment and paleosol samples for microbiological, molecular biological and biochemical analyses.....	172
	Appendix 4-5. List of sediment samples.....	173
	Appendix 4-6. List of ice and water samples.....	182
	Appendix 4-7. Collection of bone samples.....	189

1 Introduction

Lutz Schirrmeister and Mikhail N. Grigoriev

Our knowledge of the Arctic climate system has been significantly improved through multi-disciplinary investigations carried out in the Siberian Arctic during previous Russian-German projects, such as THE LAPTEV SEA SYSTEM (1994-1997), TAYMYR (1994-1997) and LAPTEV SEA 2000 (1998-2002).

Within the framework of the project SYSTEM LAPTEV SEA 2000 terrestrial expeditions to the Lena Delta and the Laptev Sea and East Siberian Sea coastal region and on New Siberian Islands were performed 1998 (Rachold and Grigoriev, 1999), 1999 (Rachold and Grigoriev, 2000), 2000 (Rachold and Grigoriev, 2001), 2001 (Pfeiffer and Grigoriev, 2002), and 2002 (Grigoriev et al., 2003). Based on this about 10 years successful research of Arctic modern and paleo environment, studies of periglacial processes and permafrost related processes were continued in the Lena River Delta (Samoylov Island) and on the coast of the Lena-Anabar lowland (Cape Mamontov Klyk) in 2003. These studies were carrying out by a multidisciplinary Russian-German team of 20 persons from spring to autumn 2003 (Table 2-1). The transition from terrestrial to sub sea permafrost, the Quaternary paleoenvironment of the Siberian arctic, microbial processes of greenhouse gas formation and the quantification of associated physicochemical conditions in tundra soils as well as recent cryogenetic and geomorphological dynamics of periglacial landscapes are the main focuses of the Lena-Anabar 2003 Expedition.

- A. Permafrost soils and ecosystems (☞ Chapter 3: *Ecological studies on permafrost soils and landscapes of the central Lena Delta*; ☞ Chapter 4.5 *Methane related studies on recent tundra soils*)
- B. Periglacial geomorphology (☞ Chapter 4.3: *Geomorphologic route along the Urasalakh River*; Chapter 4.4: *Multi-sensor optical remote sensing of periglacial tundra landscapes*)
- C. Reconstruction of Quaternary environmental changes based on the study of permafrost sequences (☞ Chapter 4.6: *The coastal section of Cape Mamontov Klyk*)
- D. Sub sea permafrost and Arctic coastal dynamics (☞ Chapter 4.7: *Studies of coastal dynamics and sub sea permafrost*)

Acknowledgments

The success of the expedition Lena-Anabar 2003 would have not been possible without the support by several Russian, Yakutian, and German institutions and authorities. In particular, we would like to express our appreciation to the Tiksi Hydrobase and the Lena Delta Reserve, special thanks to D. Melnichenko and A. Gukov. The members of the expedition wish to thank the captains and

crewmembers of the vessel “Neptun” and the staff of the biological station Samoylov.

The expedition Lena-Anabar 2003 was a contribution to the joint research project “Process studies of permafrost dynamics in the Laptev Sea” (project number 03G0589) founded by the German Federal Ministry of Education and Research (BMBF).

The coastal studies presented here are a direct contribution to Arctic Coastal Dynamics (ACD), which is a project of the International Arctic Science Committee (IASC), the International Permafrost Association (IPA) and IGBP-LOICZ. Additional financial support by INTAS (project numbers INTAS 2001-2329 and INTAS 2001-2332) is highly appreciated.

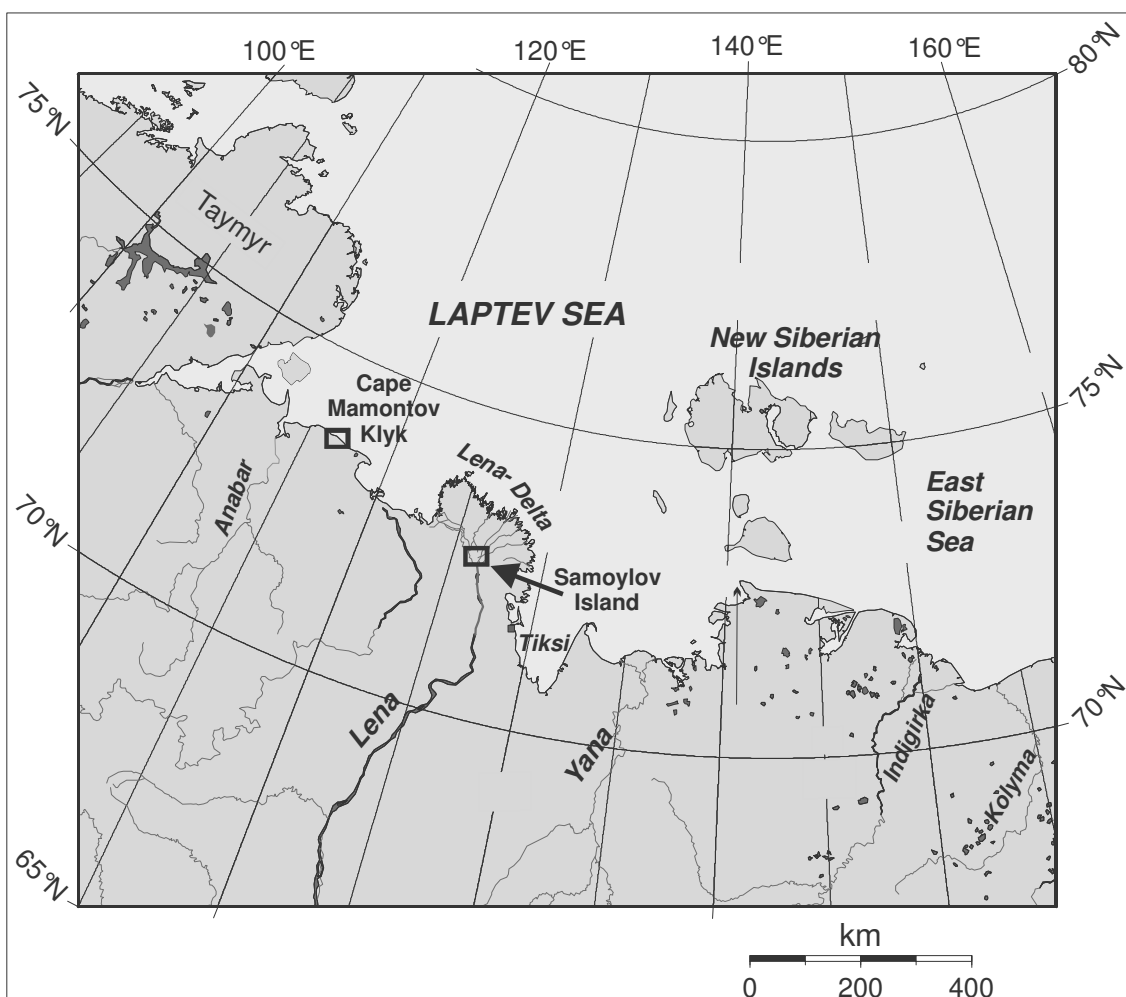


Figure 1: Map showing the location of the working area of the expedition Lena-Anabar 2003.

References

- Kassens, H., Bauch, H., Dmitrenko, I., Eicken, H., Hubberten, H.-W., Melles, M., Thiede, J. and Timokhov, L. (1999), Land-Ocean systems in the Siberian Arctic: dynamics and history. Springer, Berlin, 711pp.
- Pfeiffer E.-M. and Grigoriev, M.N. (2002): Russian-German Cooperation SYSTEM LAPTEV SEA 2000: The Expedition LENA 2001. Reports on Polar and Marine Research 426.
- Rachold, V. and Grigoriev, M.N. (1999): Russian-German Cooperation SYSTEM LAPTEV SEA 2000: The Lena Delta 1998 Expedition. Reports on Polar and Marine Research 316.
- Rachold, V. and Grigoriev, M.N. (2000): Russian-German Cooperation SYSTEM LAPTEV SEA 2000: The Expedition Lena 1999 Expedition. Reports on Polar and Marine Research 354.
- Rachold, V. and Grigoriev, M.N. (2001): Russian-German Cooperation SYSTEM LAPTEV SEA 2000: The Expedition LENA 2000. Reports on Polar and Marine Research 388.
- Rachold, V.(2002): The modern and ancient terrestrial and coastal environment of the Laptev Sea region, Siberian Arctic - A preface, Polarforschung 70
- Grigoriev, M.N.; Rachold, V., Bolshiyarov, D.Y., Pfeiffer, E.-M., Schirrmeister, L. Wagner, D. and hubberten, h.-W. (2003): Russian German Cooperation SYSTEM LAPTEV SEA. The Expedition LENA 2002. Reports on Polar and Marine Research 266.

2 Expedition itinerary and general logistics

Lutz Schirrmeister and Mikhail N. Grigoriev

With respect to the scientific program, three different teams worked during the expedition Lena-Anabar 2003 in spring, summer and autumn 2003.

Team 1 drilled on sea ice in spring on the Cape Mamontov Klyk site in order to recognize the position of the sub sea permafrost table. This Russian team of 6 peoples from Tiksi Hydrobase and the Permafrost Institute Yakutsk worked from April 11 to May 5

Chapter 4.7: Studies of coastal dynamics and sub sea permafrost

Team 2 was based on a biological station of the Lena Delta Reserve on the Island Samoylov in the central part of the Lena Delta. The team concentrated on modern processes of permafrost-affected soils, i.e. the balance of greenhouse gases (CH₄ and CO₂) and microbial process studies regarding the CH₄ cycle and carried out additional biological studies. Several smaller groups worked with a total number of 8 participants on the Samoylov Island between July 7 and October 30.

Chapter 3: Ecological studies on permafrost soils and landscapes of the central Lena Delta

Team 3 concentrated on the investigation of terrestrial permafrost environment and of the Laptev Sea coastal area around Cape Mamontov Klyk. The team consisting of 11 participants was based in a field camp and worked in total from August 4 to September 3.

Chapter 4: Periglacial features around Cape Mamontov Klyk

The general logistics of the LENA 2002 Expedition were jointly organized by the Permafrost Institute (Yakutsk), the Arctic and Antarctic Research Institute (St. Petersburg) and the Research Unit Potsdam of the Alfred Wegener Institute. Logistic operations in Tiksi (rent of busses, trucks, vessels, helicopters etc.) were organized by the Tiksi Hydrobase.

The list of participants and the addresses of the institutions involved are presented in Table 2-1 and Table 2-2.

Table 2-1. List of participants.

Name	email	Institution	Team
Ekatarina Abramova	abramova-katya@mail.ru	LDR	2
Irina Akhmetshina	abramova-katya@mail.ru	LDR	2
Dmitry Bolshiyarov	bolshiyarov@aari.nw.ru	AARI	3
Alexander Dereviagin	dereviag@online.ru	MGU	3
Mikhail Grigoriev	grigoriev@mpi.ysn.ru	PIY	1, 3
Lars Ganzert	ganzert@rz.uni/Potsdam.de	PU	2
Guido Grosse	ggrosse@awi-potsdam.de	AWI	3
Victor Kunitsky	kunitsky@mpi.ysn.ru	PIY	3
Tatyana Kuznetsova	esin@sgm.ru	MGU	3
Lars Kutzbach	lkutzbach@awi-potsdam.de	AWI	2
Alexander Makarov	bolshiyarov@aari.nw.ru	AARI	3
Hanno Meyer	hmeyer@awi-potsdam.de	AWI	3
Lutz Schirrmeister	lschirrmeister@awi-potsdam.de	AWI	3
Waldemar Schneider	w Schneider@awi-potsdam.de	AWI	2, 3
Günter Stoof	gstooof@awi-potsdam.de	AWI	2
Christian Wille	cwille@awi-potsdam.de	AWI	2
Uta Zimmermann	U.Zimmermann@ifb.uni-hamburg.de	IFB	2, 3

Table 2-2. List of participating institutions.

AARI	Arctic and Antarctic Research Institute Bering St. 38, 199397 St. Petersburg, Russia
LDR	Lena Delta Reserve 28 Academician Fyodorov St., Tiksi 678400, Yakutia, Russia
MGU	Moscow State University, Faculty of Paleontology 119899 Moscow, Russia
PIY	Permafrost Institute, Russian Academy of Science 677018 Yakutsk, Yakutia, Russia
PU	Potsdam University Am Neuen Palais 10, 14469 Potsdam
AWI	Alfred Wegener Institute, Research Unit Potsdam PO Box 60 0149, D-14401 Potsdam, Germany
IFB	Institute for Soil Science, Hamburg University Allende-Platz 2, D-20146 Hamburg, Germany

3. Ecological studies on permafrost soils and landscapes of the central Lena Delta

3.1 Aims and study area

Lars Kutzbach

Global climate models predict that global warming will have its most pronounced effect in the Arctic (Maxwell, 1992; Kattenberg et al., 1996). Tundra ecosystems and permafrost are highly sensitive to climate change (Chapin et al., 1992; Walker et al., 2001; Anisimov et al., 2002). Warmer temperatures and an increased level of permafrost thawing may have severe consequences for natural and anthropogenic systems, as extensive thermokarst subsidences (Osterkamp & Romanovsky, 1999), accelerated coastal erosion at the shores of the Arctic Ocean (Grigoriev and Rachold, 2004) or increased release of greenhouse gases from the enormous organic carbon pool within gelisols and permafrost sediments (Gorham, 1991; Roulet et al., 1992; Oechel et al., 1993). To assess the effects of climate change on Arctic ecosystems with respect to possible feedbacks to the atmospheric system, it is important to improve our understanding of the physical interaction processes between permafrost soils and sediments, tundra vegetation and the atmosphere.

Within the framework of the Russian-German cooperation project SYSTEM LAPTEV SEA, an interdisciplinary research project was started in 1998 on Samoylov Island in the central Lena Delta, which deals with the ecology, pedology, microbiology, biogeochemistry and micrometeorology of Arctic permafrost soils and landscapes (Pfeiffer et al., 1999, 2000, 2002; Wagner et al., 2001, 2003). In 2003, the research of the five previously conducted expeditions was continued. The investigations focused on

- the energy and water balance of permafrost-affected landscapes,
- the seasonal and inter-annual variability of carbon fluxes (CH₄, CO₂),
- the microbial processes that control the carbon cycle,
- the recent cryogenesis of ice wedges, permafrost sediments and gelisols of polygonal tundra
- and the dynamics and diversity of the zooplankton of the extensive freshwater bodies of the Lena Delta.

The Lena Delta is a unique permafrost landscape with a rich natural life. It is considered to be a key area for the Arctic system because of its position at the interface between the Eurasian continent and the Arctic Ocean. It has formed where the Lena River cuts through the Verkhoyansk Mountains and pours into the Laptev Sea (Figure 3.1-1). With an area of 32,000 km², it is the largest delta in the Arctic and one of the largest in the world (Walker, 1998). The fan-shaped delta is a maze of distributaries, which surround more than 1500 islands of

various sizes. It is located in the zone of continuous permafrost with permafrost depths of 500 - 600 m (Grigoriev, 1960). The climate is true-arctic, continental, and characterized by very low temperatures and low precipitation. The mean annual air temperature, measured by the weather station Stolb in the central delta, was -11.9°C during the years 2001-2003; the mean annual precipitation in the same period was 233 mm (Hydrometeorological Centre of Russia, 2004). The vegetation period lasts only three months, from the beginning of June to the end of August. On the other hand, winters are long and harsh with minimum temperatures as low as -45°C .

Samoylov Island is located at one of the main river channels, the Olenyokskaya Channel, in the southern-central part of the Lena Delta ($72^{\circ}23' \text{ N}$, $126^{\circ}29' \text{ E}$). The island is considered to be representative for the modern delta landscapes of Holocene age, that occupy about 65% of the total area of the delta, predominantly in its central and eastern part (Grigoriev, 1993; Are and Reimnitz, 2000, Schwamborn et al., 2002). Samoylov Island has a size of 7.5 km^2 and is composed of two geomorphological units. The western part (3.4 km^2) represents a modern floodplain, which is annually flooded by the Lena River. The eastern part (4.1 km^2) is build up by sediments of a Late-Holocene river terrace and is only flooded in parts during extreme flooding events.

On the island, the Lena Delta Reserve runs a small station, whose four rooms were used as bedroom, kitchen, workshop and field laboratory by the expedition team. The positions of the station and the investigation sites are shown in Figure 3.1-2.

The field work during the expedition 2003 included:

- upgrading the station with regard to the wintertime stay,
- the maintenance of the long-time meteorological and soil survey stations on Samoylov Island (Chapter 3.2),
- an intensive micrometeorological campaign (Chapter 3.3),
- chamber-based measurements of CH_4 and microbiological studies on the soil-microbial communities (Chapter 3.4),
- the continuation of a long term study on the mechanism of frost-cracking (Chapter 3.5),
- regular measurements of the small-scale spatial variability of the active-layer depth at a typical low-centre polygon (Chapter 3.6),
- air photography from helicopter for surface classification of Samoylov Island (Chapter 3.7),
- the sampling and characterisation of zooplankton from various lakes of the central Lena Delta (Chapter 3.8).

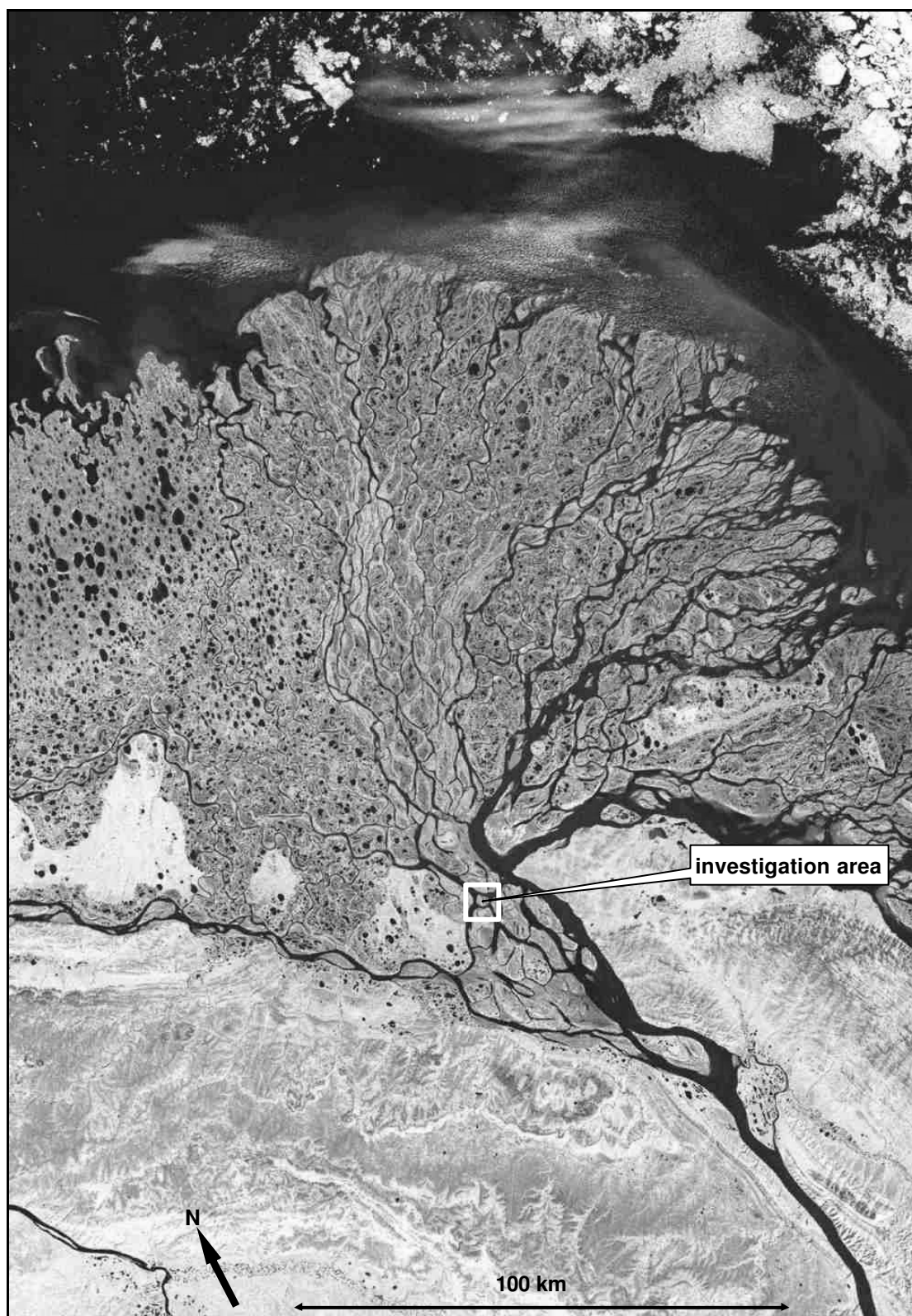


Figure 3.1-1: The Lena Delta region with the location of the investigation area on Samoylov Island (Satellite image provided by Statens Kartverk, UNEP/GRID-Arendal, and Landsat, 2000).

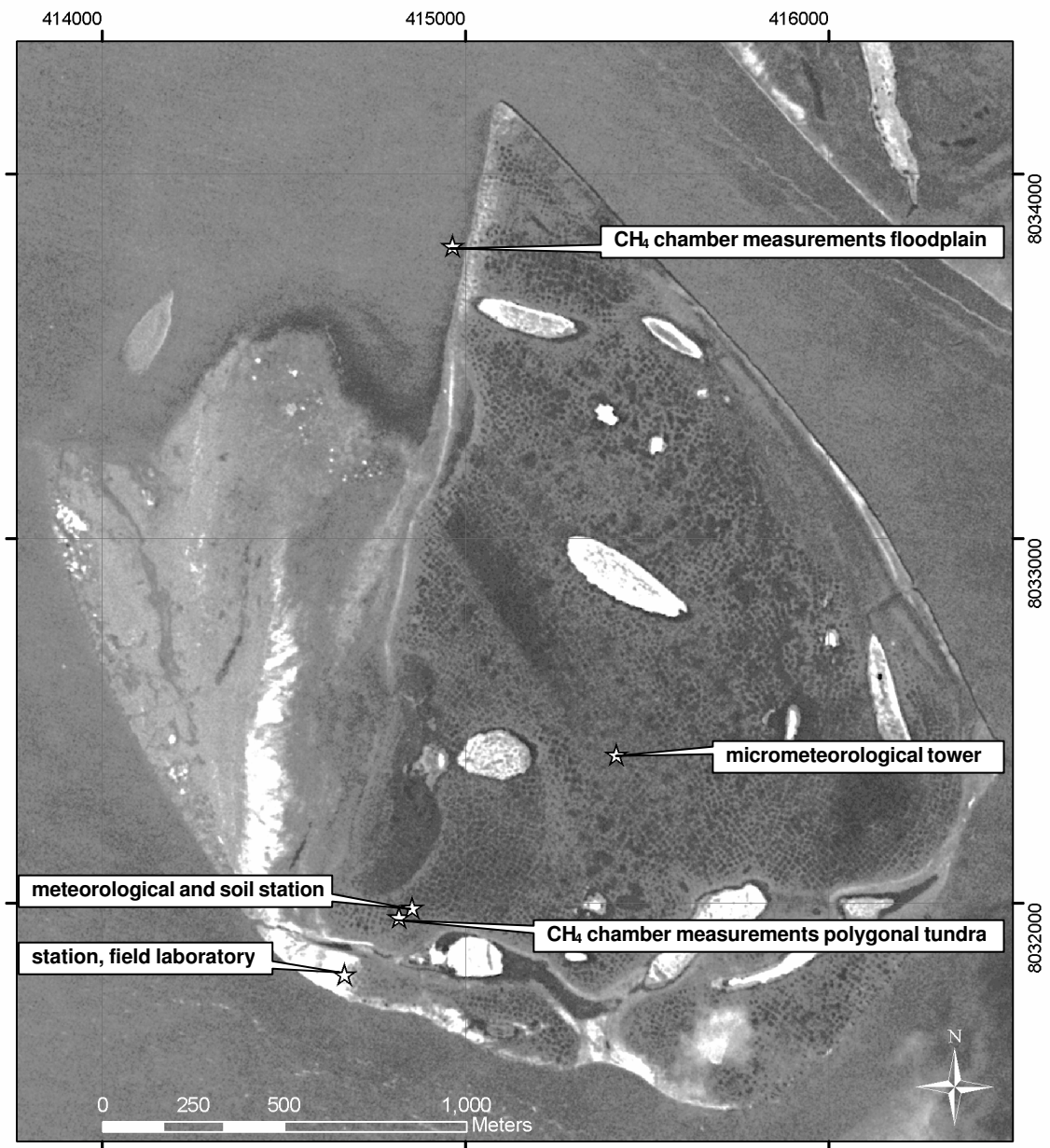


Figure 3.1-2: Site map Samoylov Island. – Positions of investigation sites; satellite image: CORONA June 22, 1964; coordinate system UTM Zone 52N, WGS84.

3.2 Energy and water budget of permafrost soils – long time meteorology and soil survey station on Samoylov Island

Christian Wille, Günther Stooß and Julia Boike

The permanent meteorology and soil survey station on Samoylov Island is situated about 200 meters northeast of the Lena Delta reserve station building on a Holocene river terrace which is characterized by polygonal tundra with raised, dry polygon rims and low, wet polygon centres. The area is drained towards lower areas and a lake in the northwest and southeast, respectively.

The station was set up during the Lena 2002 expedition and put into operation on 24.08.2002. It consists of a 3-m tower for meteorological measurements, an additional rack for the solar panel and a snow height sensor, a wind generator, a rain gauge, and two boxes for the accommodation of the soil measurement electronics, datalogger, batteries, etc. (Figure 3.3-1).



Figure 3.2-1: View of meteorology and soil survey station from southeast

The data recorded by the measurement station and the sensors used are given in Table 3.2-1. During the period 24.08.2002 – 13.08.2003, meteorological data (Pos. 1-5 in Table 3.2-1) was sampled every 20 seconds and hourly averages were stored. Soil data (Pos. 6-10 in Table 3.2-1) was sampled and stored every hour. The measurement of soil bulk electrical conductivity and soil water content were made by time domain reflectometry (TDR). Soil temperature and TDR measurements were carried out along three vertical profiles in the polygon; an additional temperature profile measurement was made at greater depth inside the ice wedge. Soil heat flux was recorded close to the soil surface in the polygon rim and center. For detailed information about the setup of the soil measurement station see Wagner et al., 2003.

Table 3.2-1: Data and sensors of permanent measurement station

Pos.	Data Measured	Sensor Type
1	Air Temperature and Relative Humidity (0.5 and 2.0 m above ground)	Rotronic Meßgeräte GmbH Meteorological Probe MP103A
2	Wind Speed & Direction (3.0 m above ground)	R M Young Company Anemometer 05103
3	Net Radiation (1.35 m above ground)	Kipp & Zonen B.V. Net Radiometer NR-Lite
4	Long wave Radiation (1.28 m above ground)	Kipp & Zonen B.V. Pyrgeometer CG1
5	Precipitation (liquid, i.e. Rain) (0.3 m above ground)	R M Young Company Tipping Bucket Rain Gauge 52203
6	Snow Height (in centre of polygon)	Campbell Scientific Ltd. Sonic Ranging Sensor SR 50
7	Soil Temperature (4 measuring profiles)	Campbell Scientific Ltd. Thermistor Soil Temperature Probe 107
8	Soil Bulk Electrical Conductivity (3 measuring profiles)	Campbell Scientific Ltd. TDR 100, Probe CS605
9	Soil Volumetric Water Content (3 measuring profiles)	Campbell Scientific Ltd. TDR 100, Probe CS605
10	Heat Flux out of / into Soil (2 measuring points)	Hukseflux Thermal Sensors Heat Flux Sensor HFP01

Due to technical problems the data series from the period 2002 – 2003 is not continuous. Table 3.2-2 shows the time periods during which data was collected by the station.

Table 3.2-2: Existing data 2002-2003

Existing Data Series 2002 - 2003
24.08.2002 - 15.12.2002
10.05.2003 - 14.06.2003
13.07.2003 - 24.10.2003

During the Expedition Lena 2003, no major changes were made to the measurement station. The meteorological sensors, the rain gauge and the snow height sensor were cleaned and checked for proper operation. The air temperature and humidity sensor at 0.5 meters height was exchanged because it had measured unrealistic humidity values. A new measurement program was installed on the soil station datalogger on 13.08.2003. With the new program, soil temperature and heat flux are measured every 15 minutes, and hourly averages are stored. The interval and averaging times of the other measurements were not changed.

The raw data will be transferred to an SQL database, which is hosted by the Institute of Environmental Physics at the University of Heidelberg and subsequently analyzed.

3.3 Micrometeorological measurements of energy, water, and carbon exchange between Arctic tundra and the atmosphere

Lars Kutzbach, Christian Wille and Günther Stooß

3.3.1 Introduction

Following the first micrometeorological field study at the polygonal tundra of Samoylov Island in 2002 (Kutzbach et al., 2003), a second campaign was performed at this site from June 18 to October 22, 2003. The campaign included the investigation of turbulent fluxes of momentum, energy, water vapour, carbon dioxide and methane by the eddy covariance technique along with supporting meteorological and soil-physical measurements. The measurement period ranged from late summer with maximal depths of the active layer to early winter when soils freeze back. The purposes of the study were:

- to characterise the seasonal progression of the exchange fluxes of energy, water and carbon, with a focus on the period of freeze-back,
- to assess the energy partitioning at the investigated tundra site,
- to quantify the exchange fluxes of water, carbon dioxide and methane on the landscape scale,
- to investigate the interactions between the energy and water balance of polygonal tundra and the carbon exchange processes between permafrost soils, tundra vegetation and the atmosphere,
- to analyse the regulation of the energy and matter fluxes by climatic forcings.

3.3.2 Experimental set-up

The investigation site for the eddy covariance and supporting measurements was established in the centre of the eastern part of Samoylov Island, which is built up by Holocene river terrace sediments and is characterised by wet polygonal tundra (UTM Zone 52 415417E 8032409N; Figure 3.3-1a). The fetch of undisturbed polygonal tundra extended at least 500 m in all directions from the tower, except for the sector from southwest to west, where all instruments and auxiliary devices were set up (Figure 3.3-1b). Data gathered during periods with winds coming from this sector were excluded from further analyses.

The technical set-up of the eddy covariance measurement system (ECS) during the campaign 2003 was basically equal to the set-up in 2002 as described in detail by Kutzbach et al. (2003a). The ECS consisted of a three-dimensional sonic anemometer (Solent 1210 R3, Gill Instruments Ltd.), an infrared gas analyser for H₂O and CO₂ (IRGA; LI-7000, LI-COR Inc.) and a CH₄ analyser

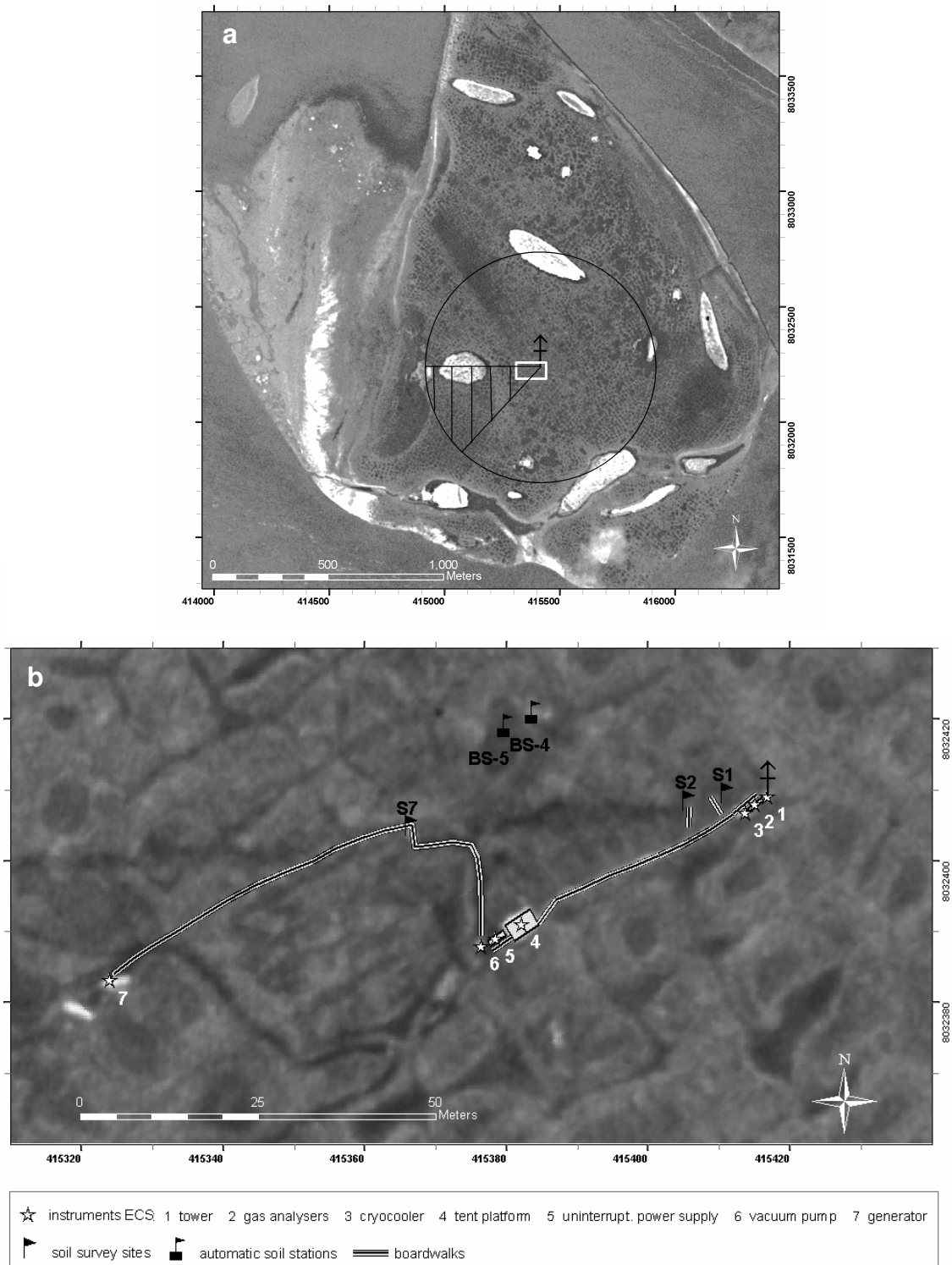


Figure 3.3-1: Maps of the micrometeorological investigation site (UTM Zone 52N, WGS84). – **a** Samoylov Island (satellite image CORONA, June 22, 1964), black circle: minimum fetch of polygonal tundra (radius 500 m), hatched area: sector of discarded data due to disturbance, white rectangle: sector shown in detail below; **b** vicinity of the eddy covariance measurement system ECS (air photograph from helicopter, June 10, 2003), positions of ECS instruments, soil survey sites and automatic soil stations.

based on tuneable laser infrared spectroscopy (TGA 100, Campbell Scientific Inc.). The sonic anemometer and the sample air intake were mounted on top of an aluminium tower at a height of 3.6 m above ground level. The gas analysers were installed in a weatherproof and temperature-regulated case at the base of the tower. Sample air was drawn from the intake through the gas analysers via a heated sampling tube (5 m long, 6.25 mm inner diameter; Dekabon 1300, Deane & Co.) by a vacuum pump (RB0021, Busch Inc.) at a flow rate of $20 \text{ dm}^3 \text{ min}^{-1}$.

The signals from the fast response sensors were digitised at 20 Hz by the anemometer and transferred via RS232 serial protocols to a portable PC housed in a tent 40 m away from the tower. The raw data were logged by the software EdiSol (University of Edinburgh) and archived on a removable hard-disc for subsequent post-processing of turbulent fluxes and micrometeorological parameters. Autonomous operation was ensured by a diesel generator (100 m away from tower) and an uninterruptible power supply.

Parallely to the eddy covariance measurements, air temperature and relative humidity were measured at a height of 2 m above ground level by a shielded meteorological probe (MP103A, ROTRONIC Messgeräte GmbH). The outputs from the meteorological probe were recorded with the anemometer at 20 Hz. Air pressure was determined with a barometric pressure sensor (RPT410, Druck Messtechnik GmbH). Incoming and surface-reflected shortwave and longwave radiation were measured by a net radiometer consisting of two pyranometers and two pyrgeometers (CNR1, Kipp & Zonen). The net radiometer was installed at the end of a 2-m cross-arm mounted on the tower at a height of 2 m. Air pressure and the constituents of the radiation balance were recorded every 10 s and averaged over 15-min periods by a data-logger (CR10, Campbell Scientific Inc.).

Soil-physical conditions were monitored automatically at two soil survey sites at the centre and at the rim of a low-centre polygon, located 35 m away from the micrometeorological tower (BS-4, BS-5). Soil heat flux density was measured at each site at a depth of 0.1 m below the soil surface by soil heat flux plates (HFP01SC, Hukseflux Thermal Sensors). Soil temperatures and soil volumetric water contents were measured in profiles by thermistor soil temperature probes (Model 107, Campbell Scientific Inc.) and time domain reflectometry probes (CS605, Campbell Scientific Ltd.), respectively. Soil heat flux density and soil temperatures were recorded every 10 min and averaged over 60-min periods by a data-logger (CR10, Campbell Scientific Inc.). Soil volumetric water content was measured every hour and recorded by the same data-logger.

Additionally, active layer depth, water level depth, soil temperature profiles and chamber-based CH_4 fluxes were measured manually in intervals of 1 to 3 days at three soil survey sites (S1, S2, S7).

Overall, the eddy covariance and the supporting measurements delivered 95 directly measured variables. 15 of these variables are micrometeorological measurements, 69 variables represent soil measurements, 8 variables are connected to the control of ECS instruments, and 3 variables contain CH₄ flux values based on chamber measurements. A list of all directly measured variables including their symbols, descriptions, measurement depths, respective instruments and measurement intervals is given in the Appendix 3-1. From the directly measured variables, a set of 51 deduced variables, including the turbulent fluxes, are calculated. A list of the calculated variables is given in the Appendix 3-2. Complementary meteorological data can be obtained from the automatic long-term meteorological and soil station on Samoylov (see Chapter 3.2) and the Russian meteorological station Stolb, which is located approximately 5 km east of Samoylov. Micrometeorological flux data were obtained from June 19, 2003, 12:45, to October 22, 2003, 11:45. The time base for all data is YAKT (Yakutsk Time), approximately 0.5 hours ahead of local solar time.

3.3.3 The observation period 2003

3.3.3.1 Wind characteristics

A summary of the wind climatology at Samoylov Island during the observation period 2003 is given as polar plots in Figure 3.3-2. The directional frequency of the wind reveals no single predominant wind direction (Figure 3.3-2a). Wind direction sectors with a higher-than-average frequency were 50°-70°, 160°-180°, or 240°-260° while winds from the sectors 10°-40°, 120°-150°, or 220°-240° were uncommon. Winds with directions not acceptable for flux calculations due to the generator disturbance (230°-270°) occurred 13.5% of the time. Overall mean wind speed was 4.7 m s⁻¹ and the maximum half-hour mean wind speed was 11.9 m s⁻¹. Strongest winds tended to come from the sectors 40°-80° and 240°-280° while the lightest winds came from the sector 100°-160° (Figure 3.3-2b). Very light winds were uncommon, with winds less than 1 m s⁻¹ observed only for 1.4% of the time. The diurnal variation of the mean wind speed was relatively small, ranging from 5.2 m s⁻¹ just after midday to 4.3 m s⁻¹ around midnight (Figure 3.3-2c). Likewise, the mean friction velocity, which is a measure of turbulence intensity, varied only weakly in the course of the day, from 0.35 m s⁻¹ at midday to 0.27 m s⁻¹ at midnight (Figure 3.3-2d). Turbulence conditions were considered to be insufficient if the friction velocity was below 0.1 m s⁻¹. Periods with such low turbulence intensity occurred 7.8% of the time and were excluded from flux calculations.

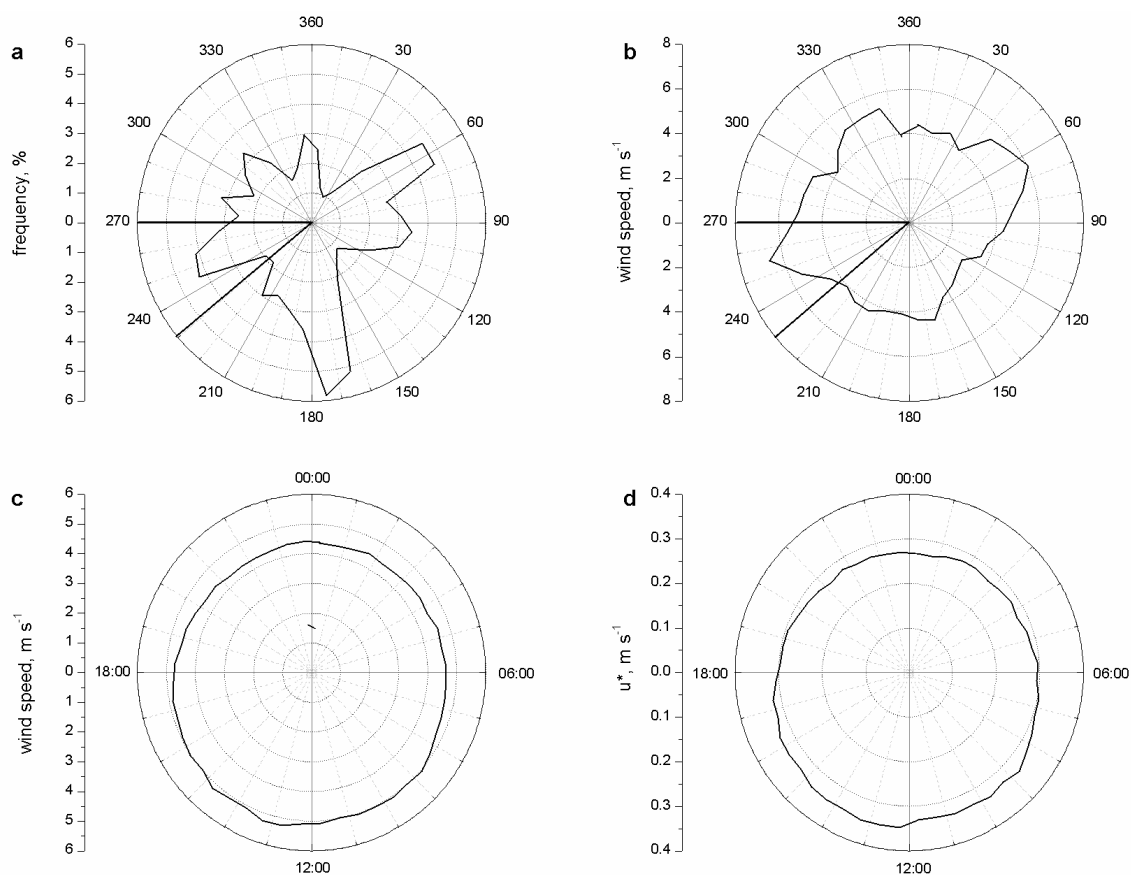


Figure 3.3-2: Summarized wind data from Samoylov Island during the micrometeorological study period, June 17 to October 22, 2003. – **a** frequency of occurrence of wind from specific sector, **b** mean wind speed versus wind direction, **c** mean wind speed versus time of day (YAKT), **d** mean friction velocity u^* versus time of day.

3.3.3.2 Meteorological conditions

The meteorological conditions on Samoylov Island during the study period 2003 are given in Figure 3.3-3. The data series of net radiation (Figure 3.3-3e) and air temperature (Figure 3.3-3d) document the distinct diurnal patterns of these parameters superimposed on their seasonal progression from late summer to the beginning of winter. The mean daily net radiation decreased from about 100 W m^{-2} at the end of July to about -30 W m^{-2} in the middle of October. The mean daily air temperature ranged from $+20^\circ\text{C}$ to -20°C in the course of the study period. Freezing of soils and lakes began not until the beginning of October due to relatively high temperatures in September. The mean September temperature was 3.3°C in 2003 while it averaged to $0.7 \pm 0.8^\circ\text{C}$ in the previous five years. At the end of the study period, the soils were frozen down to a depth of approximately 30 cm. Below the frozen top soil layer, unfrozen soil zones of several decimetres persisted until the end of the study at October 22.

Precipitation was exceptionally high in summer 2003 (Figure 3.3-3a; Hydrometeorological Centre of Russia, 2004). Summer precipitation (June-

September) amounted to 166 mm in 2003 while it averaged to only 102 ± 26 mm during the three previous years 2000-2002. A particularly strong rainfall event was observed at the beginning of the study period at the end of July (71 mm in six days). The precipitation pattern was reflected by the water table height measured at the centre and the rim of a polygon near to the micrometeorological tower (Figure 3.3-3b): Maximum water table heights were observed at the end of July, minimum water table heights at the end of the unfrozen period, at the end of September.

3.3.3.3 Turbulent fluxes

The data series of turbulent fluxes above the polygonal tundra of Samoylov Island during the study period 2003 are presented in Figure 3.3-4. Driven by the solar energy, the fluxes of heat (Figure 3.3-4b, c) and carbon dioxide (Figure 3.3-4d) showed clear diurnal and seasonal trends. On normal summer days, the sensible heat flux was positive during daytime and negative at night, it ranged between $+151 \text{ W m}^{-2}$ and -88 W m^{-2} . From September, the sensible heat flux decreased significantly, and in October it was almost permanently negative with values between $\pm 0 \text{ W m}^{-2}$ and -30 W m^{-2} . The latent heat flux was regularly greatest around midday and decreased to zero during midnight. The amplitude of the diurnal variation of the latent heat flux decreased continuously towards the end of the study period. In July, midday latent heat flux values reached 230 W m^{-2} while it was virtually zero even at midday from the middle of October, when the surface was frozen. The progression of the carbon dioxide flux behaved similarly as the heat fluxes. From July to September, it was negative during the days due to dominating photosynthesis and positive during the nights due to dominating respiration of vegetation and soils. During July and August, the carbon dioxide flux oscillated between -140 and $+65 \mu\text{g s}^{-1} \text{ m}^{-2}$. In September, the carbon dioxide flux varied between -50 and $+30 \mu\text{g s}^{-1} \text{ m}^{-2}$, and in October the flux was permanently positive with values between $+2$ and $+25 \mu\text{g s}^{-1} \text{ m}^{-2}$. In contrast to the other turbulent fluxes, the turbulent flux of methane showed no diurnal rhythm and only a slight seasonal trend (Figure 3.3-4e). It varied between 0.04 and $1.59 \mu\text{g s}^{-1} \text{ m}^{-2}$. The median methane flux of the complete study period was $0.21 \mu\text{g s}^{-1} \text{ m}^{-2}$ (about $18 \text{ mg day}^{-1} \text{ m}^{-2}$). First statistical analyses indicate that the observed variability of the methane flux can be best explained by variations of friction velocity and soil temperature. A detailed investigation of the interactions between the turbulent fluxes and the meteorological driving factors is in process.

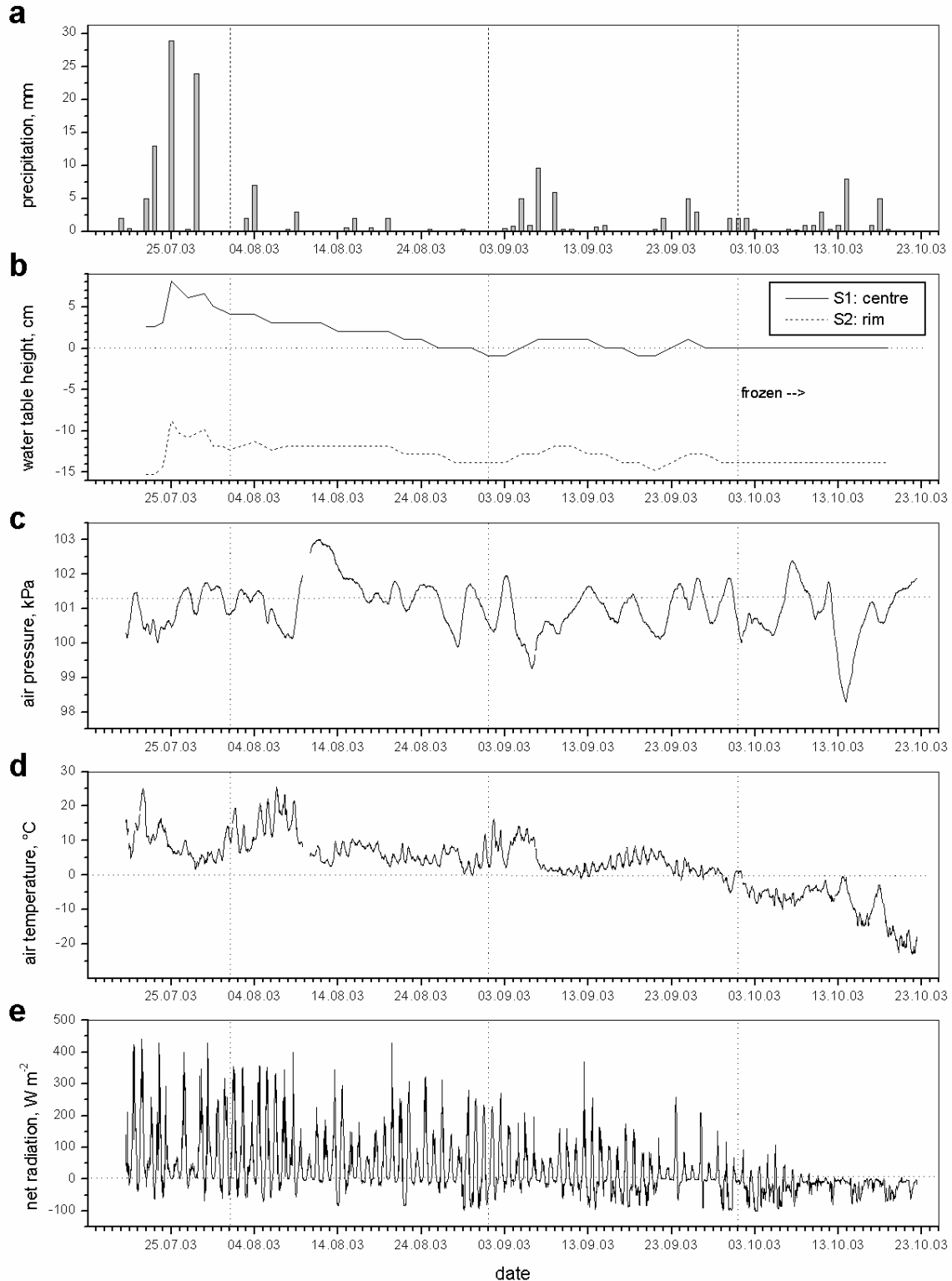


Figure 3.3-3 Time series of meteorological conditions on Samoylov Island during the study period, June 17 to October 22, 2003. – **a** precipitation (station Stolb, Hydrometeorological Centre of Russia, 2004), **b** water table height above the soil surface at the centre and the rim of a polygon (soil survey sites S1 and S2), **c** barometric air pressure, **d** air temperature (2 m above soil surface), **e** net radiation.

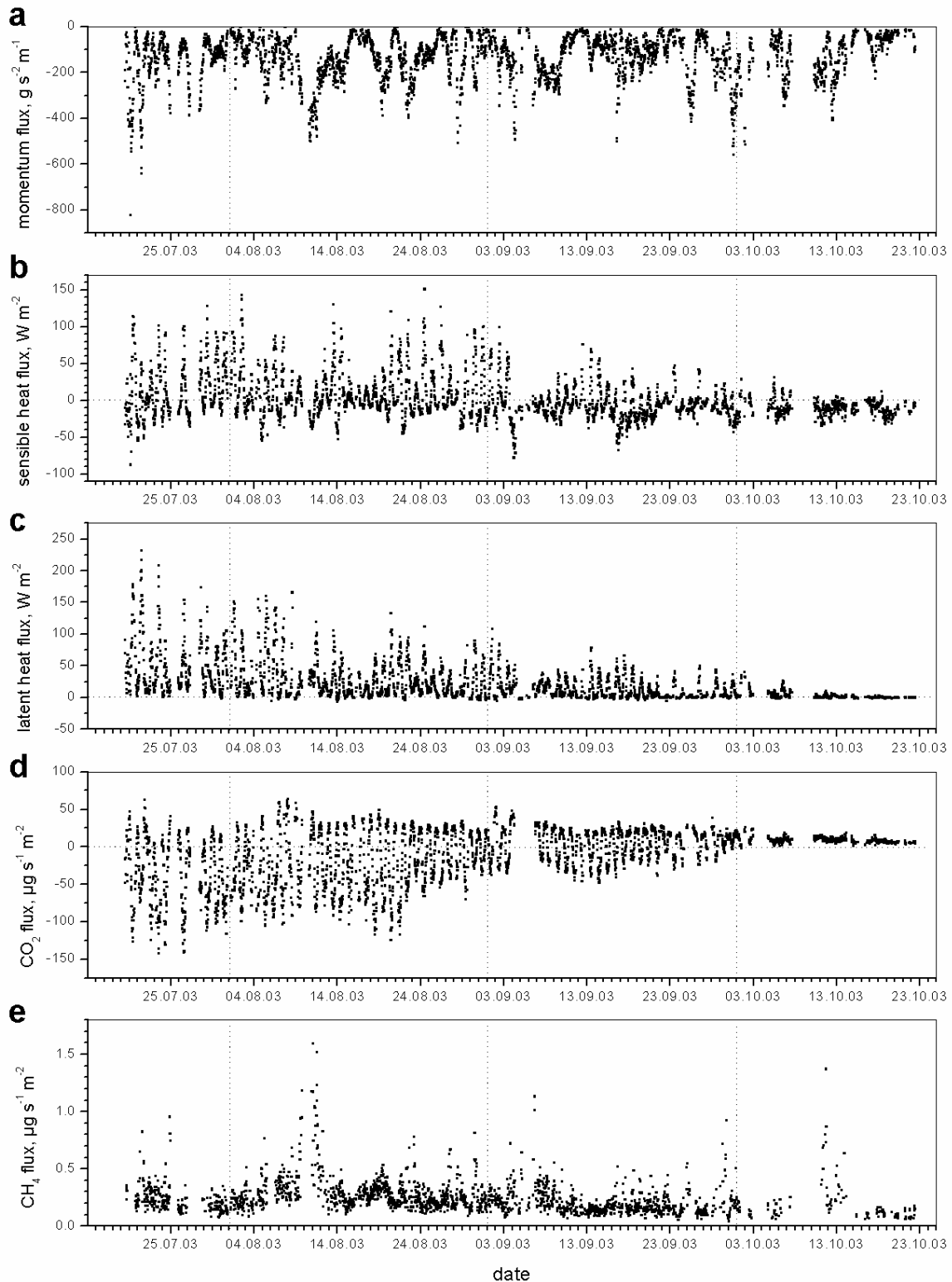


Figure 3.3-4 Turbulent flux densities during the study period June 17 to October 22, 2003. – **a** momentum flux, **b** sensible heat flux, **c** latent heat flux, **d** carbon dioxide flux, **e** methane flux. Periods with winds coming from the sector 230°-270° or with low turbulence intensity (friction velocity < 0.1) were discarded.

3.4 Microbial process studies on methane fluxes from permafrost environments

Lars Ganzert, Uta Zimmermann and Dirk Wagner

3.4.1 Introduction

The wet lowland areas of Arctic permafrost landscapes are natural sources of the climate relevant trace gas methane. The strength of permafrost, which cover nearly one fourth of the Earth's land surface (Zhang et al., 1999), as a source of methane is a still insufficiently estimated size in the global trace gas cycle.

Subarctic and arctic tundra located above 60° N covers a global area of 1.5 10⁹ km² (Harris et al. 1993). They represent the largest grouped of natural wetlands with an area of about 26 %. The reported methane emissions of wet tundra varied between 1 to 42 Tg CH₄ per year (Christensen et al. 1995). About 14 % of the global organic carbon is accumulated in permafrost soils (Post et al. 1982). The importance of this carbon pool is discussed regarding an expected climate warming. Especially, the carbon fixation in permafrost soils and the release of climate relevant trace gases like CH₄ and CO₂ due to the carbon decomposition are important for the global carbon budget.

The soil microbiological studies are focused on the seasonal variability of the modern carbon fluxes (CH₄, CO₂), the quantification of the fundamental processes (methane production and oxidation) and the structure and functioning of the microbial communities in permafrost affected soils of the Lena Delta.

During the sixth Expedition to the Lena Delta in summer 2003 the long-term studies on methane emissions from different polygonal tundra sites could be continued. The microbial methane production and oxidation of permafrost soils was studied by additional field experiments. Furthermore soil samples were taken for molecular ecological and geochemical analyses.

3.4.2 Methane emission and microbial methane production

3.4.2.1 Methods and field experiments

The investigation of methane emission as well as process studies of methane fluxes were carried out on Samoylov, a representative island in the Lena Delta.

Daily measurements of trace gas emission (CH₄), thaw depth, water surface and soil temperature were determined from July 13 to October 25, 2003 at a low-centred polygon site. Additional measurement of CH₄ release from the floodplain site on Samoylov was monitored. The used method and the main investigation sites were described previously (Wagner et al. 2003a).

The *in situ* CH₄ production was investigated considering the natural soil temperature gradient and different substrates (H₂, Acetate). At two different times, end of July and end of August, fresh soil material (20 g and 30 g,

respectively) from different soil horizons of the polygon centre and the floodplain site, respectively, was weight into 100-ml glass jars, closed gas-tight with a screw cap with septum and flushed with pure N₂. The prepared soil samples were re-installed in the same layers of the soil profile from which the samples had been taken. Gas samples were taken from the headspace with a gastight syringe and analysed for the concentration of methane by gas chromatography in the field laboratory.

Dissolved organic carbon was extracted at two different times from soil samples of three vertical profiles (polygon centre and border, floodplain). The first extraction occurred at the end of July and the second extraction at the end of August. About each 5 cm fresh soil material (9 g) was taken in July to a depth of 30 cm for the polygon centre, to a depth of 21 cm for the polygon border and to a depth of 38 cm for the floodplain. In August soil samples were taken to a depth of 41 cm for the polygon centre, to a depth of 41 cm for the polygon border and to a depth of 60 cm for the floodplain site.

The samples from each layer were weight into glass flasks (50 ml) and mixed with 45 ml distilled water. The flasks were closed and shaken for 1 h in darkness. Afterwards the suspension was filtered (mesh 0.45 µm, Gelman Science) and the clear solution was inactivated by the addition of sodium acid.

CH₄ and CO₂ concentrations were determined with a Chrompack (GC 9003) gas chromatograph in the field laboratory. The detailed configuration was described previously (Wagner et al. 2003b).

4.2.2.2. Preliminary results

The weather in summer 2003 was changeable from warm and dry to cold and stormy, with strong rain. Therefore, the measuring sites, especially the polygon centre and the floodplain were temporary water-filled and flooded, respectively. The water level for the polygon centre and the floodplain site is shown in Figure 3.4-1 and in Figure 3.4-2. As a result of the wet summer the methane emission of the polygonal tundra site showed varying methane fluxes over the vegetation period with a maximum of about 200 mg CH₄ d⁻¹ m⁻² for the polygon centre, while the dryer polygon border had a relatively constant rate with an average of about 4 mg CH₄ d⁻¹ m⁻² (Figure 3.4-3).

The maximum thaw depth of the permafrost soil was reached in August 2003: The thaw depth of the center was in average 46 cm, the border had a depth of about 47 cm (Figure 3.4-4) and the floodplain of about 66 cm (Figure 3.4-5).

The investigation of *in situ* activity of methanogenic archaea showed CH₄ production at the bottom of the active layer at temperatures around 1 °C. Figure 3.4-6 shows the activity from samples of the polygon centre at the end of August, while Figure 3.4-7 and 3-8 demonstrate the activity from samples of the floodplain at the end of July and August.

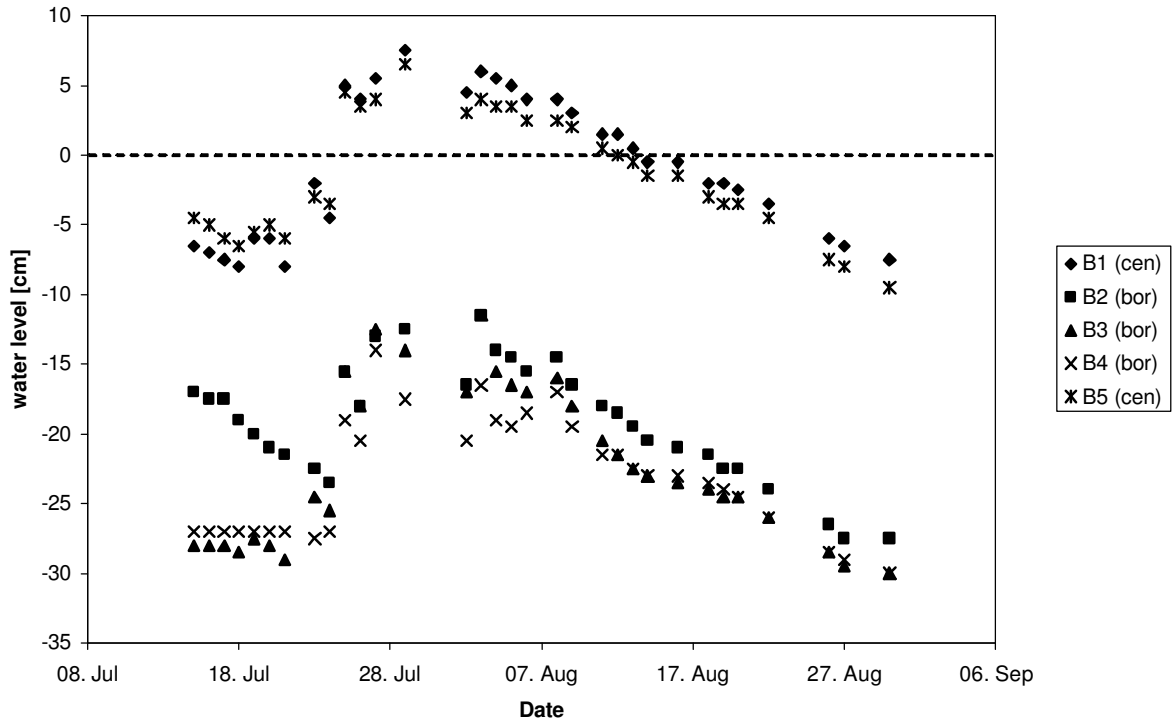


Figure 3.4-1: Water level of a low-centred polygon in summer 2003 (B1 to B5: measuring sites; bor – border, cen – centre)

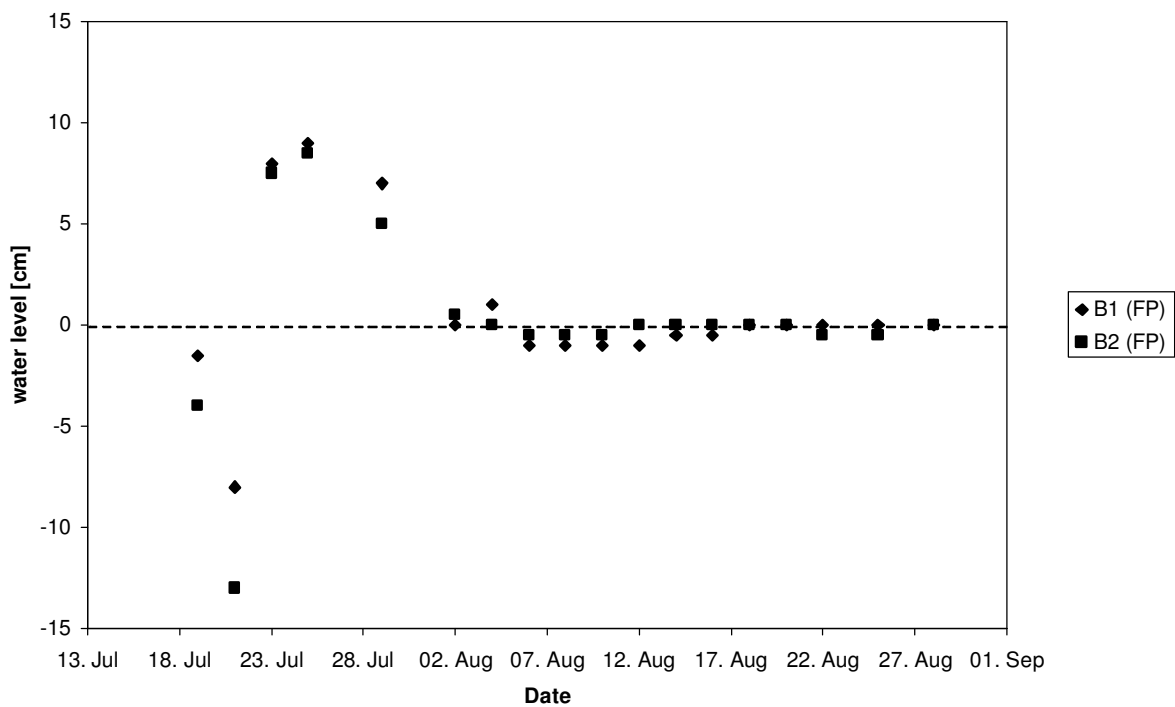


Figure 3.4-2: Water level of the floodplain site in the northern part of Samoylov Island in summer 2003 (B1 to B2: measuring sites; FP – floodplain)

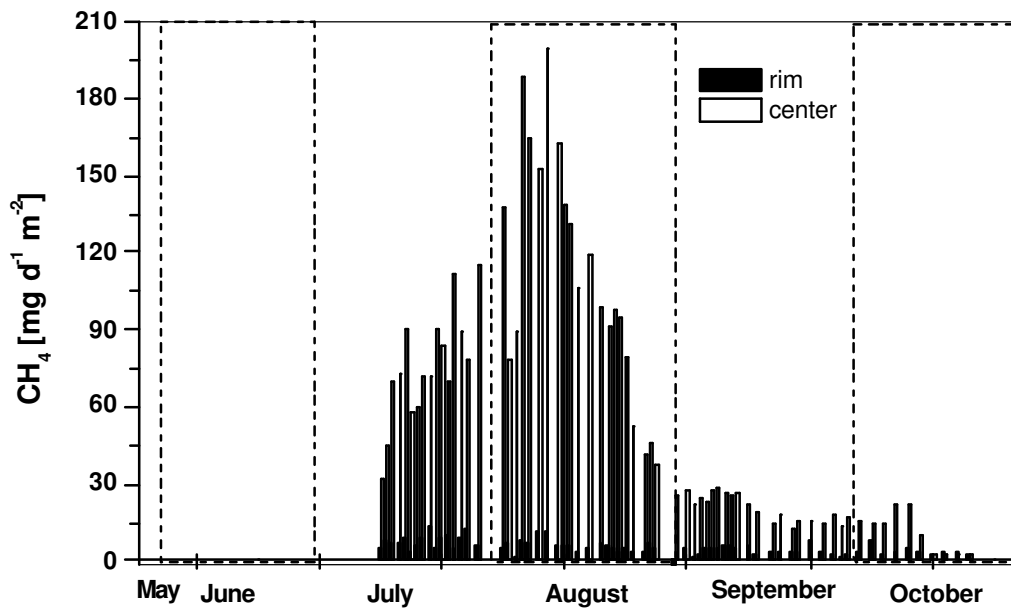


Figure 3.4-3: Methane emission of the low-centred polygonal tundra from July to October 2003.

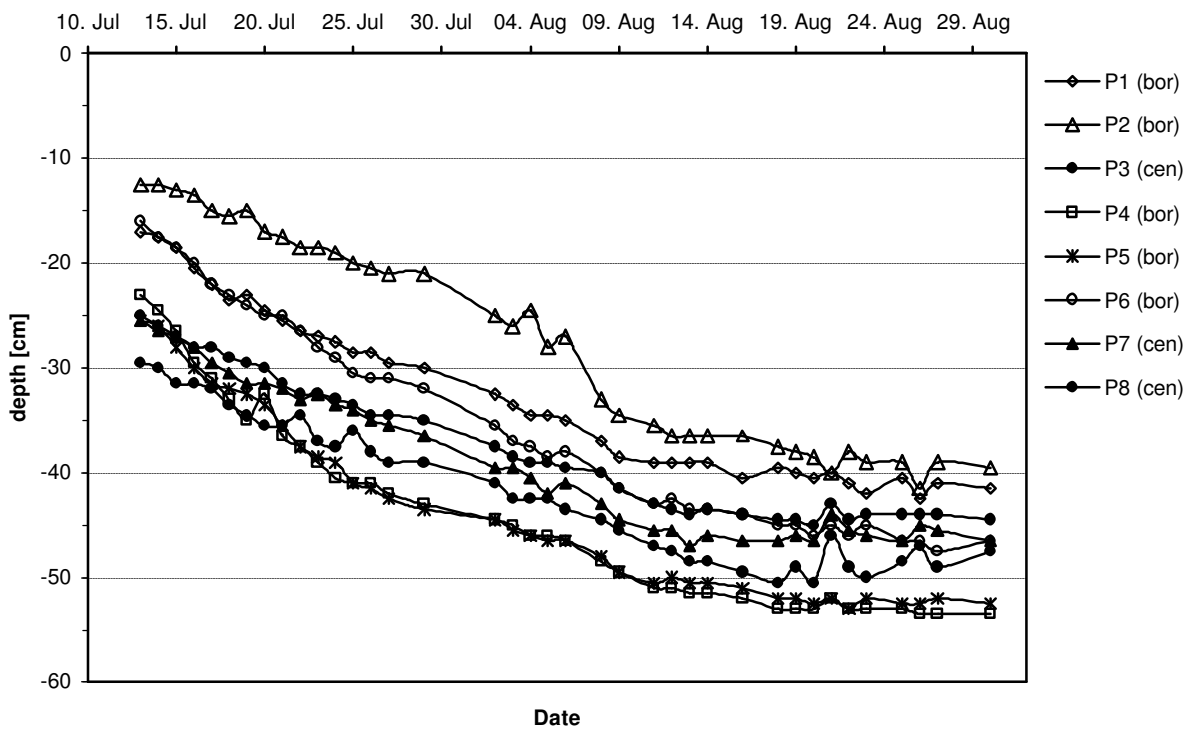


Figure 3.4-4: Thaw depth of a low-centred polygon in summer 2003 (P1 to P8: measuring sites; bor – border, cen – centre)

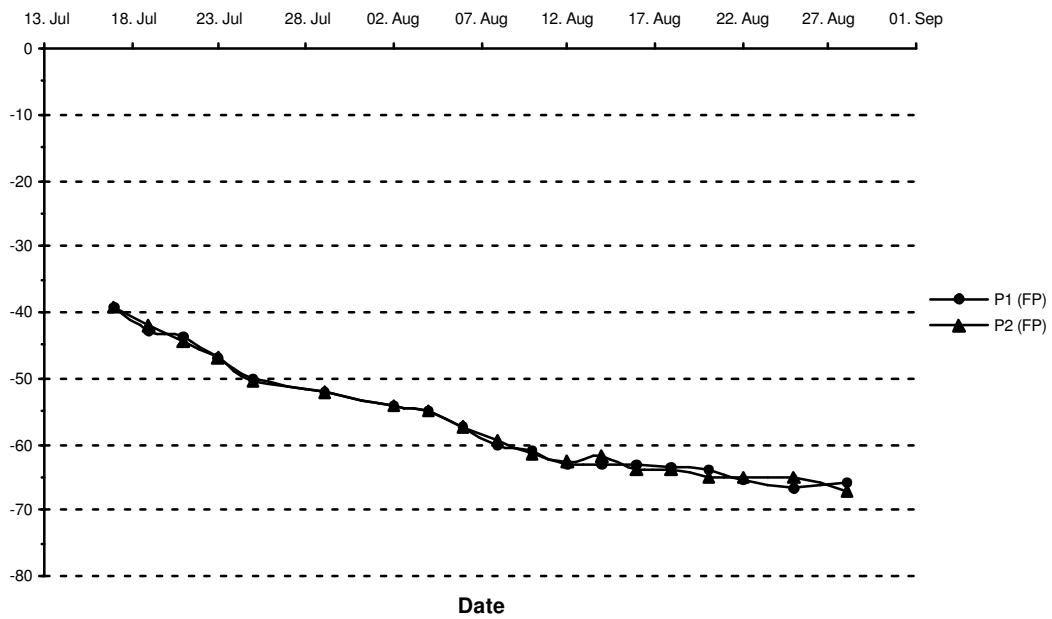


Figure 3.4-5: Thaw depth of a floodplain in the northern part of Samoylov in summer 2003 (P1 and P2: measuring sites; FP – floodplain)

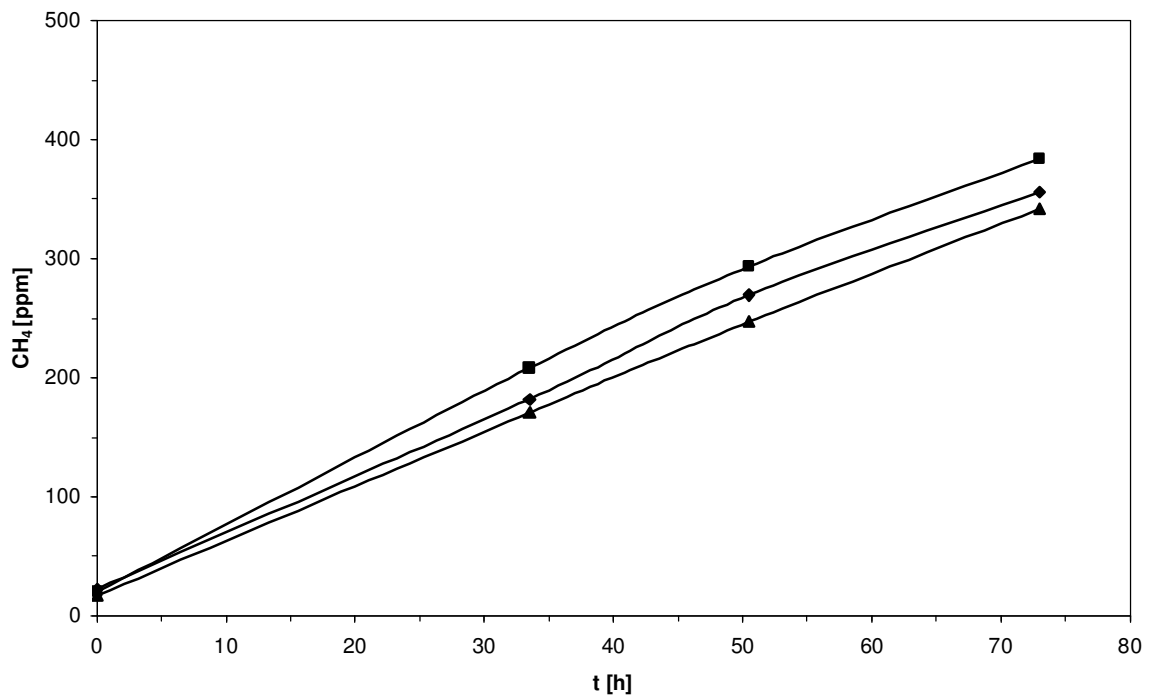


Figure 3.4-6: *In situ* methane production (3 replicates) of the bottom zone of the active layer for the polygon centre at the end of August 2003 (low temperature activity).

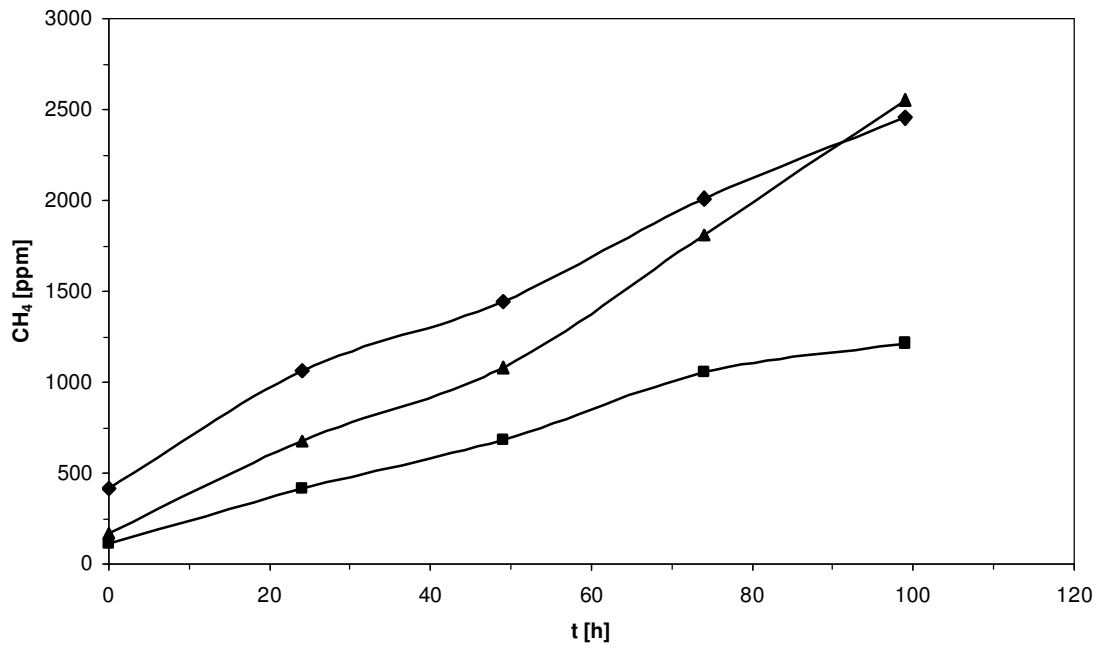


Figure 3.4-7: *In situ* methane production (3 replicates) of the bottom zone of the active layer for the floodplain at the end of July 2003 (low temperature activity).

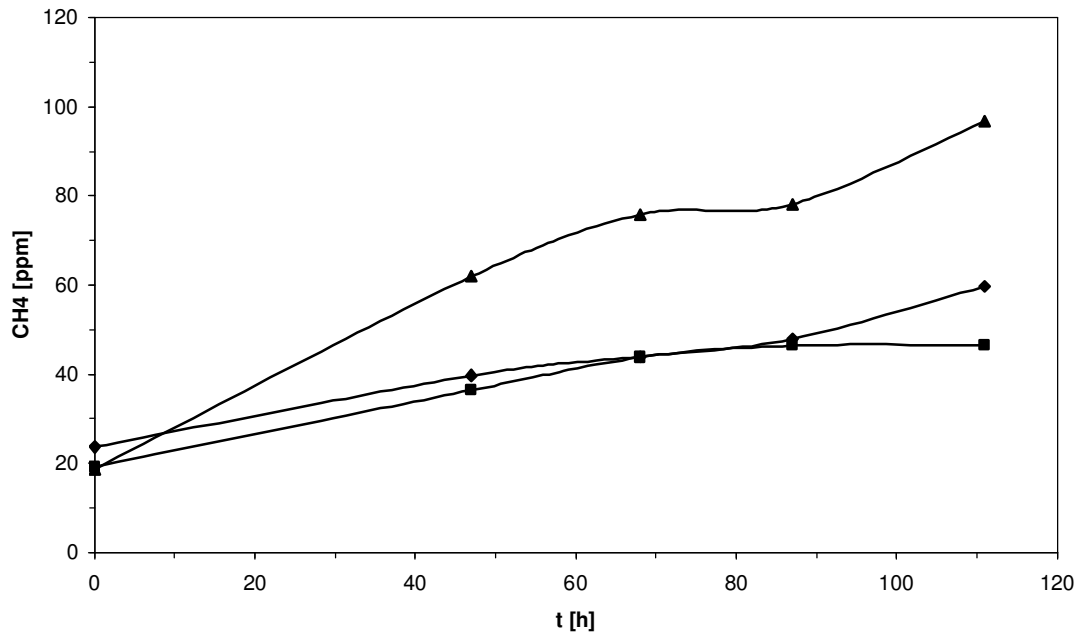


Figure 3.4-8: *In situ* methane production (3 replicates) of the bottom zone of the active layer for the floodplain at the end of August 2003 (low temperature activity).

3.4.3 Process studies on methane oxidation

3.4.3.1 Introduction and objectives

In wetland soils, microbial methane oxidation (methanotrophy) occurs at oxic-anoxic interfaces, which can be found (a) near the water table and (b) in the rhizosphere of vascular wetland plants, where O₂ leaks from the roots into the waterlogged soil. Quantitative estimates of rhizospheric methane oxidation for different northern wetlands vary widely from 0 to 50 % removal of potentially emitted methane (Frenzel and Rudolph, 1998; Moosavi and Crill, 1998; Popp et al., 2000). For wetlands of the Lena Delta, information about plant-associated methane oxidation is still lacking.

The amount of methane oxidation is affected by numerous interrelated factors, one of them being microbial community structure. Therefore, knowledge about the dynamics of methanotrophic population structure in dependence on changing environmental factors helps to understand dynamics of *in situ* methane oxidation rates and consequently methane emissions.

Major questions concerning the microbial methane oxidation were:

- What spatial and temporal differences in methanotrophic population structure can be observed in the course of the summer season, in polygon centre and border?
- How large is the amount of oxidized methane at the roots of wetland plants in waterlogged polygon centers?

3.4.3.2 Methods and field experiments

For the investigation of microbial population structures, soil samples from polygon centre and border were taken in July, August, September and October 2003 (see sample list in Appendix 3-4). These samples were immediately frozen for the transport to Germany. For each soil sampling date important environmental factors were determined, including depth of water table, soil temperatures, soil-pore-water methane concentration and vegetation growth characteristics.

Parts of the samples were prepared in the field for microbial community analyses in Germany: For molecular biological investigations (fluorescent-*in-situ*-hybridization), samples had to be fixed with formaldehyde immediately after collection. Furthermore, parts of the samples were labelled with ¹³C-enriched methane. A subsequent analysis of ¹³C-content in biomarker molecules makes it possible to characterize the active methane oxidizing population in soil. For this purpose, fresh soil material (10 g) was incubated with 100 and 1000 ppm of ¹³C-methane in air in closed 130-ml glass bottles at 0°C (corresponding to *in situ* soil temperature at time of sampling).

Measurements of pore water methane concentration were carried out by placing fresh soil samples together with a saturated NaCl solution into glass jars. After

intensive shaking of the closed jars, methane was forced from the soil solution into the headspace of the bottles and could be analysed by gas chromatography. In the waterlogged polygon centre, soil pore water was additionally collected with a syringe equipped with a steel capillary. Water samples were injected into glass tubes previously filled with saturated NaCl salt solution. Again, methane was forced into the headspace by shaking the tubes and after that analysed by gas chromatography.

In September 2003, root-associated methane oxidation was investigated in a waterlogged polygon centre at the dominant vascular plant species, *Carex aquatilis*. An inhibitor technique was applied as described in chapter 4.5. In addition to a test at single *Carex* culms, closed chambers covering an area of 0.5 x 0.5 m as described by Pfeiffer et al. (1999) were applied for a general test of the technique. For each measurement, 6 chambers were used, 3 of them serving as control. Measurements with the plant flux chambers were carried out with an inhibitor concentration of 0.5 % in the headspace; in the large chambers the inhibitor concentration was varied between 0.5 and 1.5 %.

To investigate methanotrophic population characteristics in late September / beginning of October 2003 (just at the beginning of freeze-back of the soil) potential methane oxidizing activities were determined. For this purpose, samples of polygon centre and rim from different soil depths were analysed. This measurement additionally served as control for a potential activity loss after the frozen samples have been transported to Germany. 5 g of well homogenized fresh soil material was placed in 130-ml glass bottles and incubated with 5000 ppm methane in air at 0°C, which was the approximate *in situ* soil temperature during sampling. Each sample was analysed with 3 replicates. The consumption of added methane was followed by measuring methane concentration in the headspace in regular intervals by gas chromatography.

To consider root-associated methanotrophy, potential activity at fine-root material of *Carex aquatilis* from the depth of 9-15 cm of a polygon centre was determined separately from the remaining soil.

Furthermore, in samples from 3-9 cm depth of a polygon centre the effectiveness of the gaseous inhibitor CH₂F₂, used for the *in situ* inhibitor experiment, was tested at a concentration of 1000 ppm in the headspace, with further incubation conditions as described above for potential activity measurements.

3.4.3.3 Preliminary results

The plant-mediated flux as well as the flux in large closed chambers did not change significantly after addition of the gaseous inhibitor of methane oxidation, CH₂F₂. This result confirms measurements at *Carex aquatilis* in waterlogged soils at Mamontovy Klyk in August 2003 (see chapter 4.5.3). For discussion of possible reasons see chapter 4.5.3

The separate activity measurement of fine-roots and remaining soil from 9 – 15 cm depth in a polygon centre resulted in the following: Firstly, the remaining soil without roots showed higher methane oxidation activity ($57 \pm 6 \text{ nmol CH}_4 \text{ h}^{-1} \text{ g}^{-1}$ dry material) than the whole sample including roots from the same depth ($38 \pm 8 \text{ nmol CH}_4 \text{ h}^{-1} \text{ g}^{-1}$ dry material). Secondly, roots showed a minor activity of $14 \pm 1 \text{ nmol CH}_4 \text{ h}^{-1} \text{ g}^{-1}$ dry material, indicating only small root-associated methane oxidation *in situ*.

Potential methane oxidation rates at 0°C in samples from a polygon centre are shown in Figure 3.4-9. Water table depth at sampling date was 1 cm below the surface. However, potential methane oxidation could be detected up to a depth of 27 cm with maximal activity some cm beneath the water table.

Samples incubated with 1000 ppm CH_2F_2 and 5000 ppm methane did not oxidize added methane, showing that CH_2F_2 inhibits methane oxidizing bacteria in the investigated soil even at lower concentrations than applied in the field experiments.

None of the analysed samples from the polygon border showed methane oxidizing activity at 0°C.

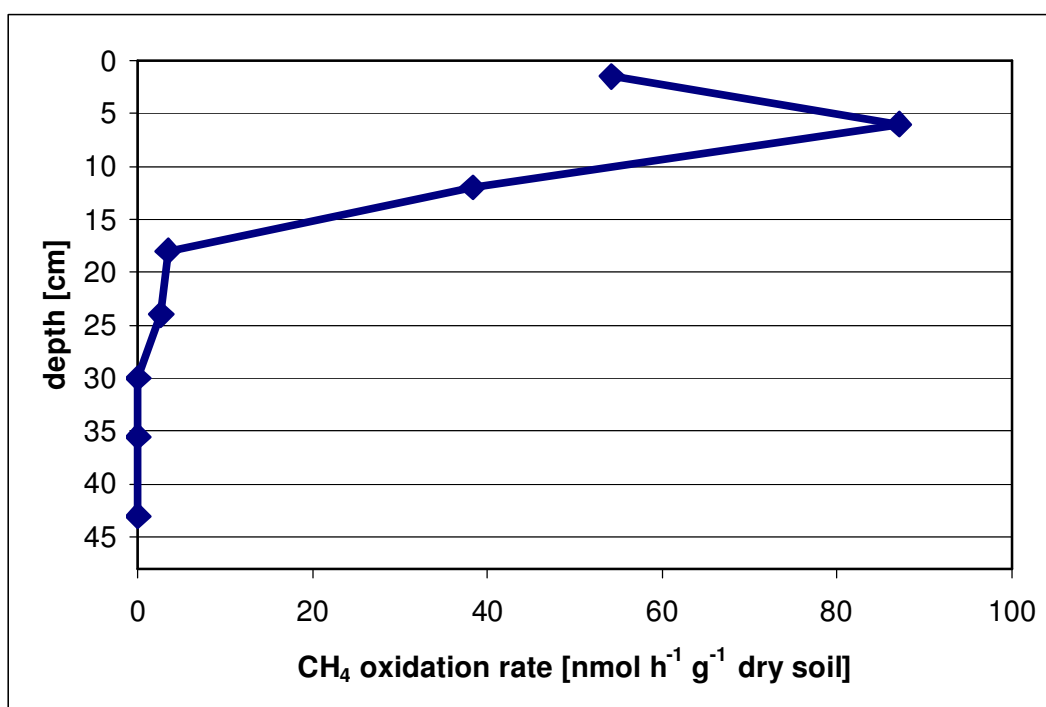


Figure 3.4-9: Vertical profile of potential methane oxidation activity at 0°C, September 2003. *In situ* water table was 1 cm below the soil surface.

3.4.4 Further investigations

The long-term studies on methane fluxes contribute to the understanding of the modern processes of the sensitive tundra ecosystem. They lay the foundation to estimate the impact on possible global climate changes.

The studies will be continued with fresh soil samples from the LENA 2003 Expedition. Especially the analyses of the organic carbon pools, the stable isotope analysis of methane and soil samples as well as the characterization of microbial community structure are still in progress. Furthermore, the isolation and characterisation of methanogenic and methanotrophic microorganisms, which are adapted to the low in situ temperature, is a time-consuming process, which will go on with established and new methods (e.g. fluorescence in situ hybridisation (FISH) and denaturing gradient gel electrophoresis (DGGE), respectively).

3.5 Studies on recent cryogenesis

Hanno Meyer and Waldemar Schneider

The main aim of studying recent cryogenesis processes is to establish a stable isotope thermometer for ice wedges. The recent ice veins are attributed to the discrete year of their formation by means of tracer experiments. A tracer (coloured lycopodium spores) is applied to a polygon with recent cryogenesis, which allows identifying all types of ground ice, which were formed in the considered year.

Studies on recent ice wedge growth were carried out for a polygon at the 1st Lena River terrace of Samoylov Island. For a detailed description of the site and the experimental set-up of the first year, see Meyer (2003). 10 different recent frost cracking experiments were carried out, for which 22 steel poles were used, two of them for survey purposes (11 and 12). The general set-up of every single experiment consists of two about 1 m long steel poles (e. g. 1A and 1B) inserted to the permafrost on both sides of a frost crack. Between two steel poles, a breaking cable was installed. Six (out of ten) experiments in 2003 were equipped with voltage data loggers (type ESIS Minidan Volt) connected to the cables, which should break at the moment of frost cracking. It is expected that the experimental set-up shows a.) if frost cracking took place and b.) the precise moment of frost cracking. The loggers measure every 20 minutes from the moment of installation until the moment of frost cracking.

Only for 5 out of 10 experiments broken cables were observed between 2002 and 2003. These were: 3A-3B, 4A-4B, 6A-6B, 9A-9B, 10A-10B. For the five other experiments, the breaking cables remained in place without cracking. Only three of the five loggers, where frost cracking occurred were equipped with a data logger (4A-4B (Volt 1), 6A-6B (Volt 3), 9A-9B (Volt 6)). Volt 3 cracked on December 9th, 2002, but had contact again on January, 8th, 2003. Volt 1 cracked on November, 27, but had contact again after that. Volt 6 did not show a clear moment of cracking. There was no clear indication which type of wire was the most suitable for the experiments: 2 out of 4 wires (Cu two-wire braid) cracked as well as 1 out of 3 wires (Cu single-wire braid) and 2 out of 3 wires (Cu wire 0.5 mm). For 2003, all experiments were equipped with two-wire braid.

The distance to two fix points (poles 11 and 5b) was measured and compared to the data of 2002 (Table 3.5-1).

Table 3.5-1: Characteristics of 22 steel poles: length, height above surface, distance to fix points (poles 11 and 5b) and depth in permafrost as well as the active layer depth.

	steel pole	2002	2003	Difference 2002-2003	2002 (09.08.)	2003 (21.07)	2003 (30.08.)	Difference 2002-2003
Steel pole	length	distance to M11	distance to M11	distance to M11	distance to 5b	distance to 5b	distance to 5b	distance to 5b
Nr.	(cm)	(cm)	(cm)	(cm)	(cm)	(cm)	(cm)	(cm)
1a	95	957,4	959,3	-1,9	-	-	-	
1b	100	930,5	932,2	-1,7	1171,8	1172	1172,4	-0,2
2a	100	866,7	869	-2,3	-	-	-	
2b	100	818,8	819,5	-0,7	944	944	945	0
3a	92	921,4	924,5	-3,1	-	-	-	
3b	100	887,2	888,4	-1,2	763,2	763,8	764,5	-0,6
4a	100	846,5	849	-2,5	-	-	-	
4b	100	806,7	807,6	-0,9	552,3	552,7	553,2	-0,4
5a	93	681,6	682,5	-0,9	-	-	-	
5b	100	660,2	660,3	-0,1	0	0	0	0
6a	92	635,4	635,6	-0,2	-	-	-	
6b	100	589,3	589,8	-0,5	465	466	464,9	-1
7a	100	977	978,5	-1,5	-	-	-	
7b	100	965	966,2	-1,2	991,1	992	992,6	-0,9
8a	92	727,5	727,7	-0,2	-	-	-	
8b	100	679,3	680,5	-1,2	977,2	979	979,6	-1,8
9a	98	531,8	532,4	-0,6	-	-	-	
9b	100	492	492,5	-0,5	1030,4	1031,3	1032,4	-0,9
10a	99,5	581,1	581,6	-0,5	-	-	-	
10b	100	555,6	557,5	-1,9	1217,3	1218	1217,4	-0,7
11	100	0	0		660,2	660	660	0,2
12	100	339,3	339,8	-0,5	472,8	474	-	-1,2

For the new installation of the experiments, the tension of the wires (Cu two-wire braid, HO3VH-H, 2x0.75) was increased by counting the turnarounds of the nut (type M5) on the thread rods (Table 3.5-2, compare Meyer, 2003).

Table 3.5-2. Ten stretching experiments with applied cables and voltmeters, the lengths of the breaking cables between the poles A and B before spanning the cable (1) and after the cables were stretched (2). The tension of the wires was increased by counting the revs (or turnarounds) of a nut (type M5) on the thread rod. In some cases, the tension was raised on August, 30th. For every cable type, maximum revs were calculated according to its length by means of the breaking experiments.

Marker	Volt-meter	Cable length		Diff.	Control	Cable length		Diff.	Turn-arounds	Turn-arounds	Max.	Tension in
		(21.7)			(30.8)	(30.8)						%
		1	2			1	2		(21.7)	(30.8)		
1A-1B	1	238	244	-6	new	211	219	-8	40	36	55	66
2A-2B	2	258	265	-7	tension control	268	271	-3	44	70	68	103
3A-3B	3	204	206	-2	new	178	186	-8	36	42	47	90

4A-4B	4	280	285	-5	tension control	288	288	0	46	58	72	81
5A-5B	5	150	152	-2	new	125	126	-1	40	20	32	63
6A-6B	6	290	294	-4	new	302	305	-3	52	39	76	51
7A-7B	7	280	283	-3	tension control	284	284	0	41	48	71	68
8A-8B	8	340	345	-5	new	340	341	-1	44	74	85	87
9A-9B	9	322	326	-4	tension control	328	328	0	39	50	82	61
10A-10B	10	175	178	-3	tension control	178	178	0	37	37	45	83

Additionally, the distances between the two poles of each experiment (e.g. 1A and 1B) was determined again in 2003 and compared to the results of 2002 (see Table 3.5-3). The poles were much (up to 152 mm !) closer to each other than in 2002.

Table 3.5-3: Ten stretching experiments with the respective distances (in mm) between the poles A and B measured from the a.) top to the top, b.) tape mark to the tape mark and c.) bottom to the bottom, after the cables were stretched .

Marker	Distance Top-Top		Diff	Distance Tape-Tape		Diff	Distance Bottom-Bottom		Diff
	2002	2003		2002	2003		2002	2003	
1A-1B	358	306	52	372	315	57	386	345	41
2A-2B	465	383	82	457	392	65	454	402	52
3A-3B	351	262	89	361	266	95	343	288	55
4A-4B	406	379	27	415	388	27	407	386	21
5A-5B	231	169	62	240	174	66	236	180	56
6A-6B	435	356	79	429	361	68	411	354	57
7A-7B	351	332	19	349	334	15	348	338	10
8A-8B	503	351	152	509	396	113	498	411	87
9A-9B	380	359	21	392	374	18	404	397	7
10A-10B	259	230	29	264	232	32	289	264	25

To understand how the low temperatures in winter penetrate the active layer and the permafrost, temperature loggers were introduced to the permafrost to derive the temperature gradients necessary for frost cracking activity. The

loggers were inserted every 15 cm in depths of 0.05 m, 0.2 m, 0.35 m and 0.5 m. In this place the active layer is 0.4 m thick.

In order to attribute an ice vein to the discrete year of its formation, tracer experiments were carried out. In late summer, 1 kg of **malachite green** coloured *lycopodium* spores was applied to the polygon walls, especially to the apexes above the frost crack to avoid drifting of the spores by wind. After application, the spores were expected to be covered by the first snow as soon as possible. In winter, when frost cracking takes place, some of the spores should fall into the frost crack. In spring, when the snow cover melts, more spores are washed into the crack. Since the melt water freezes immediately, the spores are conserved in the newly formed ice vein, which can clearly be attributed to the year of its formation.

3.6 Seasonal progression of active-layer thickness dependent on microrelief

Lars Kutzbach, Günther Stoof, Waldemar Schneider, Christian Wille and Ekaterina N. Abramova

3.6.1 Introduction

Active-layer thickness is a major factor for all physical and biological processes in permafrost soils. It is closely related to the fluxes of energy, water and carbon between permafrost landscapes and the atmosphere. Active-layer thickness is mainly driven by air temperature, but also influenced by snow cover, summer rainfall, soil properties and vegetation characteristics (Nelson et al., 1998). The typical polygonal tundra of the Lena Delta is characterised by a pronounced microrelief, which causes a high small-scale heterogeneity of soil and vegetation properties. Consequently, also the active-layer thickness varies substantially across small lateral distances of decimetres to metres. In order to up-scale results of process studies to the landscape scale, a quantification of the heterogeneity of active-layer thickness is of great interest.

3.6.2 Methods

In 2002, an active-layer thickness monitoring program was started on Samoylov Island. An investigation site of 28 m x 18 m was established on the area of a typical low-centre polygon in the vicinity of the permanent meteorological and soil survey station (Kutzbach et al., 2003b). 150 measurement points were mapped out in a regular grid of approximately 2 m x 2 m. The measurement points were grouped in classes according to their situation within the microrelief and their vegetation cover. A characterisation of the five distinguished classes is given in Table 3.6-1. At every measurement point, active-layer thickness was determined on a weekly basis by driving a steel rod into the unfrozen soil until the permafrost table was encountered. In 2003, measurements were conducted from June 15 to October 4 (2002: June 10 to August 30). In addition to the regular measurements, the mapping of the microrelief of the investigation site was refined for the production of a high-resolution 3-dimensional surface model. The new surface model is presented in Figure 3.6-1 and Figure 3.6-2.

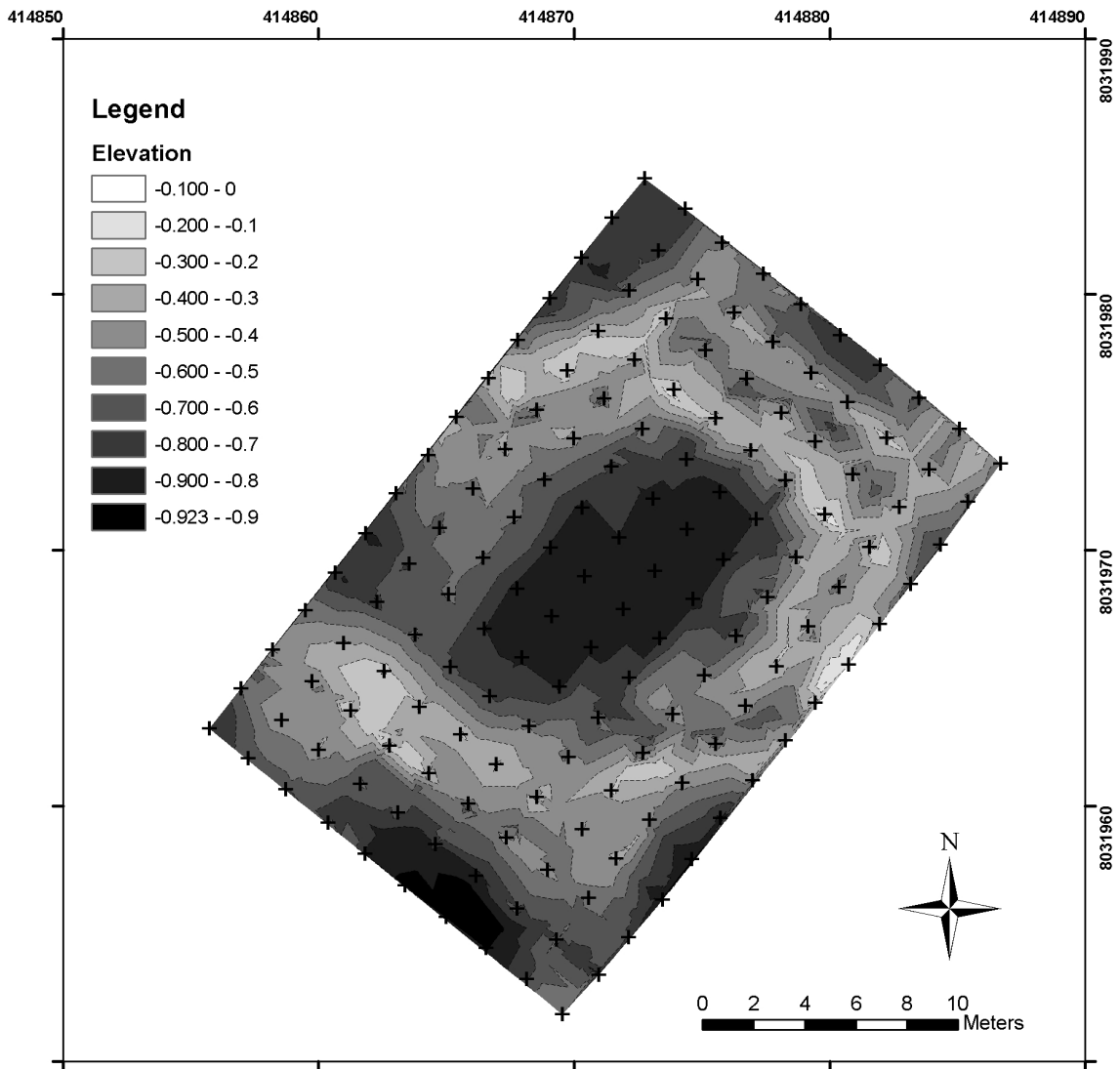


Figure 3.6-1: Map of active-layer thickness monitoring site. – Crosses: positions of measurement points. The 3D-model is based on a triangular network (TIN, 1379 points). Elevation values are relative to a reference point in metres. The coordinate system is UTM, Zone 52N, WGS84.

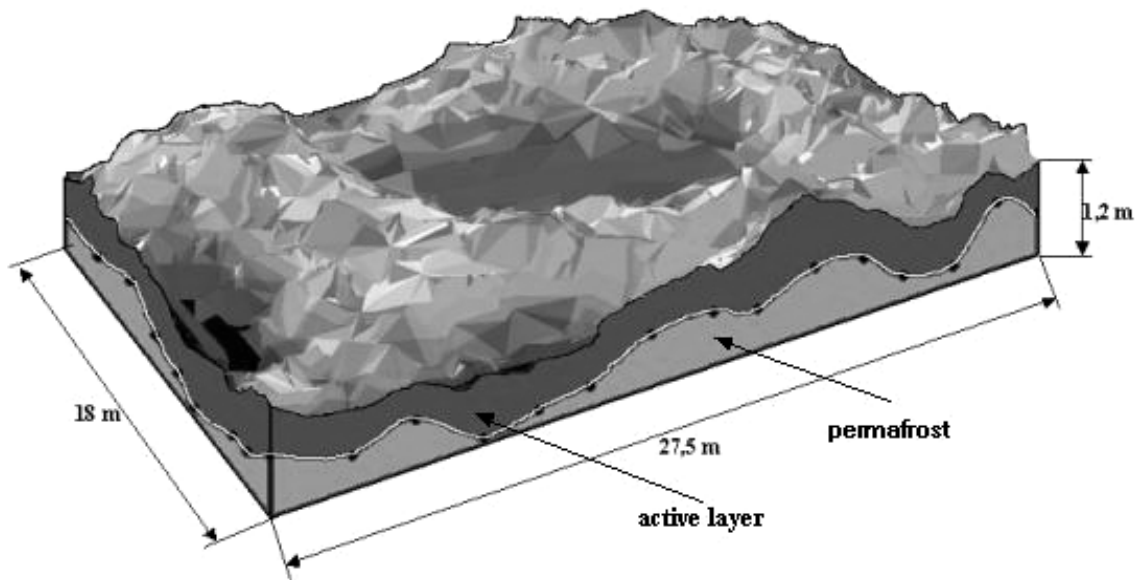


Figure 3.6-2: Three-dimensional model of the active-layer-thickness monitoring site. The white line indicates the maximum active-layer thickness in 2003 observed at the end of August. The height exaggeration factor is 4.

Table 3-6-1. Characterisation of measurement point classes at the active-layer thickness investigation site.

ID	situation within microrelief	vegetation	number of points
1	depressed polygon centre, water table at or above the soil surface	<i>Carex aquatilis</i> , <i>Limprichtia revolvens</i> , <i>Meesia longiseta</i> , <i>Calliergon giganteum</i> , <i>Meesia triquetra</i>	39
2	transition zone between centre and elevated rim	thick moss layer <i>Sphagnum orientale</i> , <i>Meesia longiseta</i> , <i>Aulacomnium palustre</i> , <i>Aulacomnium turgidum</i> , <i>Tomenthypnum nitens</i>	25
3	strongly elevated rim, strongly convex	<i>Carex aquatilis</i> , <i>Salix glauca</i> , <i>Salix reptans</i> , <i>Dryas octopetala</i> , <i>Astragalus frigidus</i> , <i>Luzula nivalis</i>	33
4	weakly elevated rim relatively flat	few <i>Carex aquatilis</i> , thick <i>Hylocomium splendens</i> layer	47
5	frost crack	<i>Limprichtia revolvens</i> , <i>Calliergon giganteum</i> , <i>Campylium stellatum</i> , <i>Tomenthypnum nitens</i>	6

3.6.3 First results

The seasonal progression of the mean active-layer thickness during the expedition periods of 2002 and 2003 is presented in Figure 3.6-3. Maximum thaw depth was observed in both years at the end of August. The mean active-layer thickness was distinctly greater in 2003 than in 2002. At the end of August, it amounted to 0.43 ± 0.08 m in 2002 and to 0.48 ± 0.07 m in 2003, respectively. It is assumed that this substantial variation between years is related to the strongly differing precipitation patterns of the years 2002 and 2003. The accumulated precipitation during June and July amounted to 46 mm in 2002, while in 2003 more than the twofold value, 110 mm, was determined for the same period (Hydrometeorological Centre of Russia, 2004). Rainfall is of high importance for the energy balance of soils, as it represents an advective heat transport from the atmosphere into the soils, increases soil moisture, and as a result alters the thermal properties of soils, as heat capacity and heat conductivity.

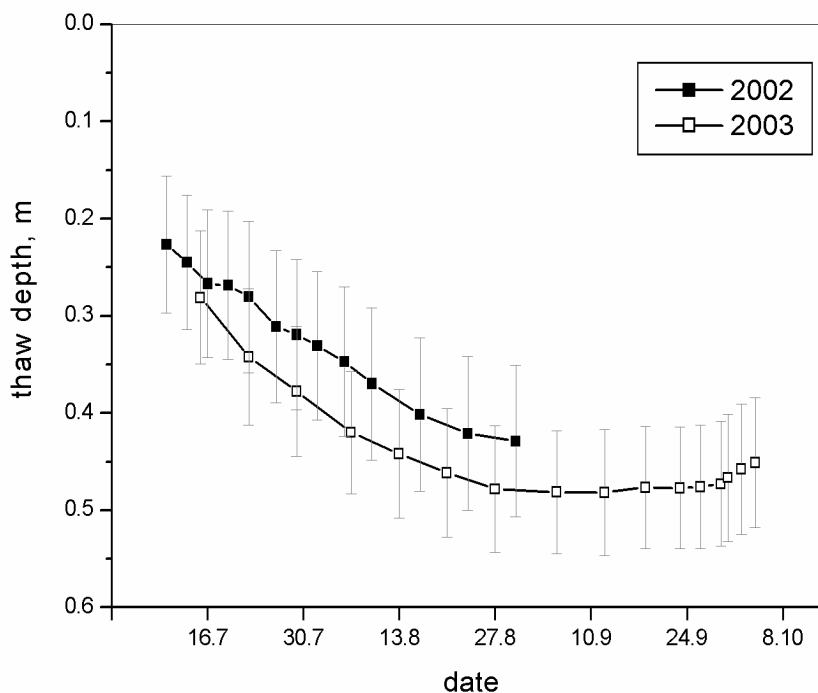


Figure 3.6-3: Seasonal progression of active-layer thickness in 2002 and 2003. Values are means of all 150 measurement points.

Figure 3.6-4 points out the strong influence of the microrelief position and vegetation cover on the active-layer thickness. In particular, the thaw depths at strongly elevated rim positions (class 3) and at weakly elevated rim positions (class 4) differ substantially. While the mean thaw depth of class 3 reached 0.53 ± 0.07 m at the end of August 2003, the mean thaw depth of class 4 reached only 0.44 ± 0.06 m. At both rim classes (3 and 4), only slow freeze-

back could be observed at the end of September. By contrast, the mean thaw depth at the depressed centre positions (class 1) decreased considerably faster at that time of season.

Further evaluation of the data will help to develop a better understanding of the spatial variability and the regulation of active-layer thickness of polygonal tundra landscapes.

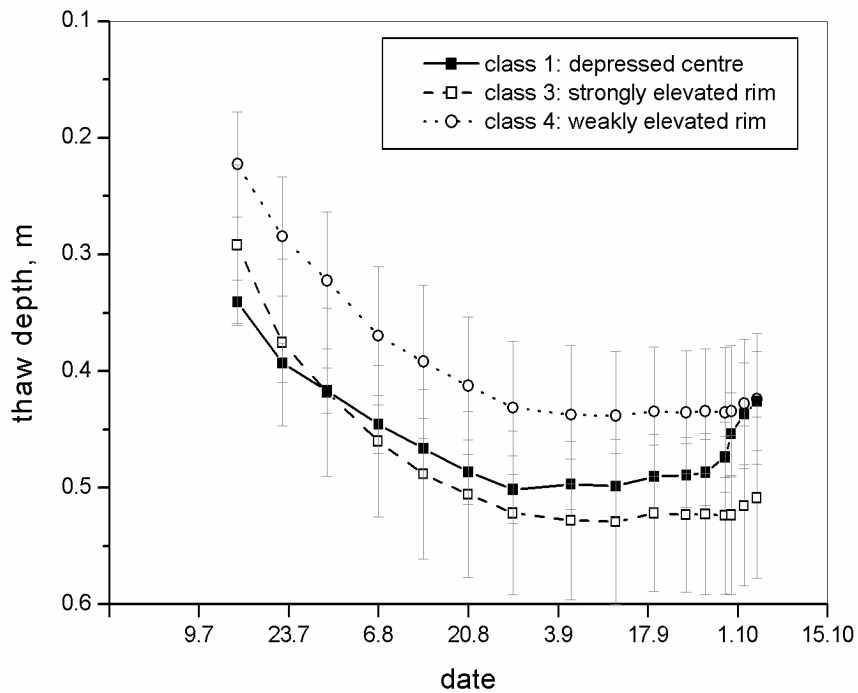


Figure 3.8-4 Seasonal progression of active-layer thickness in 2003 differentiated by situation within the microrelief (see Table 3.6-1). Values are class means (class 1: $N = 39$, class 3: $N = 33$, class 4: $N = 47$).

3.7 Air photography and surface classification of Samoylov Island

Christian Wille

For the qualitative description of surface properties like vegetation cover or land-water-ratio of Samoylov Island as well as for the evaluation of fetch homogeneity considerations of the eddy covariance measurements and for the up-scaling of chamber flux measurements, a detailed surface classification of the island at the sub-polygonal scale is necessary. However, up to know only grey-scale Corona satellite images from the 1960s with a resolution of 2 x 2 m and recent multi-spectral Landsat images with a resolution of 30 x 30 m were available for this region. Both are not useable for the desired classification because of missing spectral information and inadequate resolution, respectively.

During the Lena 2003 expedition, a survey of the island by air photography was carried out in order to obtain images for surface classification. The photographs were taken from a helicopter on 10.07.2002, using a Canon EOS100 reflex camera, a Soligor 19-23 mm lens and colour slide film. The height from which the photographs were taken was approximately 600 meters. Due to limited flight time, not all the area of the island could be photographed and some regions could only be photographed with a slanted view. As a result, the images are of a varying quality and resolution.

In Potsdam, after processing the films were scanned using a Nikon LS-2000 scanner at maximal resolution setting. This resulted in a ground resolution of the scanned images of approximately 0.3x0.3 m. The images were subsequently geo-referenced using the ENVI software and a referenced Corona image dating from 18.07.1964 (Spott, 2003). Geo-referencing was only possible for the Holocene river terrace areas; the floodplain regions in the western part of the island could not be referenced due to the lack of ground reference points. In Figure 3.7-1, the aerial view of Samoylov Island composed of the geo-referenced images is shown.

Further work is necessary for the classification and interpretation of the images. If possible, air photography surveys will be carried out during future expeditions in order to determine changes in surface pattern and composition.

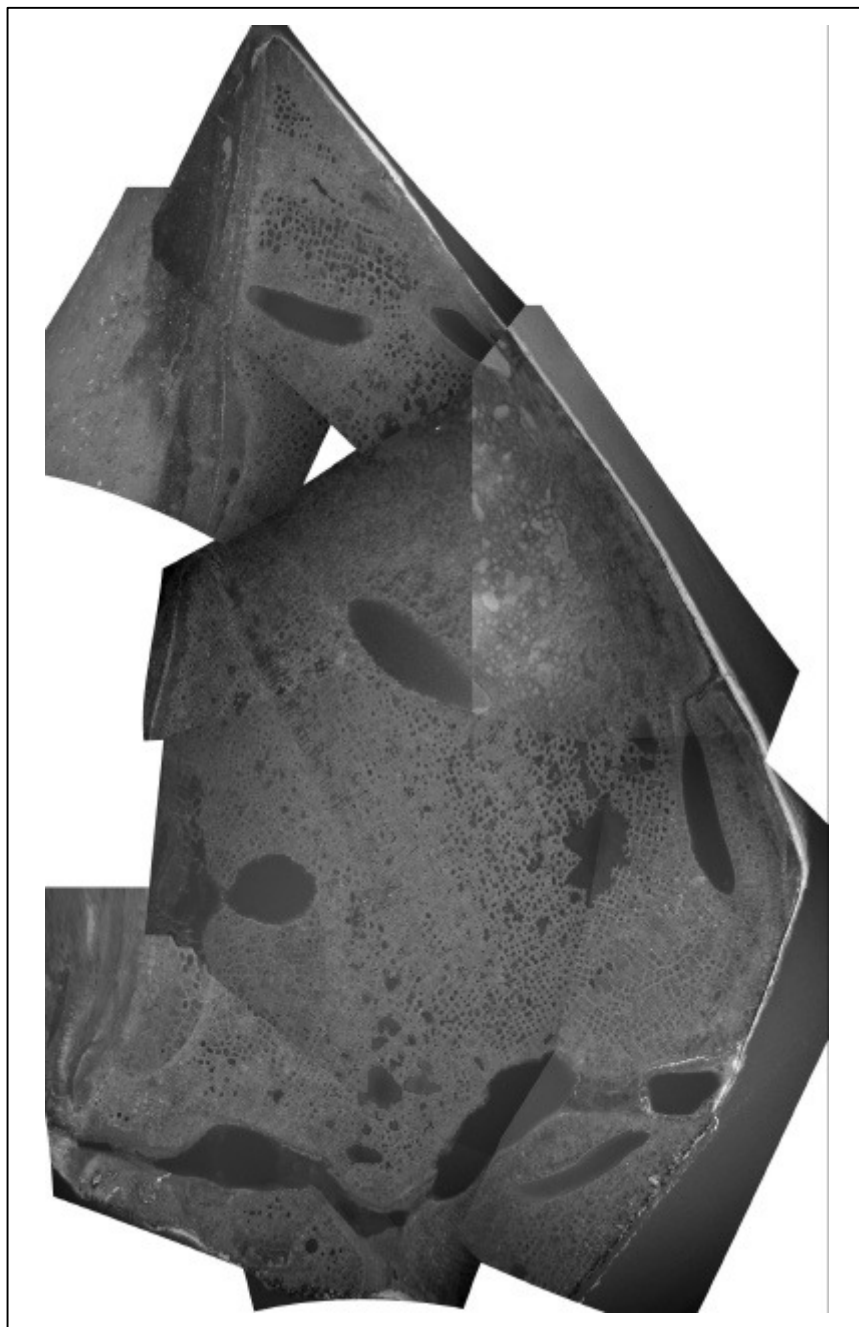


Figure 3.7-1: Composite image of Samoylov Island

3.8 Hydrobiological investigations in the Lena Delta in summer 2003

Ekatarina N. Abramova, Irina Akhmetshina, Guenther Stoof and Waldemar Schneider

3.8.1 Objectives

About 58700 lakes are situated in the Lena Delta, on average every 1000 km² incorporate 2120 small and big lakes (Mostakhov, 1973). Undoubtedly, the latter play a significant role in the delta ecosystem. Pelagic fauna of the lakes is characterized by the great variety and abundance. Among 106 zooplankton taxa found during our research last year in different reservoirs of the delta, more than 90% occurred in lakes (Abramova, 2003). Taxonomic composition of zooplankton of the Lena River itself and its channels is poor and its abundance is low. Considerable stream velocity and high concentration of suspended particulate matter hamper formation of stable zooplankton assemblages. Lake species brought into the Lena Delta and the Laptev Sea bays during flood play an important role in composition of their zooplankton associations (Gukov, 2001). Freshwater organisms constitute about 50% of the summer total zooplankton abundance in the shallow brackish water bays of the Laptev Sea (Olenek, Tumat and Yana bays) (Abramova, 2000).

Small thermokarst lakes are the most abundant type of water bodies in the Lena Delta. Polygonal tundra occupies about 1/3 (9,600 km²) of the total Lena Delta area (Grigoriev, unpublished data). The annual primary biomass production in these lakes is known to be low, but this is mainly caused by the short ice-free season. However, our preliminary data suggest that, compared to other tundra water basins, zooplankton abundance, biomass and production in small thermokarst lakes are rather high. For example, the daily production of only one dominant species *Daphnia pulex* varied from 4.3 mg/l to 5.3 mg/l during summer 2001 (Akhmetshina & Abramova, 2002). The average daily zooplankton production for different polygons changed from 0.01 to 1.5 g/m⁻³. The total absolute daily production of a medium size pond with the water volume about 82 m³ changes from 11 g to 121g a day and reaches its maximum in the periods of the most intensive reproduction of the dominant species. The average seasonal zooplankton production for an average size polygon may reach 6-7 kg. For the whole polygonal tundra of the Lena Delta, this will equal to many tons of organic material.

During the expedition “Lena-Anabar 2003” the monitoring of zooplankton in the Lena Delta was continued. We have collected zooplankton samples in different types of lakes on the Samoylov and Buor-Khaya Islands; and in the region of Cape Mamontov Klyk.

3.8.2 Research tasks

- To study species composition and distribution of zooplankton of the Lena Delta lakes;
- To investigate ecological affinity of certain species, primarily their temperature limits;
- To study biology of development of the mass Copepoda species (number of generations per season, age structure, diapausal stages, etc.)
- To analyze seasonal dynamics of zooplankton abundance and biomass in polygon lakes on the Samoylov Island
- To reveal temperature - abundance/biomass dependences;
- To determine the daily and seasonal production of zooplankton in the different lakes of the Lena Delta

3.8.3 Material and methods

Seventy-six zooplankton samples were collected during the whole period of investigation (July – October 2003) on Samoylov Island: 11 samples – from a flood-plain lake, 20 – from a deep polygon, 14 – from a shallow polygon, and 13 – from a crack between polygons. Six samples of zooplankton were collected from alases and polygons on Buor-Khaya Island and 12 from the Mamontov Klyk region (lakes and nearshore area of the Laptev Sea). Also, four samples of benthic organisms were collected to define species composition, abundance and biomass from the flood-plain lake and polygon on the Samoylov Island.

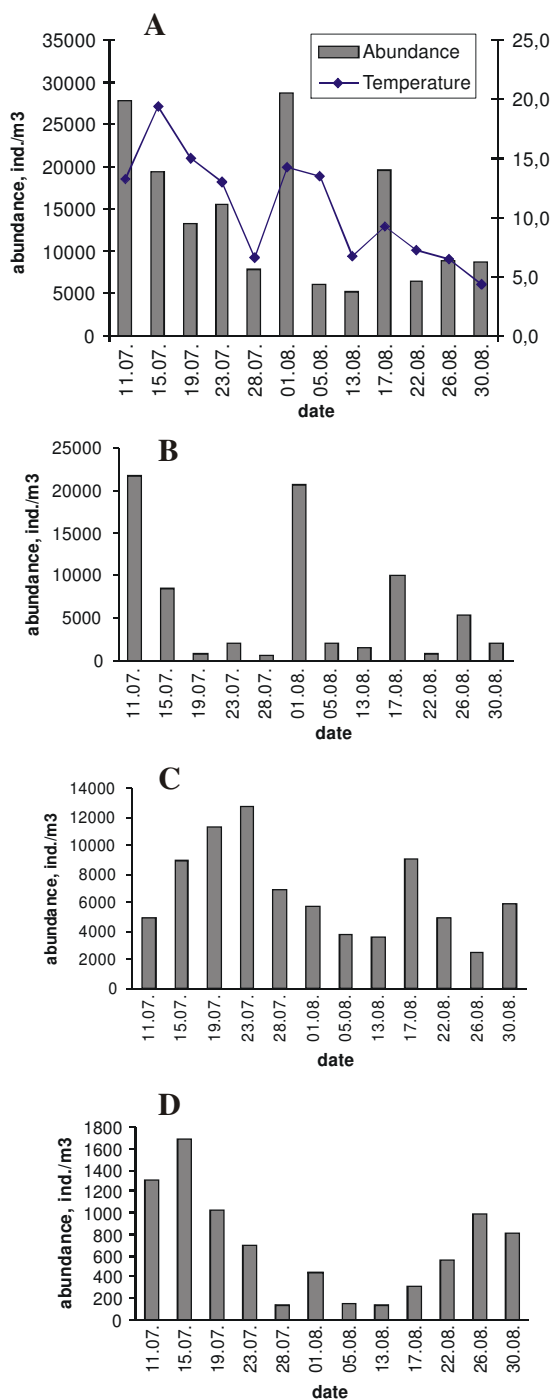
As in the previous years, sampling of zooplankton was performed by filtering of 100 litres of water through a 100- μ m mesh size net with periodicity of 5-10 days and fixation with 70% alcohol. Either the whole sample or part of it was analysed in a Bogorov chamber under a binocular microscope WESSEX WSP2. Detailed taxonomic analysis and measurements of plankton organisms (with an accuracy of one hundredth of micron) were carried out using Olympus SZX9 and Olympus BX60 microscopes with the adjusted camera and computer program “Analysis” in the Otto Schmidt Laboratory in St.-Petersburg. To identify individual weights of organisms, we used the formula: $W=ql^b$, where W is body weight, l – body length (mm), q – weight at 1 mm body length, b – index.

For benthic organisms collection Peterson grab sampler was used with the catchment area of 0.0225 m². Sediments were washed through a set of sieves ranging from 100 to 60 μ m. All organisms were fixed with 70% alcohol and analysed using binocular WESSEX WSP2. The definition of individual masses of benthos was carried out using the analytical balance Sartorius LA 230S in the Otto Schmidt Laboratory in St.- Petersburg.

To study the life cycles of two mass species of Cyclopoida a natural experiment was applied: 50-60 exemplars of naupliar stages of every species were put into two 1-liter jars covered with fine kapron gauze (mesh size - 20 μ m), which were

placed into the natural reservoir. Every two days the jars content was filtered and organisms were analysed under binocular in a small amount of water in order to define the presence or absence of the next age stages. Then the organisms were put into the jars again, and the jars were returned to the reservoir. Simultaneously, quantitative samples of zooplankton were collected, and water temperature was measured.

3.8.4 Preliminary results



Polygons are well suited for hydrobiological studies since they are small, almost closed water basins with short trophic chains, and limited active ice-free period. Species variety of zooplankton in polygons has been described earlier (Abramova, 2003). In average 30 zooplankton species occur in this type of lakes, where Copepoda, Cladocera and Anostraca are the main components of zooplankton community. Seasonal dynamics of both abundance and biomass of pelagic fauna in polygons have their own peculiarities. The maximums of the quantitative characteristics and its number usually depend on environmental conditions on a certain year and live cycle of the common zooplankton species. For instance, in summer 2001 and 2002 during the whole study period on the deep and shallow polygons of Samoylov Island Calanoida (*Heterocope borealis* and *Mixodiaptomus theeli*) predominated in the total abundance (Abramova, 2003). In summer 2003, three well-determined maxima of zooplankton abundance (first half of July, beginning and middle of August) (Figure 3.8-1A) corresponded to the appearance of young Cladocera, mainly *Daphnia pulex*. Parthenogenetic reproduction was observed for this species at least two times during the two months (in the beginning of July and August) (Figure 3.8-1B).

Figure 3.8-1. Seasonal dynamic of the total zooplankton abundance and temperature (A); and seasonal abundance fluctuation of the main zooplankton groups: Cladocera (B), Calanoida (C) and Cyclopoida (D) in the deep polygon on Samoylov Island.

Calanoida was dominated in zooplankton abundance during the second half of July (Figure 3.8-1C), in September and in the beginning of October in the deep polygon. The juvenile stages of *H. borealis* and several species of Diaptomidae were numerous in the end of summer. Cyclopoida were the most inconsiderable group in terms of abundance and biomass in our collections in summer 2003 (Figure 3.8-1D), as their intensive reproduction is usually observed in June. No investigations were carried in June 2003. The total average abundance of zooplankton for the two months (July-August) was 14000 ind./m³ in the deep polygon. Maximum abundance (about 30 thousand ind./m³) was recorded at 15°C water temperature (Figure 3.8-1A). The total average abundance of zooplankton in July-August was higher (17130 ind./m³) in the shallow polygon with maximum (31 thousand ind./m³) at 15°C water temperature also. The calanoids *H. borealis*, *M. theeli*, *Leptodiaptomus angustilobus* and immatures stages of this genus, accounted for most of the organisms found in shallow polygon in summer 2003.

One good pronounced peak of the total zooplankton biomass was recorded in deep polygons with maximum (12 g/m³) in the beginning of August (Figure 3.8-2). *Daphnia pulex* and two species of Anostraca (*Polyarthemia forcipata* and *Branchinecta paludosa*) composed more than 95% of total zooplankton biomass in this time. The average summer biomass was 3,3 g/m³ in the deep polygon and 2,4 g/m³ in the shallow polygon.

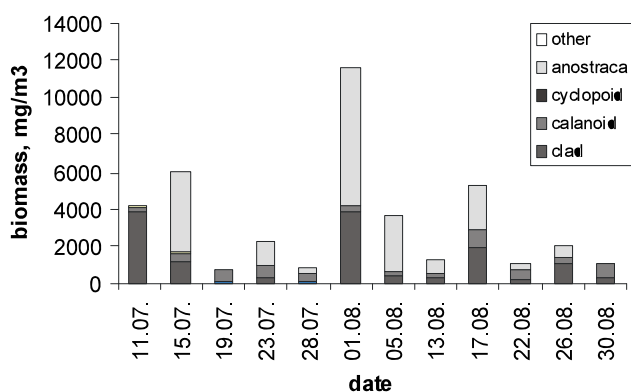


Figure 3.8-2. Seasonal dynamic of the total zooplankton biomass and the biomass of different groups of organisms in the deep polygon on the Samoylov Island in 2003

The highest zooplankton abundance (more than 40 thousand ind./m³) and lowest biomass were observed in flood-plain lakes on Samoylov Island due to the high concentration of numerous Rotatoria (>50% of the total density) and Calanoida (about 30% were made up by different stages *Eurytemora bilobata* and *Eurytemora sp.*).

In the nearshore area of the Mamontovy Klyk region (see chapter 4) the zooplankton species composition was dominated by the brackish-water complex (15 species), but fresh-water fauna was well represented too (12 species). The copepods of brackish-water complex were also dominated in abundance, especially *Eurytemora raboty*, *Tachidius sp.*, *Drepanopus bungei*, *Limnocalanus macrurus*, *Pseudocalanus sp.juv.* were numerous. *Bosmina longirostris* (Cladocera) and Rotatoria of genus *Synchaeta*, *Keratella* and *Notholca* occupied the second position in abundance.

A relatively low species diversity and abundance of benthic organisms were discovered in the lakes on the Samoylov Island. A total seven taxa were identified in the flood-plain and polygon lakes. The benthic community of the flood plain lakes were dominated of Ostracoda and Nematoda (about 73% of the total abundance) and mollusc was responsible for nearly 40% of the total biomass (Table 3.8-1). The similar situation was observed in the benthic assemblage of the polygon lake on the Samoylov Island.

Table 3.8-1. Composition, abundance and biomass of the main groups of benthic organisms in the flood-plain lake on Samoylov Island.

Taxa	abundance (ind./m ⁻³)	biomass (g/m ⁻³)
Harpacticoida	48	0.00144
Ostracoda	265	0.00053
Gammaridae	3	0.108
Mollusca	24	0.158
Hyronomidae	13	0.0177
Nematoda	146	0.00584
Annelida	60	0.0592
Other		0.0153
Total:	559	0.36601

3.9 Appendices

Appendix 3-1. Collected variables determined by direct measurements within the micrometeorological campaign Samoylov, 2003.

ID	symbol	unit	description	instrument	recording interval
Micrometeorology					
1	u_0	m s^{-1}	wind velocity components in 3 dimensions, unrotated	anemometer	0.05 s
2	v_0	m s^{-1}			
3	w_0	m s^{-1}			
4	T_{son}	$^{\circ}\text{C}$	sonic air temperature	anemometer	0.05 s
5	C_{H_2O}	mmol mol^{-1}	concentration H_2O	IRGA	0.05 s
6	C_{CO_2}	$\mu\text{mol mol}^{-1}$	concentration CO_2	IRGA	0.05 s
7	C_{CH_4}	$\mu\text{mol mol}^{-1}$	concentration CH_4	TGA	0.05 s
8	T_{air}	$^{\circ}\text{C}$	air temperature	meteorological probe	0.05 s
9	RH	%	relative humidity	meteorological probe	0.05 s
10	p	Pa	barometric pressure	pressure sensor	15 min
11	SW_{up}	W m^{-2}	incoming shortwave radiation (global rad.)	pyranometer	15 min
12	SW_{dw}	W m^{-2}	reflected shortwave radiation	pyranometer	15 min
13	LW_{up}	W m^{-2}	incoming longwave radiation	pyrgeometer	15 min
14	LW_{dw}	W m^{-2}	outgoing longwave radiation	pyrgeometer	15 min
15	h_c		canopy height	rule	one-time (=0.15m)
Instrument control					
16	z_m	m	measurement height of turbulent fluxes	rule	one-time (=3.65m)
17	z_h	m	measurement height of humidity/temperature measurement	rule	one-time (=2.0m)

Appendix 3-1. continuation

18	T_{CNR}	°C	temperature pyrgeometer	thermocouple pyrgeometer	15 min
19	T_{Li}	°C	temperature IRGA	themocouple IRGA	15 min
20	p_{Li}	kPa	pressure IRGA	pressure sensor IRGA	15 min
21	T_{case}	°C	temperature weatherproof case	thermocouple	15 min
22	T_{cryo}	°C	temperature cryocooler case	thermocouple	15 min
23	T_{air-m}	°C	air temp.	manually (temp.probe)	1-3 days
Soil Conditions					
24	Q_{G-c}	W m ⁻²	soil heat flux density polygon centre 10 cm	heat flux plate	60 min
25	Q_{G-r}	W m ⁻²	soil heat flux density polygon rim 10 cm	heat flux plate	60 min
26	T_{S-C01}	°C	soil temp. centre 1 cm	thermocouple	60 min
27	T_{S-C05}	°C	soil temp. centre 5 cm	thermocouple	60 min
28	T_{S-C10}	°C	soil temp. centre 10 cm	thermocouple	60 min
29	T_{S-C15}	°C	soil temp. centre 15 cm	thermocouple	60 min
30	T_{S-C30}	°C	soil temp. centre 30 cm	thermocouple	60 min
31	T_{S-C45}	°C	soil temp. centre 45 cm	thermocouple	60 min
32	T_{S-R01}	°C	soil temp. rim 1 cm	thermocouple	60 min
33	T_{S-R10}	°C	soil temp. rim 10 cm	thermocouple	60 min
34	T_{S-R15}	°C	soil temp. rim 15 cm	thermocouple	60 min
35	T_{S-R25}	°C	soil temp. rim 25 cm	thermocouple	60 min
36	T_{S-R30}	°C	soil temp. rim 30 cm	thermocouple	60 min
37	T_{S-R40}	°C	soil temp. rim 40 cm	thermocouple	60 min
38	θ_{S-C05}	%	soil moisture centre 5 cm	TDR	60 min
39	θ_{S-C15}	%	soil moisture centre 15 cm	TDR	60 min
40	θ_{S-C30}	%	soil moisture centre 30 cm	TDR	60 min
41	θ_{S-C45}	%	soil moisture centre 45 cm	TDR	60 min
42	θ_{S-R10}	%	soil moisture rim 10 cm	TDR	60 min
43	θ_{S-R15}	%	soil moisture rim 15 cm	TDR	60 min
44	θ_{S-R25}	%	soil moisture rim 25 cm	TDR	60 min

Appendix 3-1. continuation

45	θ_{S-R30}	%	soil moisture rim 30 cm	TDR	60 min
46	θ_{S-R40}	%	soil moisture rim 40 cm	TDR	60 min
47	d_{W-S1}	m	water level site S1	manually (in pipes)	1-3 days
48	d_{W-S2}	m	water level site S2	manually (in pipes)	1-3 days
49	d_{W-S7}	m	water level site S7	manually (in pipes)	1-3 days
50	d_{P-S1}	m	thaw depth site S1	manually (steel rod)	1-3 days
51	d_{P-S2}	m	thaw depth site S2	manually (steel rod)	1-3 days
52	d_{P-S7}	m	thaw depth site S7	manually (steel rod)	1-3 days
53	T_{air-m}	°C	air temp.	manually (temp.probe)	1-3 days
54	T_{S1-01}	°C	soil temp. site S1 1 cm	manually (temp.probe)	1-3 days
55	T_{S1-03}	°C	soil temp. site S1 3 cm	manually (temp.probe)	1-3 days
56	T_{S1-05}	°C	soil temp. site S1 5 cm	manually (temp.probe)	1-3 days
57	T_{S1-10}	°C	soil temp. site S1 10 cm	manually (temp.probe)	1-3 days
58	T_{S1-15}	°C	soil temp. site S1 15 cm	manually (temp.probe)	1-3 days
59	T_{S1-20}	°C	soil temp. site S1 20 cm	manually (temp.probe)	1-3 days
60	T_{S1-25}	°C	soil temp. site S1 25 cm	manually (temp.probe)	1-3 days
61	T_{S1-30}	°C	soil temp. site S1 30 cm	manually (temp.probe)	1-3 days
62	T_{S1-35}	°C	soil temp. site S1 35 cm	manually (temp.probe)	1-3 days
63	T_{S1-40}	°C	soil temp. site S1 40 cm	manually (temp.probe)	1-3 days
64	T_{S1-45}	°C	soil temp. site S1 45 cm	manually (temp.probe)	1-3 days
65	T_{S1-P}	°C	soil temp. site S1 permafrost table	manually (temp.probe)	1-3 days
66	T_{S2-01}	°C	soil temp. site S2 1 cm	manually (temp.probe)	1-3 days
67	T_{S2-03}	°C	soil temp. site S2 3 cm	manually (temp.probe)	1-3 days
68	T_{S2-05}	°C	soil temp. site S2 5 cm	manually (temp.probe)	1-3 days
69	T_{S2-10}	°C	soil temp. site S2 10 cm	manually (temp.probe)	1-3 days
70	T_{S2-15}	°C	soil temp. site S2 15 cm	manually (temp.probe)	1-3 days
71	T_{S2-20}	°C	soil temp. site S2 20 cm	manually (temp.probe)	1-3 days
72	T_{S2-25}	°C	soil temp. site S2 25 cm	manually (temp.probe)	1-3 days
73	T_{S2-30}	°C	soil temp. site S2 30 cm	manually (temp.probe)	1-3 days
74	T_{S2-35}	°C	soil temp. site S2 35 cm	manually (temp.probe)	1-3 days

Appendix 3-1. continuation

75	T_{S2-40}	°C	soil temp. site S2 40 cm	manually (temp.probe)	1-3 days
76	T_{S2-45}	°C	soil temp. site S2 45 cm	manually (temp.probe)	1-3 days
77	T_{S2-P}	°C	soil temp. site S2 permafrost table	manually (temp.probe)	1-3 days
78	T_{S7-01}	°C	soil temp. site S7 1 cm	manually (temp.probe)	1-3 days
79	T_{S7-03}	°C	soil temp. site S7 3 cm	manually (temp.probe)	1-3 days
80	T_{S7-05}	°C	soil temp. site S7 5 cm	manually (temp.probe)	1-3 days
81	T_{S7-10}	°C	soil temp. site S7 10 cm	manually (temp.probe)	1-3 days
82	T_{S7-15}	°C	soil temp. site S7 15 cm	manually (temp.probe)	1-3 days
83	T_{S7-20}	°C	soil temp. site S7 20 cm	manually (temp.probe)	1-3 days
84	T_{S7-25}	°C	soil temp. site S7 25 cm	manually (temp.probe)	1-3 days
85	T_{S7-30}	°C	soil temp. site S7 30 cm	manually (temp.probe)	1-3 days
86	T_{S7-35}	°C	soil temp. site S7 35 cm	manually (temp.probe)	1-3 days
87	T_{S7-40}	°C	soil temp. site S7 40 cm	manually (temp.probe)	1-3 days
88	T_{S7-45}	°C	soil temp. site S7 45 cm	manually (temp.probe)	1-3 days
89	T_{S7-50}	°C	soil temp. site S7 50 cm	manually (temp.probe)	1-3 days
90	T_{S7-55}	°C	soil temp. site S7 55 cm	manually (temp.probe)	1-3 days
91	T_{S7-60}	°C	soil temp. site S7 60 cm	manually (temp.probe)	1-3 days
92	T_{S7-P}	°C	soil temp. site S7 permafrost table	manually (temp.probe)	1-3 days
Chamber Measurements					
93	F_{CH_4-S1}	$\mu\text{g s}^{-1} \text{m}^{-2}$	CH ₄ flux chamber S1	manually + GC	1-3 days
94	F_{CH_4-S2}	$\mu\text{g s}^{-1} \text{m}^{-2}$	CH ₄ flux chamber S2	manually + GC	1-3 days
95	F_{CH_4-S7}	$\mu\text{g s}^{-1} \text{m}^{-2}$	CH ₄ flux chamber S7	manually + GC	1-3 days

Appendix 3-2. Variables derived from calculations within the micrometeorological campaign Samoylov, 2003.

ID	symbol	unit	description	calculation
101	Q_s^*	$W m^{-2}$	net radiation	$= SW_{up} + LW_{up} - SW_{dn} - LW_{dn}$
102	a	rel. value	albedo	$= \frac{SW_{dn}}{SW_{up}}$
103	T_{Sur}	$^{\circ}C$	surface radiative temperature	$\left(\frac{LW_{dw}}{\epsilon \cdot 5.67 \cdot 10^{-8}} \right)^{1/4}$
104	α	$^{\circ}$	1. rotation angle	$= \arctan \frac{\overline{v_0}}{\overline{u_0}}$
105	β	$^{\circ}$	2. rotation angle	$= \arctan \frac{\overline{w_0}}{\sqrt{\overline{u_0}^2 + \overline{v_0}^2}}$
106	u_2		u wind component rotated α, β	$= \overline{u_0} \cdot \cos \alpha \cdot \cos \beta + \overline{v_0} \cdot \sin \alpha \cdot \cos \beta + \overline{w_0} \cdot \sin \beta$
107	v_2		v wind component rotated α, β	$= -\overline{u_0} \cdot \sin \alpha + \overline{v_0} \cdot \cos \alpha$
108	w_2		w wind component rotated α, β	$= -\overline{u_0} \cdot \cos \alpha \cdot \sin \beta - \overline{v_0} \cdot \sin \alpha \cdot \sin \beta + \overline{w_0} \cdot \cos \beta$
109	γ	$^{\circ}$	3. rotation angle	$= \frac{1}{2} \cdot \arctan \frac{2 \cdot \overline{u_2} \cdot \overline{w_2}}{\overline{v_2} \cdot \overline{v_2} - \overline{w_2} \cdot \overline{w_2}}$
110	u_3	$m s^{-1}$	u wind component rotated α, β, γ	$= \overline{u_2}$
111	v_3	$m s^{-1}$	v wind component rotated α, β, γ	$= -\overline{v_2} \cdot \cos \gamma + \overline{w_2} \cdot \sin \gamma$
112	w_3	$m s^{-1}$	w wind component rotated α, β, γ	$= -\overline{v_2} \cdot \sin \gamma + \overline{w_2} \cdot \cos \gamma$
113	U	$m s^{-1}$	mean wind speed	$= \frac{1}{n} \cdot \sum_{k=1}^n \overline{u_3}$
114	U_{pr}	$m s^{-1}$	mean wind speed logarhythmic wind profile	$= \frac{U}{1 - e^{-U \cdot \kappa / u_*}} - \frac{u_*}{\kappa}$

Appendix 3-2. continuation

115	WD	°	wind direction	$\begin{cases} \arctan(v_0 / -u_0) & u \neq 0 \\ 90 & u = 0, v > 0 \\ 270 & u = 0, v < 0 \end{cases}$
116	d	m	zero-displacement height	$= \frac{2}{3} \cdot h_c$
117	z_0	m	roughness length	$= \frac{(z_m - d)}{e^{u^*/u_s}}$
118	z_{0m}	m	estimated roughness length for momentum transfer	$= 0.123 \cdot h_c$
119	z_{0h}	m	estimated roughness length for heat transfer	$= 0.1 \cdot z_{0m}$
120	r_{a1}	$s \cdot m^{-1}$	aerodynamic resistance estimated from u and u^*	$= \frac{U}{u_*^2} + \frac{4}{u_*}$
121	r_{a2}	$s \cdot m^{-1}$	aerodynamic resistance estimated from h_c	$= \frac{\ln\left(\frac{z_m - d}{z_{0m}}\right) \cdot \ln\left(\frac{z_h - d}{z_{0h}}\right)}{\kappa^2 \cdot u}$
122	λ	$J \cdot g^{-1}$	latent heat of evaporation	$= 2500.25 - 2.365 \cdot \frac{240.97 \cdot \ln \frac{e_s}{6.1121}}{17.502 - \ln \frac{e_s}{6.1121}}$
123	ρ_{air}	$g \cdot m^{-3}$	density of air (moist) at constant pressure	$= \frac{29.002 \cdot p \cdot (1 - 0.378 \cdot \frac{RH}{100} \cdot e_s)}{R \cdot (T_{air} + 273.16)}$
124	ρ_{ad}	$g \cdot m^{-3}$	density of dry air	$= \frac{29.002 \cdot p \cdot (1 - C_{H2O})}{R \cdot (T_{air} + 273.16)}$
125	ρ_{H2O}	$g \cdot m^{-3}$	density of H ₂ O	$= \frac{18.01 \cdot C_{H2O} \cdot p}{R \cdot (T_{air} + 273.16)}$
126	ρ_{CO2}	$g \cdot m^{-3}$	density of CO ₂	$= \frac{44.01 \cdot C_{CO2} \cdot p}{R \cdot (T_{air} + 273.16)}$
127	ρ_{CH4}	$g \cdot m^{-3}$	density of CH ₄	$= \frac{16.043 \cdot C_{CH4} \cdot p}{R \cdot (T_{air} + 273.16)}$
128	C_{ad}	$J \cdot g^{-1} \cdot K^{-1}$	heat capacity of dry air	$= 1.005 + \frac{(T + 23.12)^2}{3364000}$

Appendix 3-2. continuation

129	C_v	$J g^{-1} K^{-1}$	heat capacity of water vapour in air	$= 1.859 + 0.00013 \cdot RH$ $+ T_{air} \cdot (0.000193 + 0.00000569 \cdot RH)$ $+ T_{air}^2 \cdot (0.000001 + 0.00000005 \cdot RH)$
130	ρ_{si}	$K^{-1} m^{-2}$	psychrometric constant	$= \frac{C_{ad} \cdot p}{0.622 \cdot \lambda}$
131	e_s	Pa	saturation vapour pressure	$= 611.21 \cdot e^{\frac{17.502 \cdot T_{air}}{T_{air} + 240.97}}$ $\cdot (1.00072 + \frac{p \cdot (3.2 + 0.00059 \cdot T_{air}^2)}{100000000})$
132	Δ		slope of saturation vapour pressure	$= \frac{2577750 \cdot e^{17.502 \cdot T_{air} / (240.97 + T_{air})}}{(240.97 + T_{air})^2}$
133	VPD	Pa	vapour pressure deficit	$= e_s \cdot \left(1 - \frac{RH}{100}\right)$
134	u^*	$m s^{-1}$	friction velocity	$= \sqrt{ u' \cdot w' }$
135	Q_H	$W m^{-2}$	sensible heat flux	$= (\rho_{ad} \cdot C_{ad} + \rho_{H_2O} \cdot C_v) \cdot \overline{T_{son}} \cdot w'$
136	Q_E	$W m^{-2}$	latent heat flux	$= \lambda \cdot \overline{\rho_{H_2O}} \cdot w'$
137	ET	$g s^{-1} m^{-2}$	H ₂ O flux	$= \overline{\rho_{H_2O}} \cdot w'$
138	F_{CO_2}	$g s^{-1} m^{-2}$	CO ₂ flux	$= \overline{\rho_{CO_2}} \cdot w'$
139	F_{CH_4}	$g s^{-1} m^{-2}$	CH ₄ flux	$= \overline{\rho_{CH_4}} \cdot w'$
140	b	-	Bowen ratio	$= \frac{Q_H}{Q_E}$
141	ΔQ_{air}	$W m^{-2}$	heat storage in air column	$= (\rho_{ad} \cdot C_{ad} + \rho_{H_2O} \cdot C_v) \cdot \frac{dT}{dt} \cdot z_m$
142	$stab$	-	Monin-Obukhov stability parameter	$= \frac{-\kappa \cdot (z_m - d) \cdot g \cdot Q_H}{(\overline{T_{son}} + 273.16) \cdot (\rho_{ad} \cdot C_{ad} + \rho_{H_2O} \cdot C_v) \cdot u_*^3}$
143	ξ	m	Schuepp-Parameter	$= \frac{U_{pr} \cdot (z_m - d)}{\kappa \cdot u_*} \cdot (1 - 16 \cdot stab)$
144	x_{max}	m	maximum of Schuepp footprint function	$= \frac{\xi}{2}$

Appendix 3-2. continuation

145	$foot90$	m	distance of 90% Schuepp footprint	$= \xi \cdot 9.49122$
146	ET_{PM}	g s ⁻¹ m ⁻²	evapotranspiration estimated by the Penman-Monteith equation	$= \frac{1}{\lambda} \cdot \frac{\Delta \cdot (Q_s^* - Q_G) + \frac{\rho_{air} \cdot C_{ad}}{r_a} \cdot VPD}{\Delta + psi \cdot \left(1 + \frac{r_s}{r_a}\right)}$
147	r_s	s m ⁻¹	surface bulk resistance	$= \frac{VPD \cdot \rho_{air} \cdot 0.622}{ET \cdot p} + r_a \cdot \left(\frac{\Delta \cdot (Q_s^* - Q_G)}{psi \cdot \lambda \cdot ET} - \frac{\Delta}{psi} - 1 \right)$
148	ET_{PT}	g s ⁻¹ m ⁻²	evapotranspiration estimated by the Priestly Taylor equation	$= \alpha_{PT} \cdot \frac{\Delta}{\Delta + psi} \cdot (Q_s^* - Q_G)$
149	H_{PM}	W m ⁻²	sensible heat flux estimated by the Penman-Monteith model	$= a_c + b_c \left(\frac{(Q_s^* - Q_G) \cdot (r_a + r_s) - \frac{\rho_{air} \cdot C_{ad}}{psi} \cdot VPD}{\left(1 + \frac{\Delta}{psi}\right) \cdot r_a + r_s} \right)$
150	ΔQ_S	W m ⁻²	change of heat storage in the top soil consisting of i soil layers of thickness Δz_i	$= \sum_{i=1}^n C_{Si} \cdot \frac{dT_{Si}}{dt} \cdot \Delta z_i$
151	C_{Si}	J m ⁻³ K ⁻¹	heat capacity of soil layer i	$= C_{min} \cdot x_{mini} + C_{org} \cdot x_{orgi} + C_w \cdot x_{wi} + C_f \cdot x_{fi} + C_a \cdot x_{ai}$

Appendix 3-3. Constants required in calculations

152	κ	-	Karmann's constant	= 0.4
153	g	m s^{-2}	acceleration of gravity	= 9.81
154	R	$\text{J K}^{-1} \text{mol}^{-1}$	gas constant	= 8.3143
155	C_{min}	$\text{J m}^{-3} \text{K}^{-1}$	heat capacity of mineral soil material	= $1.9 \cdot 10^6$
156	C_{org}	$\text{J m}^{-3} \text{K}^{-1}$	heat capacity of organic soil material	= $2.5 \cdot 10^6$
157	C_w	$\text{J m}^{-3} \text{K}^{-1}$	heat capacity of water	= $4.2 \cdot 10^6$
158	C_i	$\text{J m}^{-3} \text{K}^{-1}$	heat capacity of ice	= $1.9 \cdot 10^6$
159	C_a	$\text{J m}^{-3} \text{K}^{-1}$	heat capacity of air	= $1.2 \cdot 10^3$
160	α_{PT}	-	Priestly-Taylor parameter, estimated	= 0.9
161	r_{se}	s m^{-1}	surface bulk resistance, estimated	= 101
162	a_c	W m^{-2}	canopy intercept coefficient heat flux estimation by Monteith-Unsworth approach	= 0.64
163	b_c	-	canopy slope coefficient heat flux estimation by Monteith-Unsworth approach	= 0.84
163	ε	-	emissivity of tundra soil, estimated	= 0.98

Appendix 3-4. List of samples for methane emission and microbial methane production studies

Numbers	Samples	Further Analyses
LD03 7048-7052	soil samples, soil extracts	geochemical ¹ , microbiological ² , DOC*
LD03 7053-7057	soil samples, soil extracts	geochemical, microbiological, DOC
LD03 7058-7063	soil samples, soil extracts	geochemical, microbiological, DOC
LD03 7064-7075	soil samples, soil extracts	geochemical, microbiological, DOC
LD03 7076-7083	soil samples, soil extracts	geochemical, microbiological, DOC
LD03 7084-7091	soil samples, soil extracts	geochemical, microbiological, DOC

¹geochemical analyses: e.g. carbon and nitrogen, Fe and Mn, cations, pH

²microbiological analyses: e.g. potential CH₄ production activity, fluorescence *in situ* hybridisation, phospholipid analysis, enrichment and characterization of microbes

*DOC = dissolved organic carbon

Appendix 3-5. List of soil samples for methane oxidation studies

no.	sample ID	date	description	Depth [cm]	planned analyses
1	LD03-3001	28.07.2004	polygon border, W 1	0-6	microbiological, biochemical
2	LD03-3002	28.07.2004	polygon border, W 1	6-10	microbiological, biochemical
3	LD03-3003	28.07.2004	polygon border, W 1	10-14	microbiological, biochemical
4	LD03-3004	28.07.2004	polygon border, W 1	14-17	microbiological, biochemical
5	LD03-3005	28.07.2004	polygon border, W 1	17-21	microbiological, biochemical
6	LD03-3006	29.07.2004	polygon centre, C 1	0-5	microbiological, biochemical
7	LD03-3007	29.07.2004	polygon centre, C 1	5-10	microbiological, biochemical
8	LD03-3008	29.07.2004	polygon centre, C 1	10-15	microbiological, biochemical
9	LD03-3009	29.07.2004	polygon centre, C 1	15-20	microbiological, biochemical
10	LD03-3010	29.07.2004	polygon centre, C 1	20-25	microbiological, biochemical
11	LD03-3011	29.07.2004	polygon centre, C 1	25-29	microbiological, biochemical
12	LD03-3012	31.07.2004	polygon border, W 2	0-4	biochemical
13	LD03-3013	31.07.2004	polygon border, W 2	4-10	biochemical
14	LD03-3014	31.07.2004	polygon border, W 2	10-15	biochemical
15	LD03-3015	31.07.2004	polygon border, W 2	15-20	biochemical
16	LD03-3016	31.07.2004	polygon border, W 2	20-25	biochemical
17	LD03-3017	31.07.2004	polygon border, W 2	25-30	biochemical
18	LD03-3018	31.07.2004	polygon border, W 2	30-35	biochemical
19	LD03-3019	31.07.2004	polygon centre, C 2	0-5	biochemical
20	LD03-3020	31.07.2004	polygon centre, C 2	5-10	biochemical
21	LD03-3021	31.07.2004	polygon centre, C 2	10-15	biochemical
22	LD03-3022	31.07.2004	polygon centre, C 2	15-20	biochemical
23	LD03-3023	31.07.2004	polygon centre, C 2	20-25	biochemical
24	LD03-3024	31.07.2004	polygon centre, C 2	25-30	biochemical
25	LD03-3025	31.07.2004	polygon centre, C 2	30-35	biochemical
26	LD03-3026	31.07.2004	polygon border, W 3	0-5	biochemical
27	LD03-3027	31.07.2004	polygon border, W 3	5-11	biochemical
28	LD03-3028	31.07.2004	polygon border, W 3	11-16	biochemical
29	LD03-3029	31.07.2004	polygon border, W 3	16-21	biochemical
30	LD03-3030	31.07.2004	polygon border, W 3	21-26	biochemical
31	LD03-3031	31.07.2004	polygon centre, C 3	0-6	biochemical
32	LD03-3032	31.07.2004	polygon centre, C 3	6-13	biochemical
33	LD03-3033	31.07.2004	polygon centre, C 3	13-18	biochemical
34	LD03-3034	31.07.2004	polygon centre, C 3	18-23	biochemical
35	LD03-3035	31.07.2004	polygon centre, C 3	23-27	biochemical
36	LD03-3036	31.07.2004	polygon centre, C 3	27-33	biochemical
37	LD03-3037	30.08.2004	polygon border, W 1	0-6	pedological, microbiological, molecularbiological, biochemical
38	LD03-3038	30.08.2004	polygon border, W 1	6-11	pedological, microbiological, molecularbiological, biochemical
39	LD03-3039	30.08.2004	polygon border, W 1	11-15	pedological, microbiological, molecularbiological, biochemical
40	LD03-3040	30.08.2004	polygon border, W 1	15-16	pedological, microbiological, molecularbiological, biochemical

Appendix 3-5. Continuation

no.	sample ID	date	description	Depth [cm]	planned analyses
41	LD03-3041	30.08.2004	polygon border, W 1	16-21	pedological, microbiological, molecularbiological, biochemical
42	LD03-3042	30.08.2004	polygon border, W 1	21-26	pedological, microbiological, molecularbiological, biochemical
43	LD03-3043	30.08.2004	polygon border, W 1	26-32	pedological, microbiological, molecularbiological, biochemical
44	LD03-3044	30.08.2004	polygon centre, C 1	0-4	pedological, microbiological, molecularbiological, biochemical
45	LD03-3045	30.08.2004	polygon centre, C 1	4-9	pedological, microbiological, molecularbiological, biochemical
46	LD03-3046	30.08.2004	polygon centre, C 1	9-14	pedological, microbiological, molecularbiological, biochemical
47	LD03-3047	30.08.2004	polygon centre, C 1	14-19	pedological, microbiological, molecularbiological, biochemical
48	LD03-3048	30.08.2004	polygon centre, C 1	19-24	pedological, microbiological, molecularbiological, biochemical
49	LD03-3049	30.08.2004	polygon centre, C 1	24-29	pedological, microbiological, molecularbiological, biochemical
50	LD03-3050	30.08.2004	polygon centre, C 1	29-34	pedological, microbiological, molecularbiological, biochemical
51	LD03-3051	30.08.2004	polygon centre, C 1	34-43	pedological, microbiological, molecularbiological, biochemical
52	LD03-3052	30.08.2004	polygon centre, C 2	0-3	biochemical
53	LD03-3053	30.08.2004	polygon centre, C 2	3-8	biochemical

3.10 References

- Abramova E.N. (2003): Species composition, ecology, population structure and seasonal dynamic of zooplankton from tundra water basins in the Lena Delta. In: Russian-German Cooperation SYSTEM LAPTEV SEA: the expedition LENA 2002. Ed. M.N. Grigoriev et al., Reports on Polar and Marine research, 466: 93-100.
- Abramova, E.N. (2000): Pelagic invertebrate fauna of the Laptev Sea shelf waters. Abstract of Ph.D. Thesis, biological sciences. St. Petersburg, pp. 1-24 (in Russian).
- Akhmetshina, I., Abramova, E. (2002): Zooplankton abundance, biomass and production in the Lena Delta polygon lakes: preliminary results. *Climate Driver of the North*, Kiel, May 8-11, Terra Nostra 2002/3: 20.
- Anisimov, O.A., A.A. Velichko, P.F. Demchenko, A.V. Eliseev, I.I. Mokhov, and V.P. Nechaev (2002): Effect of climate change on permafrost in the past, present, and future, *Izvestiya, Atmospheric and Oceanic Physics*, 38(1): 25-39.
- Are, F.E. and E. Reimnitz (2000): An overview of the Lena River Delta setting: geology, tectonics, geomorphology, and hydrology, *Journal of Coastal Research*, 16(4): 1083-1093.
- Chapin, F.S. III, R.L. Jeffries, J.F. Reynolds, G.R. Shaver, and J. Svoboda (1992): *Arctic Ecosystems in a Changing Climate: an Ecophysiological Perspective*, Academic Press, San Diego, USA. 469 pp.
- Christensen, T. R., S. Jonasson, T. V. Callaghan, and M. Havström (1995): Spatial variation in high-latitude methane flux along a transect across Siberian and European tundra environments. *J. Geophys. Res.*, 100, pp. 21035-21045.
- Frenzel, P. and Rudolph, J. (1998): Methane emission from a wetland plant: the role of CH₄ oxidation in *Eriophorum*, *Plant and Soil*, 202: 27-32.
- Gorham, E. (1991): Northern peatlands: role in the carbon cycle and probable responses to climatic warming, *Ecological Applications*, 1: 182-195.
- Grigoriev, M.N. (1993): Cryomorphogenesis of the Lena River mouth. Permafrost Institute Press, Yakutsk 176 pp. (in Russian).
- Grigoriev, M.N. and V. Rachold, V. (?2004?): The degradation of coastal permafrost and the organic carbon balance of the Laptev and East Siberian Seas, in *Proceedings of the 8th International Conference on Permafrost. Zürich (Switzerland), 21-25 July 2003*. pp. 319-324.
- Grigoriev, N.F. (1960): The temperature of permafrost in the Lena delta basin – deposit conditions and properties of the permafrost in Yakutia, *Yakutsk*, 2, 97-101 (in Russian).
- Gukov, A.Yu. (2001): *Hydrobiology of the Lena River mouth region*. M., Nauchnyi mir. 285 pp. (in Russian).
- Harris, R., K. Bartlett, S. Frolking, and P. Crill (1993): Methane emissions from northern high-latitude wetlands. In: Oremland, R. S. (ed.): *Biogeochemistry of Global Change*. New York: Chapman and Hall, pp. 449-485.
- Hydrometeorological Centre of Russia (2004): *Russia's Weather*, <http://meteo.infospace.ru>
- Kattenberg, A., F. Giorgi, H. Grassl, G.A. Meehl, J.F.B. Mitchell, R.J. Stouffer, T. Kokioka, A.J. Weaver, and T.M.L. Wigley (1996): Climate models: projections of future climate, In: J.T. Houghton et al. (eds.): *Climate Change 1995: The Science of Climate Change. Contribution of Working Group I to the Second Assessment Report of the Intergovernmental Panel on Climate Change*, pp. 285-357, Cambridge University Press, Cambridge, New York, NY, USA
- Kutzbach, L., C. Wille, and E.-M. Pfeiffer (2003a): Heat, water and carbon exchange between arctic tundra and the atmospheric boundary layer – the eddy covariance method, In: M.N. Grigoriev et al. (eds.): *Russian-German Cooperation SYSTEM LAPTEV SEA, The Expedition LENA 2002, Reports on Polar Research* 466: 8-16.
- Kutzbach, L., E.N. Abramova, and W. Schneider (2003b): Seasonal progression of thaw depth dependent on microrelief, In: M.N. Grigoriev et al. (eds.): *Russian-German Cooperation SYSTEM LAPTEV SEA, The Expedition LENA 2002, Reports on Polar Research* 466: 49-50.

- Maxwell, B. (1997): Recent climate patterns in the Arctic, in *Global Change and Arctic Terrestrial Ecosystems*, edited by Oechel et al., pp. 21-46, Springer, New York, NY, USA
- Moosavi, S.C. and Crill, P.M. (1998): CH₄ oxidation by tundra wetlands as measured by a selective inhibitor technique. *J. Geophys. Res.* 103 (D22): 29093-29106.
- Mostakhov, C.E. (1973): Lakes in the cryolithozone of the USSR. Ground waters of the cryolithozone. 2nd International Conference on Permafrost Studies. Yakutsk, vol. 5: 118-120. (in Russian).
- Nelson, F.E., K.M. Hinkel, N.I. Shiklomanov, G.R. Mueller, L.L. Miller, and D.A. Walker (1998): Active-layer thickness in north central Alaska: Systematic sampling, scale, and spatial autocorrelation, *J. Geophys. Res.*, 103 (D22): 28963-28973.
- Oechel, W.C., S.J. Hastings, G.L. Vourlitis, M. Jenkins, G. Riechers, and N. Grulke (1993): Recent Change of Arctic ecosystems from a net carbon dioxide sink to a source, *Nature*, 361: 520-523.
- Osterkamp, T.E. and V.E. Romanovsky (1999), Evidence for warming and thawing of discontinuous permafrost in Alaska, *Permafrost and Periglacial Processes*, 10, 17-37
- Pfeiffer, E.-M., Akhmadeeva, I., Becker, H., Friedrich, K., Wagner, D., Quass, W., Zhurbenko, M., Zöllner, E., Boike, J. (1999): Modern Processes in Permafrost Affected Soils. In: Rachold, V. and Grigoriev, M.N. (ed.) *Expeditions in Siberia 1998. Reports on Polar Research* 315:19-80.
- Pfeiffer, E.-M., D. Wagner, H. Becker, A. Vlasenko, L. Kutzbach, J. Boike, W. Quass, W. Kloss, B. Schulz, A. Kurchatova, V.I. Pozdnyakov, and I. Akhmadeeva (2000): Modern processes in permafrost affected soils, in *Expeditions in Siberia in 1999, Reports on Polar Research* 354, edited by V. Rachold, pp. 22-54, Alfred Wegener Institute, Bremerhaven, Germany
- Pfeiffer, E.-M., D. Wagner, S. Kobabe, L. Kutzbach, A. Kurchatova, G. Stoof, and C. Wille (2002): Modern processes in permafrost affected soils, In: E.M. Pfeiffer and M.N. Grigoriev (eds.): *Russian-German Cooperation SYSTEM LAPTEV SEA, The Expedition LENA 2001, Reports on Polar and Marine Research*, 426. 21-41.
- Popp, T.J., Chanton, J.P., Whiting, G.J. and Grant, N. (2000): Evaluation of methane oxidation in the rhizosphere of a *Carex* dominated fen in north central Alberta, Canada. *Biogeochemistry* 51: 259-281.
- Post, W.M.; Emanuel, W.R.; Zinke, P.J. & Stangenberger, A.G. (1982): Soil carbon pools and world life zones. *Nature* 298: 156-159.
- Roulet, N.T., T.R. Moore, J.L. Bubier, and P. Lafleur (1992): Northern fens: methane flux and climatic change, *Tellus*, 44B: 100-105.
- Schwamborn, G., V. Rachold, and M.N. Grigoriev (2002): Late quaternary sedimentation history of the Lena Delta, *Quaternary International*, 89: 119-134.
- Spott, O. (2003): Frostmusterbedingte Seen der Polygonalen Tundra und ihre Funktion als Quellen atmosphärischen Methans. Diploma thesis, University of Leipzig. 125pp. (in German).
- Wagner, D., Kobabe, S., Pfeiffer, E.-M. and Hubberten, H.-W. (2003b): Microbial controls on methane fluxes from a polygonal tundra of the Lena Delta, Siberia. *Permafrost Periglacial Processes*, 14: 173-185.
- Wagner, D., L. Kutzbach, C. Wille, S. Kobabe, O. Spott, A. Kurchatova, M.N. Grigoriev, G. Stoof, W. Schneider, E.N. Abramova, H. Meyer, S. Kuzmina, S. Wetterich, D. Bolshiyarov, I. Fedorova, M. Tretiakov, and E.M. Pfeiffer (2003): Ecological studies on permafrost soils and landscapes of the central Lena Delta, in: M.N. Grigoriev et al (eds.) *Russian-German Cooperation SYSTEM LAPTEV SEA, The Expedition LENA 2002, Reports on Polar and Marine Research*, 466; 5-132.
- Wagner, D.; A. Kurchatova, and G. Stoof, and (2001): Modern processes in permafrost affected soils, in *Russian-German Cooperation SYSTEM LAPTEV SEA 2000*, In: V. Rachold and M.N. Grigoriev (eds.): *The Expedition LENA 2000, Reports on Polar Research* 388: 16-23.
- Walker, D.A., N.A. Auerbach, J.G. Bockheim, et al. (1998): Energy and trace-gas fluxes across a soil pH boundary in the Arctic, *Nature*, 394: 469-472.

- Walker, H.J. (1998): Arctic deltas, *Journal of Coastal Research*, 14(3): 718-738.
- Walker, M.D., W.A. Gould, and F.S. Chapin III (2001): Scenarios of biodiversity change in Arctic and alpine tundra, in *Scenarios of Future Biodiversity*, edited by F.S. Chapin III et al., Springer, New York, NY, USA
- Zhang, T., Barry, R.G., Knowles, K., Heginbotton, J.A. and Brown, J. (1999): Statistics and characteristics of permafrost and ground-ice distribution in the northern hemisphere. *Polar Geography*, 23: 132-154.

4. Periglacial studies around Cape Mamontov Klyk

4.1 Introduction

Lutz Schirrmeister and Mikhail Grigoriev

The field campaign to the coastal region of Cape Mamontovy Klyk belongs to the research project "Process studies of permafrost dynamics in the Laptev Sea" founded by the German Federal Ministry of Education and Research (BMBF). The studies of terrestrial permafrost environment and of the Laptev Sea coastal area are essential for the investigation of transition processes from terrestrial to submarine permafrost, which is the main objective of the project. The multidisciplinary studies of paleo-ecology, geocryology, sedimentology, pedology, geomorphology as well as hydrochemistry and isotope geochemistry of ground ice were carried out in close cooperation with Russian colleagues. This approach was successfully used during former expeditions between 1998 and 2002.

The main tasks of the field campaign were:

- Geocryological and sedimentological investigations of terrestrial permafrost sequences exposed at the Laptev Sea coast of Cape Mamontovy Klyk including sample collection of frozen ground and ground ice
- Studies of periglacial morphology and surface characterisation of the coastal lowland; ground truth studies for the interpretation of remote sensing data
- Studies of methane budget of recent tundra soils and frozen paleosols including gas sampling and soil collections
- Measurement of the coastal relief dynamics and of the sea bottom bathymetry and collection of seawater and bottom sediments
- Studies of recent soil and weather conditions including sampling of precipitation and of surface water in order to get information on the local hydrological system
- Paleontological studies of the mammal fauna and fossil collection

Twelve peoples coming from Moscow, Yakutsk, Tiksi, St. Petersburg, Hamburg and Potsdam took part in this expedition.

Dimitri Bolshianov (AARI)

Guido Grosse (AWI-P)

Alexander Dereviagin (MGU)

Hanno Meyer (AWI-P)

Mikhail Grigoriev (PIY)

Lutz Schirrmeister (AWI-P)

Victor Kunitsky (PIY)

Waldemar Schneider (AWI-P)

Tatjana Kuznetsova (MGU)

Uta Zimmermann (IfB-Hamburg)

Alexander Makarov (AARI)

Jura Tjazelukhin (Tiksi)

The various special studies and sample collections were closely connected to each other. Most of the studies carried out in summer 2003 in the area of Mamontovy Klyk provide basic results for the subsequent drilling transect from terrestrial to the submarine permafrost in front of the studied coast, planned in spring 2004. This drilling project was prepared by a reconnaissance project in spring 2003 in order to investigate the position of the submarine permafrost boundary (see chapter 4.7.1).

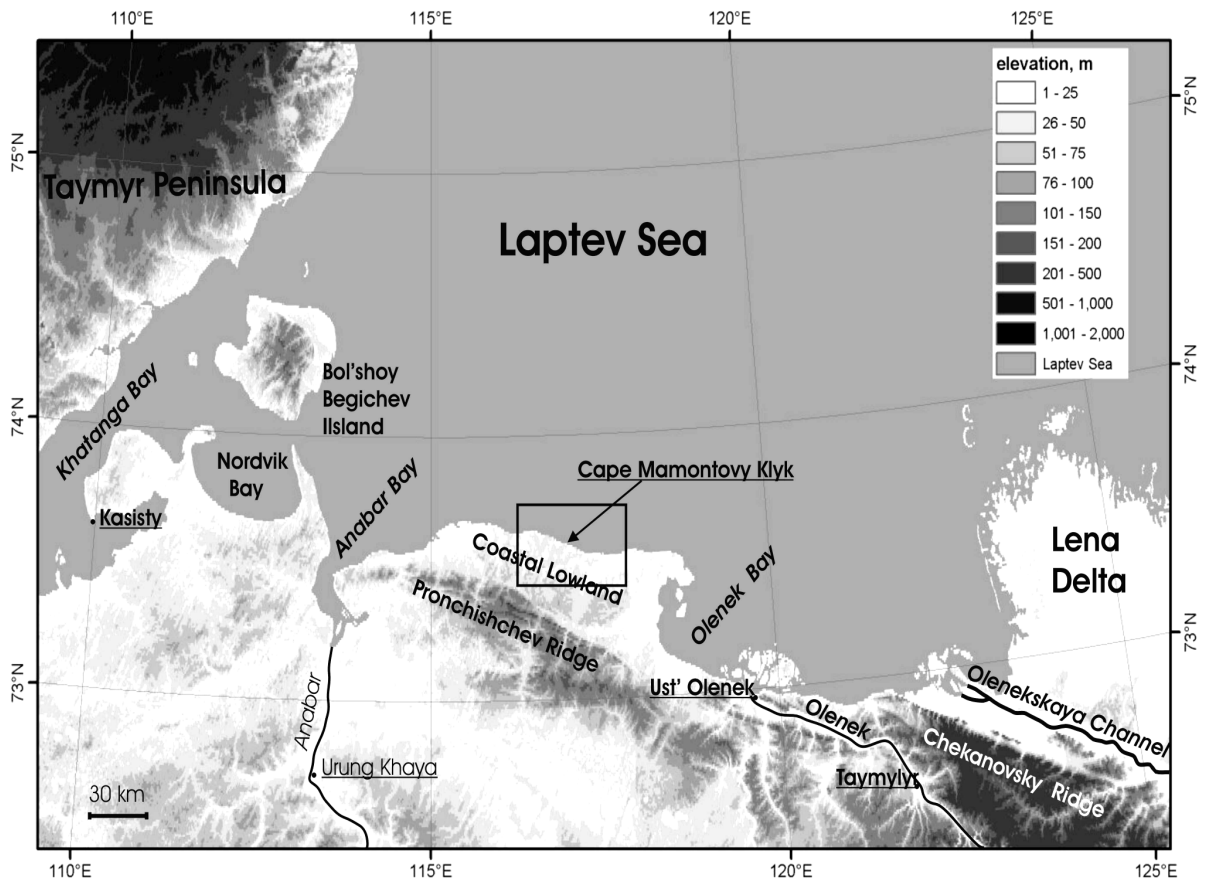


Figure 4.1-1: Position of the study area on the coast the Olenek-Anabar-interfluve in the western Laptev Sea

4.2. Geographical and geological background

Alexander Dereviagin and Viktor Kunitsky

The investigated area is located in the coastal part of the Laptev Sea between the Anabar Bay and the Olenek Bay, about of 30 km to the north of the Pronchishchev Range. The distance to Tiksi is about of 600 km (Figure 4.1-1).

The geological history of the coastal lowland is poorly understood. The Russian geologists Chekanovsky in 1874, Toll in 1894 and Tolmachev in 1905 obtained first data on geological construction of the region. Toll (1894) provided first information on nature conditions, geology and relic ground ice. According to Toll (1894) the huge relic ice bodies he observed in the costal part are defined as remains of glacier ice. He also described moraine deposits in the Anabar River valley near Cape Muus-Khaya. New and in many cases discrepant data on Quaternary geology of the lowland was obtained due to several stages of geological survey conducted later in the 20th century. Ice-rich silty sand deposits exposed in the coastal part of the lowland were considered as marine sediments (Sochava, 1933, Zhukov et. al., 1968), fluvio-glacial and fluvial-lacustrine deposits (Puminov, 1962), cryogenic-aeolian and fluvial-lacustrine deposits (Kolpakov, 1973). These investigations are usually based on the well-known stratigraphical scheme of Saks (1963) for the Russian North. Boyarsky and Mitt (1961) defined ice bodies in ice-rich sediments in the coastal outcrops, as huge syngenetic ice wedges.

The coastal lowland is a gently sloping hilly plain with elevations of about 25-35 m above sea level (a.s.l.). Altitudes gently increase towards the South, where a maximum height of 315 m is reached in the Pronchishchev Range in the riverhead of Urasalakh River.

Wide flat watersheds with gentle slopes and shallow valleys characterize the relief of the lowland, which is drained by several rivers like the Urasalakh and the Nuchcha Dzhihle Rivers and a net of thermoerosional valleys with steep slopes and plain bottoms. The Nuchcha Dzhihle River crosses the study area. The depth of the river valley is less than 10-20 meters. The stream course consists of meanders and a flat trough valley with a wide (300-400 m) flood plain near the mouth. The width of the river near the 2003 camp was about 5-7 m, and reached about 15-20 m at the mouth. The maximum depth of the river is more than 4 m when high tides and/or wind hamper the water discharge. The rising of the sea water level in the region is mainly caused by the varying of wind strength and orientation than by diurnal tides. In effect, irregular water level changes were observed. The maximum elevation of water level, marked by driftwood trunks and wood remains in the valleys, is about of 3 to 3.5 m a.s.l.. This corresponds in some of the wide valleys to locations several 100 m, in the Nuchcha Dzhihle even several kilometres inland. The main investigated outcrops are located at the bluff in the coastal part of the lowland. The height of the cliff formed by very ice-rich sediments varies from 10 to 25 m a.s.l.. The width of the beach during low sea level reaches up to several hundred meters.

In the eastern part of the investigated area a segment of the first (?) marine terrace was found. The elevation of the marine terrace is about of 1 to 1.5 m a.s.l. The terrace partly consists of sandy areas without plant cover and is covered by numerous small shallow lakes and wood remains.

The working area belongs to the subarctic tundra zone (Grigor'ev, 1956).

The nearest long-term weather stations locate in Ust'-Olenek, Saskylakh, Cape Kosisty, Nordvik and Cape Terpey-Tumusa respectively. Recently, there are only two long-term weather stations in this region Ust'-Olenek, Saskylakh (Figure 4.1-1; Table 4.2-1). Continental Arctic climate with long severe winters and short cold summers is typical for the region. Mean annual air temperature is about -14°C . Mean winter temperature is about -22°C , and mean summer temperature varies from $+5$ to $+10^{\circ}\text{C}$ (Table 4.2-1). There are about 230-270 mm of mean annual precipitation in the region, 75% of which precipitates in summer. In general, the snow cover is formed in the end of September and melts in the end of June. The thickness of snow cover is not more than 40-50 cm. A part of the snow is removed and redeposited by wind in dependence on wind conditions and geomorphological conditions. Southern and East-Southern wind directions are predominant in winter, and Northern and North-western wind directions are predominant in summer. Some times wind speed reaches about 25-30 m/sec.

Table 4.2-1. Climate data of surrounding weather stations

Long-term weather station	1	2	3	4	5	6	7	8	9	10	11	12	mean T an	Days, T<0 °C
Nordvik	-33,2	-31,1	-28,8	-20,5	-10,4	1,0	4,8	2,9	-0,8	-10,2	-24,2	-29,7	-15,0	240
Saskylakh	-35,5	-33,2	-28,8	-18,5	-6,9	6,9	11,7	8,0	1,3	-11,9	-27,6	-32,1	-14,0	254
Ust' Olenek	-34,3	-32,2	-29,0	-19,1	-7,6	2,1	8,1	6,6	1,2	-11,7	-25,3	-30,6	-14,3	258
Cape Terpey- Tumasa	-32,6	-32,5	-28,9	-20,8	-9,6	0,2	3,4	4,4	0,2	-11,0	-24,9	-30,3	-15,2	260
Cape Kasisty	-31,6	-31,7	-28,7	-20,2	-8,2	0,7	4,8	5,4	1,2	-8,9	-23,5	-28,4	-14,1	240

The study territory belongs to the zone of continuous permafrost reaching 400-600 m (Geocryology of the USSR, 1989). The geocryological conditions of the region and the cryolithology of the sediments are poorly known. No special geocryological investigations were conducted in the region. The mean annual ground temperature is about -11 to -12°C . The thickness of the active layer varies from 0.2 m to 0.4-0.5 m in July.

The working area is located at the Northeast part of Lena-Anabar depression in the Olenek zone of Late Mesozoic folded complex at the boundary of the Siberian Craton and the Laptev Paraplatformal Block (Drachev et al., 1998). The Lena-Anabar depression superposes to structures of the Lena-Anabar foredeep. The main structural elements of the studied territory are the Upper Cretaceous to Cenozoic onshore sedimentary cover (terrestrial and shelf parts)

and Lena-Taymyr Uplift (recent shelf part). The thickness of the Upper Cretaceous structural stage is about of 470 m. The Cenozoic structural stage is presented by the continental silty-sand molasse and reaches a thickness of about 300 m. The Pleistocene geological evolution of the territory is characterized by several stages of uplifts (early Pleistocene to middle Pleistocene; Late Pleistocene to Holocene) and subsidence's (Pliocene to Yearly Pleistocene; Middle Pleistocene to Late Pleistocene). That means the territory belongs to an active seismic zone.

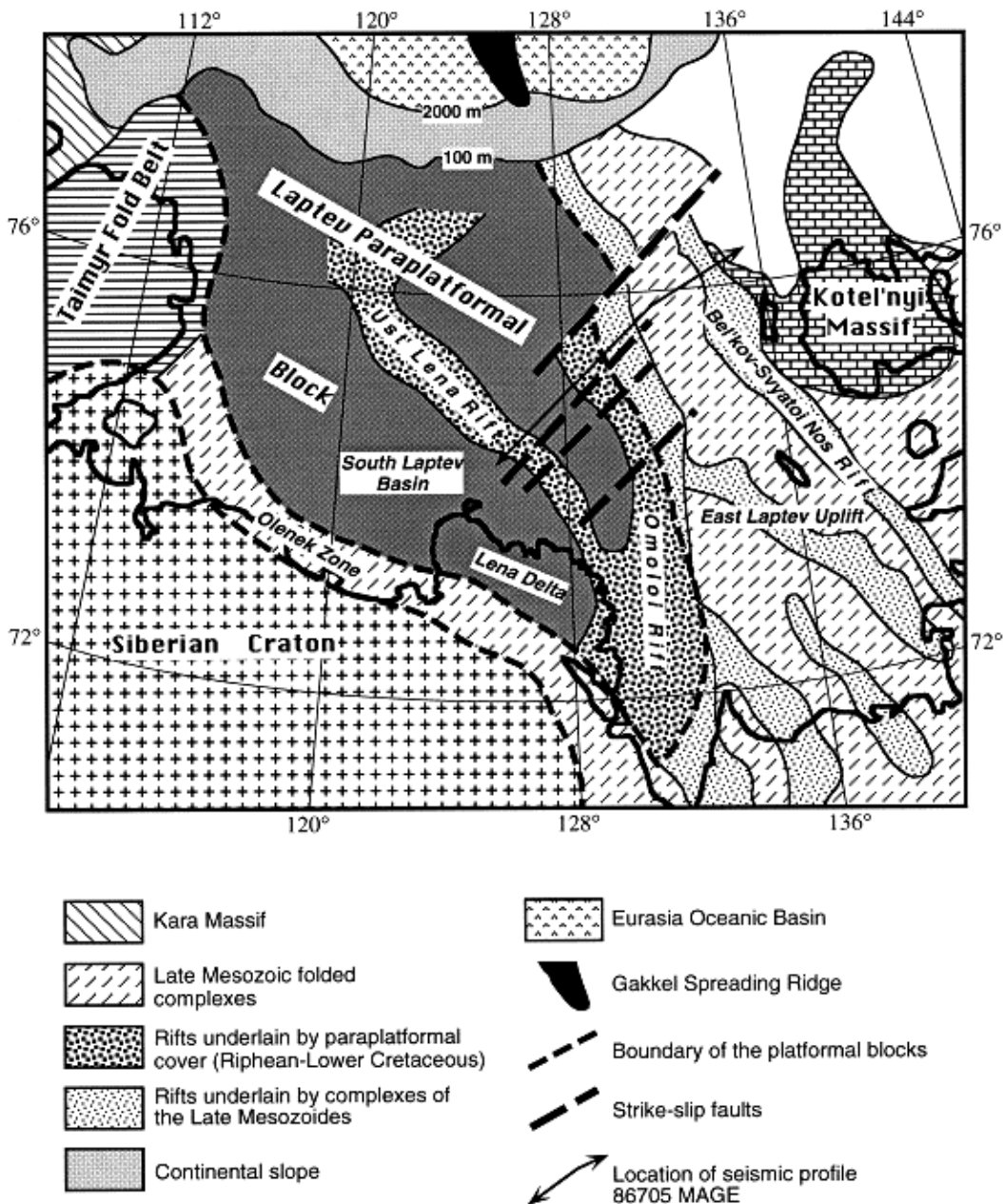


Figure 4.2-1: Tectonic zonation of the Laptev Shelf (Drachev et al. 1998)

According to Zhukov (1968) the Cenozoic sediments in the region consists of the following sequences: Late Pliocene to early Pleistocene deposits ($N_2^3 - Q_1$); middle Pleistocene to late Pleistocene non-subdivided deposits ($Q_{II} - Q_{III}^1$), including Kazantsevsky Interstadial; Late Pleistocene to Holocene non-

subdivided deposits ($Q_{III}^2 - Q_{III}^4$), including horizons of the Zyryansky Stadial, the Karginsky Interstadial and Sartansky Stadial and of the Holocene.

The Late Pliocene to early Pleistocene deposits are presented by fluvial cross bedding pebbles, gravels, badly sorted sands and silts and has local extension in the region. These deposits are partially eroded and have a specific variety of colours: orange, yellow and brown. Visible thickness is less than 10-12 m.

Middle Pleistocene to Late Pleistocene deposits are by fluvial-lacustrine fine-grained grey, yellowish-grey sands and silts with pebbles and gravels and numerous plant remains. They are characterized by lenticular, cross and ripple bedding, due to granulometric composition of sands and detritus inclusions. Peat layers are observed in the upper part of the unit. The thickness of this unit is not determined.

Late Pleistocene to Holocene deposits ($Q_{III}^2 - Q_{III}^4$) have a wide distribution in the territory and presents by very ice-rich grey, brownish-grey, and silty sediments (Ice Complex deposits). Sediments are horizontally bedded subdivided by detritus and plant remain layers, and contain fossils of mammoths. The base of Ice Complex formation is located in different heights above sea level and changes from 0 m at the North of lowland to 100 m in the Southern lowland near the Pronchishchev Range. The thickness of Ice Complex sediments is about 20-30 m.

The Holocene (Q_{IV}) consist of fluvial, thermokarst (alas, log) and marine deposits mainly defined as sand, silty-sand, peat lenses and peat layers. These sediments contain numerous plant remains.

4.3. Geomorphologic route along the Urasalakh River

Dimitri Bolshiyarov and Alexander Makarov

4.3.1 Structure of Quaternary deposits along the Urasalakh River valley

From 7 to 18 August, two investigators made a traverse from the Pronchishchev Range along the Urasalakh River to the river mouth, which is located 16 km to the west of the main camp in the vicinity of Cape Mamontov Klyk. The traverse was undertaken under the purpose to investigate the geological and geomorphologic structure of the coastal lowland between the Pronchishchev Range and the Laptev Sea. We used a rubber boat make the travel by the river.

The Pronchishchev Range in the headwaters of the Urasalakh River consists of three cuesta ridges extending from northwest to southeast. These are low mountains with heights up to 270 m formed by a monoclinical southwestward dipping strata of sandstones and siltstones and their gentle southwest slopes being concordant with the dipping of the rocks. The valleys of modern watercourses are located between the cuesta ridges. One of them is the Urasalakh River valley. The valleys between the cuesta ridges are non-terraced. Their slopes are gentle and complicated by nivation niches. The deposits at the slopes are predominantly rudaceous. The fragments are practically non-rounded.

The valleys to the north of the range cut into loose sediments of pebble-sand deposits outcropping at the foot of the hills for example at the northern slope of Lake Mentikelir East (site 1410). They are overlain by silty-sandy Ice Complex deposits containing fragments of ice veins, which are rarely exposed in the upper reaches of rivers and which are mainly detected by a thermokarst mounds relief. The coastal plain with heights up to 40-60 m a.s.l. is mainly composed of sandy-silty basin deposits. Ice Complex deposits as represented by laminated silts with a large quantity of plant detritus and ice wedges permeating them are rarely exposed in the valleys. They are observed at the eastern slope of Lake Mentikelir East (site 1401), at the east coast of Lake Tungus-Yunkyur (site 1417), in a thermokarst mound area (site 1421) – in a distance of 6 km from the Urasalakh River mouth, and in its lower reaches. Therefore, it can be concluded that typical Ice Complex deposits occur only in the coastal part of the studied area. In the upper reaches of the Urasalakh River, sand-silty deposits are only found as they underlay the Ice Complex deposits outcropping further north at the surface. These deposits are described in sections of high terraces along the Urasalakh River – sites 1415, 1418 (Figures 4.3-2, 4.3-3). In such outcrops Ice Complex deposits gradually turn to the underlying silt-sandy deposits. Sampling of sands was made for determining their age by the OSL method. Ice wedges only rarely cross the Ice Complex boundary and penetrate into the underlying sands.

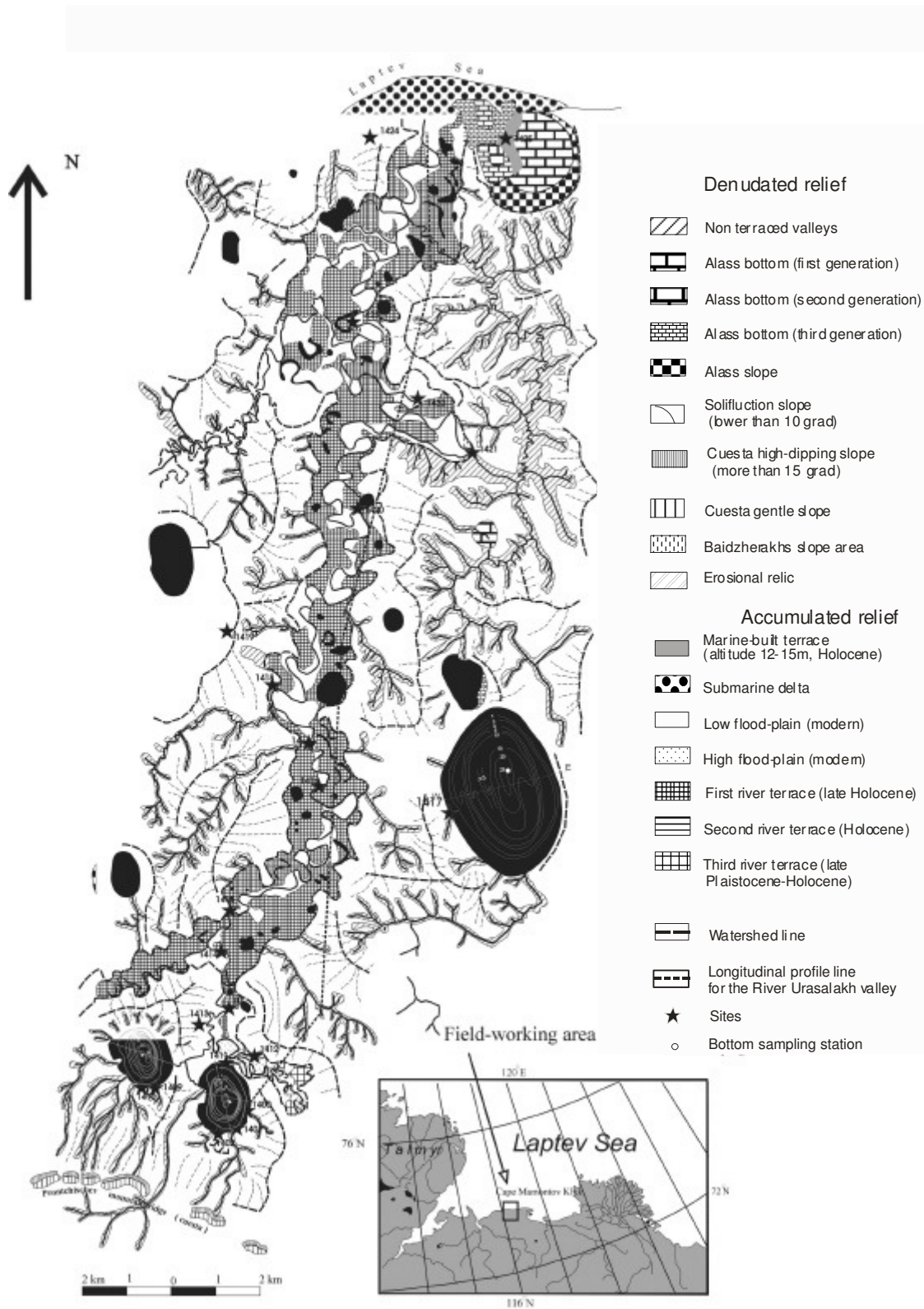


Fig.1
Figure 4.3-1: Geomorphology scheme of the Urasalakh River valley and adjacent area, south coast of the Laptev Sea.

4.3.2 Geomorphologic structure of the valley

The Urasalakh River valley extends over 20 km from the northern ridge of the Pronchishchev Range. Up to the mouth, the river freely meanders along the valley with a width of 1.2 –2 km. The channel sinuosity coefficient is 2.9.

During the traverse, the river terraces were studied conducting measurements on the height and width of the terraces and observations of their structure. This results in a longitudinal profile of the Urasalakh River valley (Figure 4.3-3). The route firstly passed along the right tributary of the Urasalakh River – the Urasalakh-Batyta River. In the main valley, low and high floodplains and three above-the-floodplain terraces are developed. In the Urasalakh-Batyta River, the low floodplain is very restricted and narrow. The floodplains are composed of alluvium. The first above-the-floodplain terrace has sometimes a basement, which consists of similar sand deposits that underlay the Ice Complex deposits near the coast. At the longitudinal profile, a straight inclined line connecting the upper point of the route with the mouth characterizes the valley bottom. Unfortunately it was impossible to measure the true bottom inclination on different river segments. However, judging by the changes of the river current speeds, the bottom profile is similarly complicated as the profile of the terraces. According to the measurements, the first terrace, which usually has a height of about 5 m on the lower segment of the valley with a length of about 2 km (between sites 1421 and 1423), rises up to 7 m to the north. Here, the river sharply goes eastward along the valley forming the most extended meander – up to 2.5 km from the general direction of the river. The ancient sandy fundament of the terrace surrounded by alluvium beds up to 1 m thickness is exposed exactly here.

In the middle reach of the river a local elevation of the second above-the-floodplain terrace was observed, which usually has a height of 10-11 m, but here, the elevation rises up to 13-14 m.

The third above-the-floodplain terrace with a height of 20-22 m is more persistent by height.

All terraces decrease in general downstream. The studies of the longitudinal profile of the terraces, which reveal their local elevation, indicate that modern block tectonic uplifts of the Earth's crust bend the terrace surface.

In the river valley, there is not only a river terrace but also a basin terrace. It was detected on the shore of the Laptev Sea where its height is 12-13 m a.s.l. Upward the valley, the terrace is traced by some relics and merges with the river valley bottom in a distance of 13-14 km from the mouth. This terrace, which was described and sampled at the site 1425, is interesting because it is located within a thermokarst depression with three various age stages of alas formation. The radiocarbon age determination of plant remains contained in the sands would be helpful to clear the age of the basin formation as well as the ages of the alas stages.

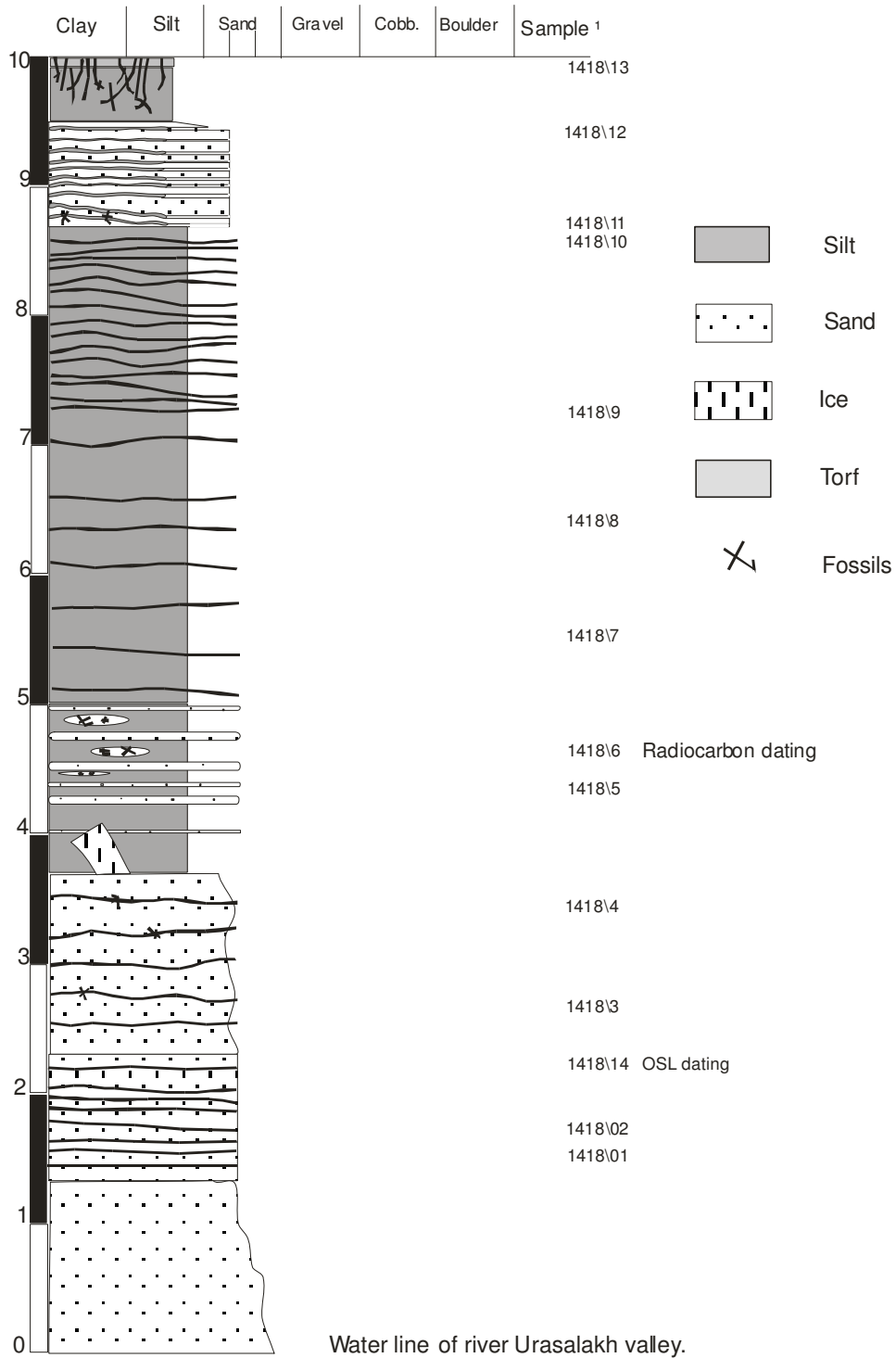


Figure 4.3-3: Profile of the exposure ¹ 1418, river Urasalakh River valley (N 73° 32,798 E 116° 23,382)

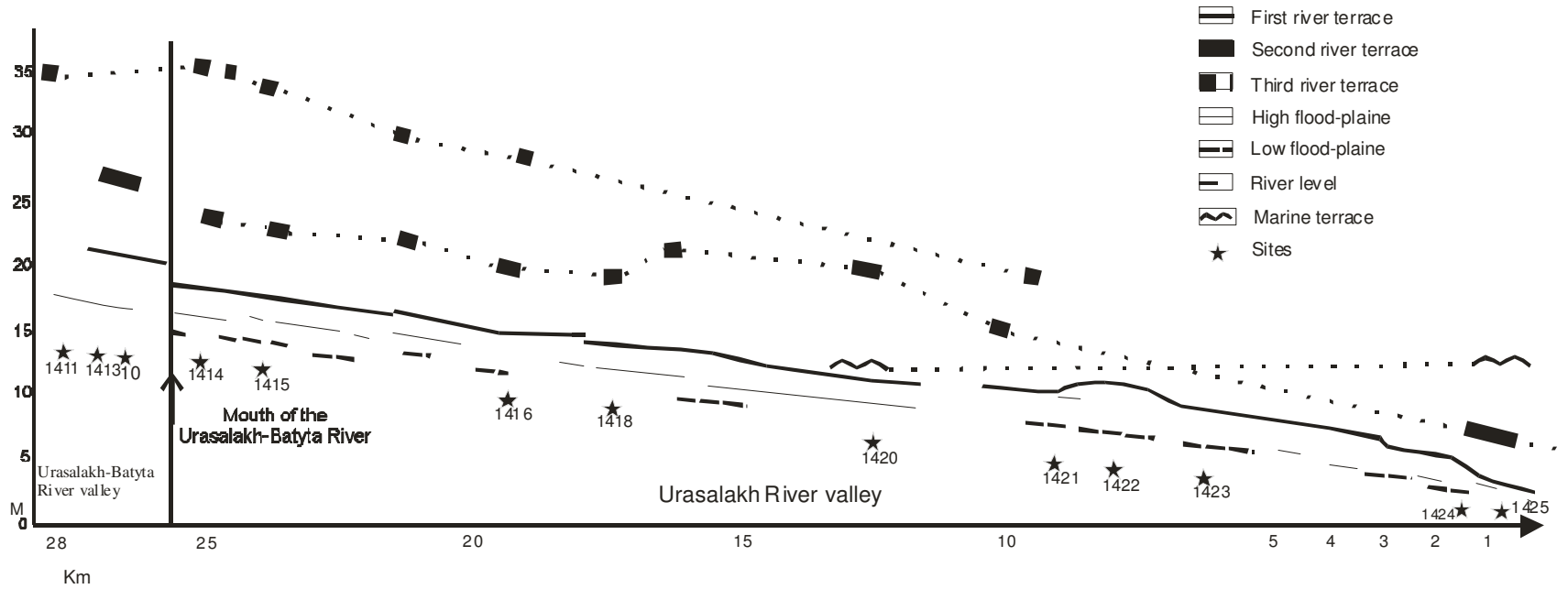


Figure 4.3-2: Gemorphological profile of the Urasalakh River valley

This basin terrace was not only revealed in the valley of the Urasalakh River, but also in other valleys of the coastal plain. In the valley of the Nucha-Dzhielyakh River where the main camp of the expedition was situated, it is well traced along the left slope of the valley having a height of 13-15 m and a width up to 500 m. There is also an extensive terrace approximately at this height in the vicinity of Cape Terpyai-Tumus, which was observed during the flight onboard of the helicopter. Thus, there are a basin terrace in the study area with a height of 13-15 m and lower marine terraces (up to 5 m) along the shore of Laptev Sea, which were also sampled for age determination of driftwood partly buried at the terrace surface.

Based on the results of en-route observations, a geomorphologic scheme of the study area was compiled, which is presented in Figure 4.3-1.

4.3.3 Studies of lakes

Two lakes near the foot of the Pronchishchev Range have been studied: their long axes from NNW to SSE orient both The Lake Mentikelir East and the Lake Mentikelir West. Their length is equal at around 1600 m. The western lake is slightly wider compared to the eastern one, and their widths obtain 1500 m and 1200 m, respectively. The eastern lake is located in 2 km distance from the northern cuesta of the range and the western lake in 2.5 km distance. This insignificant difference in the location significantly influences the sediment load flux to the lakes. The western lake is supplied by sediments of the northern range slope, while the valley of the river flowing to Lake Mentikelir East cuts the first ridge and penetrates further east to the low mountain relief of the range and collect the runoff in the depressions between the cuestas. This gives a significant superiority in the water runoff and sediment load discharge to Lake Mentikelir East compared to Lake Mentikelir West. A comparatively extensive delta is formed in the eastern lake at the flow of the supplying river. The observed rate of the water level increases in the lake during abundant precipitation comprised 30-40 cm over 24 h (8 August). The water transparency in the lakes also probably depends partly on the water and sediment load discharge when the river has a noticeable runoff. It comprises 1.3 m for the eastern lake and 3.0 m for the western lake. However, the geological structure of the shores of the lakes is of decisive importance for water saturation with suspended matter. Lake Mentikelir East has steeply shaped shores, which consist of sandy silt strata with ice wedges. These ice wedges veins are not visible today, but thermokarst mounds (baidzharakhs) are the common relief forms along the slopes of the east and north coast. In the south, the silt-clayey strata have a contact with the underlying sands and pebble-beds. In the Lake Mentikelir West mainly sands and pebble-beds existing at the water line along its coast are washed out and which are observed in a redeposited form in shallows near the shores. Due to this, the water turbidity of this lake is much lower compared to the eastern lake.

The height of lake terraces of Lake Mentikelir West is 7.5 and 10.5 m. The height of the terrace of Lake Mentikelir East is 5-7 m and the site width is 30-40 m. It is traced along the southeast, south and southwest coast. At the southwest and northwest coast, there is an additional terrace with a height of 8.5-10.5 m and a width of several tens of meters. Judging by the height of the terraces and the current level of the lakes, both terraces mark the level of one common basin that occupied both lake troughs some time in the past.

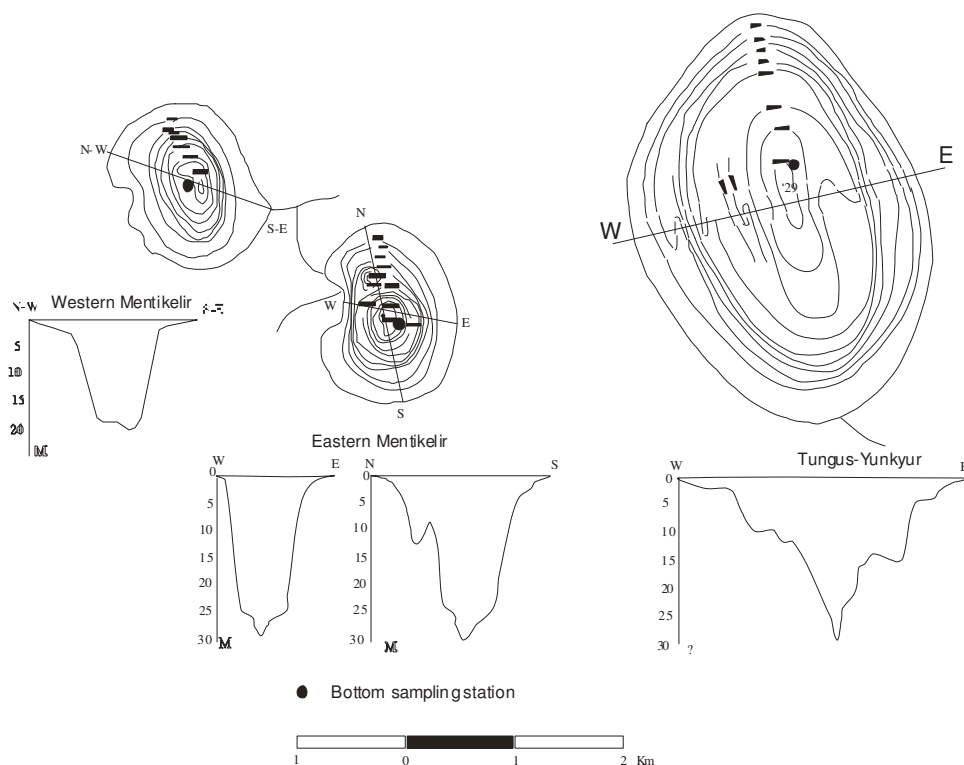


Figure 4.3-4: Bathymetric schemes and profiles Mentikelir Western, Mentikelir Eastern, Tungus-Yunkyr Lakes.

The bottom relief of both lakes is similar. These are deep troughs at the centre of the lakes with steep slopes and wide shallow water along the shores. Figure 4.3-4 presents the bathymetry maps of the lakes and the measurement profiles made by echo-sounders from a rubber boat.

The western lake has a wider shallow border. The width of the terrace with a depth of up to 1.5 m is up to 300 m. The greatest depth in the centre of an inverted saddle-shaped trough comprises 20.5 m. The eastern lake has a narrower shoal up to 150 m and a deeper trough up to 29 m. Besides, there is an additional trough in the northern part of the lake with a depth up to 14 m. The slopes of the troughs are also steep similar to the western lake.

Lake Tungus-Yunkyr located in the middle of the route along the Urasalakh River is greater in size and is also elongated from NNW to SSE similar to Lake Mentikelir. However, the trough structure is somewhat different. At the measurement profile from the west to the east shore some terrace-like benches were observed in 9-12 m depth at the west underwater slope and in 14-17 m depth in the eastern slope. The relief of these benches is complicated with steps up to 1-2 m high. The western shallow area up to 2 m depth has a width of up to 500 m and the eastern shallow area is up to 200 m wide. The maximum detected depth is 27 m, and the lake centre has not such an inverted saddle-like structure like the Lakes Mentikelir. The underwater trough slopes are less inclined (see Figure 4.3-4)

A steep eastern slope represents the part of the trough above the water level with a height up to 28 m. In the front of this slope, an ice wedge with a width up to 20 m is exposed. The entire slope is complicated with thermokarst mounds. The deposits with the ice wedges consist of sandy silt.

At the southwest lake coast, there is a pronounced terrace with a front height of 9 m and a rather steep slope ($20-25^\circ$) up to 50 m wide. Valleys of runoff streams dissect the western trough slope. The east shore does not practically have valleys and the water divide is near the water line in the lake.

The water turbidity in the lake is 3.2 m by Sekki disk.

In all three lakes, bottom sediment cores up to 60 cm length were sampled for studies of climate changes and changes of the hydrological lake regime during the last millennium.

4.4 Multi-sensor optical remote sensing of periglacial tundra landscapes

Guido Grosse

4.4.1 Research aim

The geomorphology of the region, formed by thermokarst and thermo-erosion, is an important source of information for the reconstruction of the Late Pleistocene and Holocene paleo-environment. Periglacial surface structures are indicators for certain stages of regional landscape development. To understand the extensive surface transformation since the Late Pleistocene it is essential to use remote sensing. Satellite remote sensing provides the large scale data vital for the up-scaling of geomorphological and geological field data from key sites like the area around Cape Mamontov Klyk.

It is possible to differentiate geomorphological units formed under periglacial conditions by their surface properties. Therefore the interpretation and classification of remote sensing data allows the large scale quantification of periglacial landscape units in the investigated area. Because of minor vegetation cover, relief structures like thermokarst depressions or thermo-erosional valleys are excellent to identify with satellites images in visible and infrared wavelengths. For the examination of the key site Mamontov Klyk and the coastal plain we use multi-spectral, medium resolution Landsat-7 ETM+ data together with panchromatic, high-resolution CORONA data. The extracted information can be used as an excellent complementary tool, together with sedimentological, cryological and paleontological field data, for the characterization and reconstruction of the Holocene landscape history in the region. The field data from the expedition "Lena-Anabar 2003" act as ground truth information and allow a generalization for the structures identified and mapped in the remote sensing imagery.

The resulting data is prepared for input into a geographical information system (GIS). Together with data from geological maps, geo-cryological field surveys and height information from digital elevation models (DEM), the GIS provides new insights into complex multi-source data structures.

One expected result is the estimation of quality, quantity and distribution of extensive thermokarst and thermo-erosional processes during the Holocene for the investigated region at Cape Mamontov Klyk and the entire coastal plain in front of the Pronchishchev Range.

4.4.2 Satellite data

For the investigation of the field area several satellite images are available. A Landsat-7 satellite image from 04-Aug-2000 (Path 139, Row 8) is used for the regional study of the surface conditions in the sedimentary plain from the Pronchishchev Range to the coast. The multi-spectral Landsat-7 ETM+ image has six medium-resolution data bands ranging from visible to mid-infrared wavelengths, one thermal band and one high-resolution panchromatic band (Table 4.4-1).

Table 4.4-1: Landsat-7 image properties

Band	Ground resolution (m)	Wavelength range (nm)	
1	30	450 – 520	Blue
2	30	530 – 610	Green
3	30	630 – 690	Red
4	30	780 – 900	Near infrared
5	30	1550 – 1750	Middle infrared
6	60	10400 – 12500	Thermal
7	30	2090 – 2350	Middle infrared
8	15	520 – 900	Panchromatic

Additionally, several CORONA satellite images from different dates were used during the field work (Table 4.4-2). CORONA images are very high-resolution, panchromatic images, acquired from 1960-1980. We use these images for the high-resolution study of local periglacial surface features, namely thermokarst depressions, thermokarst valleys, retrogressive thaw slumps, snow patches, pingos, and patterned ground.

Table 4.4-2: CORONA image properties

Image	Ground resolution	Acquisition date	Camera system
DS1007-1052DA030 DS1007-1052DA031 DS1007-1052DA032	9 feet (3 m)	23-06-1964	KH-4A
DS1022-1005DA047 DS1022-1005DA048	9 feet (3 m)	20-07-1965	KH-4A
DZB1210-500140L003001	30 feet (10 m)	14-07-1975	KH-9

4.4.3 General geomorphology in the Lena-Anabar interfluve

The regional scale geomorphology is determined by the Pronchishchev Range in the south, stretching parallel to the coast from NW to SE, and a 28-38 km wide sedimentary plain in front of these mountains (Figure 4.4-1). The hills are up to 270 m high. The sedimentary plain is very gently inclined towards the Laptev Sea coast with heights from 60-75 m close to the hills and 30-35 m at the coast (inclination angle of $\sim 0.07^\circ$). The river valleys in the region can be assigned to one of two major flowing directions: S-N or W-E. Some of the major rivers cross the SE Pronchishchev hills on their flow northwards. This probably points on neotectonic activity in the Pronchishchev Range. Thermokarst depressions are widely distributed in the sedimentary plain. They not only occur along river valleys but often are arranged linear on interfluves between the river valleys. This spatial pattern probably points on paleo-valley systems below the cover deposits of the Ice Complex. The cryo-lithological properties of the sediments accumulated in these supposed paleo-valleys possibly support the formation of thermokarst in the Ice Complex cover during the Holocene. Therefore the linear arrangement of large thermokarst basins is considered as a finger print of succeeding relief forms. The surface of the plain is densely incised by thermo-erosional valleys.

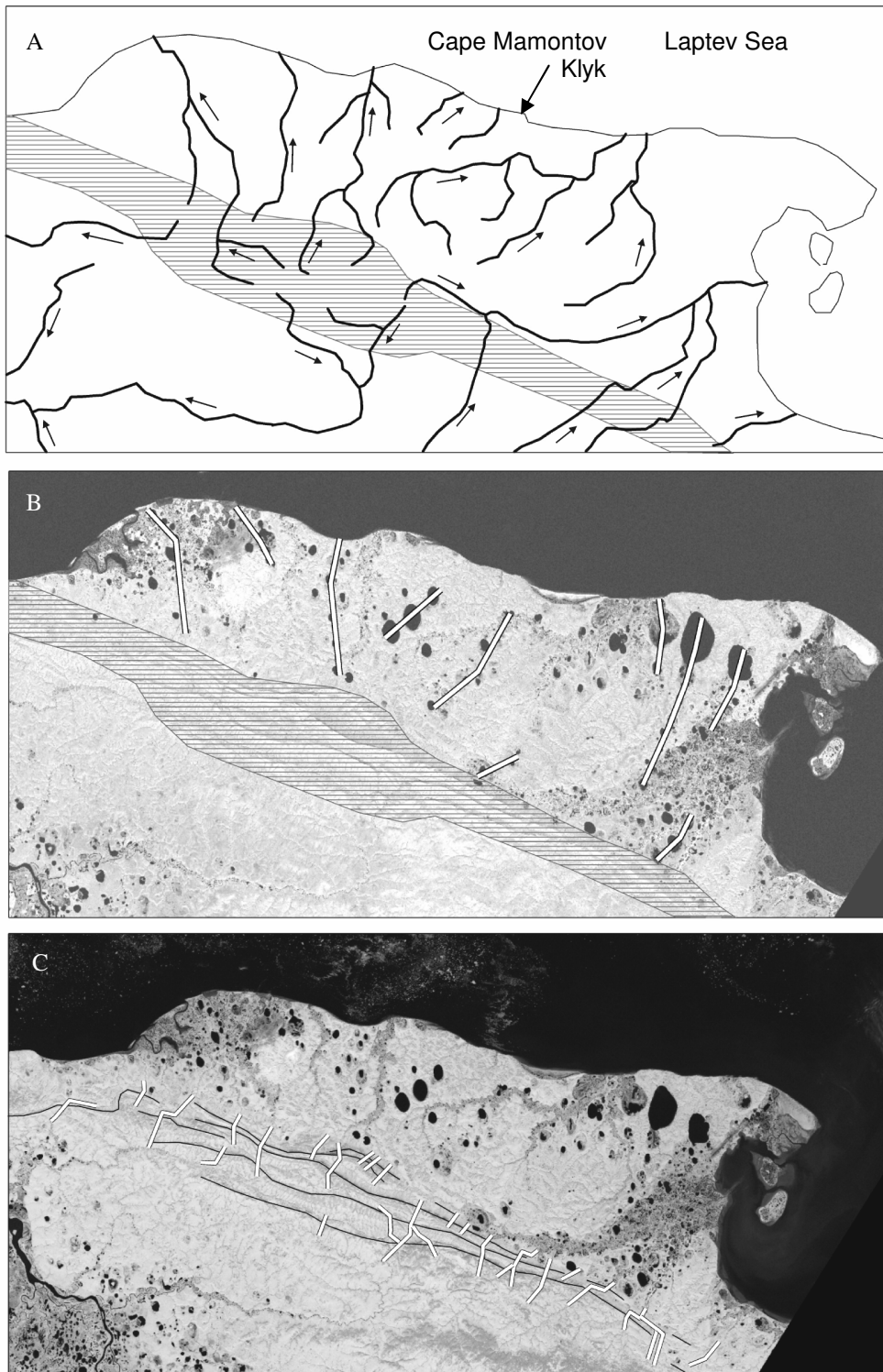


Figure 4.4-1: Regional structures in the Lena-Anabar coastal area (Landsat-7 ETM+ image)

- A – River discharge regime: North of the Pronchishchev Range (horizontal lines) the rivers flow towards N or NE; the western Pronchishchev Range acts as watershed, while the eastern Pronchishchev Range does not
- B – Linear arrangement of large thermokarst basins not connected to recent river systems possibly indicate paleo-river structures, where the cryo-lithological conditions during Ice Complex deposition within these valleys gives benefit to Holocene thermokarst formation.
- C – Black lines indicate ridges in the Pronchishchev Range, white lines represent deep valleys incising these ridges. Note the valleys in the SE, crossing the entire Pronchishchev Range.

4.4.4 Geomorphology in the investigation area near Cape Mamontov Klyk

The investigation area near Cape Mamontov Klyk consists of Edoma elevations (20-40 m a.s.l.), which are separated by erosional features and thermokarst depressions (Figure 4.4-2). A major structure is the meandering river valley of the Nuchcha-Dzhielle with sand banks, flood plains, undercut slopes, extent slip-off slopes and an estuary-like mouth. Close to the river mouth a large oxbow lake has formed, containing large amounts of driftwood. Large driftwood fields exist on the sandbanks of the estuary. Probably ice-rafted driftwood trunks several kilometres upstream indicate the occasional marine influence on the river flood land in the hinterland. Several thermo-erosional valleys incise the Edoma surface. Most of them are heading towards the river valley, only a few in the direction of the recent coast. The field camp was situated in one of these valleys close to the river. The slopes of the valleys are often covered by small thermokarst mounds (< 1m, Ø 2-4 m). The coast is subject to very fast thermal erosion and marine abrasion. Steep cliffs with 70-80° inclination have formed, in places with more gently retrogressive thaw slumps.

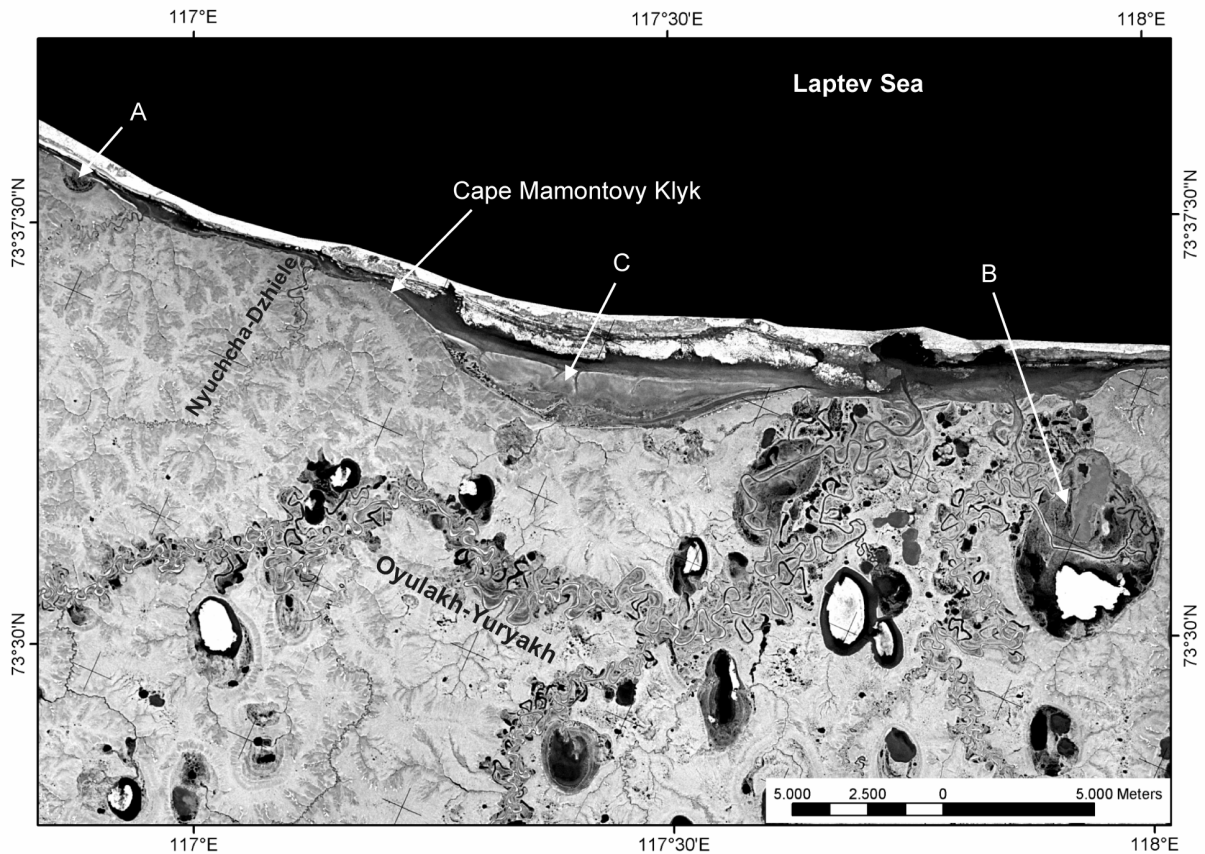


Figure 4.4-2: Satellite map (CORONA) of the region near Cape Mamontov Klyk; Note the location of the rivers Nuchcha-Dzhielle and Oyulakh-Yuryakh;

A – thermokarst site 1

B – thermokarst site 2

C – wide bay with marine terrace

One thermokarst depression occurs in the closer area of the cape. This flat depression is about 8-12 m deep and does not contain water bodies. Large nival niches with remnants of snow patches were discovered at several slopes in the depression and in some ravines heading into the depression. One thermo-erosional valley discharges from this depression towards the river Nuchcha-Dzhiele. A more remote thermokarst depression is situated 8 km NW of the river mouth (Figure 4.4-2). This depression is actively eroded by coastal erosion. Several large polygonal and irregular water bodies with more than 25 m in diameter are situated within the depression. The mean depression floor is situated 5 m a.s.l. and the surrounding surface is approximately 20-25 m a.s.l..

In the region south of Cape Mamontov Klyk the Edomas are incised by several thermo-erosional valleys. About 7 km to the south, the large river Oyulakh-Yuryakh is situated in a wide river valley. Different from all other rivers in the region, this strongly meandering river is flowing from W to E. Several thermokarst depressions are associated with the wide river valley. The river valley strongly widens when approaching the coast 18 km east of the cape. In this region, many large thermokarst depressions and thermokarst lakes are located. Some of them have already amalgamated to larger basins. In the largest at least 4 pingos occur. Between Cape Mamontov Klyk and the Oyulakh-Yuryakh River mouth a wide bay is located at the coast (Figure 4.4-2). In this bay a 11.5 km long and 1.5 km wide terrace has formed consisting of marine deposits up to 0.5-1.0 m a.s.l.. The inner zone of the terrace contains many small freshwater lakes.

4.4.5 Field data

During field work, various surface parameters were observed and described for 178 geo-located sites in the vicinity around Cape Mamontov Klyk (Figure 4.4-3). The closer area around the camp site contributes 129 sites (Figure 4.4-4) and two remote thermokarst depressions (see above) contribute another 49 geo-located sites (Figure 4.4-5 and 4.4-6). The recorded surface parameters include relief type, slope inclination, major vegetation, portion of dry vegetation, estimation of soil moisture, active layer depth and occurrence and type of small scale water bodies (Table 4.4-3). A schematic view of the parameters "major relief type", "relief position" and "slope" is shown in figure 4.4-7. In table 4.4-4 a description of the major relief features in the investigation area is given.

Samples of surface sediment were taken at 10 sites. An image database contains more than 200 photos from 115 of the geo-located sites. The detailed recordings and measurements for each site are presented in the appendix (tables Appendix 4-1 and Appendix 4-2).

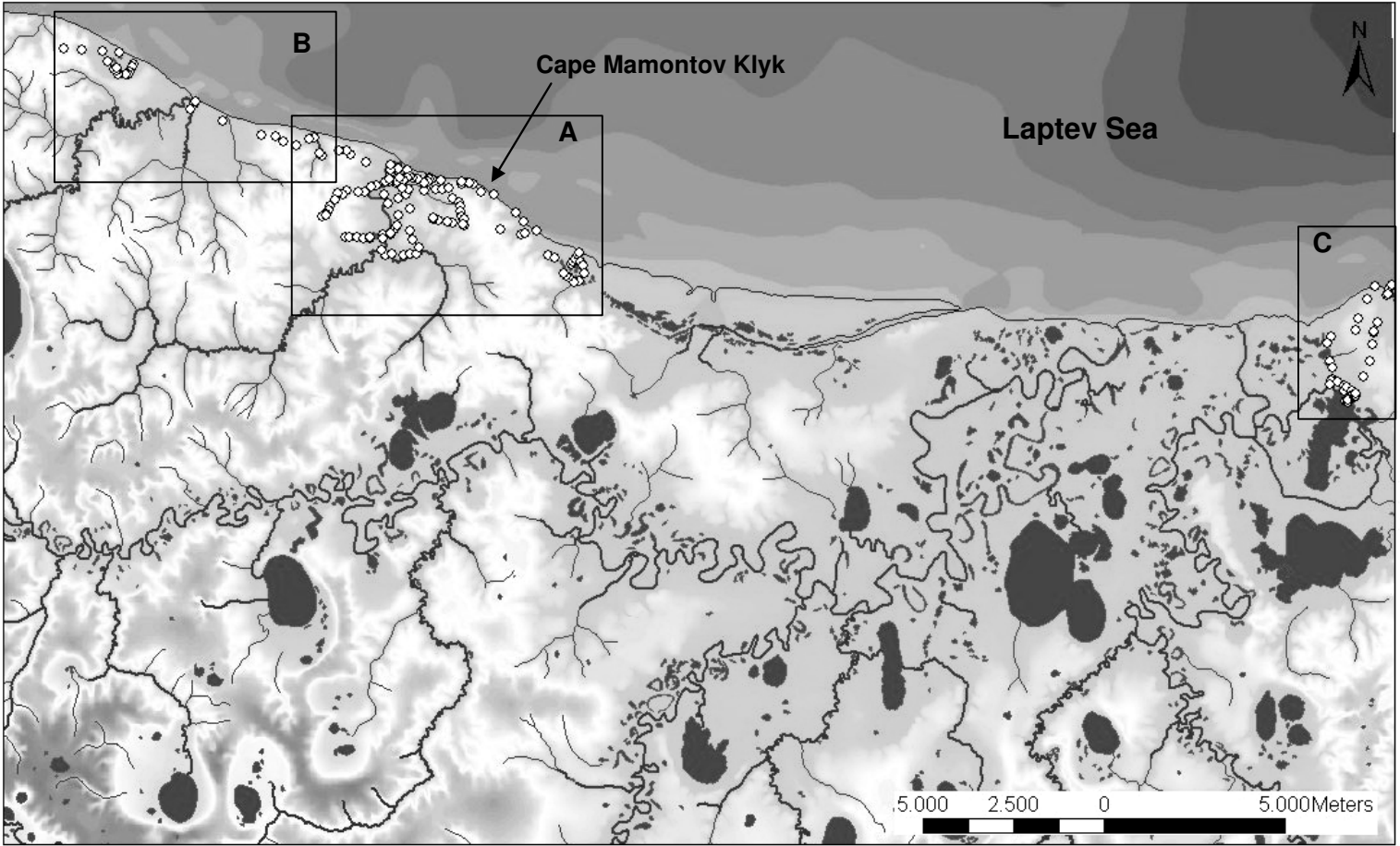


Figure 4.4-3: Elevation map with geo-located ground-truth sites (white circles); Detailed images for A, B and C are shown in separate figures

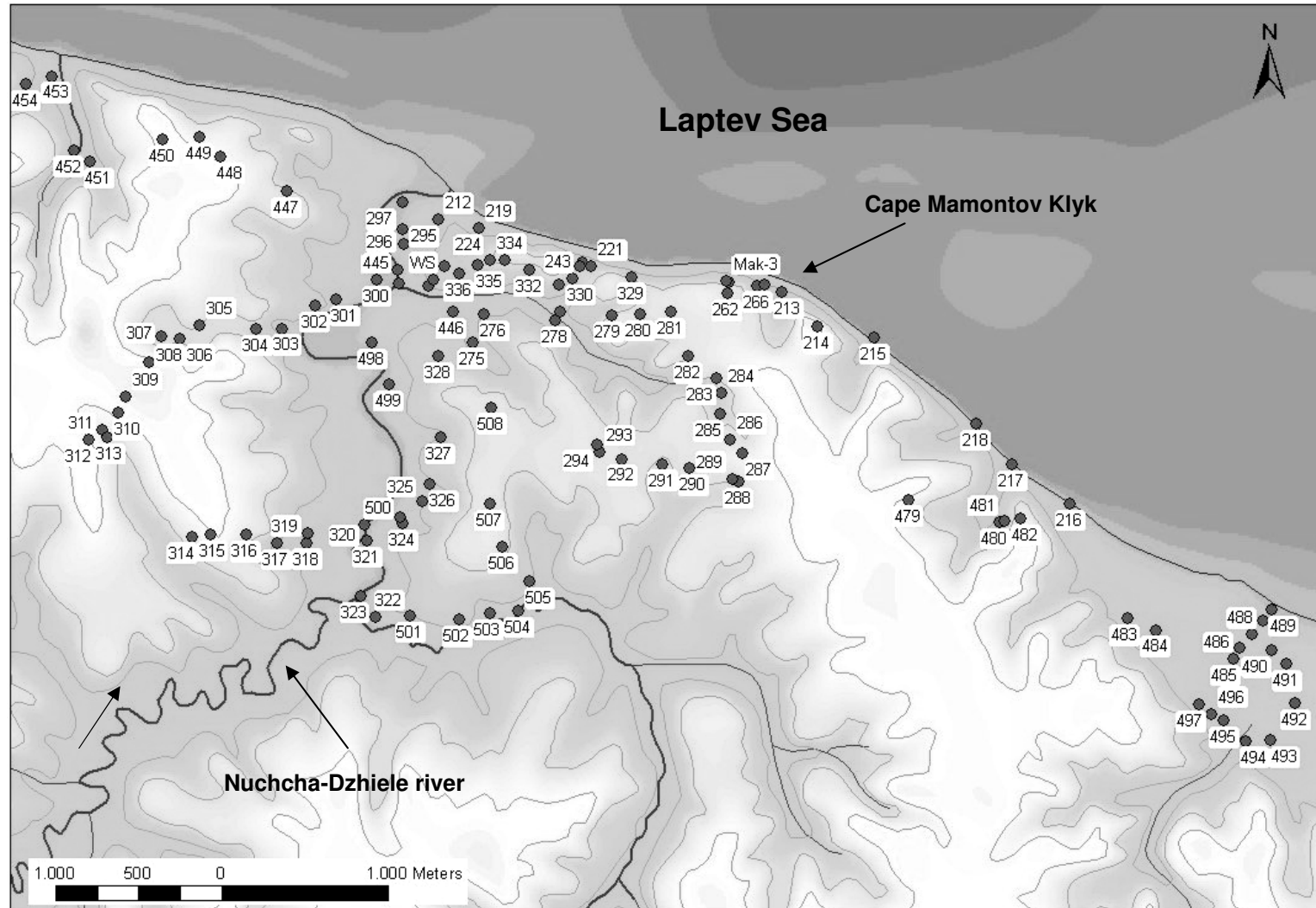


Figure 4.4-4: Detail image for Fig. 4.4-3 A with geo-located sites close to the camp at Mamontov Klyk

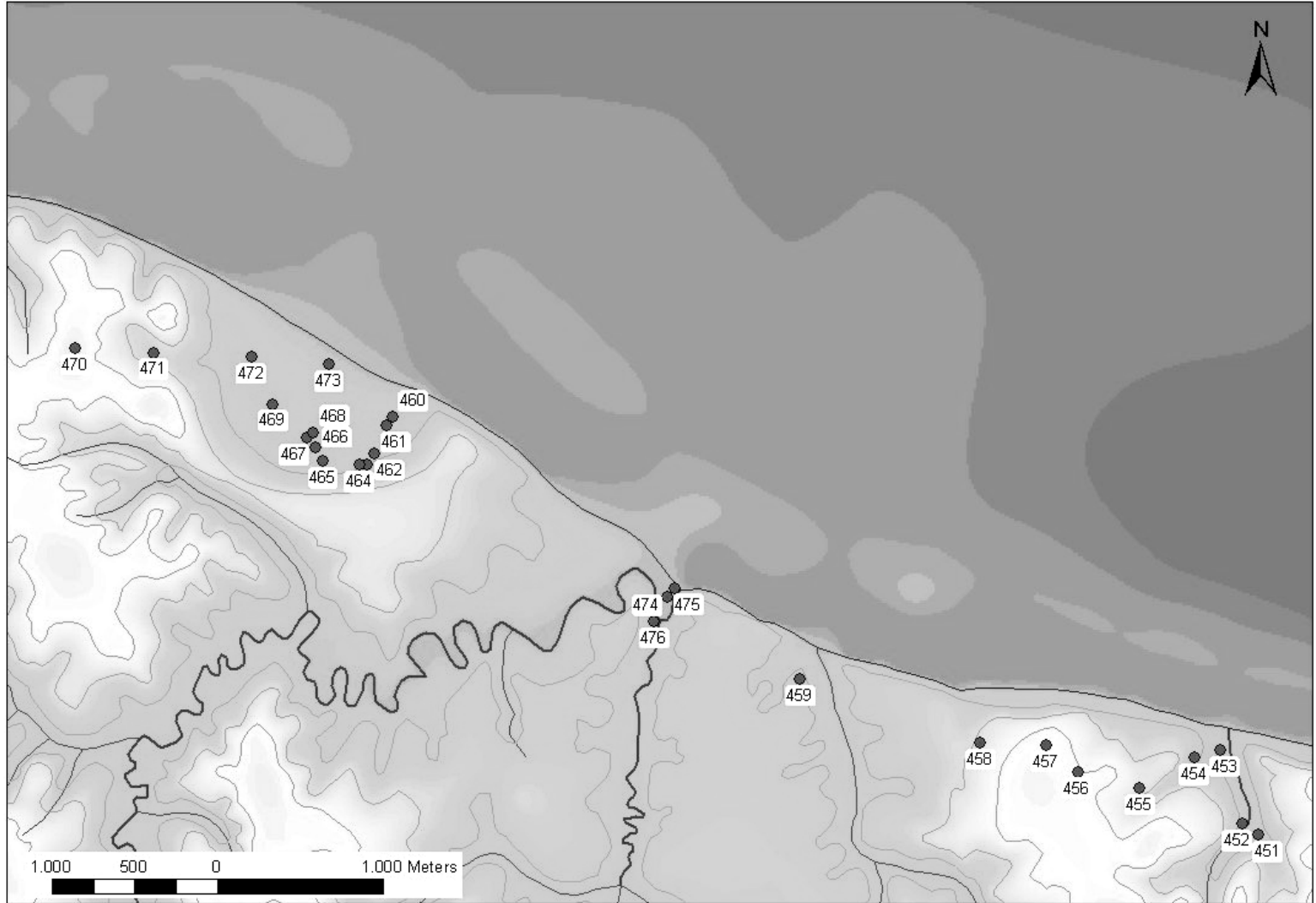


Figure 4.4-5: Detail image for Fig. 4.4-3 B with geo-located sites in a thermokarst depression west of Cape Mamontov Klyk

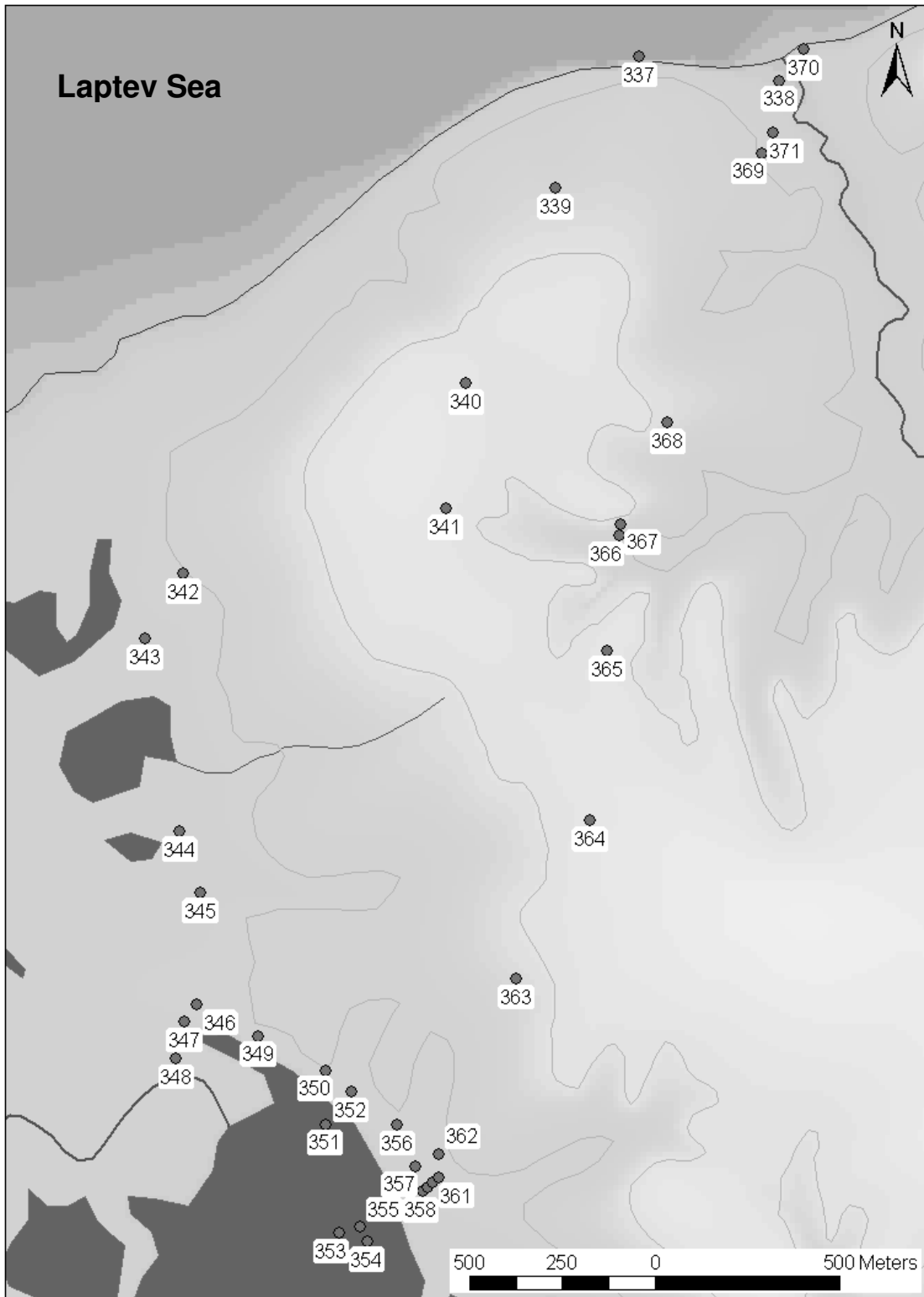


Figure 4.4-6: Detail image for Fig. 4.4-3 C with geo-located sites in a thermokarst depression east of Cape Mamontov Klyk

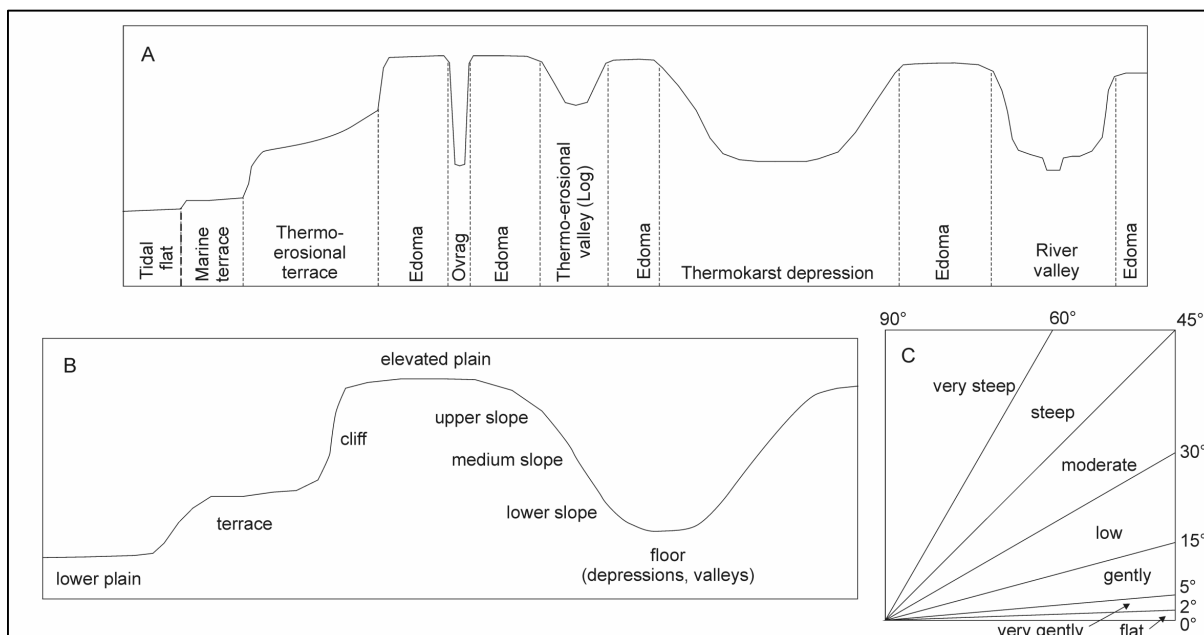


Figure 4.4-7: Classification of relief type
 A – Major relief forms; B – Site location within the relief; C – Slope inclination at site

Table 4.4-3. Variable elements of the recorded features for the geo-located ground truth sites

Recorded feature	Elements
Major relief type	Edoma, thermo-erosional valley (Log), thermokarst depression, thermo-erosional ravine (Ovrage), thermo-erosional terrace, river valley, marine terrace, tidal flat
Relief position	Elevated plain, upper slope, slope, lower slope, terrace, lower plain, floor, cliff
Meso and micro relief features	Nival niche, river bank, sand bank, sediment fan, thermokarst mounds, solifluction, mud flow, drainage channels, polygonal structures
Slope	Inclination
Active layer depth	Up to 15 measurements per site
Vegetation	Major and minor plant groups, portion of dry vegetation
Surface / soil moisture	Estimation (wet, very moist, moist, moderate moist, less moist, dry)
Water bodies	Occurrence (yes/no), type (surface discharge, polygonal, irregular, channels), size, depth
Surface sediment samples	
Photographic documentation	
Remarks	

Table 4.4-4: Description of major relief types in the investigation area

Major relief type	Description
Edoma	Frozen sequences of organic and mineral soils, containing large amounts of ground ice (ice wedges, segregated ice); erosional remnants of Late Pleistocene surface;
Thermo-erosional valley (Log)	Dendritic, U-shaped valleys with flat floor; dense grass/sedge vegetation; very moist, often with surface water and little ponds; two main types: wide and shallow, narrow and deep; length of valleys varies from 50 to 2000 m, width about 50 m;
Thermokarst depression	Deep subsidence area due to thermokarst often with large extent; associated with ice-rich permafrost; shape circular, ellipsoid or sometimes irregular; thermokarst lakes and pingos may occur in the depressions; the steep slopes are incised by erosional valleys; depressions close to each other may amalgamate; diameters range from few 100 m to several km; depth of depressions is, depending on age and subsidence rate, in coastal areas down to sea level; the depressions are dominated by wet tundra vegetation (mosses, grass), nevertheless zones from different soil moisture are visible sometimes;
Thermo-erosional ravine (Ovrag)	Deep incised V-shaped valley; formed by rapid thermo-erosion and flowing water; associated with ice-rich ground; valleys are often rather short;
Thermo-erosional terrace	Formed in front of large thermo-erosional cirques; associated with ice-rich permafrost and Edomas in the hinterland; widely U-shaped structure at coastal or fluvial sites; length of structures is 100 m up to several 100 m, width varies from 25 to 200 m;
River valley	Wide valleys with strongly meandering rivers;
Marine terrace	Coastal terrace with marine deposits, but elevated above recent sea level; often sparsely vegetated; large amounts of driftwood may occur
Tidal flat	Shallow intertidal area in front of the coast; sea level in this region fluctuates because of diurnal tides and/or wind-forcing; area is up to several 100 m wide;

4.4.6 Tachymetric survey of periglacial surface features

During the field season some periglacial surface features were surveyed in detail with a laser tachymeter. Such features were a thermo-erosional valley near the camp site (Figure 4.4-8 and 4.4-9) and thermokarst hills, where the distances between their tops were measured (Figures 4.4-10 to 4.4-14). The valley is also the location of the methane measurement site (see chapter 4.5). Thermokarst hills represent the sediment remnants of polygon centers of an eroded ice wedge polygonal net. The distance between the tops of the hills within a cluster of thermokarst hills characterizes the size of the polygons in the eroded polygonal ice wedge net. The distances also give hints on the ice wedge width between the former polygon centers. The height of the thermokarst hills is dependent on cryolithological factors, climatic factors and stage of development.

The data are used for comparison with features surveyed previously at other locations in the Laptev Sea coastal area.

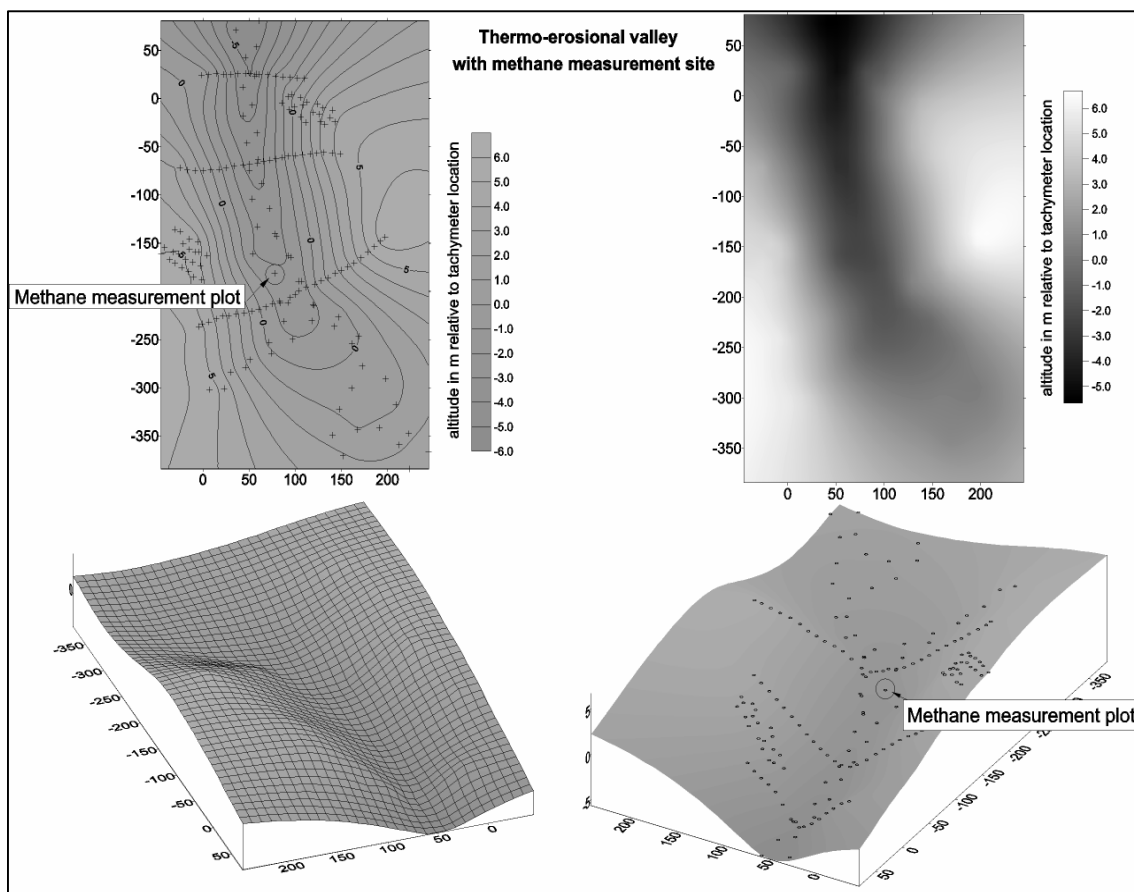


Figure 4.4-8: Elevation model of a thermo-erosional valley plotted in a xyz-coordinate system from a tachymetric survey near the camp. Altitudes are relative to the tachymeter position. The methane measurement site was situated in this valley.



Figure 4.4-9: View over the thermo-erosional valley, where methane-related studies were carried out. At the bottom of the valley, areas dominated by *Eriophorum angustifolium* (with white stands of fruit) could be observed next to wetter patches dominated by *Carex aquatilis*.

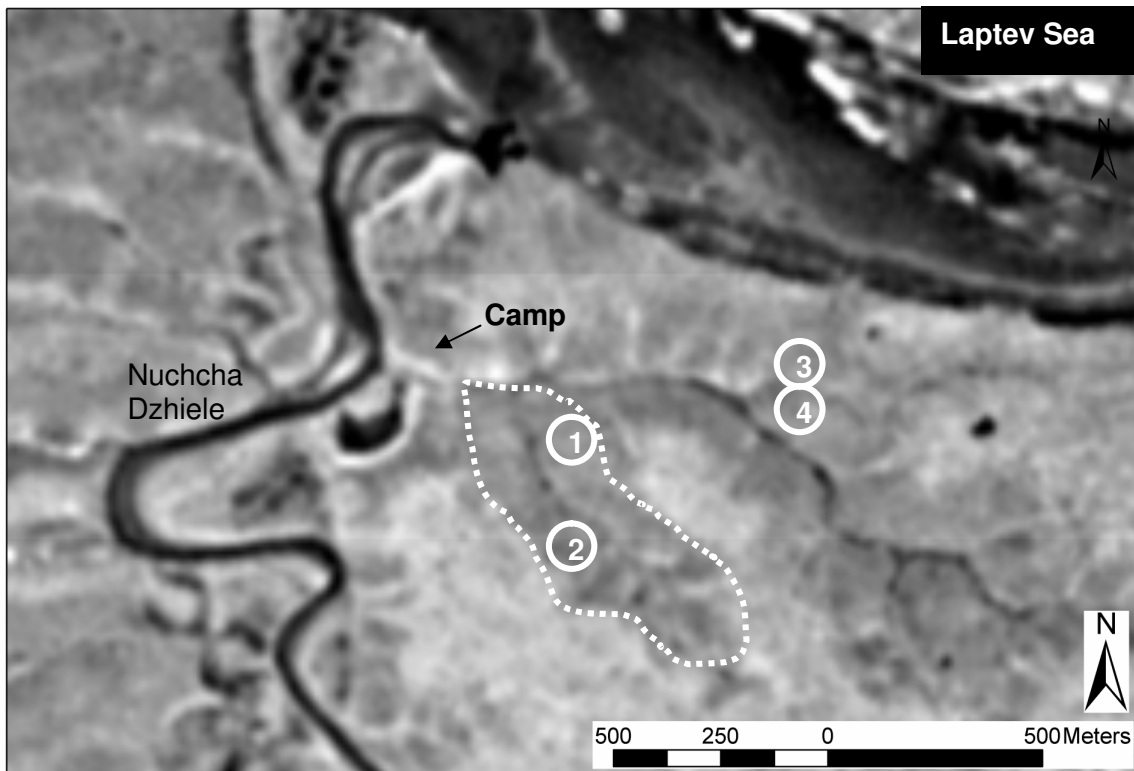


Figure 4.4-10: CORONA satellite map of the sites, where clusters of thermokarst hills were surveyed with a laser tachymeter (white circles with site numbers). The dotted white line marks the thermo-erosional valley with the methane measurement site.

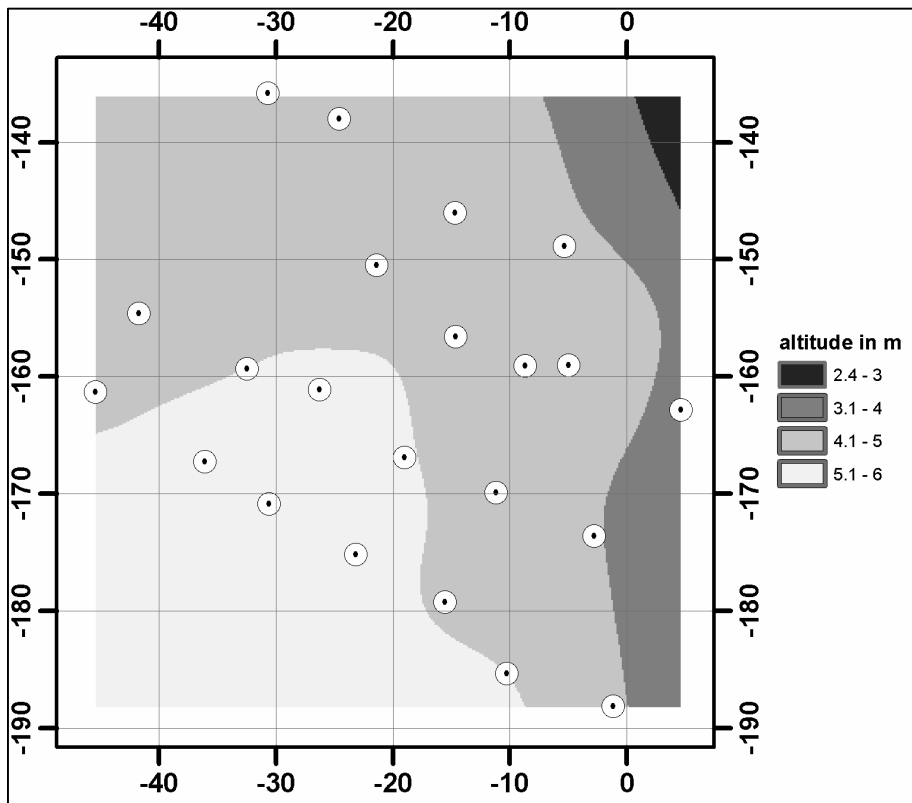


Figure 4.4-11: Survey site 1 of a thermokarst hill cluster, situated at the eastern slope of the thermo-erosional valley southeast of the camp (methane measurement site)(altitude relative to tachymeter position, xy-coordinates in m).

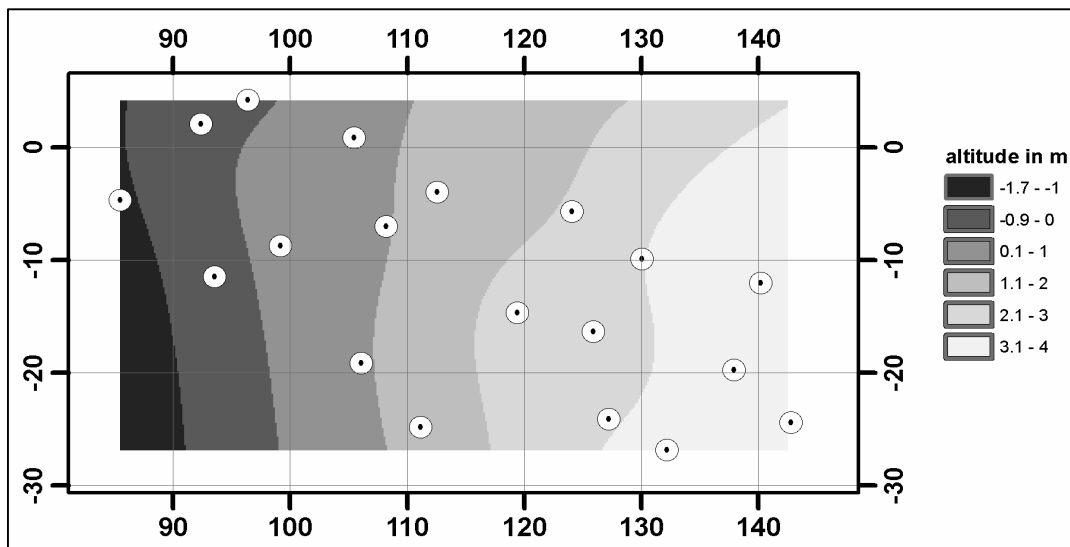


Figure 4.4-12: Survey site 2 of a thermokarst hill cluster, situated at the western slope of the thermo-erosional valley southeast of the camp (methane measurement site) (altitude relative to tachymeter position, xy-coordinates in m).

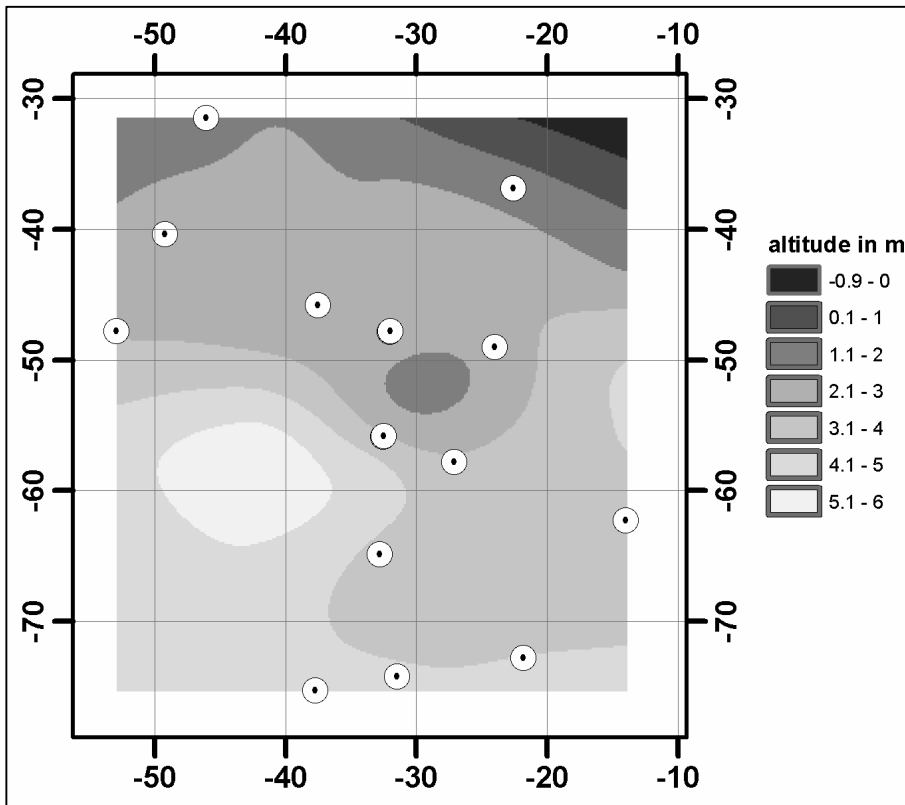


Figure 4.4-13: Survey site 3 of a thermokarst hill cluster, situated at the northern slope of a thermo-erosional valley east of the camp (altitude relative to tachymeter position, xy-coordinates in m).

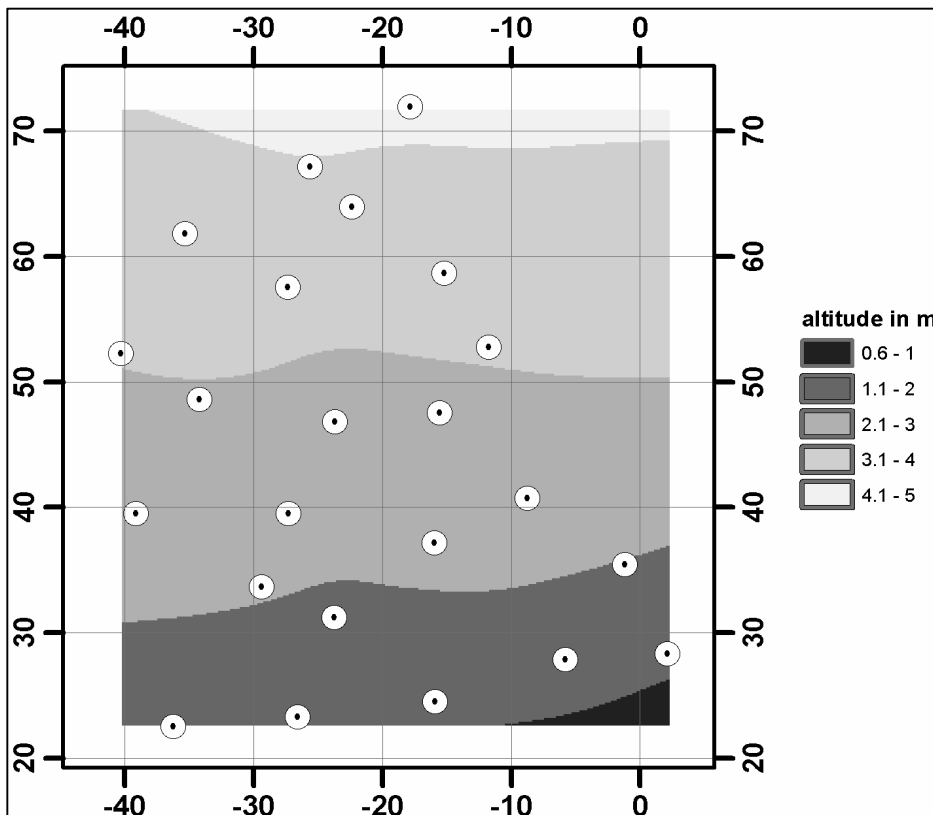


Figure 4.4-14: Survey site 4 of a thermokarst hill cluster, situated at the southern slope of a thermo-erosional valley east of the camp (altitude relative to tachymeter position, xy-coordinates in m).

4.4.7 Characterisation in situ surface properties with a soil probe at a typical elevated Edoma plain

During the field season almost continuous loggings of soil temperature and soil moisture were conducted with a soil probe at an Edoma site in the vicinity of the camp. The site at 17 m a.s.l. was chosen because of its typical appearance for an elevated tundra surface atop an Edoma. The main vegetation consisted of grass, and the soil surface was slightly tussocky. The soil probe sensors were fixed in 5 cm depth. The measurement interval was 5 min. The logging lasted from 9th August (04:38 GMT) to 26th August (03:48 GMT). The breaks in the logging period are caused by failure of power supply for the probe. Table 4.4-5 shows the extreme values during the logging. Whereas the temperature shows diurnal variation and a slight decrease during the whole period (Figure 4.4-8), the logging of volumetric soil moisture showed an almost constant moisture content of $0.4 \text{ m}^3 \times \text{m}^{-3}$ in the upper soil during the measurement period without diurnal variation.

Table 4.4-5: Values for in situ soil temperature and soil moisture (measured as electric soil voltage) logged with a soil probe in the upper 5 cm of a soil atop an Edoma surface

	Min	Max	Mean	Sd (+/-)	Logged values
Soil temperature	1.81 °C (24-08-04)	5.59 °C (13-08-04)	3.62 °C	0.84	3745
Volumetric soil moisture	$0.4 \text{ m}^3 \times \text{m}^{-3}$	$0.4 \text{ m}^3 \times \text{m}^{-3}$	$0.4 \text{ m}^3 \times \text{m}^{-3}$	0.0	3867

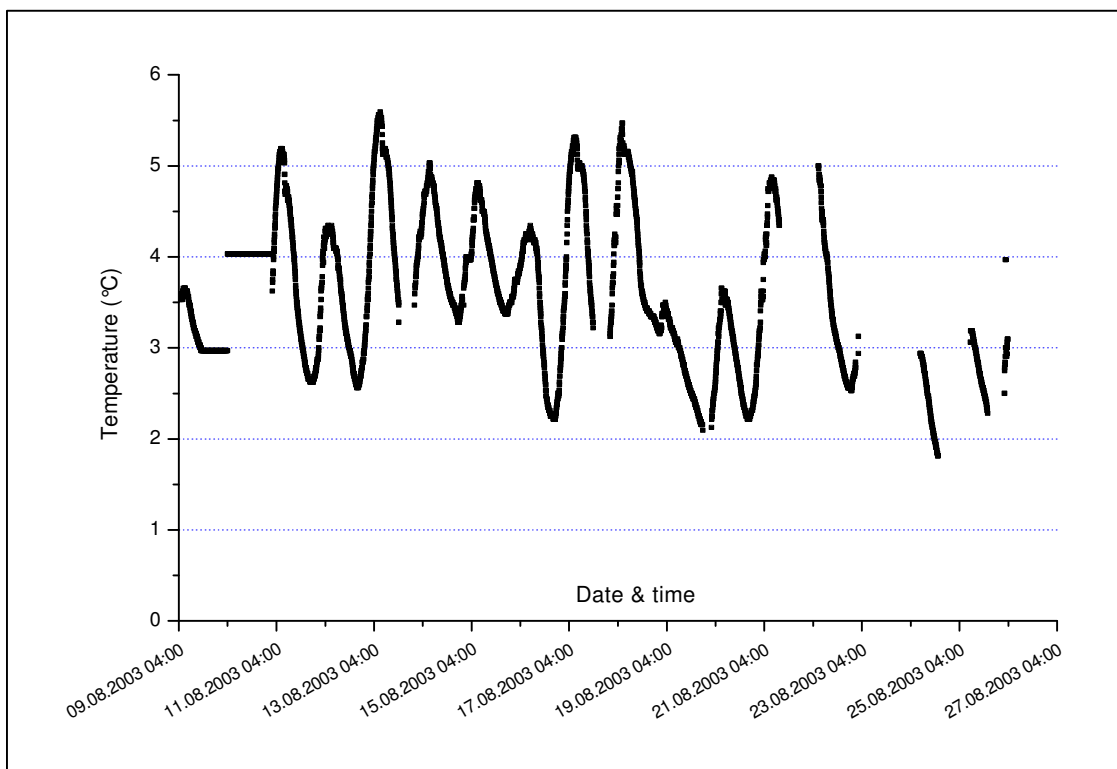


Figure 4.4-15: Diurnal variations in soil temperature within the upper 5 cm of an Edoma surface

4.5 Methane-related studies on recent tundra soils

4.5.1 Introduction and objectives

Northern wetlands presently account for 3.5-8 % of global methane emissions (Whalen & Reeburgh 1992; Christensen 1993; Harris et al. 1993; Roulet et al. 1994; Cao et al. 1996). Huge Carbon reservoirs in soils and permafrost deposits provide the potential for increased emissions in a global change scenario with rising temperatures. However, future methane fluxes depend on the interaction of numerous factors, one of them being microbial methane oxidation (methanotrophy). This process occurs at oxic-anoxic interfaces in soils, which can be found (a) near the watertable and (b) in the rhizosphere of vascular wetland plants, where oxygen leaks from the roots into the waterlogged soil.

The coastal lowland around Cape Mamontov Klyk is characterized by gently sloping hilly plains with a net of thermoerosion valleys (for details see chapter 4.4). At the bottom of the valleys, wet silty and peaty soils can be found. Methane related studies have not been conducted in this type of wetland in the Russian-German Laptev Sea Project. These investigations are supplementing the studies in the wetlands of the Lena Delta.

Major working tasks were:

- description of soils as habitat for methane producing and oxidizing microorganisms
- soil sampling for pedological analyses and for investigations of microbial communities with biochemical, molecularbiological as well as classical microbiological methods in Germany
- determination of methane emissions
- in situ investigation of microbial methane consumption at roots of vascular plants in the waterlogged soils

4.5.2 Methods

A representative thermoerosion valley with gentle slopes and waterlogged soils at the bottom was chosen for methane-related studies. Within the valley bottom, two sites with differing water table, vegetation cover and soil profile were described in detail; they will be referred to as site "Carex" and site "Eriophorum" (see Figures 4.4-8, 4.4-9).

To characterize soil profiles, soil monoliths were dug out of the waterlogged ground. The following parameters were determined in the field: soil texture, colour, quantity of roots, redox status (only in mineral horizons, with a-a-dipyridyl solution) and depth of the watertable. Soils were classified according to the "Soil Taxonomy" (Soil Survey Staff 1998).

Four types of samples were taken from different depths of each profile: (a) bulk samples for analysis of soil chemistry and texture, (b) undisturbed cores for determination of soil density, (c) samples that were immediately stored on ice for microbiological investigations and (d) samples stored in gastight jars filled with a saturated sodium chloride solution for determination of methane content (see sample list in Appendix 4.-3).

Methane emissions were determined by a closed chamber technique as described by Pfeiffer et al. (1999). At both the "Carex"- and the "Eriophorum"-site three PVC frames were installed and emissions were measured on 4 to 5 days during a period of 8 days in mid August 2003. Simultaneously, soil temperatures in different depths were recorded.

At the "Carex"-site, the root-associated methane oxidation was investigated using Difluormethane (CH_2F_2), a specific gaseous inhibitor of methane oxidizing bacteria (Krueger et al. 2001). The inhibitor can diffuse through the aerenchyma of vascular plants into the root-associated part of the soil. The proportion of oxidized methane at the roots can be calculated from the difference in methane flux with and without influence of the inhibitor (Popp et al. 2000).

For this experiment, the plant-mediated methane flux had to be measured separately from the flux through the soil surface. Therefore, special 0.5-L-glass bottles were used as closed chambers as described by Kutzbach (Kutzbach et al. 2004). These bottles were placed over single culms of *Carex aquatilis*, the dominant vascular plant species at the "Carex"-site (see Figure 4.5-1).



Figure 4.5-1: Plant flux chambers for measurement of root-associated methane oxidation at *Carex aquatilis*.

First, methane emission was measured without the inhibitor at 8 *Carex* culms. After that, CH_2F_2 was injected into 4 of the closed chambers to obtain a mixing ratio of 0.5 % CH_2F_2 in the headspace. The remaining 4 plant flux chambers served as control. After incubation of the inhibitor for 22 hours, the chambers were removed for one hour. Then the plant-mediated methane emission was measured again. This experiment was carried out twice, changing the investigated *Carex* culms.

All gas samples were stored in glass tubes filled with saturated NaCl solution until analyses of methane concentration by gas chromatography in the field laboratory on the Island Samoylov, Lena Delta.

4.5-3 First results

The most evident difference between the two investigated soils was the peat distribution in the profile, corresponding to differing depths of the watertable: At the "Carex"-site the complete profile down to the permafrost boundary consisted of peat with very small proportions of mineral substance (Figure 4.5-2). In contrast to that, the "Eriophorum"-profile had a distinct peat horizon at the top, with mineral horizons beneath (Figure 4.5-3). For more details see soil descriptions in Table 4.5-1 and Table 4.5-2.

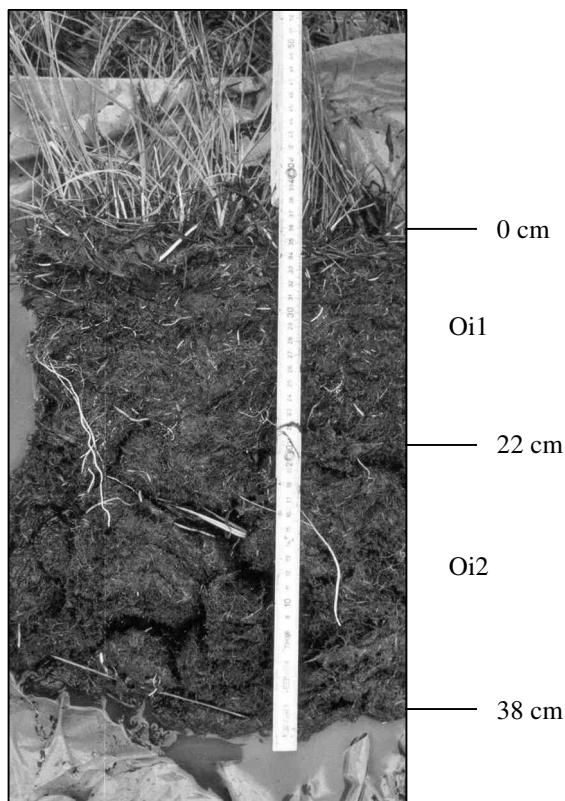


Figure 4.5-2: Photo of the *Typic Fibristel* (profile MAK-TV-1), located at the bottom of a thermoerosion valley (site "Carex").

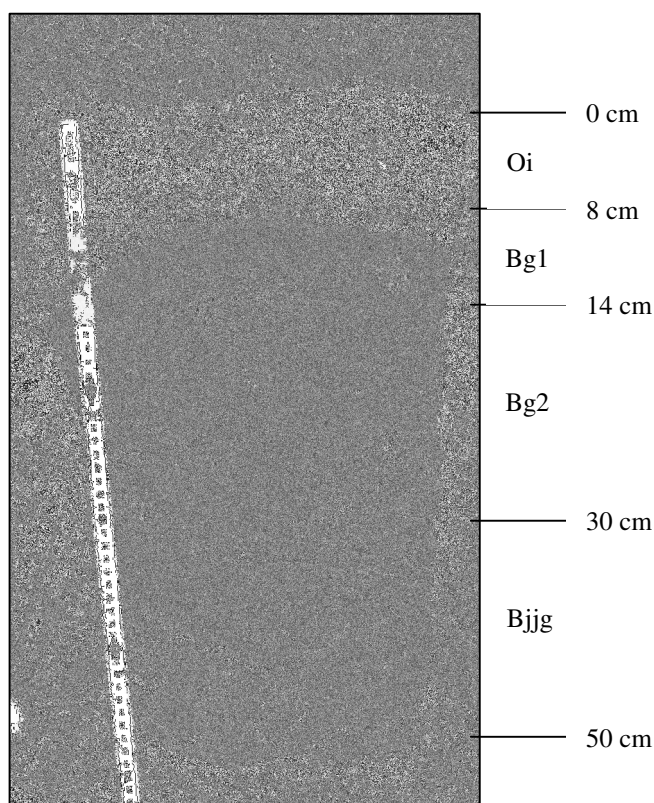


Figure 4.5-3: Photo of the *Typic Aquiturbel* (profile MAK-TV-2), located near the bottom of a thermoerosion valley (site "Eriophorum").

Table 4.5-1. Description of soil profile MAK-TV-1 (Thermoerosion valley, "Carex")

<u>Profile ID:</u> MAK-TV-1		<u>Date:</u> 25.08.2003
<u>Altitude a.s.l.:</u> 3.8 m		
<u>Location:</u> Mamontov Klyk, 73,60428° N; 117,13343° E		
<u>Relief situation:</u> bottom of thermoerosion valley		
<u>Substrate:</u> moss and sedge peat		
<u>Thawing depth:</u> 38 cm		<u>Water level depth:</u> 0 cm, partly above ground surface
<u>Vegetation (dominance in %):</u> moss layer: mosses total 55 % (remaining surface covered with shallow water); vascular plants layer: total 25 %, <i>Carex aquatilis</i> 19 %, <i>Arctagrostis latifolia</i> 5 %, <i>Arctophila fulva</i> < 0.5 %, <i>Caltha palustris</i> < 0.5 %, <i>Eriophorum angustifolium</i> < 0.5 %		
depth [cm]	horizon*	Properties
0-22	Oi1	slightly decomposed moss and sedge peat, very many fine roots, dark brown (Munsell 7.5YR3/2)
22-38	Oi2	slightly decomposed moss and sedge peat, many fine roots, dark grayish brown (Munsell 2.5Y4/2)
<u>Soil type (Soil Taxonomy):</u> Typic Fibristel		

* symbols according to Soil Taxonomy (USDA 1998)

Table 4.5-2. Description of soil profile MAK-TV-2 (Thermoerosion valley, "Eriophorum")

Profile ID: MAK-TV-2		Date: 25.08.2003
Altitude a.s.l.: 3.8 m		
Location: Mamontov Klyk, 73,60428° N; 117,13343° E		
Relief situation: near bottom of thermoerosion valley		
Substrate: shallow peat above alluvial silts		
Thawing depth: 50 cm		Water level depth: 2 cm
Vegetation (dominance in %): moss layer: mosses total 95 %; vascular plants layer: total 80 %, <i>Eriophorum angustifolium</i> 40 %, <i>Arctagrostis latifolia</i> 35 %, <i>Carex aquatilis</i> 3 %, <i>Pedicularis sudetica</i> 2 %		
depth [cm]	horizon*	Properties
0-8	Oi	slightly decomposed peat, very many fine roots, dark brown (Munsell 7.5YR3/2)
8-14	Bg1	loamy silt, coherent, 2-4 % org. matter, many fine roots, redoximorphic concretions around roots (1-2 vol.%), a-a-dipyridyl reaction positive, dark olive grey (Munsell 5Y3/2)
14-30	Bg2	loamy silt, coherent, 2-4 % org. matter, common fine roots, a-a-dipyridyl reaction positive, dark olive grey (Munsell 5Y3/2)
30-50	Bjgg	loamy silt, coherent, 4-8 % org. matter, few fine roots, a-a-dipyridyl reaction positive, dark olive grey (Munsell 5Y3/2), spots with higher content of well-decomposed org. matter
Soil type (Soil Taxonomy): Typic Aquiturbel		

* symbols according to Soil Taxonomy (USDA 1998)

In the „Carex“-site methane emissions were higher than in the “Eriophorum“-site (Figure 4.5-4), corresponding to a higher water table in the “Carex” soil. Emissions from the “Carex” site (with 77 to 114 mg CH₄ d⁻¹ m⁻²) were in the same order of magnitude as from a wet polygon tundra site with similar water table depth and vegetation cover on Samoylov Island, Lena Delta (see chapter 3.4.3).

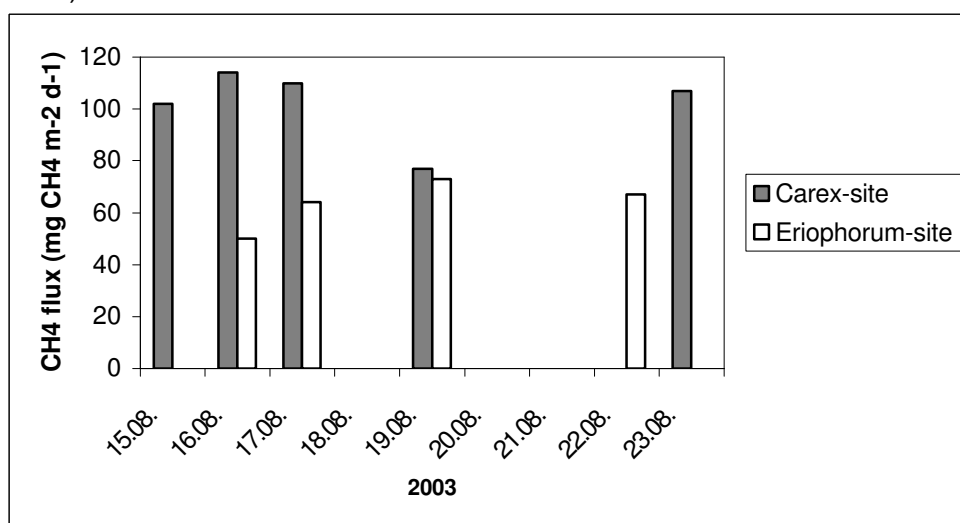


Figure 4.5-4: Methane fluxes at “Carex“- and “Eriophorum“-site in mid August 2003. Each column represents the average of 3 parallel measurements (missing columns: methane emission not determined).

Methane fluxes from single culms of *Carex aquatilis* did not significantly change after the addition of CH_2F_2 , the gaseous inhibitor of methane. This result was confirmed by measurements at *Carex aquatilis* on Samoylov, Lena Delta (see chapter 3.4.3). Possible reasons for no or minor methane oxidation at *Carex* roots are (a) not enough oxygen leaking from the plant roots (Calhoun & King 1997), (b) nitrogen limitation in the rhizosphere because of competition with *Carex* roots (Krueger et al. 2001) or (c) inhibition of methanotrophic bacteria by plant-derived substances (Amaral et al. 1998). Another possibility would be that the inhibitor did not diffuse sufficiently through the plants into the rhizosphere to inhibit methane oxidation.

4.6. The coastal section of Cape Mamontov Klyk

4.6.1 General profile

Lutz Schirrmeyer, Viktor Kunitsky, Guido Grosse, Hanno Meyer and Tatyana Kuznetsova

The coastal section studied in detail extends from the Nuchcha Dzhielle River mouth 2.2 km to the east to a deep thermo-erosional ravine close to the navigation signal of Cape Mamontov Klyk (Figure 4.4-3 box B and Figure 4.4-4). The coastal relief is characterized by the steep walls of Yedomá, which are interrupted by the wide river valley of Nuchcha Dzhielle with alluvial terraces and by flat several thermoerosional valleys (logs) and smaller deep thermoerosional ravines (ovrages)

The exposure is divided into four main units (A to D). The first three, composing the steep coastal wall, are assigned to the Late Pleistocene (?) and the fourth unit consists of the various Holocene deposits.

The lowest Unit A consists of yellowish-grey, weakly bedded fine-grained sand without visible plant remains. The cryostructure is massive and the gravimetric ice content amounts 25 to 40 wt%. Many stripped ice-ground alternations, so-called polyzatic ice wedges, were formed within the unit A. Additionally, the sand unit is penetrated from above by huge ice wedges and a few small ice wedges. A transition zone of about one meter thickness, which contains numerous *in situ* grass roots, covers the organic-free sands. The Unit A is considered as fluvial (?) deposit. The transition zone reflects shallow facies conditions of a flood plain.

The subsequent Unit B consists of an alternation of four cryoturbated peaty horizons and of weakly laminated, dark-grey silty to fine sandy interbeds. The peaty horizons mostly consist of brown moss peat and they are very ice-rich (gravimetric ice content 100 to 200 wt%). The sandy interbeds contain a lot of plant remains like grass roots and twig fragments. They are relatively ice-rich (gravimetric ice content about 80 wt%) and have a banded cryostructure. Various generations of small ice wedges were observed within unit B, which can be assigned to individual peaty horizons (s. chap. 4.6.3). Often the thin ice wedges penetrate into the lower unit A. The sediments of unit B are most probably formed by alternating processes of alluvation in the flood plain.

The transition to Unit C is gradually without a sharp boundary. The unit C represents the Ice Complex deposits with their typical huge ice wedges reaching from about 25 m a.s.l. down below the sea level in some locations. The Ice Complex sequence is composed of many paleosols with peat inclusions and numerous twig fragments. This unit is subdivided into two subunits. The lower horizon of about 0 to 2 m a.s.l. consists of cryoturbated peat soils with silty to fine sandy interbeds (alevrite). The main part of unit C is formed by several weakly developed paleosol horizons and silty to fine sandy interbeds

with in situ grass roots and fragments of shrub twigs. The gravimetric ice content of unit C varies between 50 to 100 wt% for interbeds and 100 to 150 % for paleosol horizons. The cryostructure of the segregated ground ice is banded and lens-like reticulated. The Ice Complex deposits are formed on a wide flat alluvial accumulation plain probably extending from the Pronchishchev Range to the Laptev Shelf (Figure 4.4-1). In the studied coastal outcrop the Ice Complex deposits of unit C are exposed from sea level up to 20-25 m a.s.l. between 500 and 1500 m east of the Nuchcha Dzhihle River mouth. This central part of the section is flanked in the West and the East by deposits of the units A and B outcropping up to 10 m a.s.l.. Thus we conclude, the modern coast cuts a former depression in the sandy and peaty-sandy deposits of the first units, which was filled by Ice Complex deposits in the Late Pleistocene. After filling the depression the Ice Complex sediments subsequently covered the whole area.

In places, unit C is covered by a 2 m thick sequence of peat soils representing the filling of small thermokarst ponds a polygonal ponds (so-called Bylary), which have developed on the top of the Ice Complex elevation (Yedomas). They were often observed as peat spots irregularly distributed on the Yedomas surface. These uppermost deposits were assigned to the Holocene Unit D. Additionally, the unit D includes deposits of thermoerosional valleys (logs) and of the river valley. Furthermore, thermokarst deposits, belonging to unit D, were studied in a remote alas depression (about 5 km to the west, see Figure 4.4-3, box B), which is not shown in the coastal profile of Figure 4.6.1-1.



Figure 4.6.1-1: Photo of the studied coastal section Mamontov Klyk

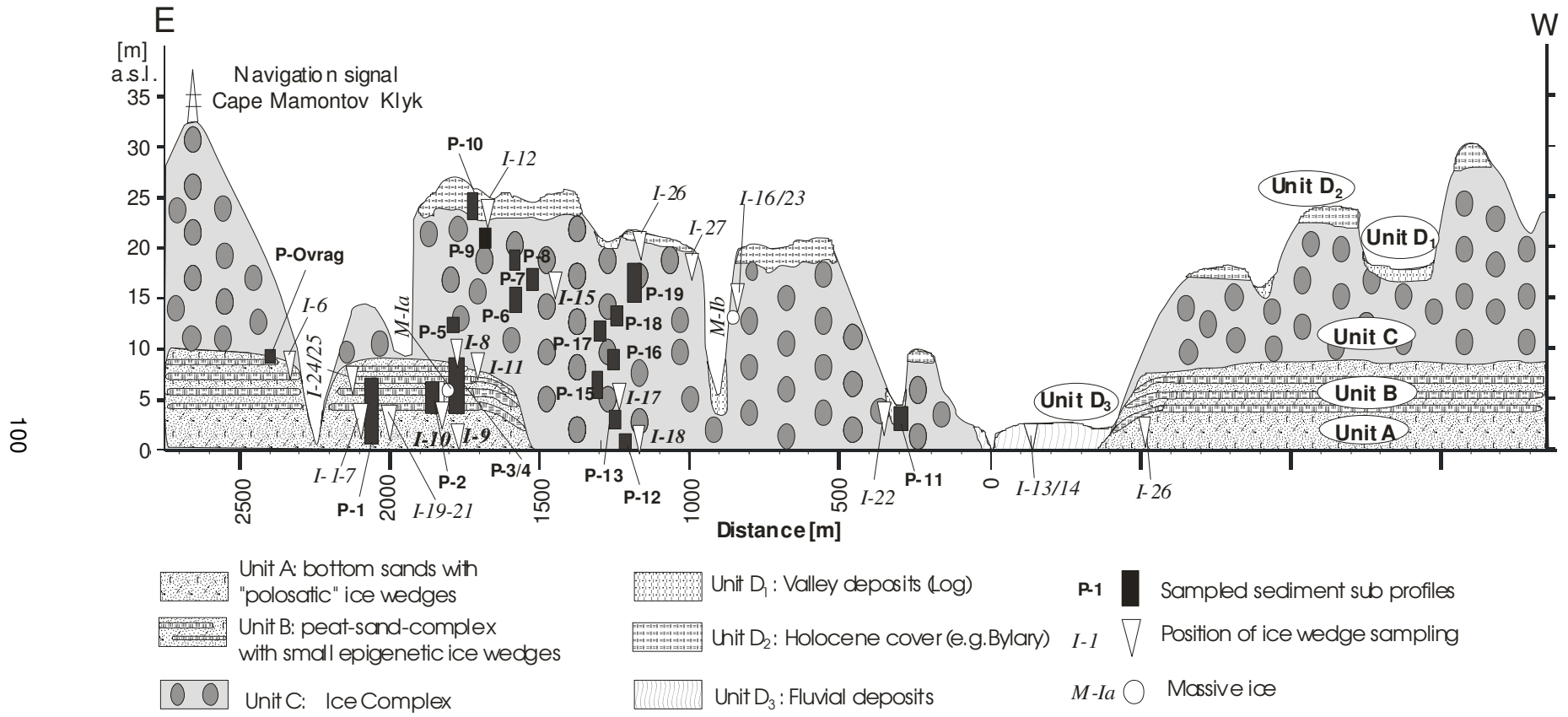


Figure 4.6.1-2: General scheme of the studied coastal section with positions of the sampled sediment: and ground ice profiles

4.6.2 Cryolithological and sedimentological studies of permafrost deposits

Lutz Schirrmeister, Viktor Kunitsky and Guido Grosse

The objectives for investigation of permafrost deposits at the coast section of Cape Mamontov Klyk are the reconstruction of Quaternary paleoenvironmental conditions and landscape history of the lowland north of the Pronchishchev Ridge. For this reason, a description and characterisation of the entire permafrost sequence was necessary concerning its stratigraphical relations as well as the cryolithological, and sedimentological features. In addition, sediment samples were collected for future paleo-ecological, sedimentological and geochemical analysis. Two composite vertical profiles as complete as possible were obtained, which extend from sea level up to the top of the coastal cliff and cover all main stratigraphical units at the site. The composite profiles consist of numerous sub-profiles, mostly exposed on thermokarst mounds (baydzherakhs). The first composed profile covers the unit A to D and the second focused on the Ice Complex deposits of unit C, which were exposed with about 20 m from the sea level to top of the cliff. Additional single sub-profiles of a Holocene thermoerosional valley (log) and of a thermokarst depression (alas) were studied (unit D), which do not belong to these composite profiles. In order to describe the special characteristics of the permafrost deposits, all sub-profiles are presented in this chapter. With this style the outcrop context for all samples becomes clear. For each sample 0.5 to 1 kg of frozen sediment was taken with a hammer and a small axe. Additional samples were collected for ice content measurement in the field lab. The gravimetric ice content is calculated in relation to the dry weight of samples. Therefore, ice supersaturated permafrost samples could have gravimetric ice contents of more than hundred percent. All sediment samples are listed in Appendix 4-5.

4.6.2.1 The first composite profile (Mak 1 to Mak 10)

The lower parts of the sub-profile Mak-1 (Fig. 6.4.2-1) and Mak-2 (Figure 6.4.2-2) expose the sandy deposits of unit A up to 4 m a.s.l.. The grey to yellowish-brown fine sand is irregularly bedded and contains single, thin, light-grey and coarser grained interbeds. No plant remains were visible. The sand seems to be completely free of organic residues. The cryostructure of this sand is massive and the gravimetric ice content is quite high for sand deposits and amounts to 25 to 40 wt %. The thaw consistence is fluid due to excessively high ice content. The samples Mak-1-1 to Mak-1-8 and Mak-2-1 belong to these deposits. In addition, the samples MAK-OSL-1 and MAK-OSL-2 were taken for further geochronological analysis with infrared stimulated luminescence (IRSL).

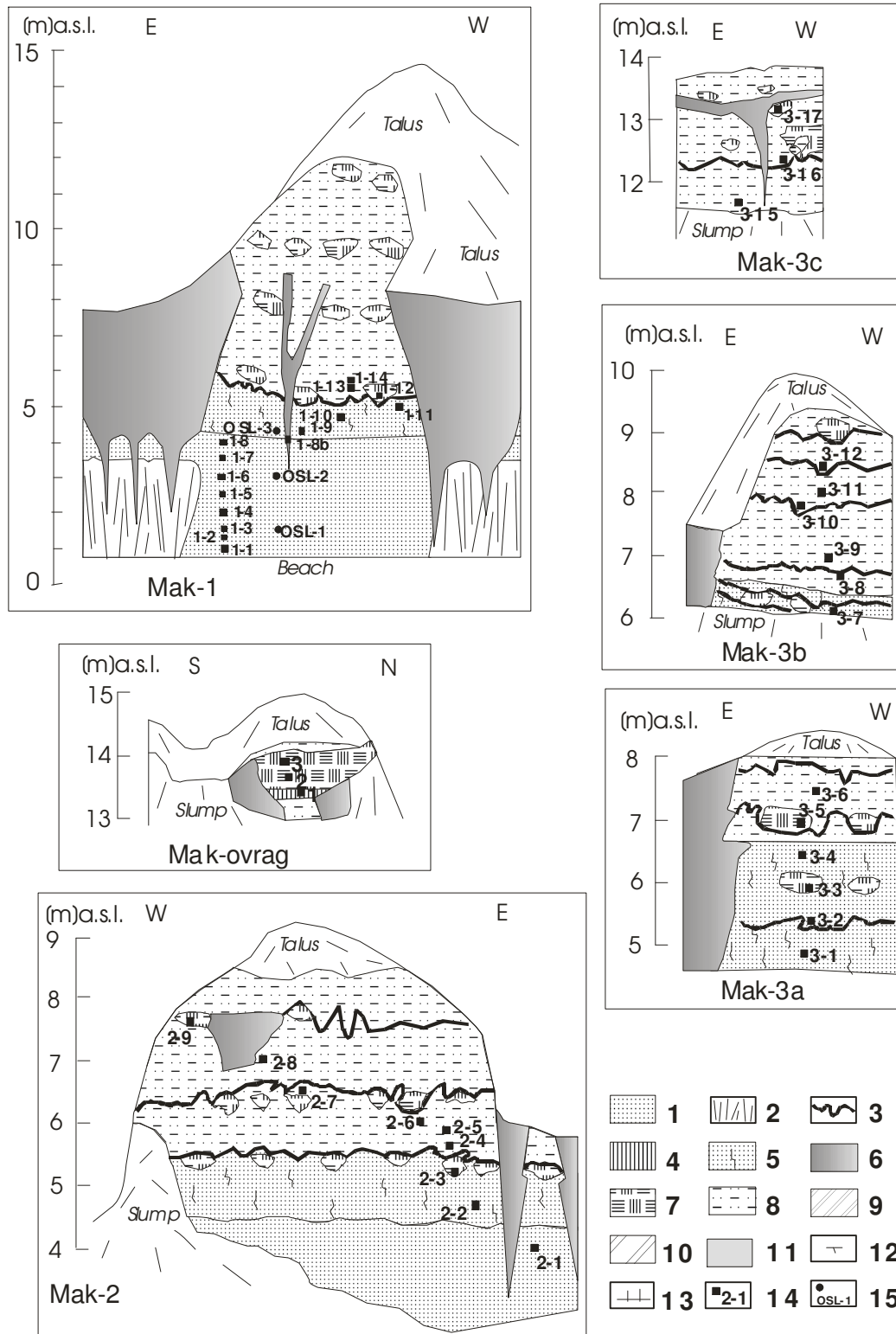


Figure 4.6.2-1: Sub profiles of the lower sands (Unit A) and of the sand-peat complex (Unit B) – lower part of the first composite profile.

A horizon of one meter thickness covers the organic-free sand deposits up to 5 m a.s.l.. It consists of similar fine-grained sand, but is containing numerous vertical *in situ* grass roots. The cryostructure is characterised by individual thin horizontal ice laminae and small vertical ice lenses around grass root remains. This horizon is considered as transition layer between unit A and the sand-peat-complex of unit B. The samples Mak-1-9 to Mak-1-11, MAK-OSL-3 and Mak-2-2 were collected from this transition layer.

The unit B, exposed between 5 to 10 m a.s.l., is characterised by an alternation of four cryoturbated peaty paleosols and three also cryoturbated sandy interbeds. This unit is exposed in the upper parts of the sub-profile Mak-1, Mak-2 and in the separately studied sub-profile Mak-ovrag (see Figure 4.6.2-1). The horizons of paleosols contain moss peat inclusions of 0.2 to 0.5 m in diameter (samples Mak-1-12 + Mak 100, Mak-1-14, Mak-2-3, 2-6 + Mak 102/103, Mak-2-9 + Mak 104). The gravimetric ice content of the peaty layer amounts to 160 to 220 wt %. The sediment direct in below the peaty layer is brownish rubiginous-spotty coloured and appears to be a former Go-soil-horizon. The dark grey silty sand interbeds contain a lot of plant detritus. Diagonally oriented black spotty lines of organic residues cross the interbeds perhaps caused by infiltration of organic matter. Special net-like structures were observed in interbed layers of the sub-profile Mak-2 that resemble syn-sedimentary water-escape structures of an instable water-supersaturated sediment. The cryostructure of the interbeds is banded (0.5 to 1 cm thick ice belts). Thin ice laminae occur parallel to the diagonal black infiltration structures. The gravimetric ice content of the interbeds amounts to 26 to 83 wt %. The samples Mak-1-12 to 14, Mak-2-3 to 2-8 and Mak-ovrag-1 to -3 belong to the sand-peat complex of unit B.

The ice wedge profiles MAK-IW-1 to MAK-IW-5 and MAK-IW-7 flank the sub profile Mak-1. The Ice wedge MAK-IW-6 adjoins to the sub-profile Mak-ovrag (see Figure 4.6.1-2 and chapter 4.6.3)

An other sand-soil sequence of unit B was studied between 4.6 to 10 m in the sub-profiles Mak-3a to Mak-3c, which were exposed at a large thermokarst mound 20 m west of the sub profile Mak-2. In contrast to the former described sub-profiles, this one does not show such a distinct peaty-sand-complex sequence. Four samples (Mak-3-1 to 3-4) were taken from a 2 m thick greyish-brown fine sand horizon with disturbed bedding, which contains small peat inclusion (1 to 10 cm), shrub root fragments. The cryostructure is massive or dotted and the gravimetric ice content reaches about 25 wt %. The sub-profile Mak-3a was studied on August 14th. One day later, the entire lower horizon was eroded and a massive ice body cropped out. Therefore, the sediment is considered as probably young reworked material. Above the massive ice body the sequence of the both sub-profiles Mak-3a and Mak-3c is the same.

Both sub-profiles continue with a 0.6 to 0.8 m thick cryoturbated paleosol horizon with peat inclusions (\varnothing 10 to 15 cm), grey to greyish-brown, black spotted silty fine sand (sample Mak-3-5, 3-7 + Mak 108). The cryostructure presents some diagonal irregularly distributed ice lenses. The gravimetric ice

content amounts to 21 to 60 wt %. The next horizon of about 1 m thickness consists of alternating bedded grey silt and light-greyish-brown fine sand layers (samples Mak-3-6, 3-8 + Mak 108, Mak-3-9). The single laminae are irregularly bedded and contain sedge remains, roots and wood fragments. The cryostructure of this layer is massive and the gravimetric ice content is of about 21 wt %. It is interpreted as a shallow part of a flood plain area. The second paleosol of the sub-profile Mak-3 is dark coloured, cryoturbated and contains a lot of detritic plant remains (sample Mak-3-10). It looks like a fluvial drift line near the shore. The sandy interbed above of about 1 m thickness (sample Mak-3-11 to 3-13) is similar to the sandy horizon described above. The third peaty paleosol at 10 m a.s.l. is also similar to the already described paleosol horizons (sample Mak-3-14).

A smaller sub-profile (Mak-3c) of only 2 m thickness was exposed near the top of the thermokarst mound between 11.7 and 13.7 m a.s.l. (Figure 4.6.2-1). A yellowish, ice-rich, fine-grained sand (sample Mak-3-14) with fine lens-like cryostructure (gravimetric ice content 50 wt %) is covered by the fourth cryoturbated paleosol with peat inclusions (sample Mak-3-15 + Mak 106, Mak 3-17 + Mak 105). This sub-profile is penetrated by the ice wedge MAK-IW-11 (see chapter 4.6.3).

The transition between unit B and the Ice Complex deposits of unit C seems to be exposed in the sub-profile Mak-4 between 11.7 and 12.7 m a.s.l. (Figure 4.6.2). The lowest part of this sub-profile is a weakly distinct, cryoturbated brownish paleosol (sample Mak-4-1). The following layer consists of yellowish-grey fine sand with some plant remains (Mak-4-2). The cryostructure is banded. Diagonal, 1 to 2 cm long fine ice lenses were observed. The gravimetric ice content is 46 to 48 wt %. The cryolithological change of the permafrost deposits is recognisable in the grey fine sandy silty sediment (alevrite) with single small shrub fragments. The cryostructure is banded and fine lens-like with broken ice lenses (samples Mak-4-3, Mak-4-4 + Mak 109). The gravimetric ice content is 64 to 70 wt %. The small ice wedge MAK-IW-8 penetrates this subprofile (see chapter 4.6.3)

The sub-profiles Mak-5 to Mak-9 reflect the sequence of the Ice Complex deposits of unit B between 13.5 and 22.5 m a.s.l.. Largely, these five sub-profiles are composed similar. Therefore, a detailed description of each several sub-profile (Figure 4.6.2-2) is dispensable. The deposits of unit C are characterised by greyish-brown fine-sandy silt (alevrite), which contains shrub wood fragments (\varnothing 0.5 to 1 cm) and smaller plant residues (e.g. in situ grass roots). Weakly developed paleosol horizons, containing small peat inclusions and more brownish coloured sediment were detected. The cryostructure of these deposits is mainly banded and lens-like (coarse to fine ice lenses). The gravimetric ice content amounts 50 to 90 wt % (max 220 wt%).

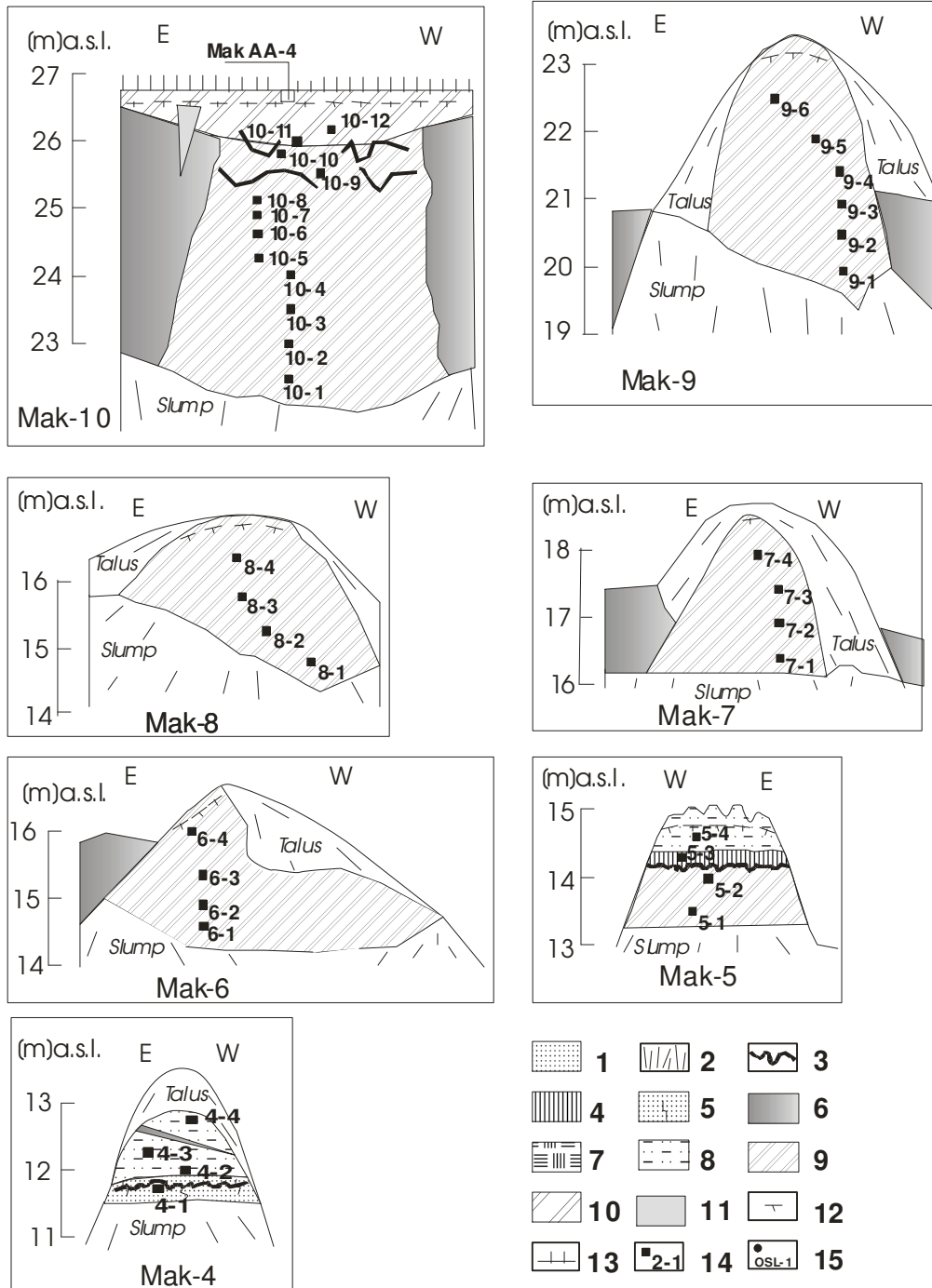


Figure 4.6.2-2: Sub profiles of the of the part of the first composite profile - Ice Complex (Unit C) and Holocene deposits (Unit D).

The transition from Unit C to Holocene deposits, which cover the Ice Complex sequence in places, is well shown by the sub-profile Mak-10 between 23 and 26.7 m a.s.l. (Figure 4.6.2-2). The lower part (samples Mak-10-1 to 10-6) of this sub-profile consists of the similar greyish-brown, ice-rich fine sandy silt as already described. The upper part of 1.5 m thickness discordantly covers the Ice Complex deposits and contains two well-developed cryoturbated peat soil horizons with loamy interbeds (samples Mak-10-7 to 10-11). The entire sub-profile was sampled additionally for pedological analysis (samples Mak 112 to 120, *see chapter 4.6.4*) The horizon is very ice-rich (gravimetric ice content 84 to 136 wt %) and the cryostructure is ice-banded and lens-like. This sub-profile exposes peaty loamy fillings of a small depression. These forms of depressions and their fillings were frequently observed in form of peat patches (10 to 50 m in diameter) on the surface of Yedoma elevations. The filling of this small thermokarst-like depression contains thin white ice wedges (MAK-IW-12, *see chapter 4.6.3*) probably of Holocene origin.

4.6.2.2 The second composite profile (Mak-12, -13 and 15 to 19)

The second composite profile covers the Ice Complex deposits of unit C from the sea level to the top of the cliff at 20 m a.s.l. (Figure 4.6.1-1). The lowest sub-profile Mak-12 exposes two cryoturbated peaty paleosols with a silty interbed between 0 and 2 m a.s.l. (Figure 4.6.2-3). The cryostructure of this interbed is banded and lens-like. Apart from these peaty horizons all other sub-profiles situated above (Mak-13 and Mak-15 to Mak-19) are more or less similar in cryolithology and sedimentology. Therefore its description will be briefly summarized only. The individual sub-profiles as well as the sample positions are presented in Figures 4.6.2-3. The Ice Complex sequence is composed of greyish-brown ice-rich fine sandy silt (alevrite) and includes weakly developed paleosol horizons with some plant remains like shrub fragments, leaves and detritic organic matter. The cryostructure is banded and dominantly lens-like, sometimes with broken ice lenses. The gravimetric ice content varies between 70 and 115 wt %. The uppermost part of the sub-profile Mak-19 probably belongs to the Holocene cover (unit D), as more sandy sediment and peat inclusions occur, and the position is directly below the Yedoma surface.

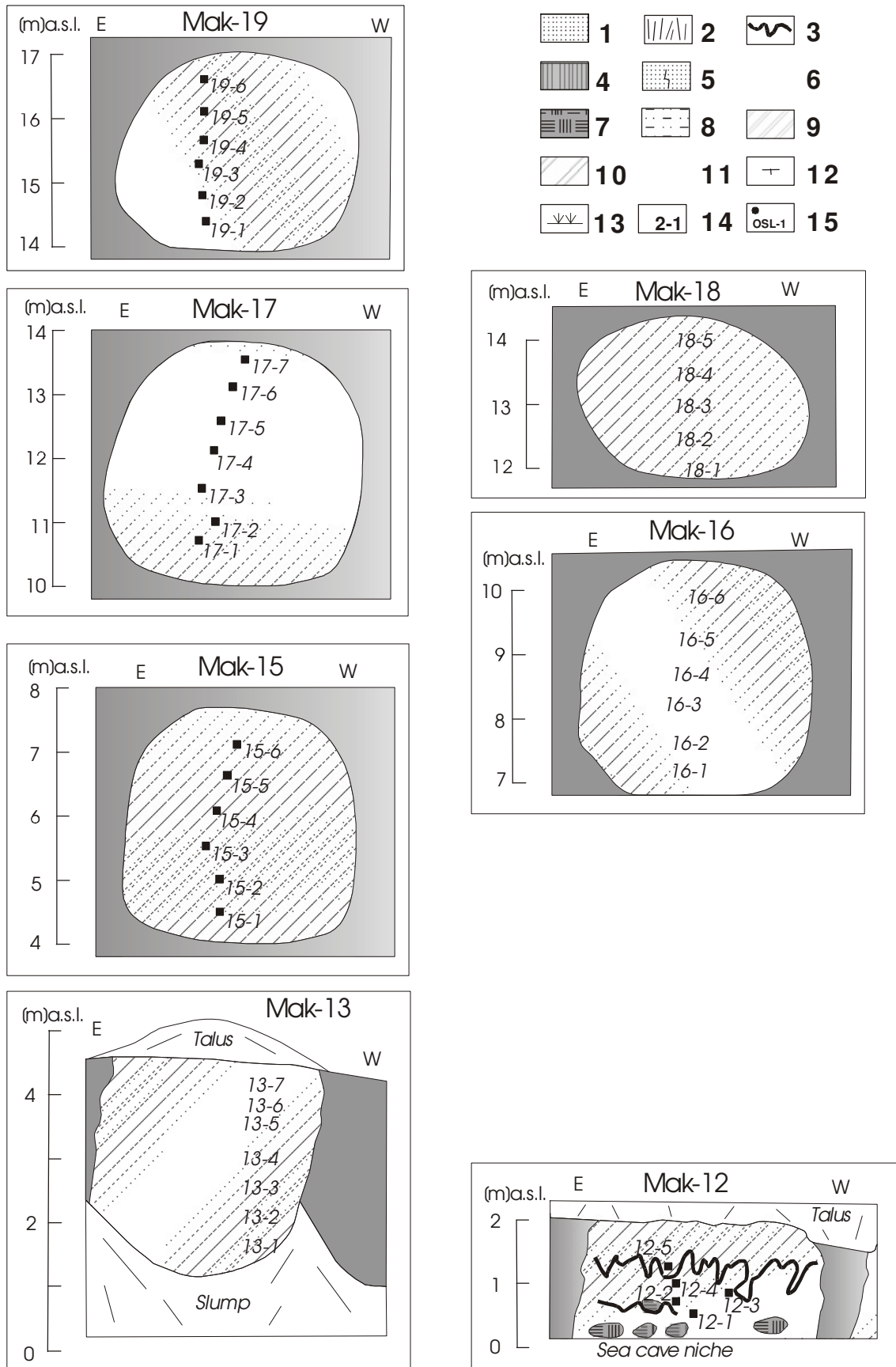


Figure 4.6.3-3: Sub profiles of the second composite profile – Ice Complex (Unit C) and Holocene deposits (Unit D)

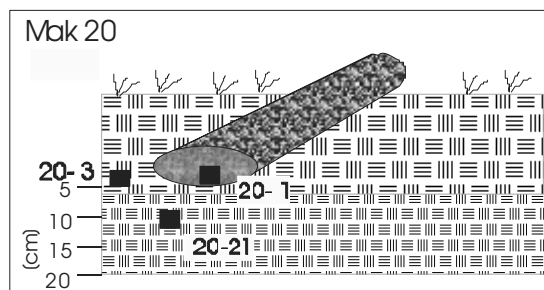
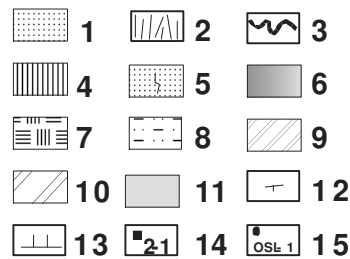
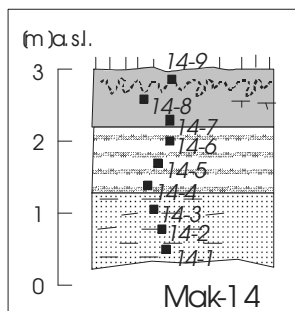
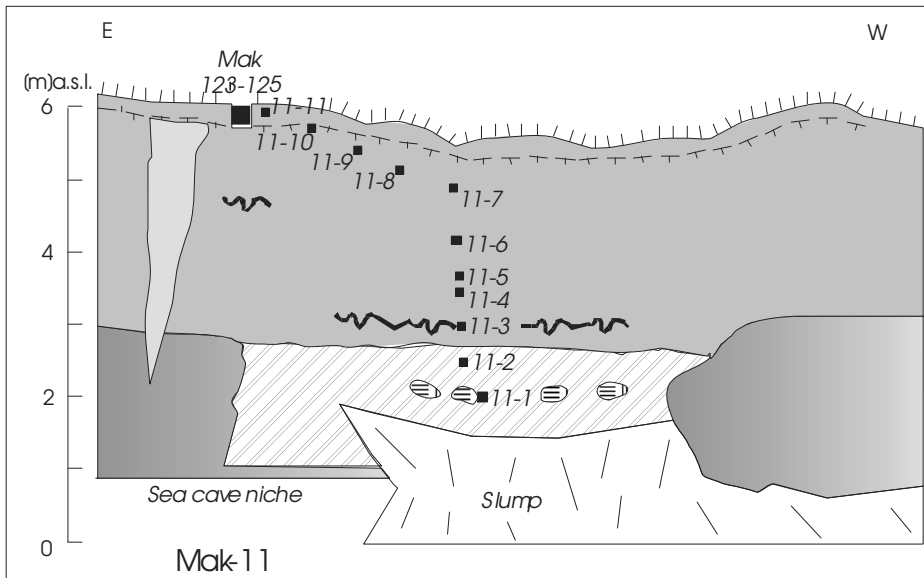


Figure 4.6.2-4: Additional sub profiles of Holocene thermokarst deposits and of a marine terrace

4.6.2.3 Additional sampled sub-profiles (Mak-11, Mak-14, Mak-20/21)

The sub-profile Mak-11 is located about 300m east of the mouth of the Nuchcha Dzhielle River (see Figure 4.6.1-2). It exposes deposits of a thermoerosional valley (unit D) between 0 and 6 m a.s.l., probably covering Ice Complex deposit (unit C). The sub-profile is flanked by ice wedges, which were especially studied (e.g. MAK-IW-22, see chap. 4.6.3). The lower part contains two greyish-brown paleosol horizons with peat inclusions (samples Mak-11-1 to 11-3). The cryostructure is banded, partly massive or lens-like reticulated. The gravimetric ice content amounts to about 50 wt %. Small ground wedges of about 10 cm length were observed 3 m a.s.l.. The upper part of the sub-profile consists of greyish-brown, well-bedded silty fine sand, with some vertically oriented grass roots. It contains additional wood fragments and peat inclusions. The cryostructure is banded with fine ice lenses, sometimes broken ice lenses (gravimetric ice content 46 to 130 wt %). The uppermost 0.5 m was sampled additionally for pedological analysis (samples Mak 123 to 125, see chapter. 4.6.4).

Deposits of a thermokarst depression (alas) were studied about 8 km west of the Nuchcha Dzhielle river mouth due to the absence of such sequences at the coast of Cape Mamontov Klyk (Figure 4.4-3, box B; Figure 4.4-5). The profile Mak-14 is composed of three different parts (Figure 4.6.2-4). The lowest meter consists of clayish fine-sandy silt with plant detritus and is partly brownish coloured. The cryostructure is coarse lens-like and the gravimetric ice content of about 30 wt %. This part is covered by a horizon of interbedding of 2-3 cm thick peat layers and sandy silt layers. Thin ice bands occur. The gravimetric ice content varies between 45 and 110 wt %). A cryoturbated peaty paleosol completes the sequence. The cryostructure is characterized by thick ice belts and vertical ice veins (gravimetric ice content 165 wt %).

Two more profiles are very small and include buried driftwood covered by moss peat. Both profiles are located at the marine terrace of the Bay Kuba Betyuene about 5 km east of Cape Mamontov Klyk (Figure 4.4.-3). The dating of the buried driftwood possibly gives a clue on the genesis of this vast marine terrace e.g. by supposed neotectonic uplift.





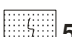








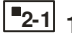
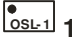
-  1 Fine-grained quartz-feldspar sand; brownish-grey (thawed), light-grey (frozen); horizontal, flaser and cross bedded; without visible plant remains, frozen; with ice cement; fluid after thawing
-  2 Sand-Ice wedge (polosatic), close alternation (mm to cm) of sand and ice veins, 2-3 m wide
-  3 Cryoturbated frozen paleosol horizon, no to scale of the profile
-  4 Cryoturbated frozen paleosol horizon, to scale of the profile
-  5 Silty fine-grained quartz-feldspar sand; brownish-grey; weakly bedded; with vertical in situ grass roots, frozen, with ice cement, in places with short ice belts near ice wedges
-  6 Ice wedge grey, compact
-  7 Autochthonous brownish peat, grass and moss remains, in places with roots and twigs of dwarf shrubs, frozen, ice-rich, formed nests (inclusions) of various diameters and several lenses
-  8 Fine-grained quartz-feldspar sand; brownish-grey; with loamy (alevrite) interbeds and lenses; with vertical in situ grass roots, in places with roots and twigs of dwarf shrubs; frozen, fine lens-like cryostructure, some banded ice belts
-  9 Dark grey loam (alevrite); alternate bedding (silt, fine sand); with vertical in situ grass roots; frozen, fine lens-like cryostructure, sequent concave banded ice belts
-  10 Dark grey loam (alevrite); with peat inclusions; bedded; with vertical in situ grass roots; frozen, horizontal ice belts
-  11 White ice wedge; less compact; with small silty parts, on the top of giant, compact grey ice wedges
-  12 Active layer boundary
-  13 Vegetation cover of subarctic tundra
-  14 Sediment sample position and sample number
-  15 Sample position for luminescence dating and sample number

Figure 4.6.2-5: Legend to the Figures 4.6.2-1 to 4.6.2-4

4.6.3 ICE WEDGES OF CAPE MAMONTOV KLYK

Hanno Meyer and Alexander Dereviagin

4.6.3.1 Introduction

The studies on ice wedges for palaeoclimate reconstruction of winter temperatures started in 1998 and, since then, were applied to different locations in the Laptev Sea region. Among these localities are the Bykovsky Peninsula (Meyer et al. 2002a), Big Lyakhovsky Island (Meyer et al. 2002b), different sites in the Lena Delta (Schirrmeister et al., 2004) and on the New Siberian Islands and Oyagoysky Yar (unpublished yet). In addition to Mamontov Klyk, sampled this year, data from several sites of Taymyr Peninsula can be used, both being located in the western Laptev Sea province representing the westernmost (closest to the Atlantic) sampling sites of all visited regions. The method is based upon the fact that the stable isotopic composition of ice wedges is genetically closely linked with the melting of the seasonal snow cover and hence, well correlated with mean winter temperatures (e.g. Vaikmäe, 1989).

Since ice wedges are predominantly vertically oriented features, they are not limited by sedimentological boundaries. Therefore, ice wedges may penetrate into older sediments (epigenetic ice wedge growth) but also keep up with the sedimentation (syngenetic ice wedge growth). Accordingly, within the same sedimentary unit, ice wedges of different generations may occur. Every ice wedge generation is related to a (new) stable surface. Consequently, the question arises from which sedimentological unit (and hence from which palaeosurface) an ice wedge originates. A detailed description of the outcrop is therefore necessary to gain an understanding of the genesis of the whole section.

During this field season, studies of the ice and water of the Cape Mamontov Klyk area were used for palaeoclimate and palaeoenvironmental interpretation of a terrestrial periglacial locality. These studies will also help to understand the genesis of subsea permafrost ice – to be drilled in the 2004 field campaign – e.g. if subsea ice is of terrestrial origin or refrozen Laptev Sea water. Therefore, the selected samples of all types of ice (recent and paleo ice wedge ice, texture ice, massive ice as well as cavity ice) and water (meteoric water, ground water, surface water) will be analysed for their stable isotope composition as well as for hydrochemistry to understand the regional hydrological and cryolithological regime. In total, 422 samples were taken, among them 226 samples from 28 ice wedges, 24 from ice-sand wedges ("polosatics"), 110 samples of texture ice, 7 of massive ice of unknown origin as well as 7 samples of snow, 5 samples of rain, 22 samples of surface water (e. g. sea water, river water, pond water) and 3 samples of ground water (see Appendix 4-6).

4.6.4.2 The ice wedges in the lower sands (Unit A) and in the sand-peat-complex (Unit B)

Section MAK-IW-1-5, MAK-IW-7 (corresponding to the sediment sub profile Mak-1, see chapter 4.6.2.1)

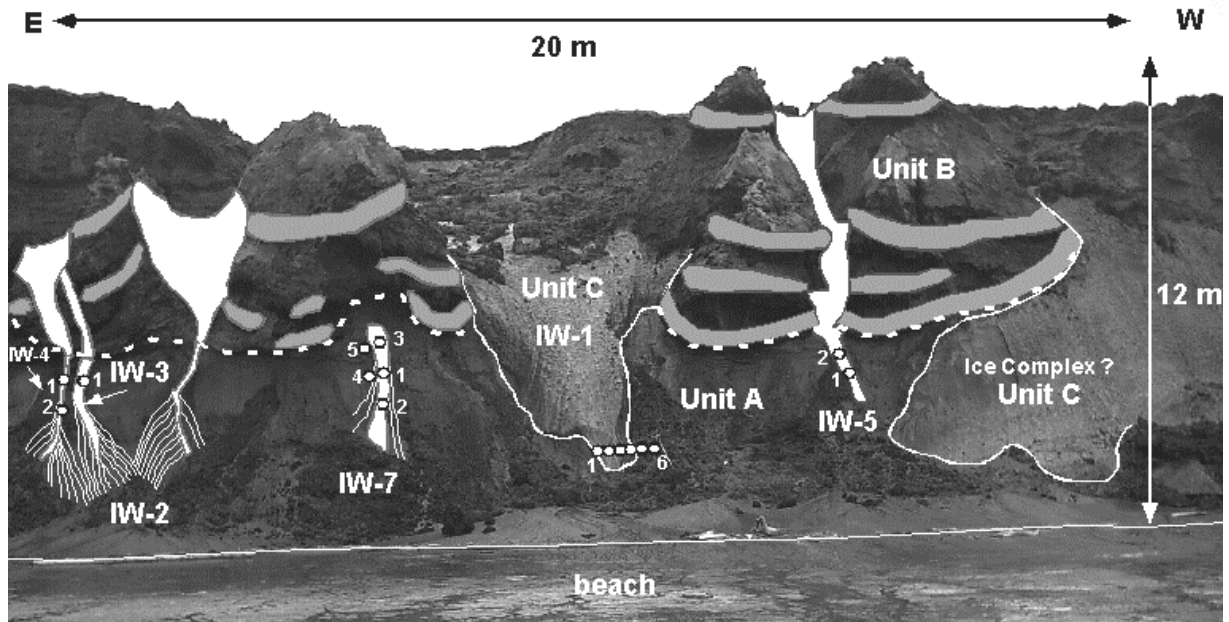


Figure 4.6.3-1: Ice wedges MAK-IW-1 to –IW-5 and MAK-IW-7 with sampling points. MAK-IW-2 is shown in detail in Figure 4.6.3-2.

The section is located at the coast and comprises Unit A (lower sands) in contact with the overlying Unit B (peat-sand complex) (Figure 4.6.3-1). The sands of Unit A contain ice-sand wedges (so called “polosatics”), which are characterised by a vertically-oriented tiger-striped sequence of ice veins and sand veins. These ice-sand wedges are the oldest cryolithological features in the section. Unit B consists of four peat horizons, which were interpreted as stable surfaces (maybe of a floodplain or old branches of a palaeo-river, which were cut from the main river and therefore fell dry and then were subsequently flooded again). Each of these stable surfaces is linked with a generation of ice wedges. These different generations of ice wedges stick one into the other. The older deposits of Unit A and Unit B are dissected by a series of very large ice wedges of Unit C, which were attributed to the Ice Complex.

MAK-IW-1

Description: MAK-IW-1 is a 7-8 m high ice wedge, which is not covered by sediment and where the upper boundary is not visible. The ice wedge shows some syngenetic structures in the upper part such as shoulders at the sides of the ice wedge, one of which seem to be associated with the first peat of Unit B (peat-sand-complex). Especially in the bottom part, the ice wedge is confined by subvertically structured very ice-rich texture ice (“polosatic”-like). The ice wedge

reaches a width of about 3.5 to 4 metres at the top and narrows downwards, where the width does not exceed 0.7 m. The ice is relatively pure and white, with milky appearance containing only small quantities of sediment and organic matter. Vertical oriented ice veins, 1-2 mm wide, are well developed. Additionally, the ice is structured by the high amount of gas bubbles, mostly < 0.5 mm, which are often arranged as "strings of beads". Four samples were taken from this ice wedge, two in the adjacent texture ice. The height of the sampling profile is 1.5 m a.s.l..

Interpretation: Most probably, MAK-IW-1 is an epigenetic ice wedge of the Ice Complex (Unit C) penetrating the lower sands of Unit A. Syngenetic forms associated with the first peat may indicate the onset of ice wedge growth at that time.

MAK-IW-2

Description: MAK-IW-2 is a sequence of ice-sand wedges ("polosatics"). At least three systems and predominant directions of these ice wedges, intersecting with each other could be distinguished, all of them associated with the lower sands of Unit A (Figure 4.6.3-2). However, these systems seem to originate in 0.2 m thin ice wedges originating from Unit B (or *vice versa* have led to the growth of these small ice wedges).

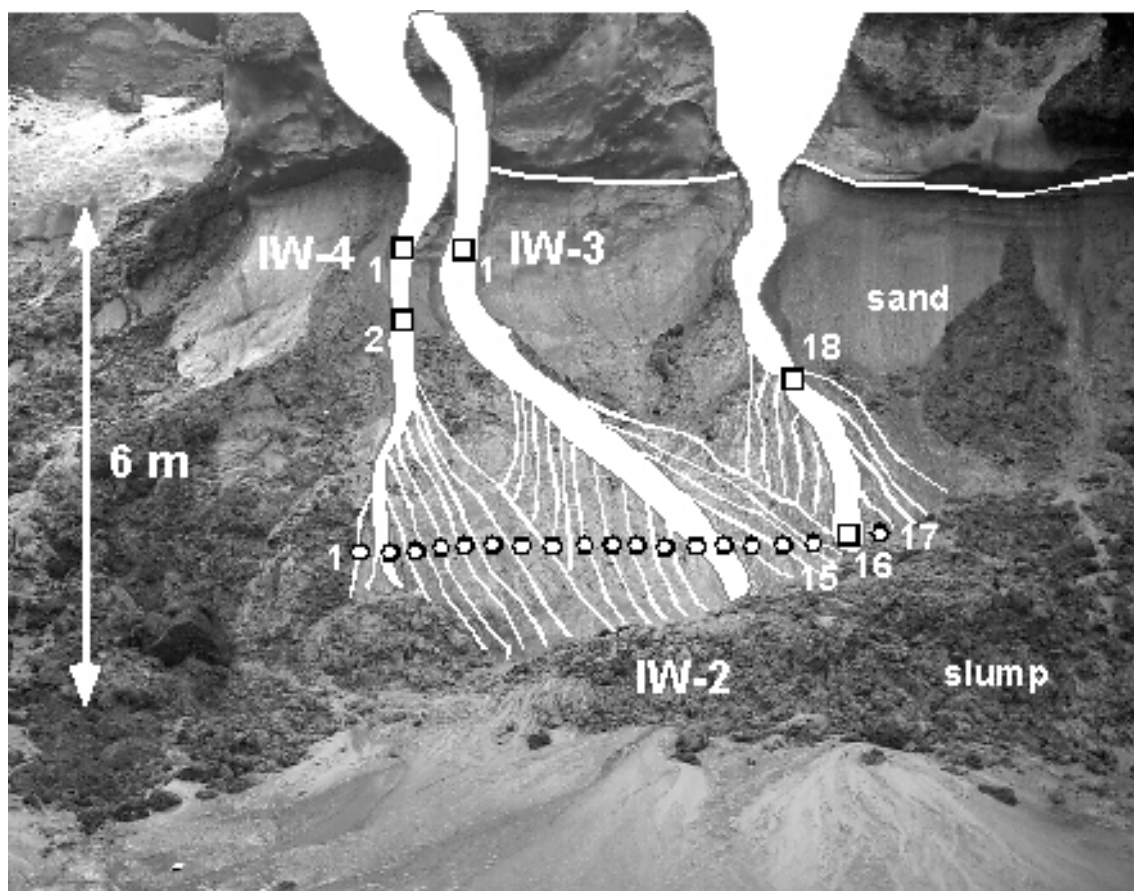


Figure 4.6.3-2: Section MAK-IW-2 with sampling points.

The ice is very pure and transparent and contains no organic matter. Single ice veins are well developed and between 4 and 12 mm (mean 8 mm) thick, interrupted by 1 m thick sediment veins. This leads to a clear subvertical structure of the ice, where eight ice veins were counted for a length of 5 cm. Gas bubbles, mostly < 1 mm, are randomly oriented in the ice. In 20 cm intervals, 17 samples were taken from this system of ice-sand wedges. The height of the sampling profile is 1 m a.s.l..

Interpretation: MAK-IW-2 is composed of different systems of ice-sand veins of the lower sands of Unit A, representing the oldest ice in the outcrop.

MAK-IW-3, IW-4, IW-5, IW-7

Description: All these ice wedges are relatively narrow, about 0.2 m wide, originate in Unit B peats and, in the lower part, are in contact with ice-sand wedges of Unit A. All four ice wedges are similar: consisting of clear, transparent ice in which vertical structures (e.g. ice veins) are recognisable. The mineral content of the ice is rather low. MAK-IW-3 contains small amounts of organic matter within the ice, but MAK-IW-4, IW-5 and IW-7 are characterised by high content of organic matter (plant remains and peat fragments). In general, the gas bubbles in these ice wedges are relatively big (= 2 mm), although smaller bubbles (in sub-mm size) occur. In total, 10 samples were taken by axe from these 4 ice wedges. The height of the sampling is around 5 m a.s.l. for ice wedges IW-3, IW-4, IW-5. Only IW-7 was sampled slightly higher above sea level (5.5 m, 6.0 m, 6.5 m)

Interpretation: MAK-IW-7 is certainly linked with the 1st peat of Unit B, whereas IW-3 and IW-4 originate at least in the 1st peat, maybe in a younger stage (2nd or 3rd peat). MAK-IW-5 is clearly associated with the 2nd peat, thus, representing the second youngest stage of Unit B ice wedges. Since all these ice wedges are relatively small, it can be assumed that they were formed relatively fast and that the stable surface conditions did not persist for a long time. Only ice wedges linked with the 3rd peat reach in some cases widths of about 1.5 m. This leads to the assumption that the stable surface condition associated with the 3rd peat may have lasted longer than the others.

MAK-IW-19 to IW-21

Description and Interpretation: The top of this 2.5 m high outcrop is located at the coast in a height of 7.5 m a.s.l.. Since it is approximately 80 m to the west of outcrop MAK-IW-1 to IW-5, mainly the same sedimentological situation is displayed here. At least four generations of ice wedges of Unit B can be distinguished. MAK-IW-21 is the oldest generation of Unit B ice wedges certainly linked with the first peat horizon. It is marked with an asterisk because it was buried again, when the photograph was taken. One sample was taken by axe from this ice wedge. MAK-IW-20 is the next younger generation of ice wedges within the second peat layer. Here, two samples were taken by axe. At

least, two more generations of Unit B ice wedges were observed: one originating under the third peat, another one originating in the third peat. Both could not be sampled due to difficult outcrop conditions. All these ice wedges are as small as 0.1 to 0.2 m in width and 0.3 m to 1.2 m in height.

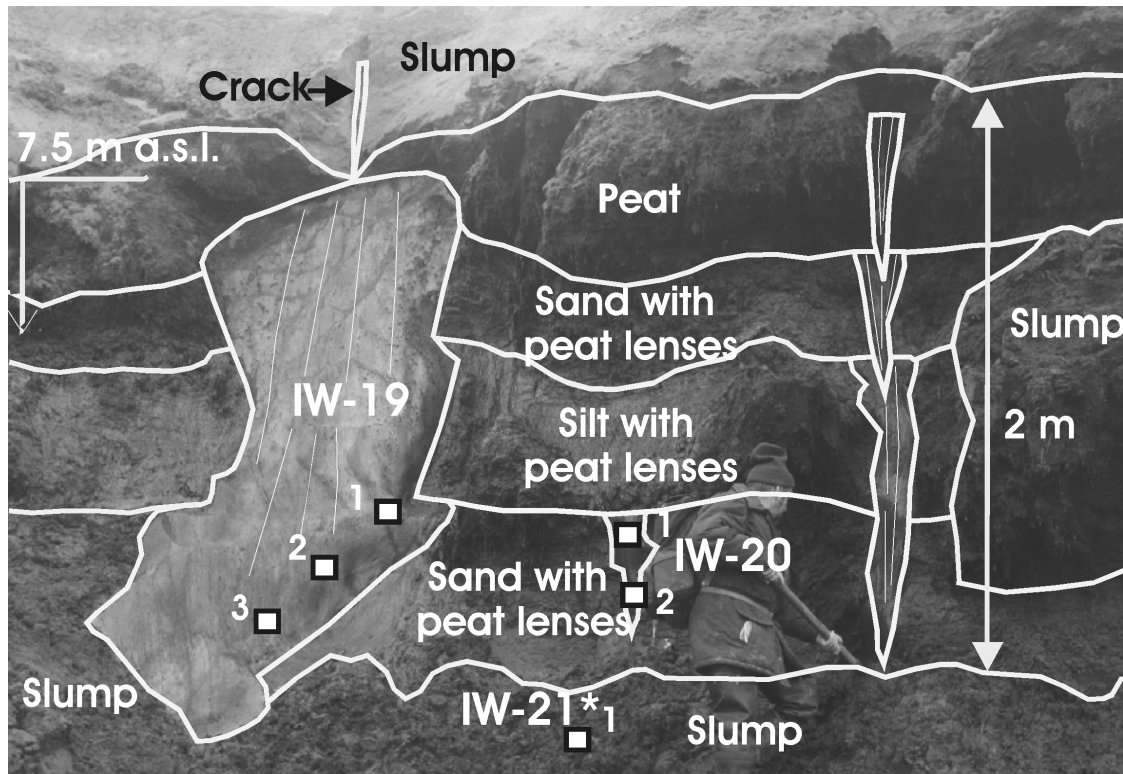


Figure 4.6.3-3: Outcrop MAK-IW-19 to -21 with sampling points

Compared to that, MAK-IW-19 is much bigger in size and at least 2.5 m high and 0.8 m wide (Figure 4.6.3-3). Three samples were retrieved by means of an axe. Similar ice wedges were observed in section MAK-IW-1 to IW-5, where outcrop conditions made sampling impossible. Additionally, MAK-IW-19 is buried by sands of Unit B and located at the same height than the 3rd peat. Therefore, this ice wedge belongs most likely to Unit B and not to the Ice Complex. A small ice vein above ice wedge MAK-IW-19 supports this assumption. The ice wedges of bigger size could signify that during the formation of Unit B, one stable surface might have persisted longer (possibly linked with the growth of the third peat). Possibly, two different types of ice wedges were formed in the same type of deposits.

Section MAK-IW-6 (corresponding to the sediment sub profile Mak-Ovrag, see chapter 4.6.2.3)

Description: At a height of about 13 m a.s.l., two ice wedges (called MAK-IW-6) were sampled in a 7 to 8 m deep thermo-erosional gully (Russian: Ovrag) approximately 100 m S the shoreline and 200 m W of the navigation signal "Cape Mamontov Klyk". Both are about 0.5 m wide and originate in a

sphagnum-rich peat of Unit B, which thickness is about 30-40 cm (Figure 4.6.3-4). The visible thickness of sand lenses enclosing the ice wedges is about 20-40 cm. The ice wedge is characterized by clean, white ice with numerous air bubbles without clear vertical structure. In total, 8 samples were taken from these two ice wedges in 15 cm increments using an ice screw. The height of the sampling profile is 13.5 m a.s.l. for the left ice wedge and slightly lower (13.3 m a.s.l.) for the right ice wedge.

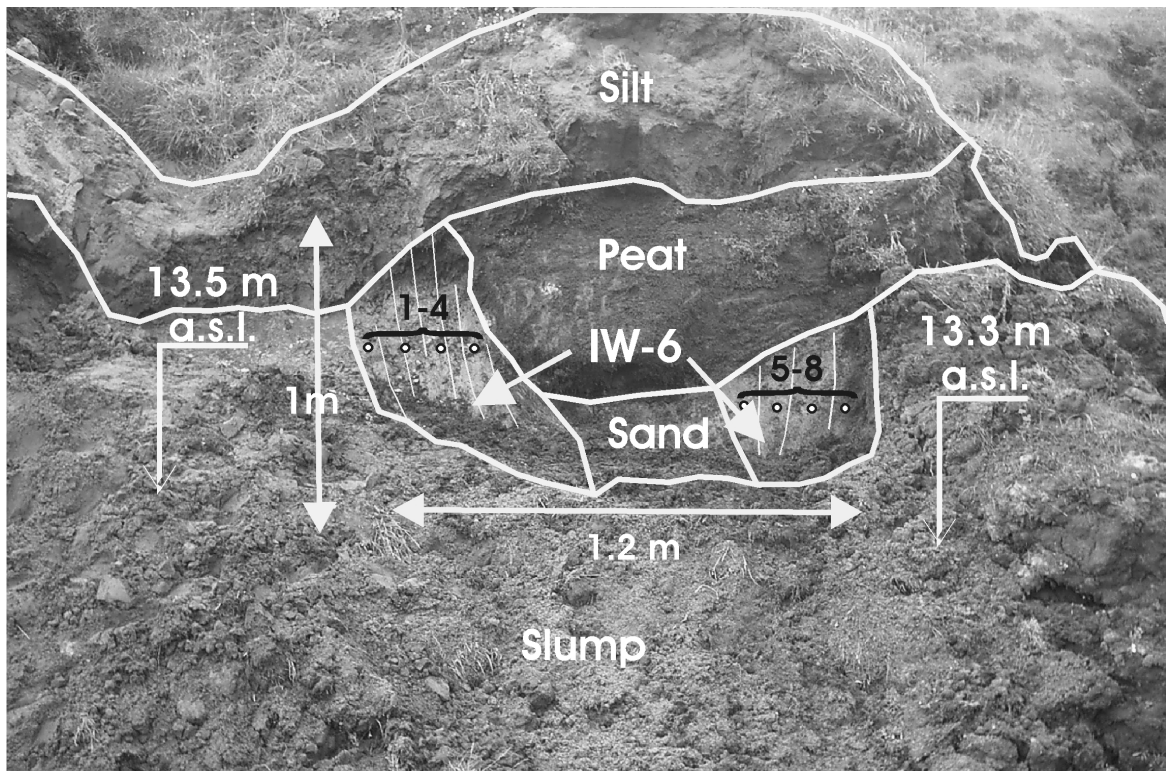


Figure 4.6.3-4: Outcrop MAK-IW-6 with sampling points (see also Figure 4.6.2-1)

Interpretation: Although it is not exactly known to which peat horizon MAK-IW-6 belongs, it is certainly a Unit B ice wedge. With regard to its height above sea level, MAK-IW-6 can most probably be attributed to the 3rd or 4th peat, thus representing a younger stage of genesis than MAK-IW-2 to IW-7.

MAK-IW-8 (corresponding to the sediment sub profile Mak-4, see chapter 4.6.2-1)

Description: At a height of about 12.5 to 13.0 m a.s.l., a 0.3 m wide ice wedge named MAK-IW-8 (see Figure 4.6.2-1 Mak-4) was sampled. Three samples were taken by axe from this ice wedge.

Interpretation: This ice wedge is located in the boundary between Ice Complex and Unit B. It is located below one of the two uppermost peat horizons of Unit B (3rd or 4th peat), most likely the 4th one. Due to the close distance and

approximately same height, it is considered as an equivalent of ice wedge MAK-IW-11.

MAK-IW-9

Description: MAK-IW-9 is a 0.2 wide ice wedge with well-developed vertical orientation (Figure 4.6.3-5). The ice is slightly milky white and transparent with clear subvertical structures. Single ice veins of 2-3 mm in width are common in this ice wedge. Many gas bubbles of different sizes (0.5 – 2 mm) but without predominant orientation occur. The content of mineral particles is medium increasing to the sides of the ice wedge, where single laminae may reach 3 mm of thickness. The organic content is low, nevertheless, numerous lemming coprolithes were found within the ice wedge and sampled for dating (MAK-¹⁴C-2). Three samples were taken from the ice wedge (in 5 cm intervals) and one sample from the adjacent ice-sand wedges.

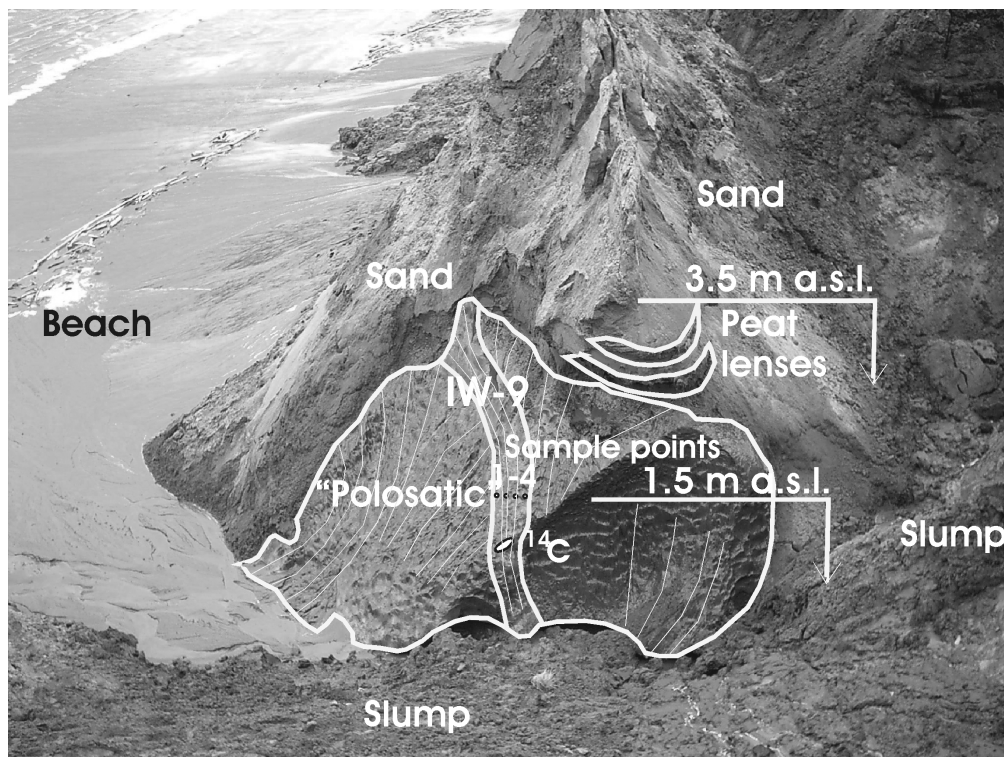


Figure 4.6.3-5: Outcrop MAK-IW-9 with sampling points

Interpretation: Genetically, this ice wedge is enclosed by ice-sand veins, which are in general discordantly cut, except in the lower parts of its landward side. MAK-IW-9 is certainly linked with the first peat horizon, thus belonging to a series of small ice wedges penetrating Unit A from above.

MAK-IW-10 (corresponding to the sediment sub profile Mak-3a, Chapter 4.6.2.1)

Description and Interpretation: Outcrop MAK-IW-10 shows the contact between Unit A and Unit B in detail. Ice-sand wedges of Unit A laterally confine a pair of twinned ice wedges. At the left side, a massive ice body of unknown origin was distinguished from ice wedge ice by the lack of vertical structures within the ice. Sedimentologically, this outcrop belongs to Unit A, nevertheless, the genesis of the ice wedges is related to Unit B. The right ice wedge is certainly linked with the first peat, whereas the left ice wedge most probably can be attributed to the second peat layer. Small ice veins of both ice wedges continue into the overlying sediment layer, where they originate in the peat layers. This may be due to a sudden increase of the sedimentation rate impeding that the ice wedges could keep up with the sedimentation. Four samples were taken from the massive ice body (* two of them approximately 2 m further to the left of Figure 4.6.3-6 and 19 samples from the ice wedges, ice-sand wedges and the small ice veins in the upper part. The height of the outcrop is between 4.7 m and 6.7 m a.s.l..

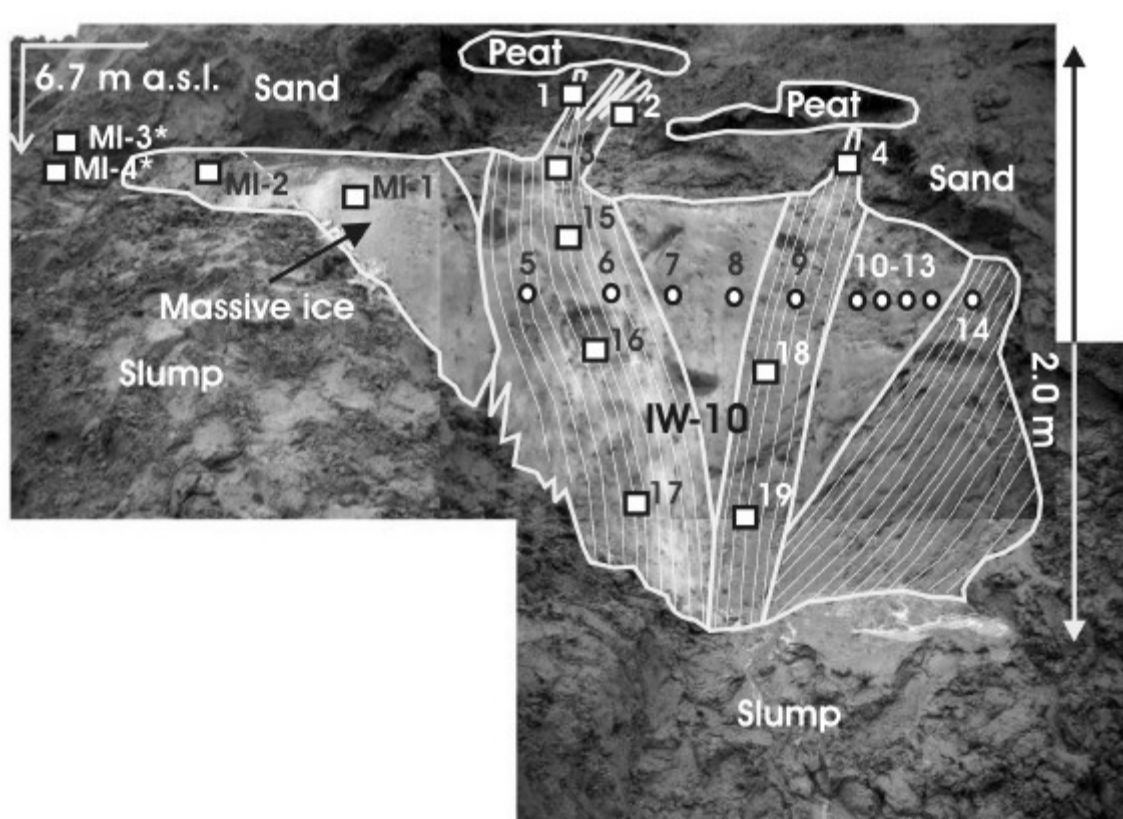


Figure 4.6.3-6: Outcrop MAK-IW-10 with sampling points (see also Figure 4.6.2-1).

MAK-IW-11 (corresponding to the sediment sub profile Mak-3c, chapter 4.6.2.1)

Description: Ice wedge MAK-IW-11 is 0.25 to 0.05 m wide narrowing from above, with vertical structures and transparent ice with brownish colour, due to a relatively high content of mineral particles. Single ice veins of 2-4 mm width are observed. The organic content is rather low, but a stick of 0.5 cm in diameter was found in the ice, in the bottom part of the ice wedge (MAK-¹⁴C-3). At the top, the ice wedge is in contact with a well-developed ice belt of 5-7 cm thickness probably characterising a stable surface. A peat layer, possibly the fourth peat within Unit B, just above the ice belt, supports this assumption. Five samples were taken from the ice wedge and two samples from the ice belts. The ice wedge is located at the top of a thermokarst mound, with a height of 12.9 m a.s.l (Figure 4.6.3-7).

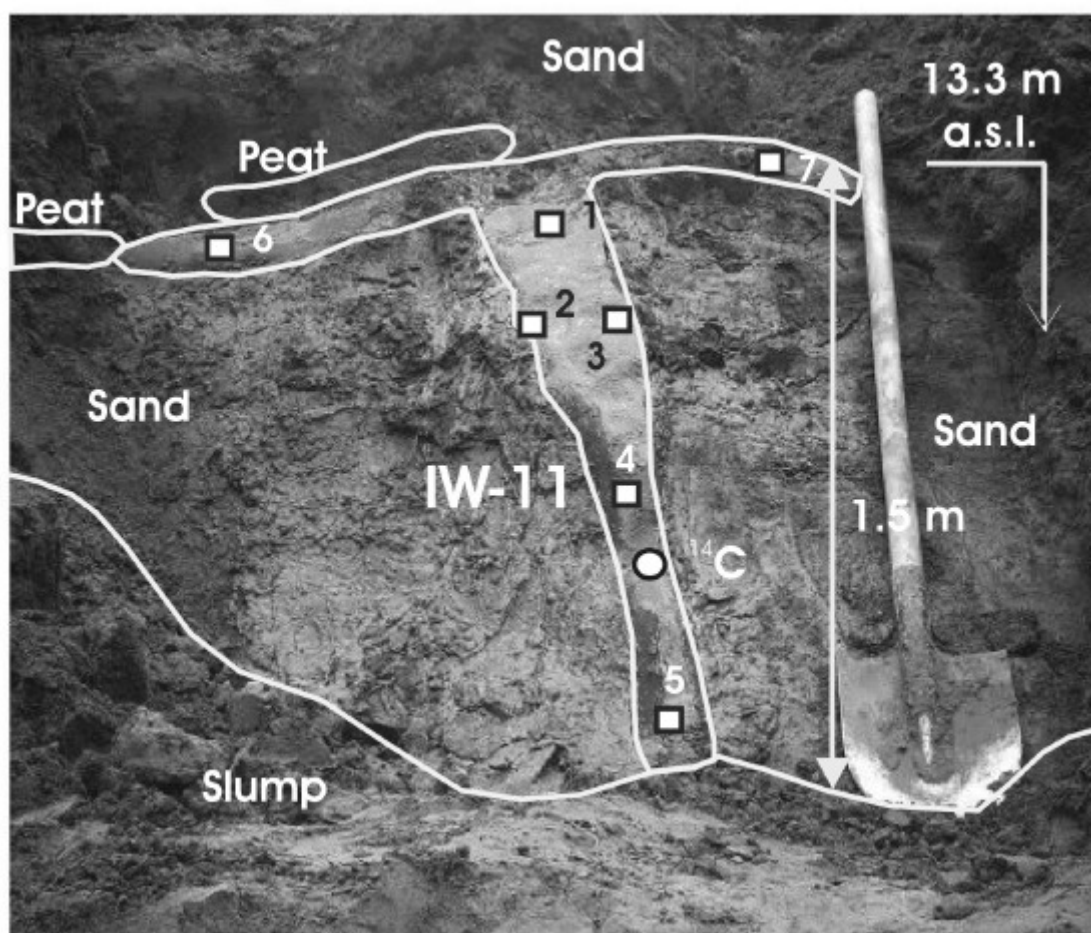


Figure 4.6.3-7: Outcrop MAK-IW-11 with sampling points (see also Figure 4.6.2-1)

Interpretation: Genetically, the ice wedge belongs to the third, or more likely, to the fourth peat of Unit B.

MAK-IW-24, IW-25

Description and Interpretation: MAK-IW-24 and IW-25 are both small ice wedges, 0.1 to 0.15 m wide, which were sampled 100 m to the west of the thermo-erosional ravine (Ovrag) and 50 m from the coast. At this location, a fourth peat horizon could be clearly differentiated and followed for several tens of metres in an estimated height of 10 to 12 m a.s.l., in general forming the tops of thermokarst mounds. The peat is about 0.5 m thick and characterised by a high content of reddish-brown *sphagnum*. Both ice wedges are linked with this fourth peat although in general, ice wedges are rather rare.

4.6.3.3 Ice wedges of the Late Pleistocene Ice Complex (Unit C) and of Holocene deposits (Unit D)

MAK-IW-12

Description: Outcrop MAK-IW-12 comprises a 2.4 m wide ice wedge of the Ice Complex (Figure 4.6.3-8) with transparent grey-yellowish and slightly tiger-striped ice and a moderate content of sediment and a low content of organic matter. Within this ice wedge, a 60 cm wide ice wedge of milky-white ice of a younger generation is observed, most likely associated with the Holocene (?) cover. Single ice veins of 3-5 mm in width are observed in this ice wedge.

From the Ice Complex ice wedge, 26 samples were taken by chain saw in a horizontal sampling transect in 1.5 cm wide slices taken in 10 cm intervals. The ice wedge is situated at the top of the Ice Complex cliff within the second thermocirque between two thermokarst mounds, with a height of the sampling profile of 17 m a.s.l.

Interpretation: Outcrop MAK-IW-12 shows the contact between Unit C (Ice Complex) and Unit D (Holocene cover) at the top of the ice cliff of the Ice Complex.

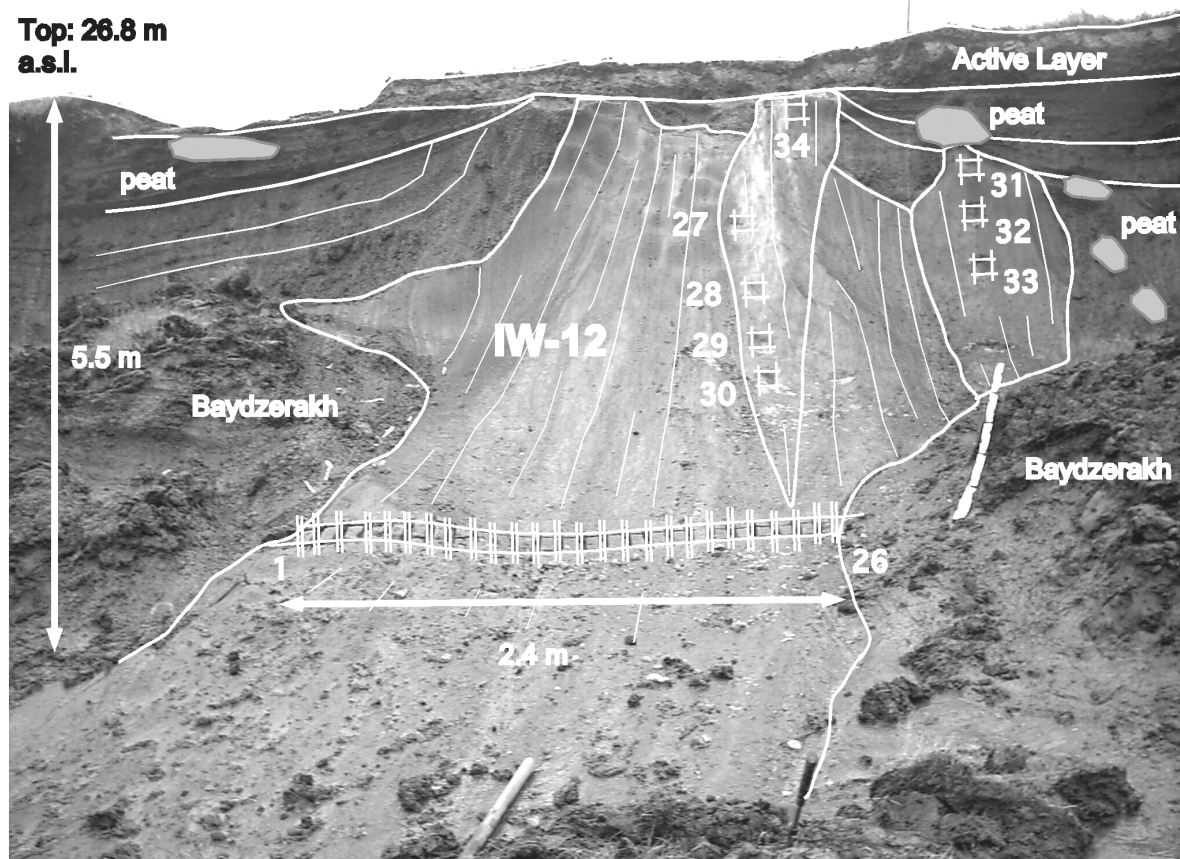


Figure 4.6.3-8: Outcrop MAK-IW-12 with sampling points

MAK-IW-13, -IW-14

Description: The ice wedges MAK-IW-13 and IW-14 are located at the Nuchcha Dzhihle River terrace (Figure 4.6.3-9) within an area of low centre polygons. The sampled outcrop is situated at the shore of the river, which cuts the studied polygon. This changed the drainage conditions and the polygon centre fell dry, whereas the frost cracks in the (former) polygon wall serve as drainage channels. Presently, the polygon walls of the old low centre polygons were lowered, sometimes more than one meter with regard to the former polygon centre, which are plain and characterised by the growth of a secondary generation of high centre polygon ice wedges. MAK-IW-13 is a remnant of an ice wedge in the wall of the former low centre polygon, which was partly eroded. MAK-IW-14 is a younger generation of high centre ice wedges in the middle of the former polygon centre. More detailed observations about the degradation of polygons due to changed drainage conditions can be obtained in Meyer (2003).

MAK-IW-13 is a 1.4 m wide ice wedge with milky, white ice and a medium content of sediment and a high content of organic matter. Well-developed vertical structures such as single, 2-4 mm wide ice veins and oriented gas bubbles are frequent. From this ice wedge, 8 samples were taken by axe in a horizontal sampling transect in 15 cm intervals between the samples. The ice wedges are situated at the western Nuchcha Dzhihle River bank with a height of the sampling profile of 1.5 m a.s.l.

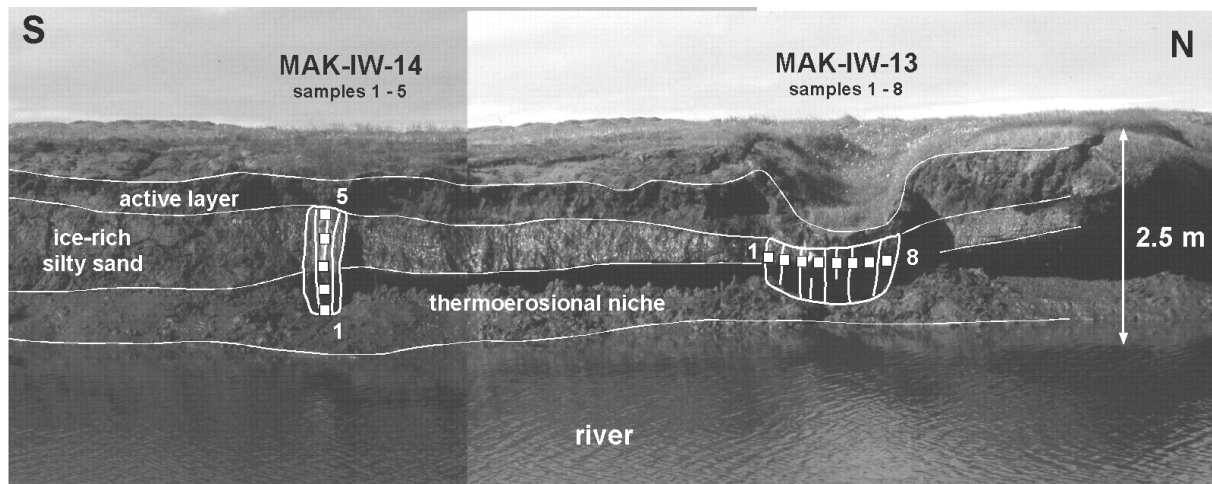


Figure 4.6.3-9: Outcrop MAK-IW-13 and -IW-14 on the Nuchcha Dzhihle River bank with sampling points

Interpretation: Both are Holocene ice wedges. The polygonal landscape and the form of the depression point to the existence of an old (Holocene) alas, which has been destroyed (and maybe also drained) by the erosional forces of the river.

MAK-IW-15

Description: MAK-IW-15 is a 2.5 m wide ice wedge of the Ice Complex (Figure 4.6.3-10) with grey-yellowish transparent ice and a medium content of sediment and of organic matter. Single 1-4 mm wide ice veins are observed. From the ice wedge, 27 samples were taken by chain saw in a horizontal sampling transect in 1.5 cm wide slices with 10 cm intervals between the samples. The first two samples from the left were taken from the ice belts. The ice wedge is situated at the bottom of the steep ice wall within the second thermocirque between two thermokarst mounds, with a height of the sampling profile of 17 m a.s.l.

Interpretation: This is an Ice Complex ice wedge.

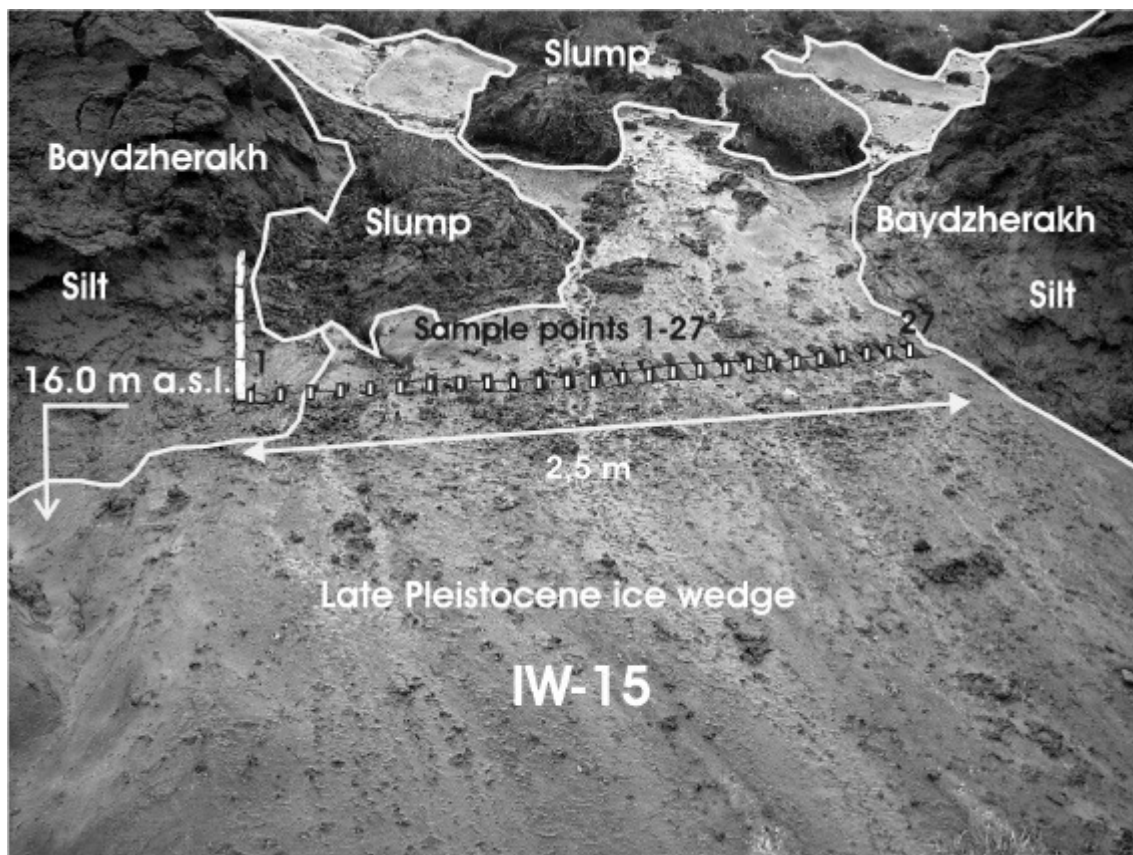


Figure 4.6.3-10: Outcrop MAK-IW-15 with sampling points

MAK-IW-16, IW-23, -MI a

Description: MAK-IW-16 is a 0.2 m wide, milky and white to yellowish ice wedge with clear vertical foliation and low sediment content. At both sides, the ice wedge is limited by subvertical schlieren-like ice-sand-veins. Four samples were taken by axe from this ice wedge. Ten metres to the east, a second ice wedge of the same generation was sampled (MAK-IW-23) and described. MAK-IW-23 is 0.1 m wide and consists of yellowish to brownish transparent ice with high organic content. Vertical structures such as single ice veins are common and well-developed. Here, one sample was taken by axe.

Five metres to the east of MAK-IW-16, a massive ice body (MAK-MI a) of unknown origin was found (Figure 4.6.3-11). The massive ice body is about 1.2 m wide and 0.8 m high and consists of two different types of ice both without preferential internal orientation: a very clear transparent part and a milky-white part rich in gas bubbles. Of both types of ice, one respective sample was taken by means of an axe. The ice wedges and the massive ice body are situated in a height of about 15 m a.s.l. at the top of the section.

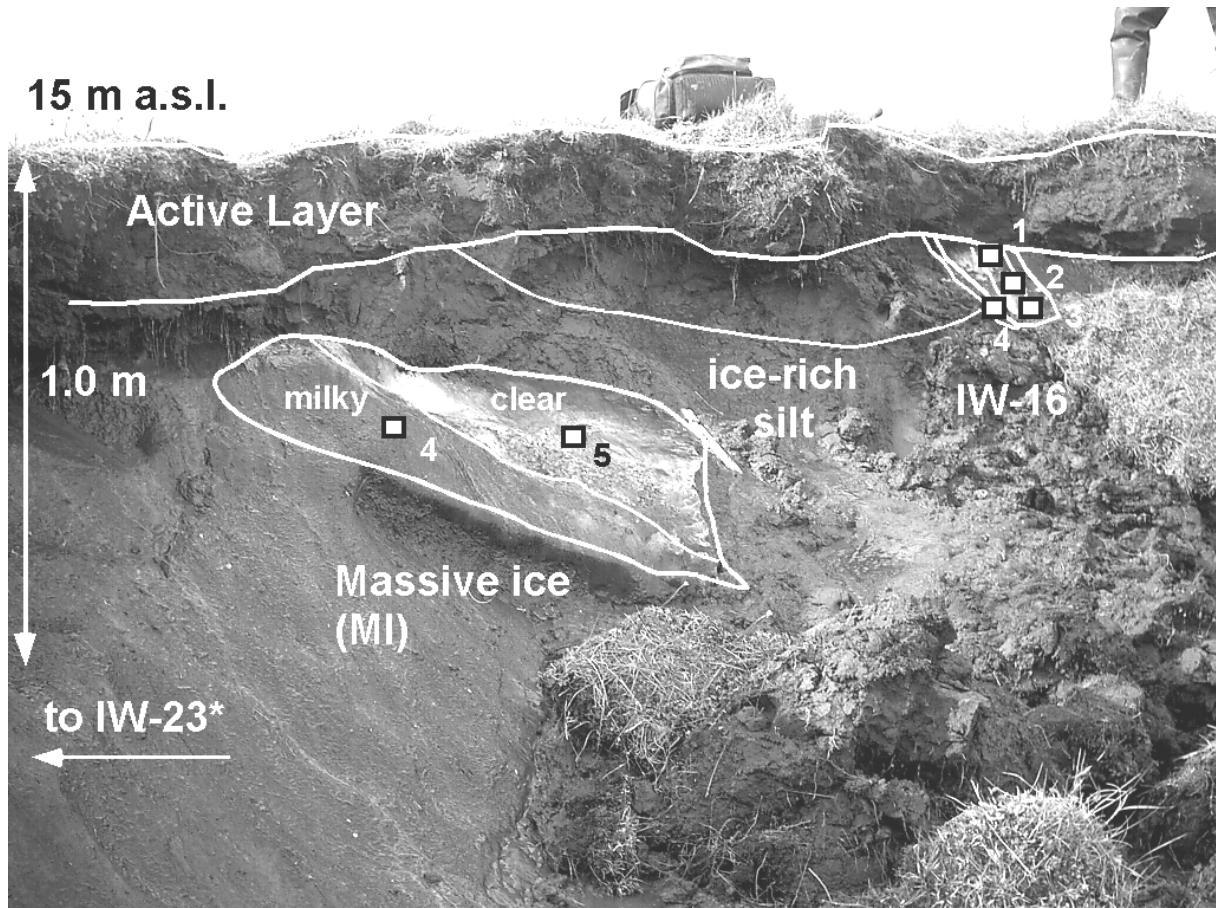


Figure 4.6.3-11: Outcrop MAK-IW-16, IW-23, -MI a with sampling points

Interpretation: The ice wedge MAK-IW-16 and -23 are probably of Holocene age and genetically correlated to the thermo-erosional valley, in which they are located on the western slope. Possibly, they are epigenetic features within older (Ice Complex) deposits. At this place, sediments of the thermo-erosional valley were not found. The massive ice body was interpreted as buried snow patch.

MAK-IW-17

Description: MAK-IW-17 is 3.2 m wide (Figure 4.6.3-12) and shows clear vertical structures, such as single ice veins of 2-4 mm in width, which may intersect each other. The ice is yellowish white to yellowish grey and turbid,

which is certainly related to the high number of very small (< 1 mm) gas bubbles, often oriented as a "string of beads". The content of mineral particles is medium and the organic content is low. On the left side, the ice wedge is in contact with single ice veins (sample MAK-IW-17.0). 33 samples were taken from the ice wedge in 10 cm intervals in horizontal direction by means of an ice screw ($\varnothing 15$ mm). Samples 1 – 16 were taken from the left, samples 29 to 45 from the right side - samples 17 to 28 are missing. The ice wedge is located at the bottom of the Ice Complex cliff, in a height of 5 m to 5.5 m a.s.l. (slightly rising from the left to the right). On the right side might be the contact to the adjacent ice wedge of the polygon.

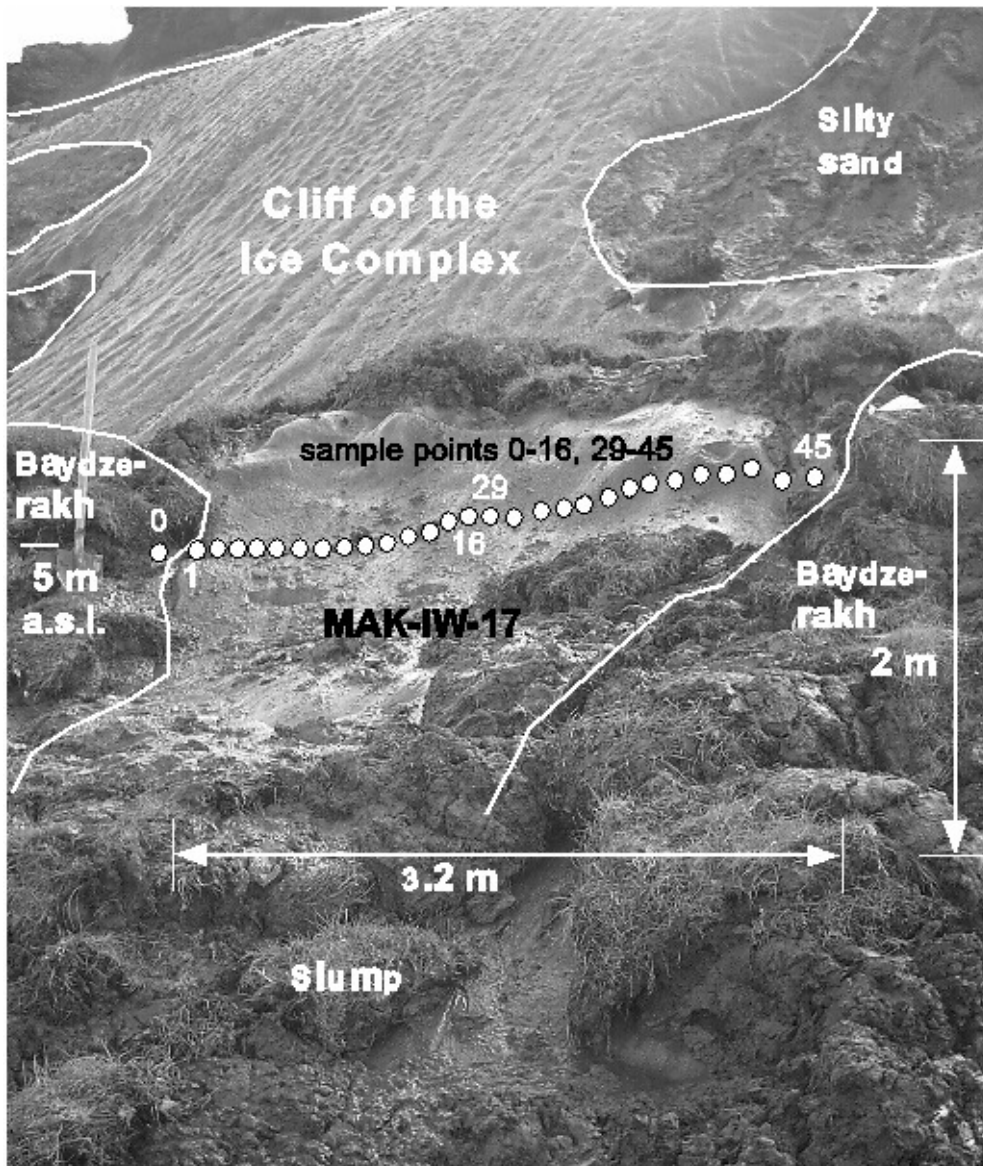


Figure 4.6.3-12: Outcrop MAK-IW-17 with sampling points

Interpretation: The ice wedge MAK-IW-17 belongs to the Ice Complex.

MAK-IW-18 (corresponding to the sediment sub profile Mak-12, Chapter 4.6.2.2)

Description: MAK-IW-18 is 0.6 m wide (Figure 4.6.3-13) and shows a moderate vertical foliation with single ice veins of 2-3 mm in width. The ice wedge is characterised by yellowish to brownish grey and transparent ice, a moderate mineral content and a low organic content. Gas bubbles are small (< 1 mm), spherical, not elongated and oriented along the ice veins. 4 samples were taken from this ice wedge by means of an ice screw (\varnothing 22 mm), again in 10 cm intervals at a height of 1.0 m a.s.l. The ice wedge is located in the second thermo-cirque near the Laptev Sea shore at a height of 1.3 m a.s.l. (top ice wedge).

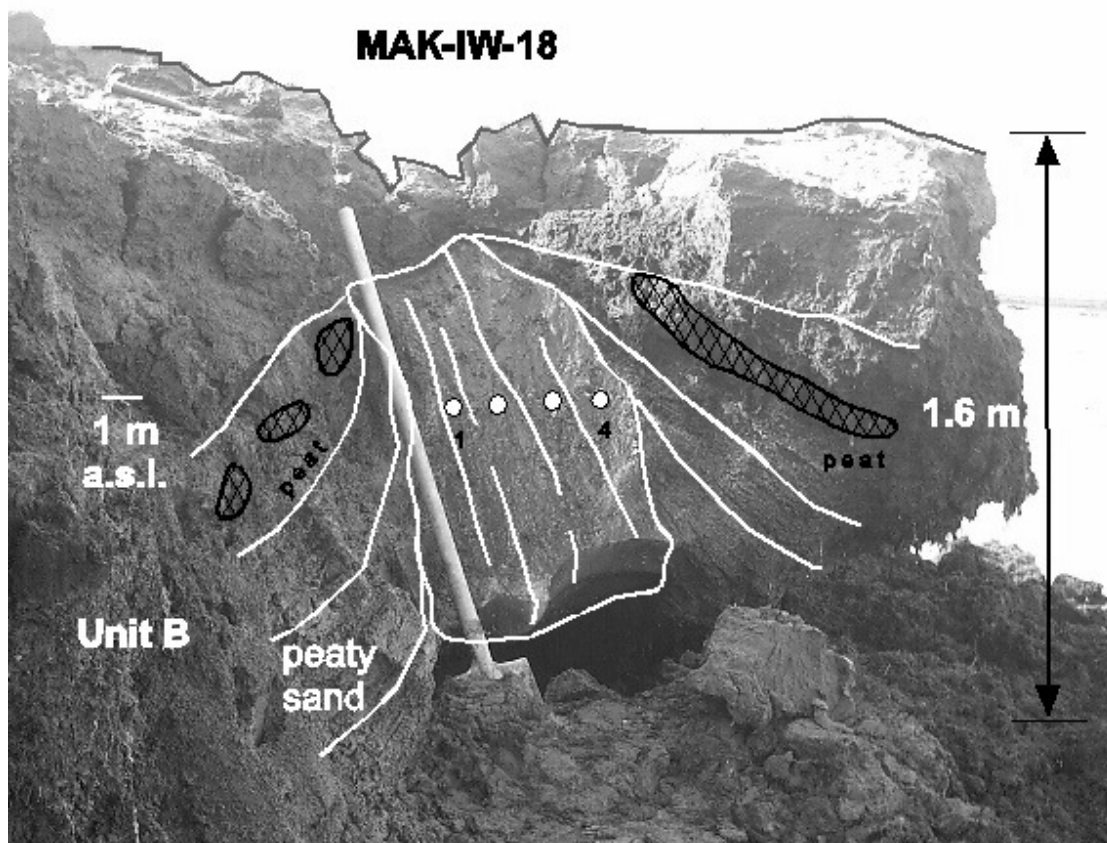


Figure 4.6.3-13: Outcrop MAK-IW-18 with sampling points (see Figure 4.6.2-3)

Interpretation: The ice wedge MAK-IW-18 belongs most likely to the uppermost peat of Unit B, but may also be a small Unit C (Ice Complex) ice wedge penetrating Unit B or a peat-rich part of Unit C. The question whether this section belongs to Unit B or C may be solved during the laboratory analyses.

MAK-IW-22

Description: MAK-IW-22 is a 1 to 1.2 m wide ice wedge and shows a well-developed vertical orientation. Vertical structures may be single ice veins of 2-7 mm in width, with clearly recognisable single ice veins and very small (< 0.5 mm) gas bubbles oriented as a "string of beads". The ice is sometimes milky white, sometimes more transparent. The content of mineral particles is rather low and the organic content is moderate. At the left side, the ice wedge is in contact with sands of Unit A/B. 14 samples were retrieved from the ice wedge by means of an ice screw (\varnothing 15 mm). 11 samples (IW-0 to IW-10) were taken in a height of 3.5 m a.s.l. in a horizontal sampling transect with 10 cm intervals. Samples 11 to 13 were sampled in the upper part by means of an axe. The ice wedge is located at the western flank of a thermo-erosional valley in a height of 3 m to 6.5 m a.s.l. (Figure 4.6.3-14).

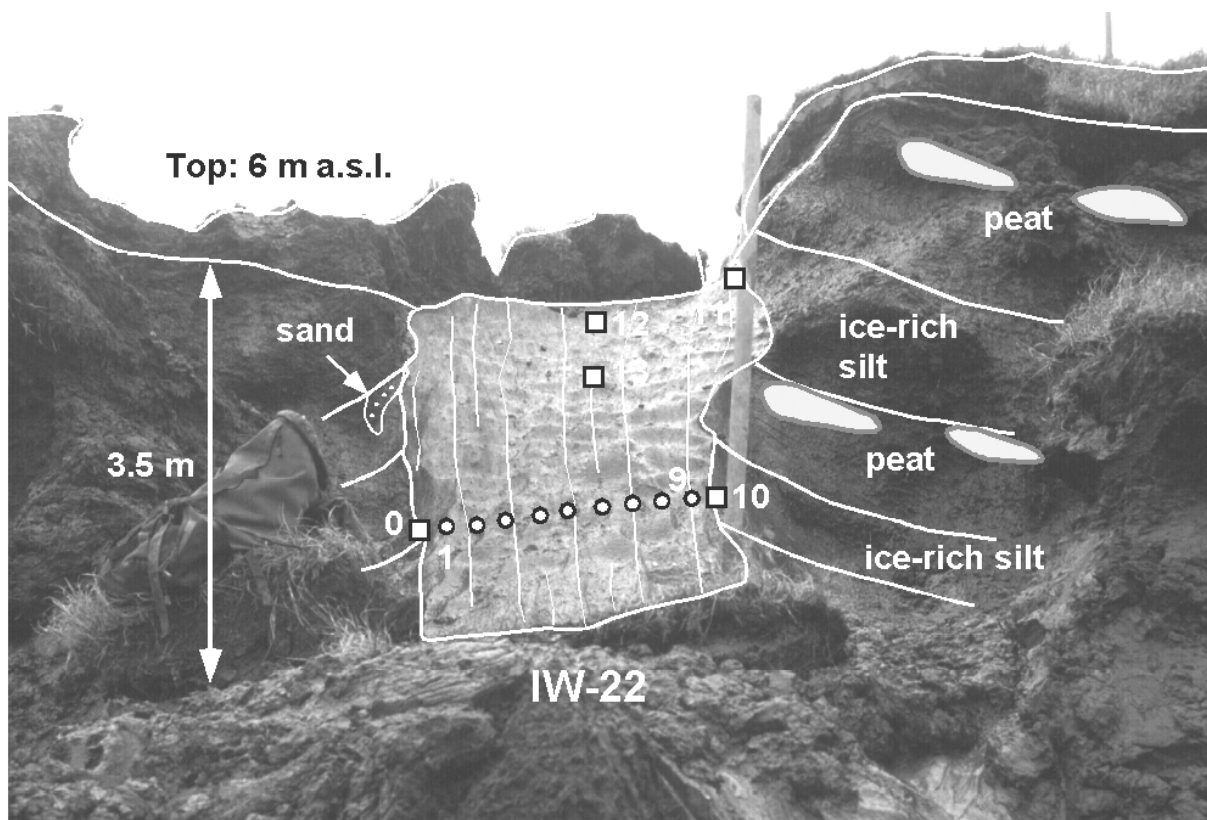


Figure 4.6.3-14: Outcrop MAK-IW-22 with sampling points

Interpretation: The genesis is still a matter of debate, since there are arguments to attribute the ice wedge to the thermo-erosional valley as well as to the Ice Complex. The Ice Complex genesis is supported by: the structure and colour of the ice, the presence of Ice Complex ice wedges 20 m to the west and the sands of Unit A or B, which are observed at the left side of the ice wedge. The size of the ice wedge, the surrounding sediment and the presence of a

thermo-erosional valley are rather favorable for a Holocene genesis within this valley. Stable isotopes will help to solve this problem.

MAK-IW-26

Description: Ice wedge MAK-IW-26 is 1.6 m wide (Figure 4.6.3-15) and was sampled in a horizontal profile in a height of 17.4 m a.s.l.. Six ice blocks, about 12 cm high and 23 to 30 cm wide, were cut by means of the chain saw. The ice was grey to white, tiger-striped with few yellowish ice veins. Single ice veins were about 2 mm wide and fell into (annual) pieces during sampling. The content of mineral particles and of organic matter was moderate. Small ice bubbles (mostly < 0.5 mm) were common, occasionally lengthened up to 4 mm within single ice veins. The right side of the ice wedge is confined by belt-like ice schlieren.

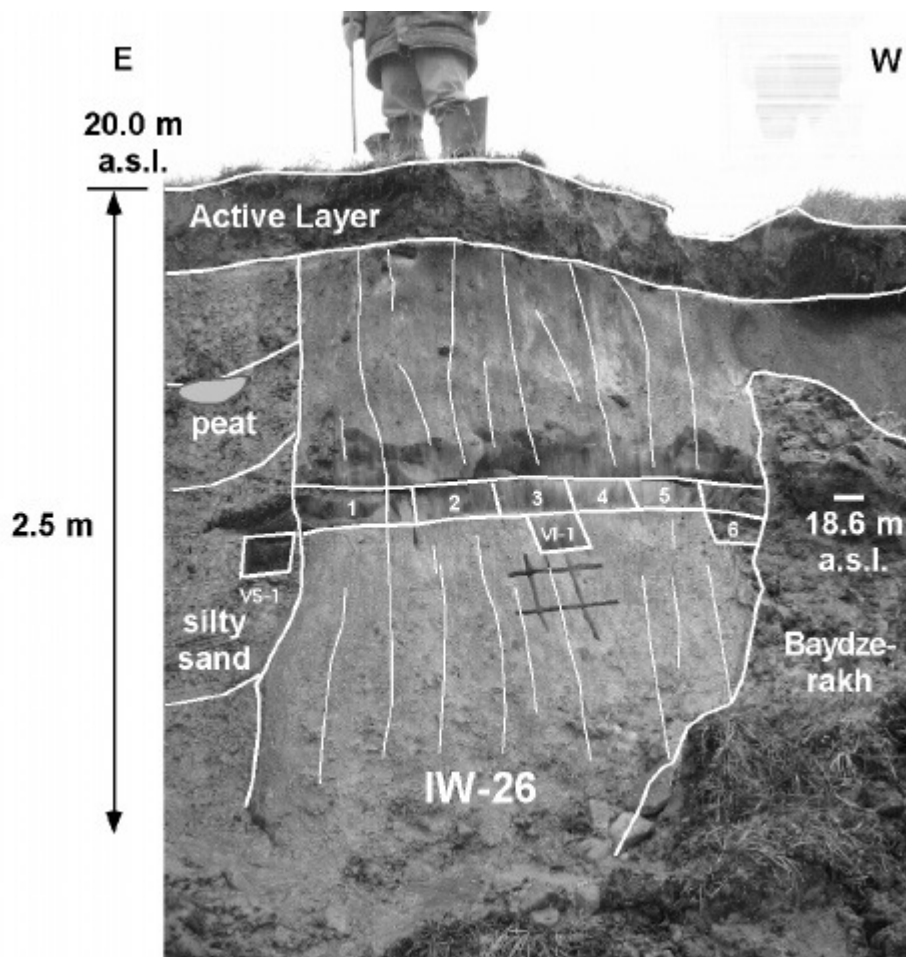


Figure 4.6.3-15: Outcrop MAK-IW-26 with sampling points

Interpretation: This is an ice wedge of the Ice Complex, which is the youngest one of the westernmost profile. The assumed age of the ice wedge is Late Pleistocene.

MAK-IW-27

Description: This ice wedge is 2.4 m wide and about 2.8 m high (Figure 4.6.3-16). Thin slices (about 15 mm wide) were cut by chain saw in 10 cm intervals from a horizontal sampling transect in an absolute height of 19 m a.s.l.. In total, 24 samples were taken. The ice is grey to yellowish-white, with single ice veins of 3 to 4 mm width. However, vertical structures are seldom clearly developed and rather moderately preserved. Gas bubbles are lengthened up to 8 mm in vertical direction. The sediment content within the ice wedge is high, the content of organic matter low. On both sides, the ice wedge is confined by ice-rich silty sands with wood fragments and banded cryostructure. Two additional samples (VI-2 and VS-2) were taken for sediment and ice analyses of the group working on coastal dynamics (see chapter 4.7.2).

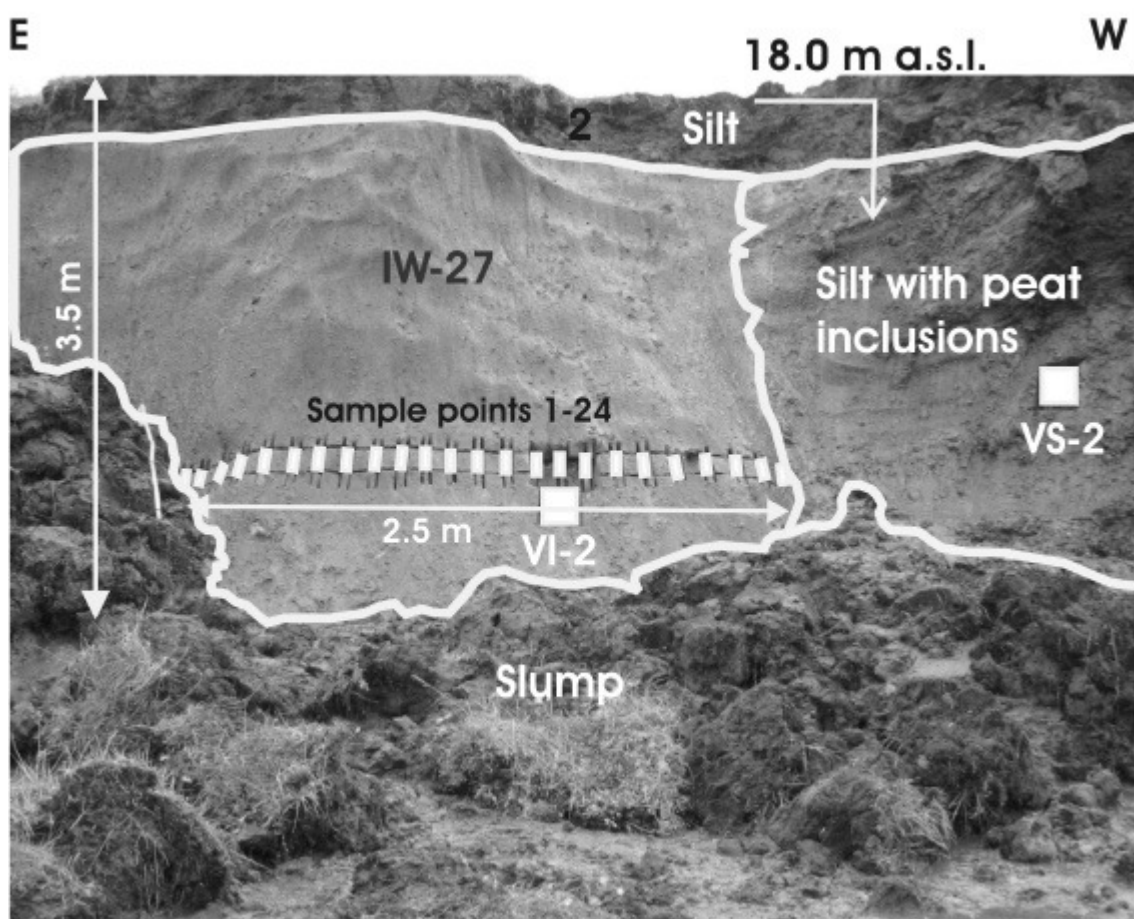


Figure 4.6.3-16: Outcrop MAK-IW-27 with sampling points

Interpretation: This ice wedge belongs to Unit C (Ice Complex).

4.6.3.4 Ground ice of unknown origin

MAK-MI b

A massive ice body (MAK-MI b) was found 20 m west of ice wedge MAK-IW-22 in a height of about 3 to 3.5 m a.s.l. presumably in Holocene log deposits. Ice lenses of massive ice are in contact with ice wedge ice, differing considerably from it. The massive ice body is composed of two different ice lenses: the upper one consists of clean transparent ice with big crystals and only a few gas bubbles, and the lower one of yellowish transparent ice with small crystals and numerous gas bubbles. The size of each of the ice lenses is approximately 0.4 x 1.5 m. Peaty silt with peat lenses encloses both massive ice and ice wedge. Three samples of massive ice and one sample of the ice wedge were taken by axe (Fig. 4.6.3-17).

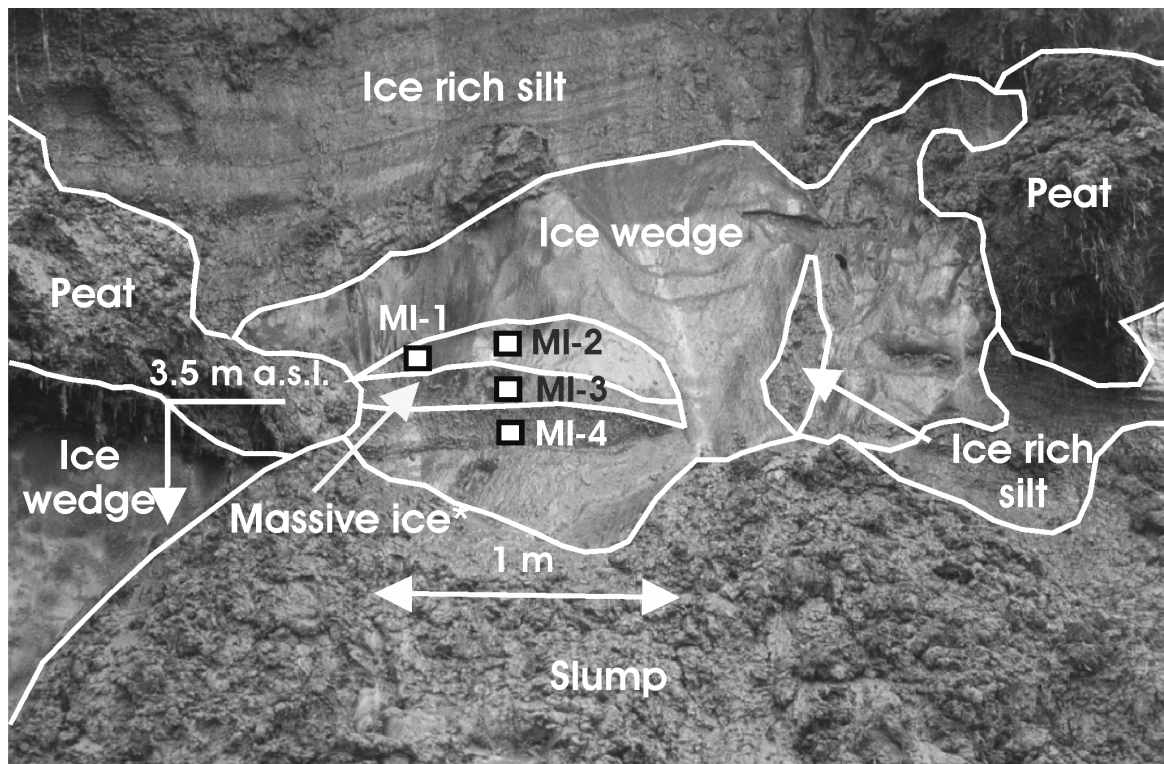


Figure 4.6.3-17: Outcrop MAK-MI b with sampling points

4.6.3.5 Ice wedge section west of the Nuchcha Dzhihle River mouth

MAK-IW-28

Description and Interpretation: This ice wedge is located on the western side of Nuchcha Dzhihle River, approximately 450 m west of the river mouth (Figure 4.6.1-2). The outcrop is a 9.5 m high very steep ice wall being located directly at the Laptev Sea coast. In the lower part, the ice wedge is laterally confined by subvertical ice-sand-wedges of Unit A (Figure 4.6.3-18). It can be clearly seen in this outcrop that these "polosatics" are limited to Unit A and that Ice Complex

ice wedges penetrate the older deposits of Unit A and Unit B. At least three, possibly four peat horizons were observed in Unit B. Unit C (Ice Complex) is only 1.5 to 2 m thick at this locality, which raises the question, whether this ice wedge is only epigenetic to Unit A and B deposits. In that case, this would lead to the assumption, that frost cracking activity during Ice Complex growth may reach depths of 8 m and more.

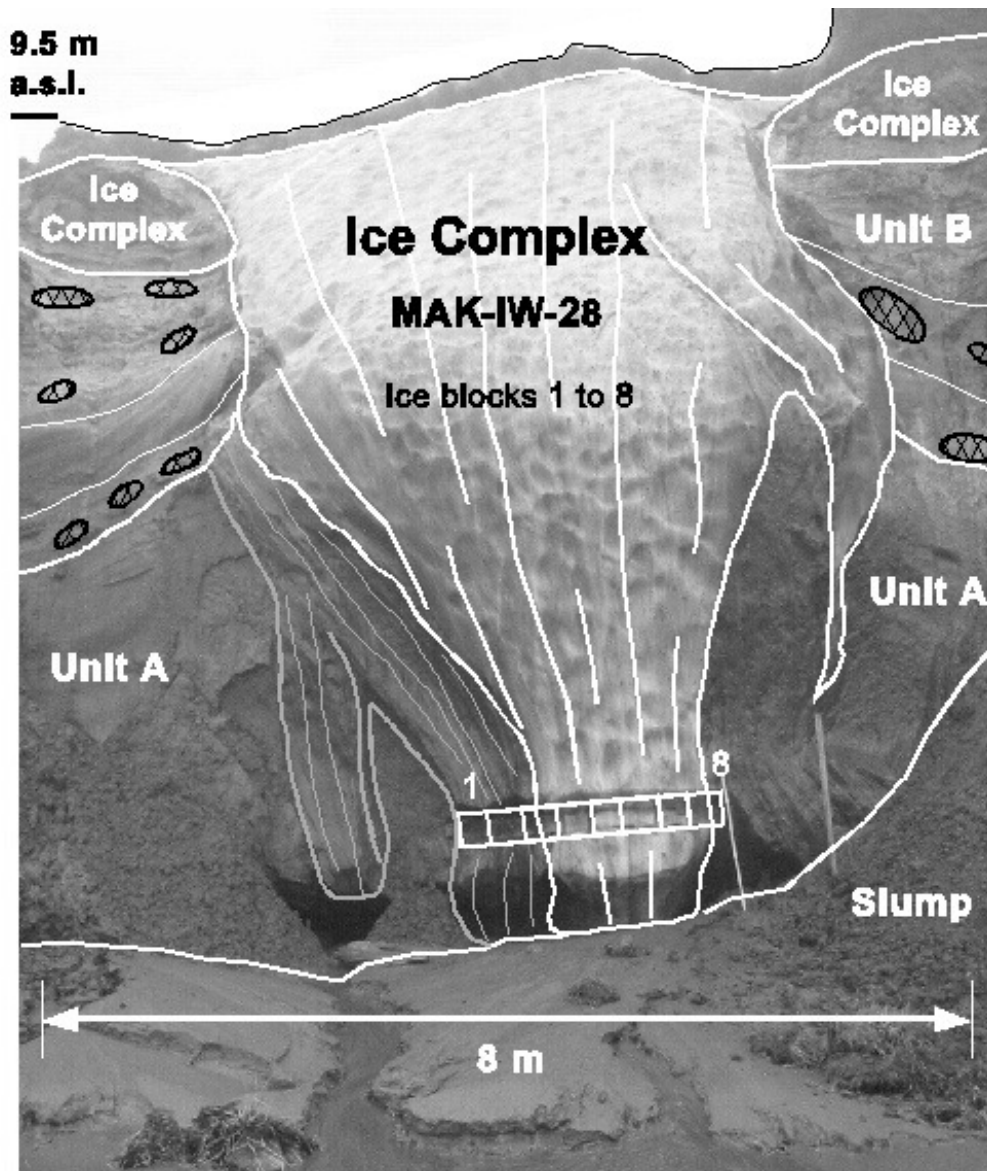


Figure 4.6.3-18: Outcrop MAK-IW-28 with sampling points

The ice of the **ice wedge** is white and milky, and cut perpendicular to the direction of frost cracking with very clear vertical structures. Narrow ice veins of 1-3 mm were observed in the ice wedge, sometimes cutting each other. The contents of organic matter and of sediment particles are both low. Gas bubbles are frequent and in general smaller than 0.5 mm. The **ice-sand-wedges** consist of single 2-8 mm wide ice veins, interrupted by < 1 mm to 2 mm wide sediment veins. The latter consist of ice-rich fine-grained sand to silt. The ice veins

originate in the adjacent ice wedge. Ice-sand veins are confined to Unit A and are cut by the first peat of Unit B.

Eight ice blocks (about 25 cm in length) were sampled by chain saw in a height of 1.5 m a.s.l.. This results in a 1.98 m long horizontal sampling profile, which includes the contact between ice-sand-wedge and Ice Complex ice wedge. Samples 1 to 3 were taken from ice sand-wedge and samples 3 to 8 from the ice wedge.

4.6.3.6 General interpretation of the sampled profile

The observation of other sampling sites such as the Bykovsky Peninsula, Oyagoysky Yar and the Big Lyakhovsky Island were confirmed during this field campaign. The Ice Complex is a Late Pleistocene formation with big syngenetic ice wedges and very ice-rich silty to sandy sediment. However, the ice wedges of Mamontov Klyk reach widths about 2.5 m, maximum 4 m, thus do not attain the dimension of their equivalents at the sampling sites mentioned above. This may point to less favourable conditions (e.g. lower water supply, higher sediment accumulation, less frequent frost cracking activity). Like at other locations, Big Lyakhovsky Island or Kurugnakh, the Ice Complex of Mamontov Klyk is underlain by a sandy facies, which may be linked to fluvial activity (at least for Kurugnakh and Mamontov Klyk). Like on Big Lyakhovsky Island, ice-sand wedges ("polosatic") occur within these sands pointing to a rather fast deposition of sediments and to the concurrency of water and sediment supply. Again, the Ice Complex is destroyed by Holocene sedimentary processes (especially by thermo-erosion in flat valleys (logs). A peculiarity is a Holocene cover above the MAK Ice Complex with a new generation of (presumably Holocene) ice wedges, which was not observed in Bykovsky Peninsula. Remarkable is the high number of massive ice bodies of unknown origin (not formed by frost cracking) which were observed and sampled in the section.

4.6.4 Geomicrobiological studies

Uta Zimmermann

4.6.4.1 Introduction and objectives

Permafrost deposits commonly contain different amounts of methane, being a potential source of this climate relevant trace gas in case of thawing (Moraes & Khalil 1993, Rivkina and Gilichinsky 1996). In addition, organic carbon presently stored in perennially frozen paleosols and sediments may be decomposed to methane when temperature rises. An increased emission of methane followed by an increase of atmospheric methane concentrations may be the result. The objective of the geomicrobiological investigations was to improve our understanding of the permafrost-inhabiting microorganisms that produce and oxidize methane. Working tasks in the field were:

- sampling of perennially frozen paleosols and sediments with differing ecological factors (pH, grain size, content of organic carbon and nutrients, age of permafrost deposits) for measurement of activity at low temperatures, abundance and diversity of methane producing and oxidizing microorganisms
- determination of methane content in permafrost deposits.

4.6.4.2 Methods

Samples were taken from different geocryological units of the coastal permafrost exposure, comprising late Pleistocene sand-peat complex, late Pleistocene ice complex, Holocene cover and Holocene thermoerosion valley deposits. All of the sampling sites were likewise described and sampled for cryolithological and sedimentological studies (see chapter 4.6.2). In total 29 samples were taken for geomicrobiological investigations (see sample list in Appendix 4-4).

After removal of thawed material at the respective points of the cliff, samples from perennially frozen parts were taken with a hammer and a small axe. For microbiological, molecularbiological and biochemical analyses, subsamples were immediately stored on ice and transported frozen to Germany. Subsamples for geochemical and -physical analyses were transported at ambient temperatures. Furthermore, methane content was determined in the field: Immediately after sampling, 10 to 20 g of frozen material was placed into gastight 50-ml-glassbottles, which were previously filled with 35 ml of a saturated sodium chloride solution. The sodium chloride prevented microbial activity and minimized methane solubility in the sample suspensions. Methane stored in the permafrost material was forced into the headspace of the bottles by vigorous shaking after thawing. Two to four weeks after sampling, gas concentrations in the headspaces were analysed by gas chromatography in the field laboratory on the Island Samoylov, Lena Delta.

4.6.4.3 First results: Methane content of permafrost samples

Table 4.6.4-1. Methane content in permafrost samples from different geocryological units (for more details about subprofiles see chapter 4.6.2.).

Cryolithological unit	Methane concentration [$\mu\text{mol/kg ice}$]	Peat	Sample number	Number of subprofile
Late Pleistocene sand-peat complex	0	+	Mak 100	MAK-1
	0	-	Mak 101	
	340	+	Mak 102	MAK-2
	139	-	Mak 103	
	22	+	Mak 104	
	2	+	Mak 105	MAK-3
	0	+	Mak 106	
	2	-	Mak 107	
	0	+	Mak 108	
Late Pleistocene Ice Complex, transition to sand-peat complex	13	-	Mak 109	MAK-4
Late Pleistocene Ice Complex	0	-	Mak 110	MAK-5
	0	-	Mak 111	
	0	-	Mak 121	MAK-9
	0	-	Mak 122	MAK-8
	429	+	Mak 126	MAK-12
	98	-	Mak 127	
	361	+	Mak 128	
Late Pleistocene ice complex, transition to Holocene cover	63	-	Mak 112	MAK-10
	131	-	Mak 113	
	290	-	Mak 114	
	423	-	Mak 115	
	662	+	Mak 116	
	115	-	Mak 117	
Holocene cover	541	+	Mak 118	MAK-10
	416	-	Mak 119	
	691	+	Mak 120	
Holocene thermoerosion valley deposits	15	+	Mak 123	MAK-11
	602	-	Mak 124	
	343	+	Mak 125	

All analysed Holocene permafrost samples contained methane (see Table 4.6.4-1), ranging from 15 to 691 $\mu\text{mol/kg ice}$. In Ice Complex samples, methane presence varied strongly between various subprofiles: 63 to 662 μmol methane per kg ice could be detected in samples from the subprofile Mak-10, which represents the transition to the Holocene cover. Mak-12 was another subprofile rich in methane (98 to 429 $\mu\text{mol/kg ice}$), representing an older part of the Ice Complex (0 to 2 m a.s.l) with marked peaty paleosoils. In contrast to that, no methane could be found in samples from subprofile Mak-5, Mak-8, Mak-9 and only a small quantity (13 $\mu\text{mol/kg ice}$) in a sample from profile Mak-4. These

lacking or minor methane contents in Ice Complex material have been earlier reported by Rivkina & Gilichinsky (1996) for various boreholes taken in the Kolyma-Indigirka Lowland, Siberia.

Samples of the sand-peat-complex were taken from three subprofiles, one of them (Mak-2) with 22 to 340 μmol methane / kg ice and two of them with lacking or minor concentrations (Mak-1, Mak-3). At the latter sites, even peaty material was free of methane, indicating oxic conditions in the peats at the time of the latest freezing.

4.6.5 Paleontological studies

Tatyana V. Kuznetsova

Paleontological studies of the Pleistocene and Holocene deposits at the Olenek - Anabar coast include collecting and determination of large and small fossil mammal remains. For the first time, special paleontological studies were carried out in this region as a part of the multidisciplinary research program. Unpublished Russian geological reports include data on a few mammal bones which were found by previous researchers.

All of the found bones and bone fragments were registered in order to obtain a complete statistic of species composition as during previous expeditions. During our work we were studying deposits a 4 km long section of the Olenek - Anabar coast – the Mamontov Klyk outcrop. We collected 501 bones and their fragments of large mammals (Appendix 4-7). Typically for permafrost regions, most bones (more than 90%) were found at the shore. The greatest part of bone fossils was collected on a small place on the shore near the mouth of the Nuchcha-Dzhiele River. Only 20% of the material was found at the Mamontov Klyk exposure itself and on the shore in front of it. The main difference of the collection from the Olenek - Anabar coast to our previous collections is the absence of complete big limb bones of woolly mammoth, horse, bison and of mammoth' teeth.

The collected bones were divided into groups by found place (location type). The group "a" contains 8 bones they were found strictly *in situ* in Ice Complex deposits. Three of them - samples O-476, O-477 and O-478 are remains probably from the one skeleton of *Mammuthus primigenius*. All big samples from this group we sent to the Radiocarbon Laboratory of the Geological Institute RAS for conventional ¹⁴C dating. Next two groups ("b" and "c") include bone found within the exposure. For 10 bones (group "b") we know the altitude of found – the level of minimum height of the original position of the bones. It gives possibility to define the area where the bones come from. Among this group there are three fragments of the upper jaw of *Equus sp.* with teeth (O-98, O-99, O-100) from one skeleton and two metapodiales (Mt III and Mt IV) of *Equus sp.* belong to another skeleton (O-102, O-103). 9 bones (group "c") were found at the exposure on or in the scree debris.

Group "d" (69 specimens) includes the bones which were collected on the shore under the Mamontov Klyk exposure. Remains of reindeer and horse are predominant, evidently reindeer remains were presented as fossil as recent bones whereas all horse bones are fossil.

Most of the material (group "e", 395 specimens) have been collected on the small part of shore near the mouth of the Nuchcha-Dzhiele River. Remains of reindeer and horse are predominant too. Several bones of *Phoca sp.* in this group are probably recent. The last two groups ("f" and "g") include bones (1 and 9 specimens) that were collected in various other areas. For example three

cervical vertebrates of *Equus sp.* from one individual were collected on the shore of middle reaches of Urasalakh River (O-161, O-162, O-163).

Table 4.6.5-1. List of mammal taxa identified in the Olenek-Anabar Region collection.

Class MAMMALIA

Order Lagomorpha

Lepus sp. (hare)

Order Carnivora

Family Canidae

Alopex lagopus (L.) (polar fox)

Canis sp. (wolf)

Order Proboscidea

Mammuthus primigenius (Blum.) (woolly mammoth)

Order Perissodactyla

Family Equidae

Equus sp. (horse)

Order Artiodactyla

Family Cervidae

Rangifer tarandus (L.) (reindeer)

Family Bovidae

Ovibos moschatus Zimm. (muskox)

Bison priscus (Boj.) (Pleistocene bison)

Order Pinnipedia

Family Phocidae

Phoca sp. (hair seals)

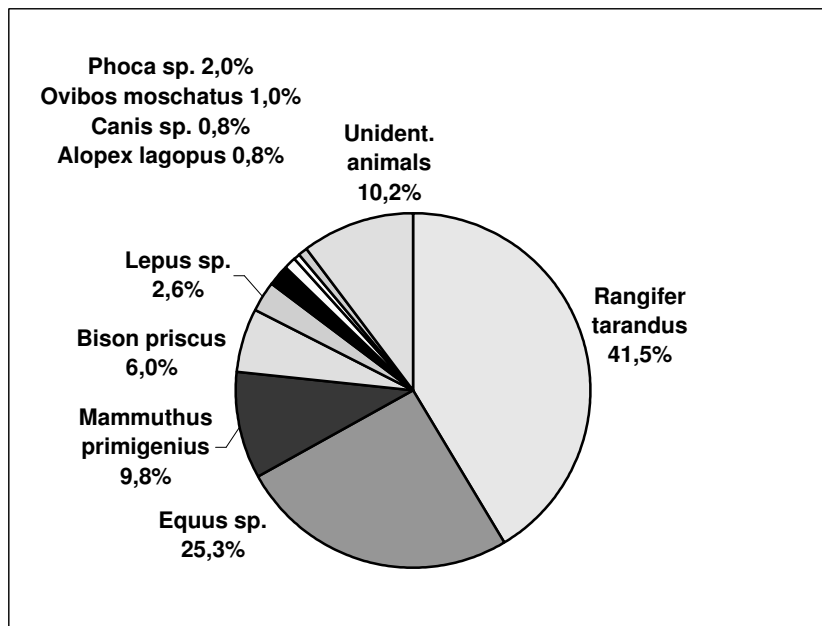


Figure 4.6.5-1: Composition on mammal bones collection from Olenek-Anabar Region, 2003, total number: 501 specimens.

In total the taxonomic composition of the collection from the Olenek-Anabar region (Table 4.6.5-1) is close to the Late Pleistocene "Mammoth" fauna from other Arctic Siberia Region. Reindeer (41.5%), horse (25.3%) and Woolly Mammoth (9.8%) fossils dominate, then followed by bison (6.0%). MuskoX and wolf each (about 1%) of the whole collection (Figure 4.6.5-1) Unusually high numbers of reindeer remains can be explained by the presence of modern bones in collection. More interesting is the predominance of horse remains compare to mammoth ones. Possibly, this depends on taphonomic factors and doesn't correspond to the composition of animal population during the Late Pleistocene in this region. Remains of polar fox and hair seals in collection are probably modern. The preservation of bones is typical for Ice Complex sites and fossil bones are not easy to distinguish from recent ones on the shore.

4.7 Studies of coastal dynamics and sub sea permafrost

4.7.1 Preliminary results of sub-sea permafrost drilling in the near-shore zone (spring 2003)

Mikhail N. Grigoriev

4.7.1.1 Introduction and background

Studies of permafrost evolution in the coastal zone allow us to understand the on-shore – offshore permafrost system evolution more precisely. One of the main tasks of the new Laptev Sea System Project "Dynamics of Permafrost" is the evolution of the sub-sea permafrost within the near-shore zone of the shallow shelf. Practically, it is very difficult to realize this task without drilling. At the Cape Mamontov Klyk Area (the coast between Olenek and Anabar Rivers, Western Laptev Sea Coast) in the frame of the Russian-German Cooperation a relatively deep drilling by professional equipment and team is planned in the nearest future. In this connection a reconnaissance drilling was carried out in order to determine the position of the near-shore sub-sea permafrost table.

There are only a few drilling transects with shore face profiles in the Asian Arctic shelf seas. These transects have been made on sea ice in spring or on small drilling platforms. As usually, within the shallow Laptev shelf at the thermal abrasion coast the sub-sea permafrost table is found by drilling at depths between 5 and 60 metres. Unfortunately, deeper boreholes do not exist in the studied near-shore area. Sometimes, formations of new sub-sea permafrost were observed within bottom deposits of the shallow sea (Grigoriev N.F., 1966, Telepnev, 1981). Our previous studies of coastal permafrost degradation at Ice Complex coasts showed that the sub-sea permafrost table slowly submerges from shoreline to the deeper parts. An inclination of the permafrost table depends on various reasons, mainly on coastal erosion retreat rates, water temperature and salinity. Previous drilling transects in front of Muostakh Island and Bykovsky Peninsula (Central Laptev Sea coast) gave us some first information about permafrost degradation at quickly retreating coasts (Grigoriev, 1993). The average inclination of the sub-sea permafrost table is 0.007 and 0,013 at these sites. The corresponding average coastal erosion rate accounts 13 and 3 m/year (Grigoriev, Kunitsky, 2000) respectively. Some natural conditions in the area of Cape Mamontov Klyk are different from Central Laptev Sea offshore parameters. For example, water salinity at Cape Mamontov Klyk exceeds salinity at the Central Laptev Sea coast 3 to 5 times. This fact is very important for the understanding of rates of sub-sea permafrost degradation.

The drilling campaign started from Tiksi on April 11, 2003. During 13 days the went on the sea ice around the Lena Delta and than across the Oleneksky Bay. The thickness of sea ice was about 1.7-2.1 m. Basic equipment (Figure 4.7-1, 4.7-2) of the drilling field team consisted of a compact drilling machine UKB-12/25, two caterpillar tractors S-130, a cross-country vehicle GAZ-71, a

habitable mobile-home "balok" and two cargo sledges. During the way to the Cape Mamontov Klyk and back we had serious hardships with obstacles like sea ice cracks and hummocks but the technical equipment has stood the test.



Figure 4.7-1: Drilling process with the drilling machine UKB-12/25 on sea ice.



Figure 4.7-2: The caterpillar tractor S-130 and habitable mobile-home "balok" on the Laptev Sea ice.

4.7.1.2 Methods and preliminary results

The drilling profile line started from the shoreline at the base of the snow-covered Ice Complex cliff (Figure 4.7-3). The profile consisted of 11 boreholes (1 to 32.5 meters deep). 10 seawater samples and 19 core samples for grain size, mineralogical and chemical analysis were collected. Because of distinctive cone-like drilling in liquefied bottom sediment it was impossible to collect a complete core. The near-bottom water temperature was measured during the drilling process.

Average erosion retreat rate of the ice-rich coast at the beginning of the drilling profile is 5.8 m/year, taking into account that the average erosion rate for the whole adjoining coastal segment is about 3-4.5 m/year. These data were obtained during our previous studies (Grigoriev et al., 2000) and by comparison of up-to date measurements with remote sensing materials.

The base of Ice Complex deposits was found near the shore in a depth of 3 meters below sea level. The underlying sand deposits were discovered down to the depth of 30 meters below sea level. The deepest borehole reached 32.5 meters and showed some unexpected results (Figure 4). Despite of a high coastal erosion rate and very low water temperatures (from -1.3 to -2.1 °C) the inclination of the permafrost table in a distance of 1.3 km from the shore was very steep (0.015) and from 1.3 to 1.4 km – extremely steep (more than 0.3). This anomaly is probably explained by ancient thermokarst processes under sub aerial conditions. Estimation show that the average rate of permafrost table degradation is about 8 cm/year or slightly more at the studied transect.

4.7.1.3 Further investigations

In order to study the sub-sea permafrost evolution within the whole shore face profile near the Cape Mamontov Klyk a deeper drilling (up to 300 m depth) is planned in spring 2005. The main tasks of this drilling campaign are:

- To drill a longitudinal borehole profile by professional drilling machine;
- To determine the sub-sea permafrost table up to 10-15 km from the shore;
- To characterise the sediments;
- To analyse temperature and salinity distribution in the boreholes;
- To estimate rates of permafrost degradation depending on coastal erosion activity and other factors

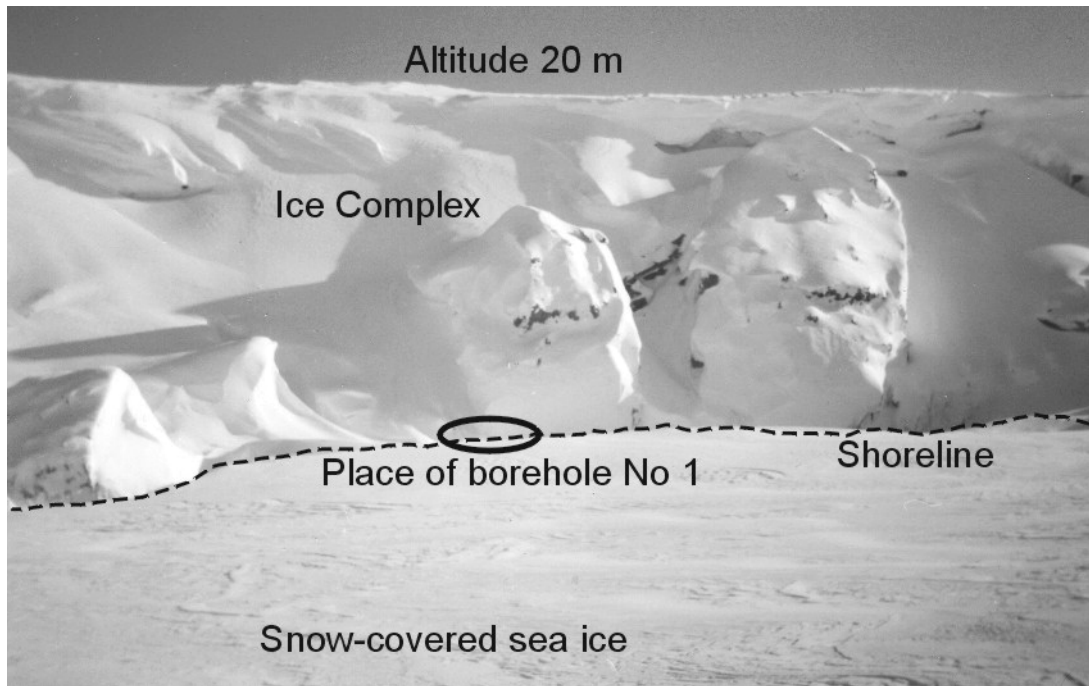


Figure 3: The beginning of drilling profile at the shore (April, 2003).

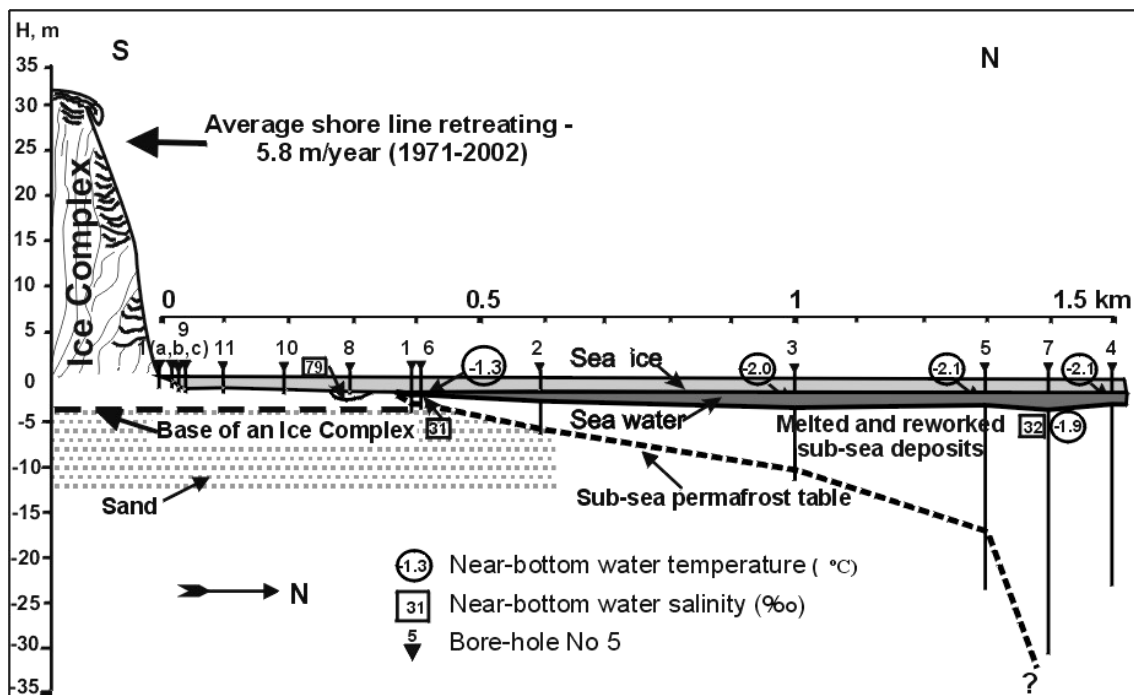


Figure 4: Reconnoitring drilling profile of degraded continental offshore permafrost at the Cape Mammoth Tusk Area, Laptev Sea (April, 2003).

Acknowledgements

The success of the spring part of expedition "Lena 2003" would not been possible without help of the Tiksi Hydrographical Base team, which organized field transportation and drilling assistance (Victor Dobrobaba, Vladimir Yakshin, Timophei Sidorov, Alexander Saphin and Sergey Kamanin). Special thanks to Dmitry Melnichenko, head of the Tiksi Hydrographical Base.

4.7.2. Measurements of the coast relief in the area of Mamontov Klyk and ice and sediment sampling

Mikhail N. Grigoriev and Waldemar Schneider

4.7.2.1. Introduction

One of the main tasks of the expedition "Lena 2003" was an estimation of coastal erosion retreat rates at the about three kilometer long coastal segment in the area of Mamontov Klyk. One of a reasons of these studies is the beginning of the new Laptev Sea System Project "Dynamics of Permafrost". In the frame of this project, during spring 2005, a relatively deep profile consisting of a number of boreholes (up to 200-250 meters in depth) is aimed in that area.

4.7.2.2. Methods

Geodetic measurements have been carried out at the key site, using a laser theodolite Elta 50 R, to obtain the modern horizontal and altitudinal position of the shore line (Figure 4.7-5). Theodolite profiles and benchmarks recorded in the field were identified and compared with the aerial photographs and maps. At erosional shores the position of the cliff base and the cliff upper edge was measured. Characteristic terrestrial features, which could also be identified on aerial photographs, such as sharp turns of small streams, small water bodies, boundaries of different types of vegetation etc., served as natural marks. A number of aerial photographs (scales 1: 30,000 – 1:50,000) and topographic maps (scales 1:25,000-200,000) were analysed. Theodolite profiles and benchmarks recorded in the field could be identified in the remote material. Furthermore, aerial photos and maps are used for long-term analysis of coastal dynamics of the key sites by computer techniques, which allow us to estimate an average rate of shoreline retreat and long-term trends of the Laptev Sea coast quite precisely.

The undisturbed sediment and ice wedge sampling was conducted from the key coastal section by chain saw (Figure 4.7-6).

Detail information concerning general goals and methods of multi-stage coastal studies of Joint German-Russian expedition is presented in previous Reports of Polar Research (Rachold, Grigoriev, 1999, 2000, 2001; Pfeiffer, Grigoriev, 2002; Grigoriev et al., 2003).



Figure 4.7-5. Theodolite survey of the coastal cliff top in the area of Mamontov Klyk (August 2003)



Figure 4.7-6. Coastal sediment and ice wedge sampling by chain saw (area of Mamontov Klyk, August 2003)

4.7.2.3. Preliminary results

The coasts of studied area mainly consist of Ice Complex deposits, which are eroded very fast (Figure 4.7-7). Primary coastal forms are: cliffs, solifluction slopes (Figure 4.7-8), alas remnants and gullies. In 2000, the first measurement of coastal erosion rates at the area of Cape Mamontov Klyk was carried out by coastal team of the Expedition "Lena 2000". It was determined that the average retreating rates of ice-rich cliff tops and cliff base of the whole observed coastal sector for long-term period (1971-2000) are about 4.0 and 4.4 m/year, respectively (Grigoriev et al., 2001).



Figure 4.7-7. 20 meters altitude icy cliff west of Mamontov Klyk Cape (August 2003)

In 2003, at this site additional coastal line measurements and observations were carried out. They have shown that the average coastal retreat rate of studied shore has kept the same range as in the previous period (about 4.0 m/year). Most active coastal retreat takes place in the sections, where the "block" type of shore destruction takes place (Figure 4.7-9). The maximum velocity of coastal erosion was observed at the local limited shore section west of the Nyuchcha-Dzhiele River mouth (up to 6 m/year) and west of Cape Mamontov Klyk (5.8 m/year). Quite moderate retreat rates have been determined on the coastal segments adjacent to mouth of the Nyuchcha-Dzhiele River and Mamontov Klyk Cape (1-3.5 m/year).



Figure 4.7-8: Typical solifluction slope adjacent to Ice Complex shore (area of Mamontov Klyk, August 2003)



Figure 4.7-9.:The "block" type of destruction of the ice-rich shore (west of mouth of the Nuchcha-Dzhiele River)

According to the task of Arctic Coastal Dynamics (ACD) Project, a number of undisturbed sediment and ice wedge samples were collected from the key coastal section and transported to Germany (Table 4.7-1). This site is located in the beginning of prospective drilling profile.

Table 4.7-1: Frozen sediment and ice wedge samples (August 2003)

No.	Name and depth	Coordinates	Description	Number of samples
1	MAK-VI (1-5) Cape Mamontov Klyk	73-36-26.9 N 117-10-38.9 E	Ice block (10x10x10 cm)	5
2	MAK-VS (1-5) Cape Mamontov Klyk	73-36-26.9 N 117-10-38.9 E	Ground block (10x10x10 cm)	5

4.7.1.4. Further investigations

We plan to continue a coastal study and sampling in the area of Cape Mamontov Klyk in the future. Probably in 2005 a deep drilling will be conducted in the coastal zone of that area. Investigated coastal segment belongs to the largest coastal section (120 km) of the Laptev Sea, which almost continuously consists of Ice Complex deposits. This segment is one of the most active in respect of coastal erosion and play a very important role in sediment and organic carbon balance of the Laptev Sea.

4.7.3 Shore face profiles in the area of Cape Mamontov Klyk: echo sounding, seawater and sea bottom deposits sampling

Mikhail N. Grigoriev and Waldemar Schneider

4.7.3.1. Introduction

One of the tasks of the expedition "Lena-Anabar 2003" was a determination of shore face features in the area of Cape Mamontov Klyk at the adjacent near-shore shelf. In this region, a bathymetric survey, seawater and bottom sediment sampling were carried out in August 2003. The main reason of seabed research is a purpose to conduct a relatively deep drilling on the shallow shelf from the sea ice in the nearest future. Previous shore face investigations in this sector of the Laptev Sea (near Terpay-Tumsa Cape) have been carried out in 2000 (Are et al., 2001).

4.7.3.2. Methods

Bathymetric studies were conducted with help the echo-sounding device and rubber boat with "Honda" engine. The field of bathymetric survey has occupied an area about 60 km² (4 x 15 km), between isobath 1 and 10 meters (Figure 4.7-10). The length of all bathymetric profiles exceeds 150 km. For bottom sediment and seawater sampling a standard sampling dredger and bathometer were used.

4.7.3.3. Preliminary results

As a result of bathymetric survey the bathymetric scheme of studied seabed was created. The mean shore face inclination at that part of the shelf is extremely slightly, about 0.0007. At least two quite evident sub-sea terraces (or terrace-like surfaces) were discovered at the shore face. The first vast sub-sea terrace is over the range of depth about 5-6 meters and another terrace begins from 9.5 meters depth (see Fig. 4.7-10).

It is very interesting that a few years ago approximately the same sub-sea terraces were found near the Cape Terpay-Tumsa in 60 km east of the Cape Mamontov Klyk (Are et al., 2001). Probably, these forms are results of several stages of coastal erosion activity. Taking into account that an average coastal retreat rate for the whole studied coast is about 4.0 m/year, the shallow sub-sea terrace, placed from 4.5 km to 11.5 km from the shoreline, was formed during a period of about 2900-1000 years BP. It is very difficult to evaluate the age of formation of the deeper terrace, beginning in a distance of about 14.5 km from the coast. It is possible that this terrace was formed during first stage of sea level stabilization in Holocene (about 5000-3600 years BP).

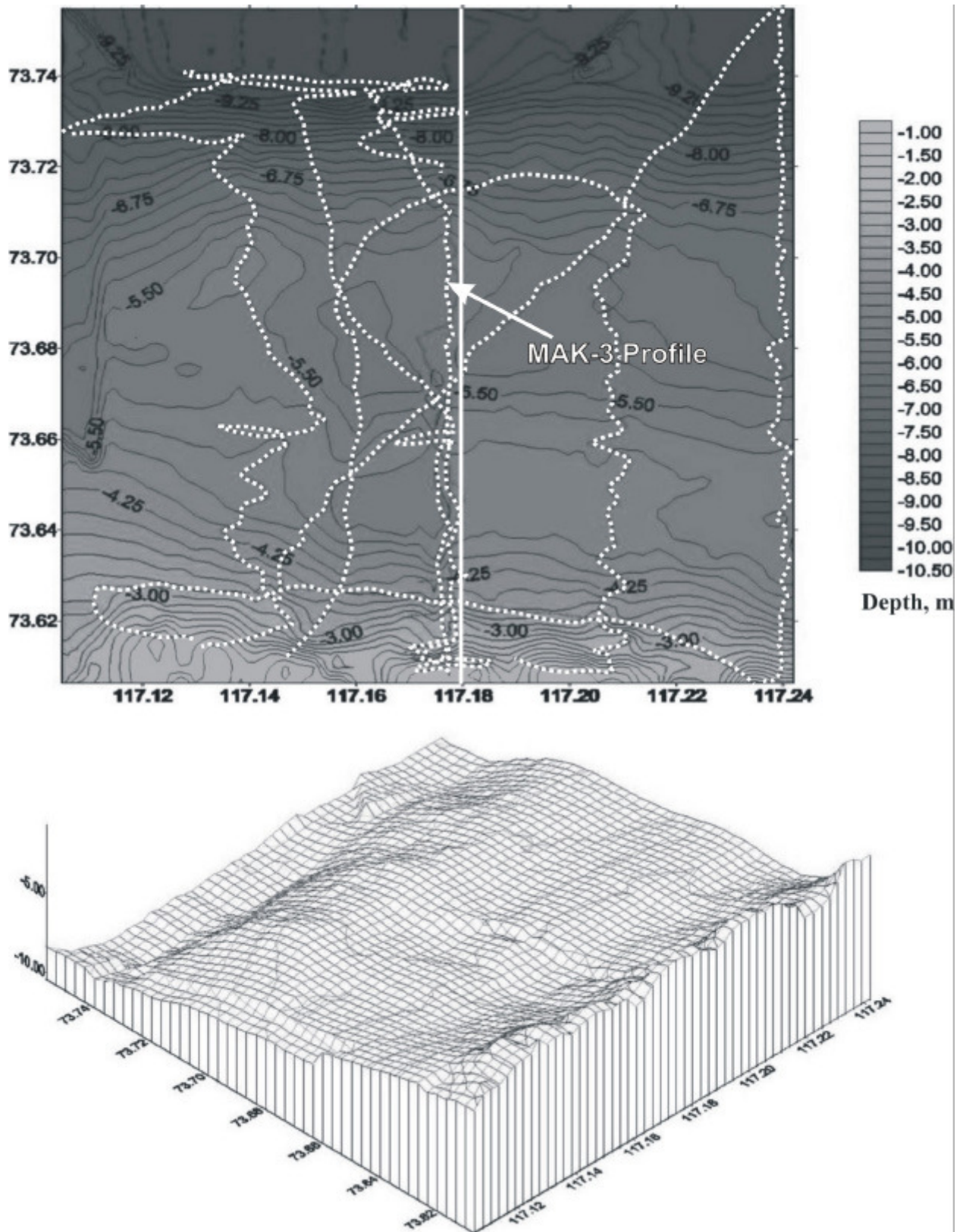


Figure 4.7-10. Bathymetric scheme and the shore face relief adjacent to the Mamontov Klyk Cape area (August 2003). Bathymetric profiles - white dotted line. Vertical white line is a location of proposed drilling profile.

During summer fieldwork 30 bottom sediments samples were collected from 0 to 10 meters depth as well as ice and frozen sediment samples from the coastal outcrops for different types of analysis, which were transported to Germany (Tabs. 4.7-2, 4.7-3). At present time all samples are processed in the laboratories.

Table 4.7-2: List of bottom sediment samples, Profile MAK-3 (August 2003)

No.	Name	Water depth (m)	Number of samples
1	S. MAK-3 (0 m)	0	3
2	S. MAK-3 (1 m)	1	3
3	S. MAK-3 (2 m)	2	3
4	S. MAK-3 (3 m)	3	3
5	S. MAK-3 (4 m)	4	3
6	S. MAK-3 (5 m)	5	3
7	S. MAK-3 (6 m)	6	3
8	S. MAK-3 (7 m)	7	3
9	S. MAK-3 (8 m)	8	3
10	S. MAK-3 (9 m)	9	3
11	S. MAK-3 (10 m)	10	3

Table 4.7-3: Frozen water and frozen sediment samples „Lena – Anabar 2003“

No.	Name	Depth (Water depth / Depth of sampling)	Description	Number of samples
1	MAK-3	0m; 2,5m; 5m; 7,5m; 10m	Frozen sea water samples	5
2	MAK-3	7/0m; 7/3,5m; 7/7m; 10/0m;10/5m;10/10m 0m;2,5/0m;5/0m;5/5m;	Frozen sea water sample (Unfiltered)	10
3	MAK-3	0/0m; 2,5/0m; 5/0m; 5/5m; 7/0m; 7/3,5m; 7/7m; 10/0m; 10/5m; 10/10m)	Frozen sea water sample (Filtered)	10

4.7.3.4. Further investigations

The study of shore face profile structure and dynamics in the area of Cape Mamontov Klyk will be continued in spring 2005. The new facts concerning development of the shore face could be very useful for study of sub-sea permafrost evolution and regional paleogeographical reconstructions on the whole.

4.8. References

- Amaral, J.A., Ekins, A., Richards, S.R. and Knowles, R. (1998). Effects of selected monoterpenes on methane oxidation, denitrification and aerobic metabolism by bacteria in pure culture. *Appl. Environ. Microbiol.* 64: 520-525.
- Are F.E., Grigoriev M. N., Rachold V., Hubberten, H.-W., Razumov S. O., and W. Schneider (2001) Shoreface profiles of the central and western Laptev Sea coast: In: Russian-German Cooperation SYSTEM LAPTEV SEA-2000: The Expedition LENA 2000. Reports on Polar Research, 388: 60-64.
- Boyarsky O.G. and Mitt K.L. (1961). New data on relic ground ice in Olenek-Anabar tundra. *Merzlotnye Issledovania, MSU*, v. 1, p.154-162. (In Russian).
- Calhoun, A. and King, G.M. (1997). Regulation of root-associated methanotrophy by oxygen availability in the rhizosphere of two aquatic macrophytes. *Appl. Environ. Microbiol.* 63 (8): 3051-3058.
- Cao, M., Marshall, S. and Gregson, K. (1996). Global carbon exchange and methane emissions from natural wetlands: application of a process-based model. *J. Geophys. Res.* 101 (D9): 14399-14414.
- Chekanovsky N.L. (1896). The daybook of the expedition at rivers Nizhniaya Tunguska, Olenek and Lena in 1873-1875. *Transactions of Russian Geographical Society*, v. XX, ? 1, (In Russian).
- Christensen, T.R. (1993). Methane emission from arctic tundra. *Biogeochemistry* 21: 117-139.
- Drachev S.S., Savostin L.A., Groshev V.G., Bruni I.E. (1998). Structure and geology of the continental shelf of the Laptev Sea, Eastern Russia Arctic., *Tectonophysics* 298: 357-393.
- Galabala R.O. (1987). New data on delta Lena construction. In "Quaternary period of Northern-East Asia. Magadan, SVKNII DVO AN SSSR, p. 152-172. (In Russian).
- Grigoriev M. N., Rachold V., Are F. E., Hubberten H.-W., Razumov S. O., and W. Schneider (2001). Coastal erosion in the Western coast of the Laptev Sea (2001). In: *The Lena Delta expedition 2000. Reports on Polar Research, Bremerhaven, Germany*, 335, p. 54-60.
- Grigoriev M. N., Rachold V., Bolshiyarov D.Yu., Pfeiffer E.-M., Schirrmeister L., Wagner D., and H.-W. Hubberten (Eds.) (2003). *Russian-German Cooperation SYSTEM LAPTEV SEA 2000: The Expedition LENA 2002. Reports on Polar and Marine Research*, 466, Bremerhaven, Germany, 341 pp.
- Grigoriev M.N. (1993). Cryomorphogenesis of the Lena River mouth area. *Permafrost Institute SB AN USSR, Yakutsk, Russia*. 176 pp. (In Russian).
- Grigoriev N.F. (1966). *Permafrost in the Yakutian coastal Zone*. Nauka Press, Moscow, Russia, 180 pp. (In Russian)
- Grigoriev, M.N., and V.V. Kunitsky (2000). Ice Complex of Yakutian Arctic Coast as a Sediment Source on the Shelf.: *Hydro meteorological and Biogeochemical Studies in the Arctic*. Vladivostok: Arctic Regional Centre, Far-Eastern Branch of RAS, Vol. 2, pp. 109-116 (in Russian).
- Harris, R.C., Bartlett, K., Frolking, S. and Crill, P. (1993). Methane emissions from northern high-latitude wetlands. In: Oremland, R.S. (ed.) *Biogeochemistry of Global Change: Radioactively Active Trace Gases*. Chapman and Hall, New York, pp. 449-485.
- Kolpakov V.V. (1973). The paleogeographical meaning of Quaternary Aeolian deposits in the North of Eastern Siberia. In "Several problems of regional geology". M. p. 38-42. (In Russian).
- Krueger, M., Frenzel, P. and Conrad, R. (2001). Microbial processes influencing methane emission from rice fields. *Global Change Biology* 7: 49-63.
- Kutzbach, L., Wagner, D. and Pfeiffer, E.-M. (2004). Effect of microrelief and vegetation on methane emission from wet polygonal tundra, Lena Delta, Northern Siberia. *Biogeochemistry* 69: 341-362.

- Meyer, H. (2003). Studies on recent cryogenesis. – In: Russian-German Cooperation SYSTEM LAPTEV SEA - The Expeditions LENA 2002, Ed.: Grigoriev et al., Reports of Polar and Marine Research 466, p. 29-48.
- Meyer, H., A. Yu. Dereviagin, C. Siegert, and H.-W. Hubberten (2002a). Paleoclimate studies on Bykovsky Peninsula, North Siberia; hydrogen and oxygen isotopes in ground ice.- Polarforschung, 70, p. 37-51.
- Meyer, H., A. Yu. Dereviagin, C. Siegert, L. Schirrmeister, and H.-W. Hubberten (2002b). Palaeoclimate reconstruction on Big Lyakhovsky Island, North Siberia; hydrogen and oxygen isotopes in ice wedges.- Permafrost and Periglacial Processes, 13, p. 91-105.
- Moraes, F. and Khalil, M.A.K. (1993). Permafrost methane content: 2. Modeling theory and results. Chemosphere 26: 595-607.
- Pfeiffer E.-M. and M.N. Grigoriev (Eds.) (2002). Russian-German Cooperation SYSTEM LAPTEV SEA 2000: The Expedition LENA 2001. Reports on Polar Research, 426, Bremerhaven, Germany, 186 pp.
- Pfeiffer, E.-M., Akhmadeeva, I., Becker, H., Friedrich, K., Wagner, D., Quass, W., Zhurbenko, M., Zöllner, E., Boike, J. (1999). Modern Processes in Permafrost Affected Soils. In: Rachold, V. and Grigoriev, M.N. (ed.) Expeditions in Siberia 1998. Reports on Polar Research 315: pp. 19-80.
- Popp, T.J., Chanton, J.P., Whiting, G.J. and Grant, N. (2000). Evaluation of methane oxidation in the rhizosphere of a *Carex* dominated fen in north central Alberta, Canada. Biogeochemistry 51: 259-281.
- Puminov A.P. (1962). Covering Quaternary deposits of Anabar-Olenek interfluves. In "Quaternary geology and geomorphology of Siberia". Novosibirsk, Publications of IGI G SO AN SSSR, v. 27., p. 102-117. (In Russian).
- Rachold V., and M. N. Grigoriev (Eds.) (1999). Russian-German Cooperation SYSTEM LAPTEV SEA-2000: The Expedition LENA DELTA 1998. Reports on Polar Research, 315, Bremerhaven, Germany, 259 pp.
- Rachold V., and M. N. Grigoriev (Eds.) (2000). Russian-German Cooperation SYSTEM LAPTEV SEA-2000: The Expedition LENA 1999. Reports on Polar Research, 354, Bremerhaven, Germany, 269 pp.
- Rachold V., and M. N. Grigoriev (Eds.) (2001). Russian-German Cooperation SYSTEM LAPTEV SEA-2000: The Expedition LENA 2000. Reports on Polar Research, 388, Bremerhaven, Germany, 135 pp.
- Rivkina, E. and Gilichinsky, D. (1996). Methane as a paleoindicator of the dynamics of permafrost deposits. Lithology and Mineral Resources 31 (4), 396-399.
- Roulet, N.T., Jano, A., Kelly, C.A., Klinger, L.F., Moore, T.R., Protz, R., Ritter, J.A. and Rouse, W.R. (1994). Role of the Hudson Bay lowland as a source of atmospheric methane. J. Geophys. Res. 99 (D1). 1435-1454.
- Saks V.N. (1963). Quaternary period in Soviet Arctic. Publications of NIIGA, v. 77. (In Russian).
- Schirrmeister, L., Grosse, G., Schwamborn, G., Andreev, A.A., Meyer, Kunitsky, V.V., Kuznetsova, T.V., Dorozkina, M.V., Pavlova, Y.Y, Bobrov, A., Oezen, D. (2004). Late Quaternary history of the accumulation plain north of the Chekanovsky Ridge (Lena Delta, Russia). A multidisciplinary approach.- Polar geography, 27: 277-319.
- Sochava V.B. (1933). Tundra of Anabar River basin. Publications of Geographical Society, v. 65, ? 4. (In Russian).
- Soil Survey Staff, Soil Conservation Service, USDA (1998). Keys to Soil Taxonomy 8th edition. Pocahontas, Blacksburg, Virginia.
- Telepnev E.V. (1981). Sub-sea frozen zone of the near-shore part of the Big Lyakhovsky Island. In: Cryolithozone of the Arctic Shelf. Permafrost Institute SB AN USSR, Yakutsk, Russia, pp. 44-53 (In Russian).
- Toll E.V. (1894). The expedition of Academy of Science to New Siberian Islands and Coast of North Ocean. Izvestia Russkogo Geographicheskogo obshestva, v. 30, ? 4. (In Russian).

- Tolmachev I.P. (1904). New founding on Siberia's geology. Publications of St.-Petersburg's Community of Natural Scientists, v. XXXIV, ? 1. (In Russian).
- Vaikmäe, R. (1989). Oxygen Isotopes in Permafrost and Ground Ice - A new Tool for paleoclimatic Investigations.- Proceedings of the 5th Working Meeting Isotopes in Nature, Leipzig, September 1989, p. 543-553.
- Whalen, S.C., Reeburgh, W.S. (1992). Interannual variations in tundra methane emission: a 4-year time series at fixed sites. Global Biogeochem. Cycles 6: 139-159.
- Zhukov V.V., Gorina I.F., Pinchuk L.Ya. (1968). Cenozoic diamondiferous of Anabar-Olenek interfluves. Publications of NIIGA, v.156. (In Russian).

4.9. Appendices

Appendix 4-1. Surface parameters for the studied geolocated sites around Cape Mamontov Klyk	155
Appendix 4-2. Active layer data of the geo-located sites.....	170
Appendix 4-3. List of soil samples (active layer); collected in the coastal lowland.....	171
Appendix 4-4. List of permafrost sediment and paleosol samples for microbiological, molecular biological and biochemical analyses.....	172
Appendix 4-5. List of sediment samples.....	173
Appendix 4-6. List of ice and water samples.....	182
Appendix 4-7. Collection of bone samples.....	189

Appendix 4-1. Surface parameters for the studied geolocated sites around Cape Mamontov Klyk

Site	Latitude	Longitude	Date	Major relief type	Relief position	Meso- and Micro relief features	Slope inclination	Mean slope (°)	Soil moisture	Water bodies	Water depth (cm)	Photo
Mklyk	73,6073	117,1249	08. 08	Edoma	lower slope	thermokarst hills	very gently	3	moderate moist	-	-	yes
212	73,6109	117,1268	10. 08	River valley (mouth)	terrace	sand bank	flat	1	moist	-	-	-
213	73,6069	117,1925	10. 08	Ovrag (mouth)	medium slope	-	very steep	65	moist	-	-	-
214	73,6051	117,1994	10. 08	Edoma	elevated plain	-	very gently	2,5	dry	-	-	yes
215	73,6045	117,2102	10. 08	Ovrag (mouth)	medium slope	mud flows	very steep	65	very moist	-	-	yes
216	73,5955	117,2475	10. 08	Marine terrace	lower plain	-	flat	1,5	very moist	small ponds	n.a.	yes
217	73,5976	117,2365	10. 08	Log	floor	-	very gently	3,5	wet	-	-	-
218	73,5998	117,2295	10. 08	Log	floor	-	very gently	3,5	wet	-	-	-
219	73,6104	117,1347	11. 08	Tidal flat	lower plain	-	flat	1,5	wet	surface water	5	-
220	73,6085	117,1544	11. 08	Tidal flat	lower plain	-	flat	1,5	wet	surface water	5	-
221	73,6083	117,1561	11. 08	Tidal flat	lower plain	-	flat	1,5	wet	surface water	5	-
224	73,6104	117,1346	12. 08	Log	floor	-	flat	2	very moist	-	-	-
243	73,6083	117,1540	12. 08	Log	floor	-	flat	2	very moist	-	-	-
262	73,6069	117,1821	12. 08	Log	lower slope	-	very gently	4	moist	-	-	-
266	73,6073	117,1879	12. 08	Ovrag	medium slope	mud flows	steep	50	very moist	-	-	-
Mak-1	73,6074	117,1892	12. 08	Cliff	lower slope	mud flows	very steep	80	wet	-	-	yes
Mak-2	73,6075	117,1825	14. 08	Cliff	lower slope	mud flows	very steep	70	wet	-	-	yes
Mak-3	73,6075	117,1819	14. 08	Cliff	lower slope	mud flows	very steep	75	wet	-	-	yes
275	73,6043	117,1334	15. 08	Log	floor	-	very gently	3	wet	surface water	5	-
276	73,6058	117,1355	15. 08	Log	medium slope	thermokarst hills	gently	12	moist	-	-	yes
277	73,6059	117,1501	15. 08	Log	medium slope	-	low	25	moist	-	-	yes
278	73,6055	117,1493	15. 08	Log	medium slope	-	low	25	moist	-	-	yes
279	73,6057	117,1601	15. 08	Edoma	upper slope	thermokarst hills	very gently	7,5	moderate moist	-	-	yes
280	73,6058	117,1653	15. 08	Edoma	elevated plain	polygonal structures	flat	1	very moist	large irregular polygonal pond	22	yes
281	73,6059	117,1713	15. 08	Edoma	elevated plain	-	flat	1	moist	small ponds	<40	yes
282	73,6035	117,1746	15. 08	Edoma	upper slope	-	gently	14	very moist	-	-	yes
283	73,6023	117,1799	15. 08	Edoma	upper slope	thermokarst hills	moderate	18	moist	-	-	yes

284	73,6015	117,1810	15. 08	Log	floor	-	flat	1	wet	surface water	10	yes
285	73,6004	117,1808	15. 08	Log	floor	-	flat	1	wet	large pond	>50	yes
286	73,5990	117,1826	15. 08	Edoma	elevated plain	polygonal structures	flat	2	moist	small ponds	12	yes
287	73,5983	117,1849	15. 08	Edoma	elevated plain	polygonal structures	flat	2	moist	small ponds	12	yes
288	73,5967	117,1842	15. 08	Log	floor	-	flat	1	wet	large pond	30	yes
289	73,5969	117,1829	15. 08	Edoma	medium slope	thermokarst hills	low	16	less moist	-	-	-
290	73,5974	117,1749	15. 08	Edoma	upper slope	-	gently	7,5	moist	-	-	-
291	73,5977	117,1697	15. 08	Edoma	medium slope	-	gently	13	less moist	-	-	yes
292	73,5980	117,1619	15. 08	Edoma	elevated plain	polygonal structures	flat	1	moist	small polygonal ponds	n.a.	yes
293	73,5983	117,1576	15. 08	Edoma	elevated plain	polygonal structures	flat	1	very moist	large pond	20	yes
294	73,5988	117,1571	15. 08	Edoma	elevated plain	polygonal structures	flat	1	very moist	large irregular polygonal pond	n.a.	yes
295	73,6096	117,1202	18. 08	River valley	terrace	sand bank	flat	1	moist	-	-	yes
296	73,6104	117,1200	18. 08	River valley	terrace	sand bank	flat	1	moist	-	-	yes
297	73,6118	117,1200	18. 08	River valley	terrace	sand bank	flat	2	moist	-	-	yes
298	73,6077	117,1259	18. 08	Edoma	medium slope	thermokarst hills	low	25	less moist	-	-	-
299	73,6075	117,1193	19. 08	River valley	terrace	sand bank	gently	4	very moist	-	-	yes
300	73,6077	117,1151	19. 08	River valley	terrace	sand bank	flat	1	moist	surface water	5	yes
301	73,6066	117,1072	19. 08	Edoma	medium slope	thermokarst hills	gently	12,5	less moist	-	-	yes
302	73,6063	117,1033	19. 08	Edoma	medium slope	thermokarst hills	gently	7,5	moist	-	-	yes
303	73,6050	117,0970	19. 08	Ovrag	medium slope	solifluction, nival niche	moderate	35	moist	-	-	yes
304	73,6050	117,0921	19. 08	Log	medium slope	nival niche	moderate	32,5	moist	-	-	yes
305	73,6052	117,0813	19. 08	Log	floor	-	flat	1	very moist	surface water	10	yes
306	73,6045	117,0775	19. 08	Edoma	elevated plain	-	very gently	4	dry	-	-	yes
307	73,6046	117,0739	19. 08	TK depression	floor	sediment fan	very gently	2	moist	-	-	yes
308	73,6032	117,0715	19. 08	Edoma	elevated plain	polygonal structures	flat	1	moderate moist	some polygonal ponds	<40	yes
309	73,6014	117,0671	19. 08	Edoma	upper slope	-	gently	7,5	less moist	-	-	-
310	73,6005	117,0656	19. 08	Edoma	medium slope	-	low	15	less moist	-	-	yes
311	73,5996	117,0626	19. 08	Log	floor	-	flat	1	very moist	surface water	6	-

312	73,5990	117,0600	19. 08	Edoma	medium slope	thermokarst hills	low	16	less moist	-	-	-
313	73,5992	117,0634	19. 08	Log	floor	-	flat	1	wet	surface water & small pond	5 & 40	-
314	73,5938	117,0797	19. 08	Edoma	medium slope	thermokarst hills	low	16	moderate moist	-	-	-
315	73,5939	117,0833	19. 08	Edoma	upper slope	drainage channels	gently	6	less moist	-	-	-
316	73,5939	117,0900	19. 08	Ovrag	medium slope	mud flows, solifluction	steep	50	very moist	-	-	-
317	73,5934	117,0960	19. 08	Log	floor	-	flat	1	wet	-	-	yes
318	73,5935	117,1017	19. 08	River valley	terrace	-	flat	1	wet	-	-	-
319	73,5940	117,1018	19. 08	River valley	terrace	polygonal structures	very gently	2,5	moist	polygonal ponds	n.a.	yes
320	73,5944	117,1128	19. 08	River valley	terrace	sand bank	very gently	2,5	moist	-	-	yes
321	73,5936	117,1132	19. 08	River valley	terrace	polygonal structures	very gently	4	moderate moist	-	-	yes
322	73,5895	117,1148	19. 08	River valley	terrace	polygonal structures	flat	1	very moist	large irregular polygonal pond	n.a.	-
323	73,5906	117,1119	19. 08	River valley	terrace	-	flat	1	very moist	river channel	n.a.	-
324	73,5945	117,1200	19. 08	River valley	terrace	polygonal structures	flat	1	very moist	polygonal ponds	n.a.	yes
325	73,5957	117,1238	19. 08	Edoma	medium slope	thermokarst hills	low	30	less moist	-	-	-
326	73,5966	117,1251	19. 08	Log	floor	-	flat	1	wet	surface water	5	yes
327	73,5991	117,1272	19. 08	Edoma	upper slope	-	gently	13	moderate moist	-	-	-
328	73,6035	117,1269	19. 08	Edoma	upper slope	-	gently	7,5	moist	-	-	-
329	73,6078	117,1638	20. 08	Thermoerosional terrace	lower slope	mud flows	moderate	32	very moist	-	-	yes
330	73,6077	117,1525	20. 08	Log	floor	-	very gently	3	wet	surface water	5	-
331	73,6074	117,1499	20. 08	Edoma	medium slope	thermokarst hills	low	16	moderate moist	-	-	-
332	73,6082	117,1443	20. 08	Edoma	medium slope	-	low	16	moderate moist	-	-	-
333	73,6087	117,1397	20. 08	Log	upper slope	-	gently	7	moist	-	-	-
334	73,6087	117,1368	20. 08	Edoma	elevated plain	-	flat	1	moist	-	-	-
335	73,6084	117,1345	20. 08	Edoma	upper slope	-	gently	8	moderate moist	-	-	-
336	73,6080	117,1308	20. 08	Log	medium slope	-	low	20	moist	-	-	-
337	73,5794	117,9832	21. 08	Tidal flat	lower plain	-	flat	1	moist	-	-	-
338	73,5788	117,9952	21. 08	River valley (mouth)	terrace	sand bank	flat	1	dry	-	-	yes

339	73,5763	117,9758	21. 08	Edoma	elevated plain	polygonal structures	flat	0	moist	some polygonal ponds	n.a.	yes
340	73,5716	117,9679	21. 08	Edoma	elevated plain	polygonal structures	flat	0	very moist	many polygonal ponds	n.a.	yes
341	73,5686	117,9660	21. 08	Ovrag	medium slope	solifluction	steep	50	moist	-	-	yes
342	73,5671	117,9434	21. 08	TK depression	medium slope	thermokarst hills	low	27,5	dry	-	-	yes
343	73,5655	117,9400	21. 08	TK depression	lower slope	polygonal structures	gently	7,5	wet	polygonal ponds	10	yes
344	73,5608	117,9428	21. 08	TK depression	floor	polygonal structures	flat	1	wet	surface water & polygonal ponds	5 & 20	yes
345	73,5593	117,9444	21. 08	TK depression	lower slope	polygonal structures	gently	7,5	moist	-	-	yes
346	73,5566	117,9440	21. 08	TK depression	upper slope	-	low	20	dry	-	-	yes
347	73,5562	117,9429	21. 08	TK depression	floor	-	flat	1	wet	surface water	5	yes
348	73,5553	117,9422	21. 08	TK depression	floor	-	flat	1	very moist	water channel	>80	yes
349	73,5558	117,9492	21. 08	Log	floor	sediment fan	very gently	3	moist	-	-	-
350	73,5550	117,9549	21. 08	Log	floor	sediment fan	very gently	3	moist	-	-	-
351	73,5537	117,9548	21. 08	TK depression	floor	-	flat	1	very moist	-	-	yes
352	73,5545	117,9571	21. 08	Log	floor	sediment fan	very gently	3	moist	-	-	-
353	73,5510	117,9558	21. 08	TK depression	floor	-	flat	2	very moist	-	-	yes
354	73,5508	117,9582	21. 08	TK depression	floor	-	flat	1	very moist	-	-	yes
355	73,5512	117,9577	21. 08	TK depression	floor	-	flat	1	wet	surface water	5	yes
356	73,5536	117,9610	21. 08	Log	floor	sediment fan	very gently	4	moist	-	-	-
357	73,5526	117,9624	21. 08	TK depression	floor	polygonal structures	very gently	4	wet	polygonal pond	<50	yes
358	73,5520	117,9631	21. 08	TK depression	floor	polygonal structures	very gently	4	wet	polygonal pond	25	yes
359	73,5521	117,9635	21. 08	TK depression	floor	polygonal structures	very gently	4	wet	polygonal pond	50	yes
360	73,5522	117,9640	21. 08	TK depression	floor	polygonal structures	very gently	4	wet	polygonal pond	50	yes
361	73,5523	117,9645	21. 08	TK depression	floor	polygonal structures	very gently	4	wet	polygonal pond	50	yes
362	73,5529	117,9645	21. 08	Log	floor	sediment fan	very gently	4	moist	-	-	-
363	73,5571	117,9714	21. 08	Log	floor	-	very gently	5	wet	surface water	5	yes
364	73,5609	117,9779	21. 08	Edoma	elevated plain	polygonal structures	flat	1	moist	some polygonal ponds	n.a.	yes

365	73,5651	117,9796	21. 08	Ovrag	medium slope	thermokarst hills, solifluction	moderate	45	moist	-	-	yes
366	73,5678	117,9808	21. 08	Log	floor	thermokarst hills	flat	1	wet	-	-	yes
367	73,5681	117,9809	21. 08	Log	medium slope	thermokarst hills	moderate	45	dry	-	-	yes
368	73,5706	117,9851	21. 08	Log	floor	thermokarst hills	flat	1	wet	-	-	yes
369	73,5771	117,9935	21. 08	Elevated plain (no Edoma)	upper slope	-	low	17,5	dry	-	-	yes
370	73,5796	117,9973	21. 08	Tidal flat	lower plain	-	flat	2	very moist	-	-	yes
371	73,5776	117,9945	21. 08	Log	floor	-	very gently	5	moist	-	-	-
WS	73,6084	117,1280	22. 08	Edoma	upper slope	-	very gently	5	moist	-	-	yes
445	73,6082	117,1191	22. 08	River valley	terrace	sand bank	flat	2	moist	-	-	-
446	73,6059	117,1298	22. 08	Edoma	medium slope	thermokarst hills	gently	10	moderate moist	-	-	-
447	73,6125	117,0979	23. 08	Edoma	elevated plain	thermokarst hills	very gently	4	moderate moist	-	-	-
448	73,6143	117,0852	23. 08	Edoma	elevated plain	polygonal structures	flat	2	moist	some polygonal ponds	n.a.	yes
449	73,6154	117,0813	23. 08	Edoma	medium slope	-	gently	12,5	very moist	-	-	-
450	73,6153	117,0743	23. 08	Edoma	elevated plain	polygonal structures	flat	1	very moist	polygonal ponds	n.a.	yes
451	73,6141	117,0603	23. 08	Ovrag	lower slope	mudflow, thermokarst hills	steep	50	moist	-	-	-
452	73,6147	117,0573	23. 08	Ovrag	lower slope	mudflow, thermokarst hills	steep	50	moist	-	-	yes
453	73,6187	117,0531	23. 08	Ovrag	lower slope	mudflow	steep	50	moist	-	-	-
454	73,6183	117,0480	23. 08	Log	medium slope	-	steep	50	n.a.	-	-	yes
455	73,6166	117,0376	23. 08	Log	medium slope	thermokarst hills	gently	12,5	dry	-	-	yes
456	73,6175	117,0256	23. 08	Edoma	elevated plain	polygonal structures	flat	1	very moist	polygonal ponds	n.a.	-
457	73,6190	117,0195	23. 08	Edoma	elevated plain	polygonal structures	flat	1	very moist	polygonal ponds	n.a.	yes
458	73,6191	117,0069	23. 08	Edoma	upper slope	drainage channels	gently	10	very moist	-	-	-
459	73,6226	116,9723	23. 08	Edoma	medium slope	polygonal structures	low	15	moist	-	-	-
460	73,6367	116,8939	23. 08	TK depression	floor	polygonal structures	flat	0	wet	large polygonal ponds	10	yes

461	73,6363	116,8929	23. 08	TK depression	floor	polygonal structures	flat	0	wet	large polygonal pond	40	yes
462	73,6348	116,8905	23. 08	TK depression	floor	polygonal structures	flat	0	wet	polygonal pond	50	-
463	73,6341	116,8890	23. 08	TK depression	lower slope	thermokarst hills	gently	12	dry	-	-	yes
464	73,6341	116,8876	23. 08	TK depression	lower slope	thermokarst hills	gently	12	dry	-	-	yes
465	73,6343	116,8806	23. 08	TK depression	floor	polygonal structures	flat	0	wet	polygonal pond	40	yes
466	73,6351	116,8791	23. 08	TK depression	floor	-	flat	0	wet	irregular lake	38	yes
467	73,6356	116,8774	23. 08	TK depression	floor	-	flat	0	wet	surface water	3	yes
468	73,6359	116,8787	23. 08	TK depression	floor	-	flat	0	wet	irregular lake	80	yes
469	73,6374	116,8709	23. 08	TK depression	floor	polygonal structures	flat	1	very moist	polygonal ponds	n.a.	yes
470	73,6404	116,8329	23. 08	Edoma	elevated plain	-	flat	1	moderate moist	-	-	yes
471	73,6402	116,8480	23. 08	Log	floor	-	gently	10	wet	surface water	10	yes
472	73,6400	116,8668	23. 08	TK depression	floor	polygonal structures	flat	1	very moist	polygonal ponds	n.a.	-
473	73,6396	116,8817	23. 08	TK depression	floor	-	flat	0	n.a.	-	-	yes
474	73,6270	116,9469	23. 08	River valley (mouth)	terrace	sand bank	very gently	5	moderate moist	-	-	yes
475	73,6275	116,9483	23. 08	River valley (mouth)	terrace	sand bank	very gently	5	moist	-	-	yes
476	73,6257	116,9443	23. 08	River valley	terrace	-	gently	12	moderate moist	-	-	-
479	73,5957	117,2166	26. 08	Log	lower slope	thermokarst hills	gently	10	less moist	-	-	yes
480	73,5945	117,2339	26. 08	Log	lower slope	-	low	25	less moist	-	-	-
481	73,5945	117,2349	26. 08	Log	medium slope	-	low	25	less moist	-	-	-
482	73,5947	117,2380	26. 08	Log	upper slope	thermokarst hills	low	18	less moist	-	-	-
483	73,5892	117,2585	26. 08	Marine terrace	lower slope	sediment fan, polygonal structures	gently	7,5	very moist	-	-	yes
484	73,5886	117,2637	26. 08	Marine terrace	lower plain	-	very gently	3	wet	surface water & small lakes	5 & 60	yes
485	73,5870	117,2786	26. 08	Marine terrace	lower plain	-	flat	2	wet	surface water	5	yes
486	73,5877	117,2797	26. 08	Marine terrace	lower plain	-	flat	1	wet	surface water	5	yes
487	73,5884	117,2820	26. 08	Tidal flat	lower plain	-	flat	1	moist	-	-	yes
488	73,5891	117,2841	26. 08	Tidal flat	lower plain	-	flat	1	moist	-	-	yes
489	73,5897	117,2859	26. 08	Tidal flat	lower plain	-	flat	1	moist	-	-	yes
490	73,5875	117,2860	26. 08	Tidal flat	lower plain	-	flat	1	moist	-	-	-

491	73,5867	117,2887	26. 08	Marine terrace	lower plain	-	flat	2	wet	surface water & small lakes	5 & 60	-
492	73,5846	117,2903	26. 08	Marine terrace	lower plain	-	flat	2	wet	surface water & small lakes	5 & 60	yes
493	73,5826	117,2856	26. 08	Marine terrace	lower plain	-	flat	1	wet	surface water	5	yes
494	73,5826	117,2809	26. 08	Marine terrace	lower slope	sediment fan	gently	7,5	wet	surface water	5	yes
495	73,5837	117,2767	26. 08	Marine terrace	lower slope	sediment fan	gently	7,5	wet	ponds	n.a.	yes
496	73,5841	117,2744	26. 08	Marine terrace	lower slope	-	gently	7,5	wet	ponds	n.a.	yes
497	73,5846	117,2720	26. 08	Marine terrace	lower slope	solifluction	low	18	moist	-	-	yes
498	73,6043	117,1142	28. 08	River valley	terrace	polygonal structures	very gently	3	very moist	polygonal ponds	n.a.	yes
499	73,6020	117,1174	28. 08	River valley	terrace	polygonal structures	gently	7,5	moderate moist	-	-	yes
500	73,5948	117,1195	28. 08	River valley	terrace	polygonal structures	very gently	3	very moist	polygonal throughs	n.a.	-
501	73,5895	117,1214	28. 08	Edoma	medium slope	polygonal structures	low	25	moist	-	-	-
502	73,5893	117,1308	28. 08	Edoma	medium slope	polygonal structures	low	20	moist	-	-	-
503	73,5897	117,1366	28. 08	Ovrag	medium slope	mud flows	steep	50	moist	-	-	yes
504	73,5898	117,1421	28. 08	River valley	terrace	-	flat	1	less moist	oxbow lake	n.a.	yes
505	73,5913	117,1442	28. 08	Edoma	medium slope	thermokarst hills	low	15	wet	-	-	yes
506	73,5932	117,1391	28. 08	Edoma	elevated plain	-	gently	6	very moist	few small ponds	n.a.	yes
507	73,5956	117,1367	28. 08	Edoma	elevated plain	-	flat	1	very moist	few small ponds	n.a.	yes
508	73,6008	117,1370	28. 08	Edoma	elevated plain	polygonal structures	flat	1	very moist	few small ponds	n.a.	-

Site	Major vegetation	Minor vegetation	Dry vegetation (%)	Samples	Remarks
Mklyk	grass	-	n.a.	-	camp Mamontovy Klyk 2003, kitchen tent; initial thermokarst hills <30cm high
212	-	-	-	-	estuary of the Nyuchcha-Dzhiele, start point of the Eastern coastal section
213	-	grass	n.a.	-	
214	moss, lichen	grass	55	Mak-AA-1	signal tower, frost boils
215	-	grass	n.a.	-	erosional ravine, disturbed surface
216	-	grass	n.a.	Mak-G-1	grey-black silt, covering peat and wood accumulations, terrace 0.5 m asl
217	n.a.	n.a.	n.a.	-	
218	n.a.	n.a.	n.a.	-	
219	-	-	-	Mak-11	in front of the coastal cliff, wave ripples, accumulation of organic matter, Mak-11 at the cliff
220	-	-	-	-	in front of the coastal cliff, wave ripples, accumulation of organic matter
221	-	-	-	-	in front of the coastal cliff, wave ripples, accumulation of organic matter
224	n.a.	n.a.	n.a.	-	upper cliff
243	n.a.	n.a.	n.a.	-	upper cliff
262	n.a.	n.a.	n.a.	-	upper cliff
266	-	grass	n.a.	-	upper cliff, small erosional ravine, disturbed surface
Mak-1	-	-	-	Mak-1	
Mak-2	-	-	-	Mak-2	
Mak-3	-	-	-	Mak-3	
275	grass, sedges	Eriophorum	n.a.	Methane sampling	methane measurement site
276	grass	Eriophorum, moss, lichen	n.a.	Mak-G-2	grass tussocks, thermokarst hills >1 m high & 4 m in diameter
277	grass, Eriophorum	moss, lichen	n.a.	-	active layer depth cross-profile
278	grass, Eriophorum	moss, lichen	n.a.	-	active layer depth cross-profile
279	grass	moss, Eriophorum	n.a.	-	
280	grass, Eriophorum, moss	-	10	Mak-AI-1, Mak-96-02, Mak-AA-2	water-filled polygonal trough

281	grass, Eriophorum, moss	-	25	-	undulating surface, small moss patches
282	grass, Eriophorum	moss	30	-	surrounded by slopes with thermokarst hills
283	grass, moss	-	40	-	thermokarst hills 4 m in diameter & with wide interspaces
284	sedges	Eriophorum, moss	7,5	-	8-10 m wide floor
285	sedges	Eriophorum, moss	7,5	Mak-96-03, Mak-AA-3, Mak-CE-1	small hills of accumulated moss, 1.2 m in diameter and 70 cm high
286	moss, Eriophorum	-	35	-	large moss-peat patches, 5-6 m in diameter, dried-up polygonal ponds ?
287	moss, Eriophorum	-	35	-	large moss-peat patches, 5-6 m in diameter, dried-up polygonal ponds ?
288	sedges	Eriophorum, moss	n.a.	-	slopes covered with thermokarst hills
289	grass	moss, lichen	n.a.	-	thermokarst hills 1.5 m high
290	grass, Eriophorum	-	20	-	
291	grass, lichen	-	62,5	-	grass tussocks
292	grass, moss, Eriophorum	-	50	-	water-filled polygonal troughs
293	grass, Eriophorum	sedges, moss	n.a.	-	
294	grass, Eriophorum	moss	n.a.	-	
295	-	grass	n.a.	-	large driftwood accumulation, grass in patches (4 m in diameter)
296	-	grass	n.a.	-	strong peat accumulation, some driftwood, grass in patches
297	-	-	-	-	small peat accumulations 10 cm in diameter
298	grass	-	n.a.	-	thermokarst hills 0.5 m high
299	-	-	-	-	slip-off slope, dark grey sand
300	grass	-	n.a.	-	river mouth, dark grey sediment
301	grass, moss	lichen	65	-	small sediment patches, grass tussocks
302	grass	-	55	-	grass tussocks, thermokarst hills <0.5 m high
303	-	grass	n.a.	-	8-10 m above valley floor
304	Eriophorum	grass	n.a.	-	strong erosion, disturbed surface, formation of steps
305	sedges, grass, moss	Eriophorum	n.a.	-	
306	grass	-	n.a.	-	large, peak-like erosional remnant within depression, steep slopes

307	grass, sedges	Eriophorum	10	-	8-12 m deep, slopes 40-45°, nival niches & sediment fans, thermokarst hills 1.5m high
308	grass	Eriophorum	35	-	
309	grass, Eriophorum, moss	-	35	-	
310	grass	Eriophorum, moss	60	-	grass tussocks
311	grass, Eriophorum, sedges	moss	5	-	
312	grass, Eriophorum	-	n.a.	-	grass tussocks
313	grass, sedges, moss	-	n.a.	-	pond 12x18 m
314	grass	-	55	-	grass tussocks
315	grass	Eriophorum, moss	55	-	slightly tussocky
316	-	grass	n.a.	-	black-grey sediment, snow patch area
317	Eriophorum, sedges, grass	-	5	-	
318	grass, Eriophorum	-	40	-	
319	grass, moss	-	45	Ice wedge ice sample	polygons >10 m in diameter
320	-	-	-	Mak-G-3, Mak-G-4	dark-grey to greyish-brown river sediments, large peat accumulations (2 m high)
321	grass	Eriophorum	65	-	slip-off slope with polygons orthogonal to the river course, polygons 15-20 m wide
322	sedges, grass, moss	Eriophorum	n.a.	-	
323	n.a.	n.a.	n.a.	-	mouth of small river into large river
324	sedges, grass, moss, Eriophorum	-	40	-	old river bank, low centre polygons
325	grass	-	55	-	thermokarst hills up to 1.5m high
326	Eriophorum, grass	-	5	-	
327	grass, Eriophorum	-	40	-	grass tussocks

328	grass, moss	Eriophorum	50	-	grass tussocks
329	-	grass	-	Mak-12, Mak-13	disturbed surface
330	Eriophorum, sedges, gras, moss	-	5	-	
331	grass	-	60	-	thermokarst hills >50 cm high, grass tussocks
332	grass	-	45	-	50 m wide slope area without thermokarst hills
333	grass	Eriophorum	30	-	
334	Eriophorum, grass	-	30	-	
335	grass	Eriophorum	25	-	grass tussocks
336	grass, moss	Eriophorum	15	-	
337	-	-	-	-	landing location
338	grass	-	n.a.	-	camp / fireplace
339	grass	Eriophorum, moss	40	-	
340	grass, Eriophorum, moss	-	n.a.	-	
341	-	grass	n.a.	-	disturbed surface
342	grass, moss, lichen	-	55	-	thermokarst hills 30-40 cm high (initial)
343	grass, sedges, moss	-	35	-	low centre polygons 10m diameter, centres+troughs lowered 20-30 cm
344	sedges, moss	Eriophorum	15	-	
345	grass	moss, Eriophorum	25	-	polygons 20-25m diameter
346	lichen, moss	grass	n.a.	-	grass tussocks
347	grass	-	5	-	short red-green grass
348	grass	-	5	-	short red-green grass, marginal area of a large water channel
349	grass, Eriophorum	-	n.a.	-	
350	grass, Eriophorum	-	n.a.	-	wide (20m) shallow valley
351	-	grass	5	Mak-G-5	area between 2 water channels, often flooded, drying cracks, wave ripples
352	grass, Eriophorum	-	n.a.	-	short valley
353	grass	-	5	-	small island (0.5m high, 20m diameter) between water channels, rarely flooded

354	grass	-	5	-	small island (0.5m high, 5m diameter) between water channels, rarely flooded
355	-	-	-	-	marginal area of water channels, with shallow water, yellowish-brown sediment
356	grass, Eriophorum	-	n.a.	-	wide, shallow valley
357	sedges, moss	Eriophorum	35	-	orthogonal low centre polygons 10x15m to 15x20m diameter, walls 20-30 cm high
358	sedges, moss	Eriophorum	35	-	orthogonal low centre polygon 10x15m diameter, walls 20-30 cm high
359	sedges, moss	Eriophorum	35	-	orthogonal low centre polygon 8x12m diameter, walls 20-30 cm high
360	sedges, moss	Eriophorum	35	-	orthogonal low centre polygon 8x8m diameter, walls 20-30 cm high
361	sedges, moss	Eriophorum	35	-	orthogonal low centre polygon 6x12m diameter, walls 20-30 cm high
362	grass	Eriophorum	n.a.	-	
363	grass, moss	Eriophorum	15	-	shallow valley (< 2m deep), 8m wide
364	grass, Eriophorum, moss	-	50	-	high-centre polygons, moss patches
365	-	grass, lichen	n.a.	-	thermokarst hills 3-6m high, 7-8m diameter, grass tussocks, disturbed surface
366	grass, sedges	Eriophorum	0	-	valley floor ca. 10m wide, slopes very dry, poorly vegetated thermkarst hills
367	-	grass, lichen	70	Mak-G-6	sandy sediments, poorly vegetated
368	grass, sedges	Eriophorum	0	-	valley floor ca. 10m wide, slopes very dry, poorly vegetated
369	lichen, moss, grass	-	70	-	sandy sediments
370	-	-	-	-	peat detritus, wave ripples, ufS
371	moss, grass	Eriophorum	20	-	
WS	grass	-	n.a.	-	weather station, grass tussocks
445	-	-	-	Mak-G-7	river sand
446	grass	-	n.a.	-	tachymeter location in Uta's valley
447	grass	-	55	-	thermokarst hill <60cm high, grass tussocks
448	grass, Eriophorum	sedges	35	-	
449	grass, Eriophorum	moss	n.a.	-	slope towards shallow Log valley, grass tussocks
450	Eriophorum, grass	sedges, moss	25	-	dried up ponds with moss patches
451	-	-	-	-	Ovrag junction, driftwood trunks, steep slopes ca. 4-5m high, disturbed surface
452	-	-	-	-	Ovrag junction, driftwood trunks, steep slopes ca. 4-5m high, disturbed surface
453	-	-	-	-	Log flows into Ovrag

454	grass	-	n.a.	-	Log turns into ovrag, disturbed surface
455	grass	-	75	-	sediment patches, thermokarst hills <30cm high, grass tussocks
456	Eriophorum, grass	sedges, moss	25	-	dried up ponds with moss patches
457	Eriophorum, grass	sedges, moss	25	-	dried up ponds with moss patches
458	grass	Eriophorum	20	-	grass tussocks
459	grass	Eriophorum	20	-	grass tussocks
460	peat, moss, sedges, grass	Eriophorum	20	-	ponds several m in diameter, red and green sedges, brown peat
461	sedges, moss, peat	-	20	-	pond 30-40m in diameter, red and green sedges, brown peat, green and red moss
462	sedges, moss, peat	-	20	-	pond 15x20m in diameter
463	lichen, grass	moss	80	-	small terrace between depression floor and sandy slope
464	lichen, grass	moss	80	Mak-G-8	fS-mS
465	sedges, moss, peat	-	20	-	pond 15x20m in diameter
466	sedges	-	0	-	lake centre, red sedges, lake diameter ca. 50m
467	grass, Eriophorum, moss	-	0	-	oily film on water surface, moss: green and black Sphagnum
468	sedges, moss	-	0	-	red and green sedges, sphagnum moss on lake floor
469	grass, Eriophorum, sedges, moss	-	40	-	orthogonal low centre polygons, 15x20m diameter
470	grass, Eriophorum	moss	50	-	triangulation sign
471	grass, sedges, Eriophorum	-	10	-	wide Log valley towards thermokarst depression
472	grass, Eriophorum, sedges, moss	-	40	-	orthogonal low centre polygons, 15x20m diameter
473	n.a.	n.a.	n.a.	Mak-14	alas profile
474	-	-	-	-	river bank with sediments near river mouth
475	-	-	-	-	river bank with recent peat accumulation near river mouth
476	grass	-	n.a.	-	mouth of small river into large river

479	grass	-	55	-	wide Log valley, small sediment patches 10-15cm in diameter, grass tussocks
480	grass	-	50	-	wide Log valley, grass tussocks
481	grass, moss	-	55	Plant sample P481	small sediment patches 10-15cm in diameter, grass tussocks
482	grass	-	45	-	thermokarst hills 1.5m high, grass tussocks
483	grass, Eriophorum, moss	-	n.a.	-	lagoon coast
484	grass, sedges, Eriophorum	-	15	-	some driftwood trunks, Eriophorum only in areas without surface water
485	sedges, gras	-	n.a.	-	few driftwood trunks, flodding area of lakes
486	sedge	-	n.a.	Water sample P486, plant sample P486	almost no driftwood, one plant species only
487	-	sedges	n.a.	Mak-G-9, plant sample P487	grey to reddish-grey sediments, wave ripples, drying cracks
488	-	-	-	Mak-G-10	small peat patches, sandy sediments, drying cracks
489	-	-	-	-	peat patches & accumulation, shell remains, drying cracks
490	-	-	-	-	peat patches & accumulation, shell remains, one plant species only, few driftwood
491	sedges, gras	-	n.a.	Water sample P491, plant sample P491	few driftwood trunks
492	sedges, gras	-	n.a.	-	few driftwood trunks
493	Eriophorum, sedges	-	15	-	driftwood trunks
494	grass, Eriophorum, sedges, moss	-	n.a.	Mak-CE-2	driftwood trunks, sediment fan of a small ravine
495	grass, Eriophorum, sedges, moss	-	n.a.	Water sample P495	mouth area of small ravine
496	moss, grass, Eriophorum, sedges	-	30	Wood samples Mak-20-1 to -3	black peat accumulations, buried driftwood trunks

497	grass, Eriophorum	-	45	Wood sample Mak-20-4	buried driftwood
498	grass, Eriophorum, sedges, moss	-	55	-	low centre polygons 10-12m in diameter, black-brown peat
499	grass	Eriophorum	15	-	slip-off slope, mainly one reddish-green grass species, some driftwood trunks
500	grass, Eriophorum	-	50	-	low centre polygons, thick peat accumulation, water-filled troughs, few driftwood
501	grass, Eriophorum	-	45	-	high centre polygons and initial thermokarst hills
502	grass, Eriophorum	-	45	-	high centre polygons and initial thermokarst hills
503	-	grass	n.a.	-	depth ca. 6m, disturbed surface
504	-	lichen	n.a.	-	strongly meandering small river, grass tussocks
505	Eriophorum	grass	n.a.	-	thermokarst hills ca. 80cm high, 2-5m in diameter, distances ca. 6-8m
506	grass	Eriophorum, moss	50	-	moss patches, ca. 10m in diameter, grass tussocks
507	grass, moss	Eriophorum	50	-	moss patches, ca. 10m in diameter, grass tussocks
508	grass, moss	Eriophorum	50	-	moss patches, ca. 10m in diameter, polygonal troughs 20-40 incised

Appendix 4-2. Active layer data of the geo-located sites

Site	Active layer depth (cm)			N
	mean	min	max	
276	62	50	75	9
277	56	50	62	15
278	50	41	60	15
279	42	40	43	8
280	29	17	40	15
281	36	30	40	8
282	42	38	50	9
283	55	42	75	11
284	43	40	45	6
285	36	30	41	13
286	34	29	37	10
288	43	37	53	6
290	35	31	40	5
291	46	41	52	8
292	37	32	42	8
293	45	45	45	1
294	24	19	29	3
298	54	47	60	6
299	-	>80	-	1
300	41	36	45	5
301	48	44	52	5
302	53	44	68	7
303	45	36	55	4
304	51	50	53	3
305	51	50	52	3
307	41	40	43	4
308	36	30	44	5
309	42	35	49	4
310	49	42	56	5
311	32	30	35	4
312	46	31	59	5
313	39	36	42	5
314	51	32	74	4
315	37	32	40	4
317	49	46	51	4
318	43	42	45	4
319	44	35	50	3
320	-	70	-	2
321	56	52	61	4
322	55	55	55	1
326	44	43	46	3
327	43	33	52	4
328	38	27	48	4
339	36	33	38	3
340	33	22	47	4
342	61	52	77	4
343	42	30	62	4
344	32	19	45	6
345	52	50	54	3
(N - Number of measurements) (period from 2004-08-15 to 2004-08-28)	total			

Site	Active layer depth (cm)			N
	mean	min	max	
346	53	45	61	4
347	40	39	40	3
348	44	40	47	3
351	-	92	-	2
354	98	92	105	3
357	37	36	38	3
363	43	38	48	3
364	37	35	38	3
366	65	63	70	3
369	71	68	74	3
447	51	40	70	3
448	39	35	42	3
449	41	40	42	3
450	34	32	35	4
451	70	66	72	3
455	59	49	66	5
456	38	34	41	3
457	34	33	35	3
458	40	39	40	3
459	33	31	35	3
460	64	48	74	5
463	64	52	88	4
467	53	40	60	4
479	52	50	55	3
480	39	30	53	5
481	50	46	55	4
482	62	46	86	5
483	48	46	53	3
484	36	35	38	3
485	42	39	46	4
486	-	>110	-	3
487	-	>100	-	1
488	-	>100	-	1
489	-	>100	-	1
492	45	44	46	3
493	39	38	40	3
494	29	27	31	3
495	38	35	45	3
496	37	36	38	3
498	39	33	42	4
499	45	43	47	3
500	25	22	32	4
501	36	28	47	4
502	38	32	45	3
504	72	62	80	3
505	42	32	54	4
506	39	38	39	3
507	32	30	35	3
508	38	38	39	3
98	45	40	51	435

Appendix 4-3. List of soil samples (active layer); collected in the coastal lowland

no.	sample ID	date	location	description	depth [cm]
1	Mak 200	25.08.	73,60428 ° N 117,13343 ° E	bottom of thermoerosion valley (Mak-tv-1)	0-1
2	Mak 201			bottom of thermoerosion valley (Mak-tv-1)	1-8
3	Mak 202			bottom of thermoerosion valley (Mak-tv-1)	8-15
4	Mak 203			bottom of thermoerosion valley (Mak-tv-1)	15-23
5	Mak 205			bottom of thermoerosion valley (Mak-tv-1)	23-29
6	Mak 206			bottom of thermoerosion valley (Mak-tv-1)	29-39
7	Mak 208			near bottom of thermoerosion valley (Mak-tv-2)	0-8
8	Mak 209			near bottom of thermoerosion valley (Mak-tv-2)	8-14
9	Mak 210			near bottom of thermoerosion valley (Mak-tv-2)	14-22
10	Mak 211			near bottom of thermoerosion valley (Mak-tv-2)	22-30
11	Mak 212			near bottom of thermoerosion valley (Mak-tv-2)	30-38
12	Mak 213			near bottom of thermoerosion valley (Mak-tv-2)	38-50
13	Mak 214	26.08.	73,61043 ° N 117,13470 ° E	dry tundra near cliff (Mak-dr-1)	0-4
14	Mak 215			dry tundra near cliff (Mak-dr-1)	4-6
15	Mak 216			dry tundra near cliff (Mak-dr-1)	6-15
16	Mak 217			dry tundra near cliff (Mak-dr-1)	15-25
17	Mak 218			dry tundra near cliff (Mak-dr-1)	25-32
18	Mak 219			dry tundra (Mak-dr-2)	0-18
19	Mak 220			dry tundra (Mak-dr-2)	18-40
20	Mak 221	26.08.	73,60731 ° N 117,12492 ° E	wet polygonal tundra (Mak-po-1)	0-6
21	Mak 222			wet polygonal tundra (Mak-po-1)	6-12
22	Mak 223			wet polygonal tundra (Mak-po-1)	12-17
23	Mak 224			wet polygonal tundra (Mak-po-1)	17-22
24	Mak 225			wet polygonal tundra (Mak-po-1)	22-29
25	Mak 226			wet polygonal tundra (Mak-po-1)	29-36
26	Mak 227			wet polygonal tundra (Mak-po-1)	36-44

Appendix 4-4. List of permafrost sediment and paleosol samples for microbiological, molecular biological and biochemical analyses.

no.	sample ID	date	corresponding sample ID for cryolithological analyses (see Appendix 4-5)	no. of sub profile
1	Mak 100	14.08.	Mak 1-12	Mak 1
2	Mak 101	14.08.	-	Mak 1
3	Mak 102	14.08.	Mak 2-6	Mak 2
4	Mak 103	14.08.	-	Mak 2
5	Mak 104	14.08.	Mak 2-9	Mak 2
6	Mak 105	16.08.	Mak 3-17	Mak 3
7	Mak 106	16.08.	Mak 3-16	Mak 3
8	Mak 107	16.08.	Mak 3-8	Mak 3
9	Mak 108	16.08.	Mak 3-7	Mak 3
10	Mak 109	16.08.	Mak 4-4	Mak 4
11	Mak 110	16.08.	Mak 5-3	Mak 5
12	Mak 111	16.08.	Mak 5-4	Mak 5
13	Mak 112	18.08.	Mak 10-1	Mak 10
14	Mak 113	18.08.	Mak 10-2	Mak 10
15	Mak 114	18.08.	Mak 10-3	Mak 10
16	Mak 115	18.08.	Mak 10-4	Mak 10
17	Mak 116	18.08.	Mak 10-5	Mak 10
18	Mak 117	18.08.	Mak 10-6	Mak 10
19	Mak 118	18.08.	Mak 10-7	Mak 10
20	Mak 119	18.08.	Mak 10-9	Mak 10
21	Mak 120	18.08.	Mak 10-10	Mak 10
22	Mak 121	18.08.	Mak 9-1	Mak 9
23	Mak 122	18.08.	Mak 8-2	Mak 8
24	Mak 123	18.08.	Mak 11-9	Mak 11
25	Mak 124	24.08.	Mak 11-10	Mak 11
26	Mak 125	24.08.	Mak 11-11	Mak 11
27	Mak 126	24.08.	Mak 12-2	Mak 12
28	Mak 127	24.08.	Mak 12-3	Mak 12
29	Mak 128	24.08.	Mak 12-5	Mak12

Appendix 4-5. List of sediment samples

No.	sample	Height m asl	lithology	colour	cryostructures	ice abs.	ice grav.	carb.
Mak-1; 73.6074° N, 117.189° E; 12.08.2003								
1	Mak-1-1	1	fine sand to silt	yellowish-brown	massive	25,8	34,7	-
2	Mak-1-2	1,3	fine sand to silt	yellowish-brown	massive			
3	Mak-1-3	1,55	fine sand to silt	yellowish-brown	massive			
4	Mak-1-4	2,05	silty fine sand, laminated	yellowish-brown	massive			
5	Mak-1-5	2,55	silty fine sand, laminated	yellowish-brown	massive	19,9	24,8	-
6	Mak-1-6	3	laminated	yellowish-brown	massive			
7	Mak-1-7	3,5	fine sand to silt	yellowish-brown	massive			
8	Mak-1-8	4	fine sand to silt	yellowish-brown	massive	28,7	40,2	-
9	Mak-1-8b	4,1	polosatic	yellowish-brown				
10	Mak-1-9	4,3	fine-sand silt, grass roots	yellowish-brown	massive			
11	Mak-1-10	4,7	fine sand to silt		banded, massive interlayers	21,1	26,7	+
12	Mak-1-11	5	fine sand to silt	yellowish-brown	banded, diagonal			
13	Mak-1-12	5,3	peaty paleosol	brown to brownish-grey	banded	68,8	220,3	-
14	Mak-1-13	5,5	silty interlayer	grey to greyish-brown	banded			
15	Mak-1-14	5,7	peaty paleosol, peat inclusion	brown				
Mak-2; 73.6075° N, 117.1824° E; 14.08.2003								
16	Mak-2-1	6,2	sand, organic free		massive	20,5	25,8	-
17	Mak-2-2	6,9	fine sand silt, grass roots	yellowish-brown	massive	20,9	26,4	-
18	Mak-2-3	7,4	peaty paleosol, cryoturbated, peat inclusion	brown		67,6	208,4	-
19	Mak-2-4	7,8	fine sand silt, interlayer, plant remains	grey	ice rich, banded, granular in interlayers			
20	Mak-2-5	8,1						
21	Mak-2-6	8,3	peaty paleosol, cryoturbated, peat inclusion	brown		62	163,1	-
22	Mak-2-7	8,7	fine sand silt, interlayer, plant remains, net like structures	brownish-grey	ice rich	45,6	83	+
23	Mak-2-8	9,2	fine sand to silt	grey	ice rich, banded	22,1	28,3	+
24	Mak-2-9	9,8	peaty paleosol, cryoturbated, peat inclusion	brownish		61,8	162,1	-

Appendix 4-5: Continuation

No.	sample	Height m asl	lithology	colour	cryostructures	ice abs.	ice grav.	carb.
Mak-3; 73.6075 °N, 117.1819 °E; 14./15.08.2003								
25	Mak-3-1	4,9	fine sand, peat inclusions		reworked slope material			
26	Mak-3-2	5,4	reworked slope material ?			20,1	26,4	-
27	Mak-3-3	5,9	reworked, refrozen slope material?, peat inclusion					
28	Mak-3-4	6,4	fine sand	yellowish grey	dotted, massive	19,6	24,4	-
29	Mak-3-5	6,9	paleosol, fine- sand silt, spotty , peat inclusion	brownish- grey, black spots	diagonal ice lenses	37,7	60,4	+
30	Mak-3-6	7,4	fine-sand, laminated	light brownish		17,2	20,8	-
31	Mak-3-7	7	peaty paleosol, see Mak-3-5			17,2	20,8	-
32	Mak-3-8	7,5	fine-sand, irregular laminated	grey		53,9	117,1	+
33	Mak-3-9	7,9	fine sand, irregular laminated, sedge remains	grey	massive			
34	Mak-3-10	8,4	paleosol, sedge (?) remains	grey		26,3	35,6	+
35	Mak-3-11	8,9	fine-sand interlayer, irregular laminated	grey	massive	18,3	22,4	-
36	Mak-3-12	9,4	paleosol, sedge (?) remains	grey		23,9	31,5	++
37	Mak-3-13	9,9	fine sand, interlayer, laminated	grey	massive	28,4	39,4	++
38	Mak-3-14	10,3	peaty paleosol, peat inclusions	brown		36	56,3	++
39	Mak-3-15	11,7	fine sand, few plant remains	yellowish grey	laminated, fine lens-like	33,5	50,5	-
40	Mak-3-16	12,4	peaty paleosol, peat inclusion	brownish		41,3	70,2	-
41	Mak-3-17	13,2	peaty paleosol, peat inclusion	brownish				

Appendix 4-5: Continuation

No.	sample	Height m asl	lithology	colour	cryostructures	ice abs.	ice grav.	carb.
Mak-4, 73.6075°N, 117.1819°E; 15.08.2003								
42	Mak-4-1	11,7	paleosol, cryoturbated	brownish		33,2	49,8	-
43	Mak-4-2	12	fine sand, single plant remains	yellowish grey	banded, diagonal ice lenses	31,9	46,8	-
44	Mak-4-3	12,3	fine-sand silt, wood remains (twigs, roots)	grey	banded, fine lens- like	39,1	64,3	++
45	Mak-4-4	12,7	fine-sand silt, wood remains (twigs, roots)	grey	banded, fine lens- like	41,3	70,2	++
Mak-5; 73.6075°N, 117.1824°E; 16.08.2003								
46	Mak-5-1	13,5	fine-sand silt	grey-brown	banded, broken lens-like	48,4	93,9	++
47	Mak-5-2	14	fine-sand silt	greyish- brown	banded, broken lens-like	41,1	69,7	++
48	Mak-5-3	14,3	paleosol, peat inclusion, wood remains (twigs, roots)	brownish- grey		70	232,8	++
49	Mak-5-4	14,6	silty sand, grass roots, weakly laminated, sand laminae	grey-brown	massive	36,8	58,2	
Mak-6; 73.6075°N, 117.1824°E; 16.08.2003								
50	Mak-6-1	14,8	sandy silt, twigs	grey-brown	banded, horizontal lenses	41,6	71,1	++
51	Mak-6-2	14,9	sandy silt, vertical grass roots	brownish- grey	thin, parallel small ice layers			
52	Mak-6-3	15,4	sandy silt, vertical grass roots	brownish- grey	thin, parallel small ice layers	42	72,4	++
53	Mak-6-4	16	sandy silt, vertical grass roots	brownish- grey	thin, parallel small ice layers			
Mak-7; 73.6075°N, 117.1824°E; 16.08.2003								
54	Mak-7-1	16,4	silty sand, vertical grass roots	grey-brown	small ice layers, fine lens-like	33,8	51	++
55	Mak-7-2	16,9	fine-sand silt, wood remains	grey-brown	thin, parallel small ice layers			
56	Mak-7-3	17,4	silty sand, vertical grass roots	grey-brown	small ice layers, fine lens-like	35,9	56,1	++
57	Mak-7-4	17,9	fine-sand silt,	grey-brown	small ice layers, fine lens-like			

Appendix 4-5: Continuation

No.	sample	Height m asl	lithology	colour	cryostructures	ice abs.	ice grav.	carb.
Mak-8; 6075°N, 117.1819°E; 16.08.2003								
58	Mak-8-1	14,8	fine-sand silt, vertical grass roots	grey	banded, broken small ice lenses			
59	Mak-8-2	15,3	fine-sand silt, vertical grass roots	grey	banded, broken small ice lenses	40,9	69,2	++
60	Mak-8-3	15,8	peaty paleosol, peat inclusion, wood remains	brownish- grey				
61	Mak-8-4	16,3	peaty paleosol, peat inclusion, wood remains	brownish- grey		43,6	77,4	+
Mak-9; Mak-2; 73.6075°N, 117.1824°E; 17.08.2003								
62	Mak-9-1	19,9	fine-sand silt, small plant remains	grey-brown	banded, interlayers massive to fine lens-like	35,7	55,5	++
63	Mak-9-2	20,4	fine-sand silt, small plant remains	grey-brown	few ive bands, partly broken lens-like			
64	Mak-9-3	20,9	fine-sand silt, wood remains	Grey-brown	banded, fine lens- like	42,2	73,1	+
65	Mak-9-4	21,4	fine-sand silt, wood remains	grey-brown	banded, coarse lens-like	40,1	66,9	+
66	Mak-9-5	21,9	fine-sand silt, wood remains	grey-brown	fine lens-like reticulated			
67	Mak-9-6	22,4	fine-sand silt, wood remains	grey-brown	banded, coarse lens-like	34	51,5	+
Mak-10; Mak-2; 73.6075°N, 117.1824°E; 17.08.2003								
68	Mak-10-1	22,5	paleosol, wood remains	grey-brown	banded	38	61,3	++
69	Mak-10-2	23	silty fine-sand	grey-brown	thigh banded, lens-like			
70	Mak-10-3	23,5	silty fine-sand	grey-brown	banded, fine lens- like	49,8	99,4	+
71	Mak-10-4	24	paleosol, wood remains	grey-brown	broken lens-like			
72	Mak-10-5	24,3	cryoturbated paleosol, peat inclusion	brown		73,7	280,7	-
73	Mak-10-6	24,6	silty fine-sand interlayer	grey-brown	banded,			
74	Mak-10-7	24,9	peaty paleosol, peat inclusion	brown				
75	Mak-10-8	25,2	cryoturbated paleosol, peat inclusion	brownish		45,6	83,9	-
76	Mak-10-9	25,5	silty fine-sand	greyish brown	banded			
77	Mak-10-10	25,75	paleosol, peat inclusion	brown		57,7	136,4	-
78	Mak-10-11	26	paleosol, peat inclusion	brown				
79	Mak-10-12	26,2	modern soil, cryoturbated	greyish brown	diagonal ice veins	56	127,3	-

Appendix 4-5. Continuation

No.	sample	Height m asl	lithology	colour	cryostructures	ice abs.	ice grav.	carb.
Mak-11; 73.6104°N, 117.1347°E, 20.08.2003								
80	Mak-11-1	2	paleosol	brownish-grey	massive to fine lens-like	36,6	50,5	-
81	Mak-11-2	2,5	sandy silt, plant remains	greyish-brown	lensed, lens-like reticulated			
82	Mak-11-3	3	paleosol, light-dark laminated	grey-brown	banded, fine lens-like, ground wedge	46,1	85,4	-
83	Mak-11-4	3,5	paleosol, wood remains	brownish-grey	banded, coarse lens-like reticulated			
84	Mak-11-5	3,7	silty fine sand, laminated, grass roots	grey-brown	banded	30,7	44,3	-
85	Mak-11-6	4,2	silty fine sand, laminated, grass roots	grey-brown	banded			
86	Mak-11-7	4,9	peaty paleosol, peat inclusions	dark-grey	broken lenses	56,4	130,1	-
87	Mak-11-8	5,2	peaty soil, peat inclusions	grey-brown	banded			
88	Mak-11-9	5,5	peat inclusion	grey-brown	banded	49	96,2	-
89	Mak-11-10	5,8	fine sand to silt	grey	banded			
90	Mak-11-11	6	transition layer, soil	brown	diagonal			
Mak-12; 73.6078°N, 117.1638°E, 20.08.2003								
91	Mak-12-1	0,5	peaty paleosol, peat inclusion	brown-grey	banded, lens like	59,8	148,6	-
92	Mak-12-2	0,75	peaty paleosol, peat inclusion	brown-grey	banded, lens like			
93	Mak-12-3	0,85	fine sand to silt	grey	lens-like	48,6	94,5	-
94	Mak-12-4	1	peaty paleosol, peat inclusion	brownish-grey	banded, lens-like	59,7	148,2	-
95	Mak-12-5	1,25	cryoturbated paleosol, peat inclusion	brownish-grey	banded	50,3	101,4	-
Mak-13; 73.6078°N, 117.1638°E, 20.08.2003								
96	Mak-13-1	1,8	sandy silt, few organic, wood remains	grey	banded, lens-like	42,8	74,8	+
97	Mak-13-2	2,2	fine-sand silt, few organic, wood remains	grey	banded, lens-like			
98	Mak-13-3	2,7	fine-sand silt, few organic, wood remains	grey	banded, lens-like	52,6	110,9	+
99	Mak-13-4	3,2	fine-sand to silt, few organic, wood remains	grey	banded, lens-like			
100	Mak-13-5	3,7	fine-sand silt, few organic, wood remains	grey	banded, lens-like	41,6	71,3	+
101	Mak-13-6	4	silty fine sand, few organic, wood remains	grey	banded, lens-like			
102	Mak-13-7	4,3	fine-sand silt, few organic, wood remains	grey	banded, lens-like	32,1	47,4	+

Appendix 4-5. Continuation

No.	sample	Height m asl	lithology	colour	cryostructures	ice abs.	ice grav.	carb.
Mak-14; 73.6396°N, 116.8817°E; 23.08.2003								
103	Mak-14-1	0,5	alas deposit, silty sand, plant remains	brownish	coarse lens-like reticulated			
104	Mak-14-2	0,8	alas deposit	brownish		25,7	34,7	-
105	Mak-14-3	1,1	alas deposit	grey				
106	Mak-14-4	1,4	alas deposit, interbedding, peaty layers (2-4 cm)	grey/brown	lens-like, sub vertically	81,6	44,9	-
107	Mak-14-5	1,7	alas deposit, sand-peat interbedding	grey/brown	small ice bands			
108	Mak-14-6	2	alas deposit, sand-peat interbedding	grey/brown	small ice bands	52,6	111,2	-
109	Mak-14-7	2,3	alas deposit, sand-peat interbedding, more peaty	brown	banded, thick ice bands			
110	Mak-14-8	2,6	alas deposit, peaty soil	brown	banded	62,2	164,6	-
111	Mak-14-9	2,9	alas deposit, cryoturbated peat soil, peat inclusion	brown	banded, vertical ice veins			
Mak-15; 73.6078°N, 117.1638°E; 25.08.2003								
112	Mak-15-1	4,5	fine sand to silt		banded,	53,5	115,2	+
113	Mak-15-2	5	fine sandy silt, roots	grey-brown	broken lens-like			
114	Mak-15-3	5,5	fine-sandy silt, plant remains					
115	Mak-15-4	6,1	fine-sandy silt			42,6	74,2	-
116	Mak-15-5	6,6	fine-sand to silt, wood (twigs, roots)	grey	banded, lens-like to massive			
117	Mak-15-6	7,1	fine-sand to silt, wood (twigs, roots)			52,6	112,2	-
Mak-16; 73.6078°N, 117.1638°E; 25.08.2003								
118	Mak-16-1	7,3	fine-sand to silt, small plant remains	grey	broken ice bands, broken fine lens-like			
119	Mak-16-2	7,8	fine-sand to silt,	grey		45,5	83,5	+
120	Mak-16-3	8,3	fine-sand to silt, wood (twigs, roots)	grey	broken lens-like, sub vertically			
121	Mak-16-4	8,8	fine-sand to silt, wood (twigs, roots)	grey	coarse lens-like, broken	53,2	113,8	+
122	Mak-16-5	9,3	fine-sand to silt, wood (twigs, roots)	grey	coarse lens-like			
123	Mak-16-6	10	sand	yellowish-grey	banded, fine lens-like	45,2	82,4	++

Appendix 4-5. Continuation

No.	sample	Height m asl	lithology	colour	cryostructures	ice abs.	ice grav.	carb.
Mak-17; 73.6078°N, 117.1638°E; 25.08.2003								
124	Mak-17-1	10,7	fine-sand to silt, small wood remains	greyish brown	banded, alternation of broken coarse and fine lens-like	45,9	84,9	+
125	Mak-17-2	11	paleosol	brownish	not banded, broken fine lens- like			
126	Mak-17-3	11,5	peaty paleosol, wood remains,	brownish, spotty	banded, alternation of broken lens-like and fine lens-like			
127	Mak-17-4	12,1	paleosol, wood remains (twigs, roots)	brownish	banded, alternation of broken lens-like and fine lens-like	42,2	73,1	+
128	Mak-17-5	12,6	paleosol, many wood remains	brownish	banded			
129	Mak-17-6	13,1	sandy silt, wood remains	grey	sparsely banded, fine lens-like to massive			
130	Mak-17-7	13,6	paleosol	grey, brownish spotty	banded, alternation of fine lens-like and broken coarse lens-like	42,8	75,8	++
Mak-18; 73.6078°N, 117.1638°E; 25.08.2003								
131	Mak-18-1	12,1	fine sand silt, paleosol, leafs	brownish- grey, spotty	banded, irregular fine lens-like to massive			
132	Mak-18-2	12,6	sandy silt	brown-grey	widely banded, broken lens-like			
133	Mak-18-3	13,1	paleosol, leafs	blondish spotty	tightly banded, alternation of broken ice bands and fine lens like to massive	51,5	106,2	+
134	Mak-18-4	13,6	paleosol, spot with leafs	dark-brown spotty	tightly banded, alternation of broken ice bands and fine lens like to massive			
135	Mak-18-5	14,1	paleosol, spot with leafs		tightly banded, alternation of broken ice bands and fine lens like to massive	53,3	114,3	+

Appendix 4-5. Continuation

No.	sample	Height m asl	lithology	colour	cryostructures	ice abs.	ice grav.	carb.
Mak-19; 73.6078°N, 117.1638°E; 25.08.2003								
136	Mak-19-1	14,4	fine sandy silt, few small wood remains	greyish- brown	banded, lens-like, fine lens-like to massive			
137	Mak-19-2	14,8	paleosol, fewer wood remains	brownish, irregular	widely banded, massive	42,1	72,8	+
138	Mak-19-3	15,3	sand, few wood remains, finely distributed plant remains	greyish- brown- to yellowish- brown, spotty	banded, massive to fine lens-like			
139	Mak-19-4	15,6	paleosol, many wood remains, organic-rich spots	dark grey, spotty	widely banded	47,3	89,8	+
140	Mak-19-5	16,1	paleosol, spots with leaf remains	grey, yellowish- brown spotted	tinny banded, fine lens-like to massive	43,9	78,1	+
141	Mak-19-6	16,6	sand,	yellowish- grey	dotted			
142	Mak-19-7	17,1	sandy silt	grey	not banded, broken lens-like to massive	50,5	101,8	+
143	Mak-19-8	17,5	modern cryosol, peat inclusions, transition zone	greyish- brown	diagonal, lens-like			
Mak-20; 73.5841°N, 117.2744°E; 26.08.2003								
144	Mak-20-1	1,5	driftwood					
145	Mak-20-2	1,45	moss peat	brown				
146	Mak-20-3	1,4	peaty silt					
147	Mak-20-4	1,5	driftwood					
Mak-Ovrag, 15.08.2003								
165	Mak-Ovrag-1	15,0	peat lens	brown				
166	Mak-Ovrag-2	15,5	peat lens	brown		92,6	1248	
167	Mak-Ovrag-3	16	peat lens	brown				

Appendix 4-5. Continuation

Surface samples							
No.	sample		material	Latitude	Longitude		
148	Mak-AA-1		surface vegetation	73.6051	117.1994		
149	Mak-AA-2			73,6058	117,1653		
150	Mak-AA-3			73,6004	117,1808		
151	Mak-AA-4		modern soil		-		
152	Mak-C-1		moss				
153	Mak-C-2		moss				
154	Mak-G-1			73,5955	117,2475	10.08.	
155	Mak-G-10		marine sand	73,5891	117,2841	26.08.	
156	Mak-G-11		peat, beach deposit				
157	Mak-G-2			73,6058	117,1355	15.08.	
158	Mak-G-3			73,5944	117,1128	19.08	
159	Mak-G-4		river sand	73,5944	117,1128	19,08.	
160	Mak-G-5		dried alas bottom, surface,	73,5537	117,9548	21.08.	
161	Mak-G-6		surface, sand, thermokarst hill,.	73,5681	117,9809	21.08.	
162	Mak-G-7		river sand, near the camp,	73,6082	117,1191	22.08.	
163	Mak-G-8		sand of alas surface, 23.08.	73,6341	116,8876	23.08.	
164	Mak-G-9		beach sand	73,5884	117,2820	26.09.	

ice abs. – absolute ice content [weight %]

ice grav. – gravimetric ice content [weight %]

carb. – carbonate (HCl-test)

Appendix 4-6. List of ice and water samples

Nr.	date	sample	type	Isotopes			Chemistry		LF μS/cm	pH	REMARKS
				¹⁸ O	² H	³ H	anion/ cation	HCO ₃			
1	09.08.2003	MAK-99/01	RW	X	X	X	X	X	117,6	7,00	
2	10.08.2003	MAK-99/02	RW	X	X	X	X	X	108	6,95	
3	11.08.2003	MAK-CI-1	CI	X	X	X	X	-	51,9	6,63	
4	11.08.2003	MAK-97/01	SP	X	X	X	X	X	11,7	6,72	
5	11.08.2003	MAK-97/02	SP	X	X	X	X	X	3,6	6,53	
6	11.08.2003	MAK-97/03	SP	X	X	X	X	X	6,6	6,69	
7	11.08.2003	MAK-96/01	SW	X	X	X	X	-	90,1	6,36	signal tower lake
8	13.08.2003	MAK-IW-1.1	IW	X	X	-	-	-	98,5	8,74	
9	13.08.2003	MAK-IW-1.2	IW	X	X	-	-	-	119,8	8,08	
10	13.08.2003	MAK-IW-1.3	IW	X	X	-	-	-	148,5	7,18	
11	13.08.2003	MAK-IW-1.4	IW	X	X	X	-	-	-	-	
12	13.08.2003	MAK-14C-1	ORG	-	-	-	-	-	-	-	lednik
13	13.08.2003	MAK-3 (10m) tief	SW	X	X	-	X	-	30400	7,86	Sal 20,5
14	12.08.2003	MAK-1-13.TI	TI	X	X	-	X	-	2400	7,43	Sal 1,3
15	12.08.2003	MAK-1-10.TI	TI	X	X	-	-	-	-	-	
16	12.08.2003	MAK-1-9.TI	TI	X	X	-	-	-	-	-	
17	12.08.2003	MAK-1-8B.TI	TI	X	X	-	X	-	632	8,00	
18	12.08.2003	MAK-1-8.TI	TI	X	X	-	-	-	-	-	
19	12.08.2003	MAK-1-7.TI	TI	X	X	-	-	-	-	-	
20	12.08.2003	MAK-1-6.TI	TI	X	X	-	-	-	-	-	
21	12.08.2003	MAK-1-2.TI	TI	X	X	-	-	-	-	-	
22	12.08.2003	MAK-1-1.TI	TI	X	X	-	-	-	-	-	
23	13.08.2003	MAK-2-4.TI	TI	X	X	-	-	-	-	-	
24	13.08.2003	MAK-2-5.TI	TI	X	X	-	-	-	-	-	
25	13.08.2003	MAK-2-7.TI	TI	X	X	-	X	-	674	8,10	
26	13.08.2003	MAK-2-8.TI	TI	X	X	-	X	-	859	7,43	
27	14.08.2003	MAK-IW-1.5	PO	X	X	-	-	-	-	-	
28	14.08.2003	MAK-IW-1.6	PO	X	X	-	-	-	1677	7,72	
29	14.08.2003	MAK-IW-2.1	PO	X	X	-	-	-	-	-	
30	14.08.2003	MAK-IW-2.2	PO	X	X	-	X	-	1258	7,80	
31	14.08.2003	MAK-IW-2.3	PO	X	X	-	-	-	1523	7,84	
32	14.08.2003	MAK-IW-2.4	PO	X	X	-	-	-	-	-	
33	14.08.2003	MAK-IW-2.5	PO	X	X	-	X	-	663	8,25	
34	14.08.2003	MAK-IW-2.6	PO	X	X	-	-	-	-	-	
35	14.08.2003	MAK-IW-2.7	PO	X	X	-	-	-	309	8,57	
36	14.08.2003	MAK-IW-2.8	PO	X	X	-	-	-	-	-	
37	14.08.2003	MAK-IW-2.9	PO	X	X	-	-	-	-	-	
38	14.08.2003	MAK-IW-2.10	PO	X	X	-	X	-	112,4	8,65	
39	14.08.2003	MAK-IW-2.10a	PO	X	X	-	X	-	-	-	
40	14.08.2003	MAK-IW-2.11	PO	X	X	-	-	-	-	-	
41	14.08.2003	MAK-IW-2.12	PO	X	X	-	X	-	117,2	8,65	
42	14.08.2003	MAK-IW-2.13	PO	X	X	-	-	-	-	-	
43	14.08.2003	MAK-IW-2.14	PO	X	X	-	-	-	-	-	
44	14.08.2003	MAK-IW-2.15	PO	X	X	-	X	-	85,2	8,91	
45	14.08.2003	MAK-IW-2.16	PO	X	X	-	-	-	-	-	
46	14.08.2003	MAK-IW-2.17	PO	X	X	-	X	-	119,7	8,65	
47	14.08.2003	MAK-IW-2.18	PO	X	X	-	-	-	-	-	
48	14.08.2003	MAK-IW-3.1	IW	X	X	-	X	-	92,6	8,42	
49	14.08.2003	MAK-IW-4.1	IW	X	X	-	-	-	-	-	
50	14.08.2003	MAK-IW-4.2	IW	X	X	-	X	-	83,5	8,1	
51	14.08.2003	MAK-IW-5.1	IW	X	X	-	X	-	184,7	8,13	
52	14.08.2003	MAK-IW-6.1	IW	X	X	-	-	-	92,9	8,71	
53	14.08.2003	MAK-IW-6.2	IW	X	X	-	X	-	-	-	
54	14.08.2003	MAK-IW-6.3	IW	X	X	-	-	-	187	7,36	
55	14.08.2003	MAK-IW-6.4	IW	X	X	-	-	-	-	-	
56	14.08.2003	MAK-IW-6.5	IW	X	X	-	-	-	117	7,92	
57	14.08.2003	MAK-IW-6.6	IW	X	X	-	X	-	194,3	7,93	
58	14.08.2003	MAK-IW-6.7	IW	X	X	-	-	-	-	-	
59	14.08.2003	MAK-IW-6.8	IW	X	X	-	-	-	122	8,03	
60	15.08.2003	MAK-IW-7.1	IW	X	X	-	-	-	-	-	
61	15.08.2003	MAK-IW-7.2	IW	X	X	-	X	-	73,7	8,24	
62	15.08.2003	MAK-IW-7.3	IW	X	X	-	-	-	-	-	
63	15.08.2003	MAK-IW-7.4	PO	X	X	-	-	-	274	8,33	
64	15.08.2003	MAK-IW-7.5	PO	X	X	-	-	-	-	-	
65	15.08.2003	MAK-96/02	SW	X	X	X	X	X	107,7	6,92	
66	15.08.2003	MAK-96/03	SW	X	X	X	X	-	160,9	6,88	
67	15.08.2003	MAK-AL-1	AL	X	X	X	-	-	68,5	6,53	
68	15.08.2003	MAK-IW-8.1	IW	X	X	-	-	-	-	-	
69	15.08.2003	MAK-IW-8.2	IW	X	X	-	X	-	120,1	8,45	
70	15.08.2003	MAK-IW-8.3	IW	X	X	-	-	-	-	-	

Appendix 4-6. Continuation

Nr.	date	sample	type	Isotopes			Chemistry		LF μS/cm	pH	REMARKS
				¹⁸ O	² H	³ H	anion/ cation	HCO ₃			
71	15.08.2003	MAK-IW-9.1	IW	X	X	-	-	-	-	-	
72	15.08.2003	MAK-IW-9.2	IW	X	X	-	X	-	120	8,22	
73	15.08.2003	MAK-IW-9.3	IW	X	X	-	-	-	-	-	
74	15.08.2003	MAK-IW-9.4	PO	X	X	-	X	-	275	8,46	
75	15.08.2003	MAK-14C-2	ORG	-	-	-	-	-	-	-	
76	15.08.2003	MAK-MI-1	MI	X	X	X	X	-	63,5	9	
77	15.08.2003	MAK-MI-2	MI	X	X	X	X	-	62,9	9,2	
78	15.08.2003	MAK-MI-3	MI	X	X	X	-	-	63,6	9,21	
79	15.08.2003	MAK-MI-4	MI	X	X	X	-	-	66,1	9,4	
80	15.08.2003	MAK-IW-10.1	IW	X	X	-	-	-	-	-	
81	15.08.2003	MAK-IW-10.2	IW	X	X	-	X	-	95,5	8,65	
82	15.08.2003	MAK-IW-10.3	IW	X	X	-	-	-	-	-	
83	15.08.2003	MAK-IW-10.4	IW	X	X	-	X	-	302	7,58	
84	15.08.2003	MAK-IW-11.1	IW	X	X	-	-	-	-	-	
85	15.08.2003	MAK-IW-11.2	IW	X	X	-	X	-	89,5	8,58	
86	15.08.2003	MAK-IW-11.3	IW	X	X	-	-	-	-	-	
87	15.08.2003	MAK-IW-11.4	IW	X	X	-	X	-	90,8	8,62	
88	15.08.2003	MAK-IW-11.5	IW	X	X	-	-	-	-	-	
89	15.08.2003	MAK-IW-11.6	TI	X	X	-	-	-	-	-	
90	15.08.2003	MAK-IW-11.7	TI	X	X	-	X	-	83,6	7,92	
91	14.08.2003	MAK-3-12.TI	TI	X	X	-	-	-	-	-	
92	14.08.2003	MAK-3-13.TI	TI	X	X	-	X	-	565	7,91	
93	14.08.2003	MAK-3-14.TI	TI	X	X	-	-	-	768	7,28	
94	16.08.2003	MAK-99/03	RW	X	X	X	X	-	50	5,64	
95	14.08.2003	MAK-IW-5.2	IW	X	X	-	-	-	-	-	
96	15.08.2003	MAK-14C-3	14C	X	X	-	-	-	-	-	
97	16.08.2003	MAK-IW-10.5	IW	X	X	-	-	-	-	-	
98	16.08.2003	MAK-IW-10.6	IW	X	X	-	-	-	-	-	
99	16.08.2003	MAK-IW-10.7	IW	X	X	-	X	-	107,5	9,34	
100	16.08.2003	MAK-IW-10.8	IW	X	X	-	-	-	-	-	
101	16.08.2003	MAK-IW-10.9	IW	X	X	-	-	-	-	-	
102	16.08.2003	MAK-IW-10.10	IW	X	X	-	-	-	-	-	
103	16.08.2003	MAK-IW-10.11	IW	X	X	-	X	-	149,3	7,39	
104	16.08.2003	MAK-IW-10.12	IW	X	X	-	-	-	-	-	
105	16.08.2003	MAK-IW-10.13	IW	X	X	-	-	-	-	-	
106	16.08.2003	MAK-IW-10.14	IW	X	X	-	X	-	312	7,48	
107	16.08.2003	MAK-IW-10.15	IW	X	X	-	-	-	-	-	
108	16.08.2003	MAK-IW-10.16	IW	X	X	-	X	-	72,4	8,78	
109	16.08.2003	MAK-IW-10.17	IW	X	X	-	-	-	-	-	
110	16.08.2003	MAK-IW-10.18	IW	X	X	-	X	-	119,9	8,42	
111	16.08.2003	MAK-IW-10.19	IW	X	X	-	-	-	-	-	
112	18.08.2003	MAK-IW-13.1	TI	X	X	-	-	-	-	-	
113	18.08.2003	MAK-IW-13.2	IW	X	X	-	X	-	116,6	6,93	
114	18.08.2003	MAK-IW-13.3	IW	X	X	-	-	-	-	-	
115	18.08.2003	MAK-IW-13.4	IW	X	X	-	-	-	-	-	
116	18.08.2003	MAK-IW-13.5	IW	X	X	-	X	-	48,4	6,71	
117	18.08.2003	MAK-IW-13.6	IW	X	X	-	-	-	-	-	
118	18.08.2003	MAK-IW-13.7	IW	X	X	-	-	-	-	-	
119	18.08.2003	MAK-IW-13.8	IW	X	X	-	X	-	47,5	6,61	
120	18.08.2003	MAK-IW-14.1	IW	X	X	-	-	-	-	-	
121	18.08.2003	MAK-IW-14.2	IW	X	X	-	X	-	157,6	6,48	
122	18.08.2003	MAK-IW-14.3	IW	X	X	-	-	-	-	-	
123	18.08.2003	MAK-IW-14.4	IW	X	X	-	X	-	91,1	6,67	
124	18.08.2003	MAK-IW-14.5	IW	X	X	-	-	-	-	-	
125	18.08.2003	MAK-96/04	SW	X	X	X	X	X	389	7,95 small lake on fluvial terrace	
126	18.08.2003	MAK-96/05	SW	X	X	X	X	X	8280	8,07 river mouth, SAL=5,0	
127	18.08.2003	MAK-96/06	SW	X	X	X	X	X	1704	8,2 polygonal pond , SAL=0,8	
128	18.08.2003	MAK-d13C-1	ORG	-	-	-	-	-	-	-	
129	18.08.2003	MAK-d13C-2	ORG	-	-	-	-	-	-	-	
130	18.08.2003	MAK-d13C-3	ORG	-	-	-	-	-	-	-	
131	18.08.2003	MAK-d13C-4	ORG	-	-	-	-	-	-	-	
132	18.08.2003	MAK-d13C-5	ORG	-	-	-	-	-	-	-	
133	18.08.2003	MAK-d13C-6	ORG	-	-	-	-	-	-	-	
134	18.08.2003	MAK-d13C-7	ORG	-	-	-	-	-	-	-	
135	18.08.2003	MAK-3 (0 m)	SW	X	X	-	X	-	11190	8,97 SAL=9,0	
136	18.08.2003	MAK-3 (2,5 m)	SW	X	X	-	X	-	17890	8,67 SAL=11,6	
137	18.08.2003	MAK-3 (5 m)	SW	X	X	-	X	-	25520	8,23 SAL=16,9	
138	18.08.2003	MAK-3 (7,5 m)	SW	X	X	-	X	-	22700	8,07 SAL=14,9	

Appendix 4-6. Continuation

Nr.	date	sample	type	Isotopes			Chemistry		LF μS/cm	pH	REMARKS
				¹⁸ O	² H	³ H	anion/ cation	HCO ₃			
139	18.08.2003	MAK-3 (10 m)	SW	X	X	-	-	-	21500	8,14	SAL=14,0
140	18.08.2003	MAK-4/5/5	SW	X	X	-	X	-	25400	8,02	SAL=16,9
141	18.08.2003	MAK-4/10/5	SW	X	X	-	X	-	24300	8,07	SAL=16,1
142	18.08.2003	MAK-4/7,5/3,7	SW	X	X	-	X	-	26100	8,02	SAL=17,4
143	18.08.2003	MAK-4/7,5/7,5	SW	X	X	-	X	-	28100	8,02	SAL=18,9
144	14.08.2003	MAK-3-15.TI	TI	X	X	-	-	-	-	-	-
145	15.08.2003	MAK-4-1.TI	TI	X	X	-	X	-	477	7,32	-
146	15.08.2003	MAK-4-2.TI	TI	X	X	-	-	-	-	-	-
147	15.08.2003	MAK-4-3.TI	TI	X	X	-	X	-	929	7,53	-
148	16.08.2003	MAK-5-2.TI	TI	X	X	-	-	-	-	-	-
149	16.08.2003	MAK-5-3.TI	TI	X	X	-	-	-	-	-	-
150	16.08.2003	MAK-6-1.TI	TI	X	X	-	-	-	2150	7,61	-
151	16.08.2003	MAK-6-3.TI	TI	X	X	-	X	-	1365	7,61	-
152	16.08.2003	MAK-6-4.TI	TI	X	X	-	-	-	-	-	-
153	16.08.2003	MAK-7-2.TI	TI	X	X	-	-	-	-	-	-
154	16.08.2003	MAK-7-3.TI	TI	X	X	-	-	-	-	-	-
155	16.08.2003	MAK-7-4.TI	TI	X	X	-	-	-	-	-	-
156	16.08.2003	MAK-8-2.TI	TI	X	X	-	-	-	-	-	-
157	16.08.2003	MAK-8-3.TI	TI	X	X	-	-	-	537	7,68	-
158	16.08.2003	MAK-8-4.TI	TI	X	X	-	X	-	674	7,79	-
159	15.08.2003	MAK-Ovrag-1	TI	X	X	-	X	-	1001	6,45	-
160	15.08.2003	MAK-Ovrag-2	TI	X	X	-	X	-	376	7,55	-
161	15.08.2003	MAK-Ovrag-3	TI	X	X	-	X	-	355	7,41	-
162	15.08.2003	MAK-4-4.TI	TI	X	X	-	X	-	1081	7,72	-
163	16.08.2003	MAK-5-4.TI	TI	X	X	-	-	-	-	-	-
164	19.08.2003	MAK-95/01	RIW	X	X	-	X	-	37,1	5,71	-
165	19.08.2003	MAK-IW-12.1	IW	X	X	-	-	-	-	-	frozen
166	19.08.2003	MAK-IW-12.2	IW	X	X	-	-	-	-	-	frozen
167	19.08.2003	MAK-IW-12.3	IW	X	X	-	-	-	-	-	frozen
168	19.08.2003	MAK-IW-12.4	IW	X	X	-	-	-	-	-	frozen
169	19.08.2003	MAK-IW-12.5	IW	X	X	-	-	-	-	-	frozen
170	19.08.2003	MAK-IW-12.6	IW	X	X	-	-	-	-	-	frozen
171	19.08.2003	MAK-IW-12.7	IW	X	X	-	-	-	-	-	frozen
172	19.08.2003	MAK-IW-12.8	IW	X	X	-	-	-	-	-	frozen
173	19.08.2003	MAK-IW-12.9	IW	X	X	-	-	-	-	-	frozen
174	19.08.2003	MAK-IW-12.10	IW	X	X	-	-	-	-	-	frozen
175	19.08.2003	MAK-IW-12.11	IW	X	X	-	-	-	-	-	frozen
176	19.08.2003	MAK-IW-12.12	IW	X	X	-	-	-	-	-	frozen
177	19.08.2003	MAK-IW-12.13	IW	X	X	-	-	-	-	-	frozen
178	19.08.2003	MAK-IW-12.14	IW	X	X	-	-	-	-	-	frozen
179	19.08.2003	MAK-IW-12.15	IW	X	X	-	-	-	-	-	frozen
180	19.08.2003	MAK-IW-12.16	IW	X	X	-	-	-	-	-	frozen
181	19.08.2003	MAK-IW-12.17	IW	X	X	-	-	-	-	-	frozen
182	19.08.2003	MAK-IW-12.18	IW	X	X	-	-	-	-	-	frozen
183	19.08.2003	MAK-IW-12.19	IW	X	X	-	-	-	-	-	frozen
184	19.08.2003	MAK-IW-12.20	IW	X	X	-	-	-	-	-	frozen
185	19.08.2003	MAK-IW-12.21	IW	X	X	-	-	-	-	-	frozen
186	19.08.2003	MAK-IW-12.22	IW	X	X	-	-	-	-	-	frozen
187	19.08.2003	MAK-IW-12.23	IW	X	X	-	-	-	-	-	frozen
188	19.08.2003	MAK-IW-12.24	IW	X	X	-	-	-	-	-	frozen
189	19.08.2003	MAK-IW-12.25	IW	X	X	-	-	-	-	-	frozen
190	19.08.2003	MAK-IW-12.26	IW	X	X	-	-	-	-	-	frozen
191	19.08.2003	MAK-IW-12.27	IW	X	X	-	-	-	-	-	frozen
192	19.08.2003	MAK-IW-12.28	IW	X	X	-	-	-	-	-	frozen
193	19.08.2003	MAK-IW-12.29	IW	X	X	-	-	-	-	-	frozen
194	19.08.2003	MAK-IW-12.30	IW	X	X	-	-	-	-	-	frozen
195	19.08.2003	MAK-IW-12.31	IW	X	X	-	-	-	-	-	-
196	19.08.2003	MAK-IW-12.32	IW	X	X	-	X	-	-	-	-
197	19.08.2003	MAK-IW-12.33	IW	X	X	-	-	-	-	-	-
198	19.08.2003	MAK-IW-15.1	IW	X	X	-	-	-	-	-	frozen
199	19.08.2003	MAK-IW-15.2	IW	X	X	-	-	-	-	-	frozen
200	19.08.2003	MAK-IW-15.3	IW	X	X	-	-	-	-	-	frozen
201	19.08.2003	MAK-IW-15.4	IW	X	X	-	-	-	-	-	frozen
202	19.08.2003	MAK-IW-15.5	IW	X	X	-	-	-	-	-	frozen
203	19.08.2003	MAK-IW-15.6	IW	X	X	-	-	-	-	-	frozen
204	19.08.2003	MAK-IW-15.7	IW	X	X	-	-	-	-	-	frozen
205	19.08.2003	MAK-IW-15.8	IW	X	X	-	-	-	-	-	frozen
206	19.08.2003	MAK-IW-15.9	IW	X	X	-	-	-	-	-	frozen
207	19.08.2003	MAK-IW-15.10	IW	X	X	-	-	-	-	-	frozen
208	19.08.2003	MAK-IW-15.11	IW	X	X	-	-	-	-	-	frozen
209	19.08.2003	MAK-IW-15.12	IW	X	X	-	-	-	-	-	frozen

Appendix 4-6. Continuation

Nr.	date	sample	type	Isotopes			Chemistry		LF		REMARKS
				¹⁸ O	² H	³ H	anion/ cation	HCO ₃	μS/cm	pH	
210	19.08.2003	MAK-IW-15.13	IW	X	X	-	-	-	-	-	frozen
211	19.08.2003	MAK-IW-15.14	IW	X	X	-	-	-	-	-	frozen
212	19.08.2003	MAK-IW-15.15	IW	X	X	-	-	-	-	-	frozen
213	19.08.2003	MAK-IW-15.16	IW	X	X	-	-	-	-	-	frozen
214	19.08.2003	MAK-IW-15.17	IW	X	X	-	-	-	-	-	frozen
215	19.08.2003	MAK-IW-15.18	IW	X	X	-	-	-	-	-	frozen
216	19.08.2003	MAK-IW-15.19	IW	X	X	-	-	-	-	-	frozen
217	19.08.2003	MAK-IW-15.20	IW	X	X	-	-	-	-	-	frozen
218	19.08.2003	MAK-IW-15.21	IW	X	X	-	-	-	-	-	frozen
219	19.08.2003	MAK-IW-15.22	IW	X	X	-	-	-	-	-	frozen
220	19.08.2003	MAK-IW-15.23	IW	X	X	-	-	-	-	-	frozen
221	19.08.2003	MAK-IW-15.24	IW	X	X	-	-	-	-	-	frozen
222	19.08.2003	MAK-IW-15.25	IW	X	X	-	-	-	-	-	frozen
223	19.08.2003	MAK-IW-15.26	IW	X	X	-	-	-	-	-	frozen
224	19.08.2003	MAK-IW-15.27	IW	X	X	-	-	-	-	-	frozen
225	19.08.2003	MAK-95/02	RIW	X	X	X	-	-	-	-	
226	17.08.2003	MAK-9-1.TI	TI	X	X	-	-	-	-	-	
227	17.08.2003	MAK-9-2.TI	TI	X	X	-	-	-	-	-	
228	17.08.2003	MAK-9-4.TI	TI	X	X	-	-	-	1115	7,48	
229	17.08.2003	MAK-9-6.TI	TI	X	X	-	-	-	1488	7,68	
230	17.08.2003	MAK-10-1.TI	TI	X	X	-	-	-	-	-	
231	17.08.2003	MAK-10-2.TI	TI	X	X	-	X	-	1962	7,67	
232	17.08.2003	MAK-10-3.TI	TI	X	X	-	-	-	1652	7,45	
233	17.08.2003	MAK-10-4.TI	TI	X	X	-	-	-	-	-	
234	17.08.2003	MAK-10-5.TI	TI	X	X	-	-	-	-	-	
235	17.08.2003	MAK-10-6.TI	TI	X	X	-	X	-	608	7,16	
236	17.08.2003	MAK-10-7.TI	TI	X	X	-	-	-	-	-	
237	17.08.2003	MAK-10-8.TI	TI	X	X	-	X	-	524	7,15	
238	17.08.2003	MAK-10-9.TI	TI	X	X	-	X	-	648	7,27	
239	17.08.2003	MAK-10-10.TI	TI	X	X	-	-	-	520	7,14	
240	17.08.2003	MAK-10-12.TI	TI	X	X	-	-	-	-	-	
241	20.08.2003	MAK-97/04	SP	X	X	X	X	-	28	7,14	
242	20.08.2003	MAK-97/05	SP	X	X	X	X	-	-	-	
243	21.08.2003	MAK-IW-16.1	IW	X	X	-	X	-	44,1	7,16	
244	21.08.2003	MAK-IW-16.2	IW	X	X	-	-	-	-	-	
245	21.08.2003	MAK-IW-16.3	IW	X	X	-	X	-	101,2	8,08	
246	21.08.2003	MAK-IW-16.4	IW	X	X	-	-	-	-	-	
247	21.08.2003	MAK-IW-17.0	TI	X	X	-	X	-	386	7,7	
248	21.08.2003	MAK-IW-17.1	IW	X	X	-	X	-	230	8,02	
249	21.08.2003	MAK-IW-17.2	IW	X	X	-	-	-	-	-	
250	21.08.2003	MAK-IW-17.3	IW	X	X	-	X	-	202	8,03	
251	21.08.2003	MAK-IW-17.4	IW	X	X	-	-	-	-	-	
252	21.08.2003	MAK-IW-17.5	IW	X	X	-	X	-	171,2	7,94	
253	21.08.2003	MAK-IW-17.6	IW	X	X	-	-	-	-	-	
254	21.08.2003	MAK-IW-17.7	IW	X	X	-	-	-	154,7	8,06	
255	21.08.2003	MAK-IW-17.8	IW	X	X	-	-	-	-	-	
256	21.08.2003	MAK-IW-17.9	IW	X	X	-	X	-	212	7,97	
257	21.08.2003	MAK-IW-17.10	IW	X	X	-	-	-	-	-	
258	21.08.2003	MAK-IW-17.11	IW	X	X	-	-	-	165,7	8,05	
259	21.08.2003	MAK-IW-17.12	IW	X	X	-	-	-	-	-	
260	21.08.2003	MAK-IW-17.13	IW	X	X	-	-	-	201	8,07	
261	21.08.2003	MAK-IW-17.14	IW	X	X	-	-	-	-	-	
262	21.08.2003	MAK-IW-17.15	IW	X	X	-	-	-	189,9	8,01	
263	21.08.2003	MAK-IW-17.16	IW	X	X	-	-	-	-	-	
264	21.08.2003	MAK-IW-17.29	IW	X	X	-	X	-	181,9	8,18	
265	21.08.2003	MAK-IW-17.30	IW	X	X	-	-	-	-	-	
266	21.08.2003	MAK-IW-17.31	IW	X	X	-	-	-	230	8,04	
267	21.08.2003	MAK-IW-17.32	IW	X	X	-	-	-	-	-	
268	21.08.2003	MAK-IW-17.33	IW	X	X	-	X	-	181,1	8,12	
269	21.08.2003	MAK-IW-17.34	IW	X	X	-	-	-	-	-	
270	21.08.2003	MAK-IW-17.35	IW	X	X	-	-	-	154,9	8,18	
271	21.08.2003	MAK-IW-17.36	IW	X	X	-	-	-	-	-	
272	21.08.2003	MAK-IW-17.37	IW	X	X	-	X	-	157,7	8,15	
273	21.08.2003	MAK-IW-17.38	IW	X	X	-	-	-	-	-	
274	21.08.2003	MAK-IW-17.39	IW	X	X	-	X	-	146,4	8,14	
275	21.08.2003	MAK-IW-17.40	IW	X	X	-	-	-	-	-	
276	21.08.2003	MAK-IW-17.41	IW	X	X	-	X	-	135	8,13	
277	21.08.2003	MAK-IW-17.42	IW	X	X	-	-	-	133,8	8,14	
278	21.08.2003	MAK-IW-17.43	IW	X	X	-	-	-	-	-	
279	21.08.2003	MAK-IW-17.44	IW	X	X	-	-	-	-	-	
280	21.08.2003	MAK-IW-17.45	IW	X	X	-	-	-	-	-	

Appendix 4-6. Continuation

Nr.	date	sample	type	Isotopes			Chemistry		LF μS/cm	pH	REMARKS
				¹⁸ O	² H	³ H	anion/ cation	HCO ₃			
281	21.08.2003	MAK-IW-18.1	IW	X	X	-	X	-	95,2	8,15	
282	21.08.2003	MAK-IW-18.2	IW	X	X	-	-	-	-	-	
283	21.08.2003	MAK-IW-18.3	IW	X	X	-	X	-	69,1	8,31	
284	21.08.2003	MAK-IW-18.4	IW	X	X	-	-	-	-	-	
285	21.08.2003	MAK-IW-19.1	IW	X	X	-	-	-	-	-	
286	21.08.2003	MAK-IW-19.2	IW	X	X	-	X	-	91,1	8,13	
287	21.08.2003	MAK-IW-19.3	IW	X	X	-	-	-	-	-	
288	21.08.2003	MAK-IW-20.1	IW	X	X	-	-	-	-	-	
289	21.08.2003	MAK-IW-20.2	IW	X	X	-	X	-	92,3	8,66	
290	21.08.2003	MAK-IW-21.1	IW	X	X	-	X	-	194,3	8,38	
291	21.08.2003	MAK-95/03	RIW	X	X	X	X	-	66,5	7,43	
292	22.08.2003	MAK-95/04	RIW	X	X	-	X	-	75,1	7,43	
293	22.08.2003	MAK-96/07	SW	X	X	X	X	-	412	8,44	
294	22.08.2003	MAK-96/08	SW	X	X	X	X	-	337	8,05	
295	22.08.2003	MAK-96/09	SW	X	X	X	X	-	442	8,13	
296	20.08.2003	MAK-11-3.TI	TI	X	X	-	-	-	-	-	
297	20.08.2003	MAK-11-8.TI	TI	X	X	-	X	-	120,7	6,13	
298	20.08.2003	MAK-11-10.TI	TI	X	X	-	-	-	-	-	
299	20.08.2003	MAK-11-11.TI	TI	X	X	-	-	-	128,3	5,6	
300	20.08.2003	MAK-11-9.TI	TI	X	X	-	-	-	-	-	
301	20.08.2003	MAK-12-5.TI	TI	X	X	-	-	-	-	-	
302	20.08.2003	MAK-11-6.TI	TI	X	X	-	-	-	-	-	
303	20.08.2003	MAK-11-7.TI	TI	X	X	-	X	-	172,1	6	
304	20.08.2003	MAK-11-4.TI	TI	X	X	-	-	-	-	-	
305	20.08.2003	MAK-11-2.TI	TI	X	X	-	X	-	598	7,28	
306	20.08.2003	MAK-12-1.TI	TI	X	X	-	X	-	648	7,37	
307	20.08.2003	MAK-12-3.TI	TI	X	X	-	-	-	-	-	
308	20.08.2003	MAK-13-1.TI	TI	X	X	-	-	-	-	-	
309	20.08.2003	MAK-13-2.TI	TI	X	X	-	X	-	695	7,46	
310	20.08.2003	MAK-13-3.TI	TI	X	X	-	-	-	-	-	
311	20.08.2003	MAK-13-4.TI	TI	X	X	-	X	-	468	7,67	
312	20.08.2003	MAK-13-5.TI	TI	X	X	-	X	-	616	7,69	
313	23.08.2003	MAK-IW-22.0	IW	X	X	-	X	-	85,6	7,71	
314	23.08.2003	MAK-IW-22.1	IW	X	X	-	X	-	88,7	7,66	
315	23.08.2003	MAK-IW-22.2	IW	X	X	-	-	-	-	-	
316	23.08.2003	MAK-IW-22.3	IW	X	X	-	-	-	-	-	
317	23.08.2003	MAK-IW-22.4	IW	X	X	-	-	-	-	-	
318	23.08.2003	MAK-IW-22.5	IW	X	X	-	X	-	73,2	7,73	
319	23.08.2003	MAK-IW-22.6	IW	X	X	-	-	-	-	-	
320	23.08.2003	MAK-IW-22.7	IW	X	X	-	X	-	89,2	6,92	
321	23.08.2003	MAK-IW-22.8	IW	X	X	-	-	-	-	-	
322	23.08.2003	MAK-IW-22.9	IW	X	X	-	-	-	-	-	
323	23.08.2003	MAK-IW-22.10	IW	X	X	-	X	-	65,3	7,11	
324	23.08.2003	MAK-IW-22.11	IW	X	X	-	X	-	65,8	7,19	
325	23.08.2003	MAK-IW-22.12	IW	X	X	-	-	-	-	-	
326	23.08.2003	MAK-IW-22.13	IW	X	X	-	-	-	-	-	
327	23.08.2003	MAK-IW-23-1	IW	X	X	-	-	-	-	-	
328	23.08.2003	MAK-IW-24.1	IW	X	X	-	-	-	95	9,01	
329	23.08.2003	MAK-IW-24.2	IW	X	X	-	X	-	-	-	
330	23.08.2003	MAK-98/01	GW	X	X	X	X	-	368	6,58	
331	23.08.2003	MAK-98/02	GW	X	X	X	-	-	-	-	
332	23.08.2003	MAK-98/03	GW	X	X	X	X	-	126,3	5,92	
333	23.08.2003	MAK-95/05	RIW	X	X	X	X	-	41,7	6,48	
334	23.08.2003	MAK-IW-12.34	IW	X	X	-	-	-	-	-	
335	23.08.2003	MAK-MI-5	MI	X	X	X	X	-	40,5	7,39	
336	23.08.2003	MAK-MI-6	MI	X	X	X	-	-	-	-	
337	23.08.2003	MAK-MI-7	MI	X	X	X	X	-	60,4	7,72	
338	23.08.2003	MAK-IW-25.1	IW	X	X	-	-	-	-	-	
339		MAK-14-1.TI	TI	X	X	-	-	-	-	-	
340		MAK-14-2.TI	TI	X	X	-	-	-	-	-	
341		MAK-14-3.TI	TI	X	X	-	-	-	-	-	
342		MAK-14-5.TI	TI	X	X	-	-	-	-	-	
343		MAK-14-7.TI	TI	X	X	-	-	-	-	-	
344		MAK-14-8.TI	TI	X	X	-	-	-	-	-	
345	25.08.2003	MAK-IW-26.1	IW	-	-	-	-	-	-	-	frozen
346	25.08.2003	MAK-IW-26.2	IW	-	-	-	-	-	-	-	frozen
347	25.08.2003	MAK-IW-26.3	IW	-	-	-	-	-	-	-	frozen
348	25.08.2003	MAK-IW-26.4	IW	-	-	-	-	-	-	-	frozen
349	25.08.2003	MAK-IW-26.5	IW	-	-	-	-	-	-	-	frozen
350	25.08.2003	MAK-IW-26.6	IW	-	-	-	-	-	-	-	frozen
351	25.08.2003	MAK-IW-27.1	IW	-	-	-	-	-	-	-	frozen

Appendix 4-6. Continuation

Nr.	date	sample	type	Isotopes			Chemistry		LF μS/cm	pH	REMARKS
				¹⁸ O	² H	³ H	anion/ cation	HCO ₃			
352	25.08.2003	MAK-IW-27.2	IW	-	-	-	-	-	-	frozen	
353	25.08.2003	MAK-IW-27.3	IW	-	-	-	-	-	-	frozen	
354	25.08.2003	MAK-IW-27.4	IW	-	-	-	-	-	-	frozen	
355	25.08.2003	MAK-IW-27.5	IW	-	-	-	-	-	-	frozen	
356	25.08.2003	MAK-IW-27.6	IW	-	-	-	-	-	-	frozen	
357	25.08.2003	MAK-IW-27.7	IW	-	-	-	-	-	-	frozen	
358	25.08.2003	MAK-IW-27.8	IW	-	-	-	-	-	-	frozen	
359	25.08.2003	MAK-IW-27.9	IW	-	-	-	-	-	-	frozen	
360	25.08.2003	MAK-IW-27.10	IW	-	-	-	-	-	-	frozen	
361	25.08.2003	MAK-IW-27.11	IW	-	-	-	-	-	-	frozen	
362	25.08.2003	MAK-IW-27.12	IW	-	-	-	-	-	-	frozen	
363	25.08.2003	MAK-IW-27.13	IW	-	-	-	-	-	-	frozen	
364	25.08.2003	MAK-IW-27.14	IW	-	-	-	-	-	-	frozen	
365	25.08.2003	MAK-IW-27.15	IW	-	-	-	-	-	-	frozen	
366	25.08.2003	MAK-IW-27.16	IW	-	-	-	-	-	-	frozen	
367	25.08.2003	MAK-IW-27.17	IW	-	-	-	-	-	-	frozen	
368	25.08.2003	MAK-IW-27.18	IW	-	-	-	-	-	-	frozen	
369	25.08.2003	MAK-IW-27.19	IW	-	-	-	-	-	-	frozen	
370	25.08.2003	MAK-IW-27.20	IW	-	-	-	-	-	-	frozen	
371	25.08.2003	MAK-IW-27.21	IW	-	-	-	-	-	-	frozen	
372	25.08.2003	MAK-IW-27.22	IW	-	-	-	-	-	-	frozen	
373	25.08.2003	MAK-IW-27.23	IW	-	-	-	-	-	-	frozen	
374	25.08.2003	MAK-IW-27.24	IW	-	-	-	-	-	-	frozen	
375	26.08.2003	MAK-99/04	RW	X	X	X	X	-	-		
376	26.08.2003	MAK-Aq. Dest.	DW	-	-	-	X	-	-		
377	26.08.2003	MAK-IW-28.1	IW	-	-	-	-	-	-	frozen	
378	26.08.2003	MAK-IW-28.2	IW	-	-	-	-	-	-	frozen	
379	26.08.2003	MAK-IW-28.3	IW	-	-	-	-	-	-	frozen	
380	26.08.2003	MAK-IW-28.4	IW	-	-	-	-	-	-	frozen	
381	26.08.2003	MAK-IW-28.5	IW	-	-	-	-	-	-	frozen	
382	26.08.2003	MAK-IW-28.6	IW	-	-	-	-	-	-	frozen	
383	26.08.2003	MAK-IW-28.7	IW	-	-	-	-	-	-	frozen	
384	26.08.2003	MAK-IW-28.8	IW	-	-	-	-	-	-	frozen	
385	27.08.2003	MAK-99/04	RW	X	X	-	-	-	-		
386		MAK-97/06	SP	X	X	X	-	-	-	1405/1	
387		MAK-97/07	SP	X	X	X	-	-	-	1405/2	
388	26.08.2003	MAK-P486	SW	X	X	-	-	-	-	Pt Guido	
389	26.08.2003	MAK-P491	SW	X	X	-	-	-	-	Pt Guido	
390	26.08.2003	MAK-P495	SW	X	X	-	-	-	-	Pt Guido	
391	25.08.2003	MAK-15-1.TI	TI	X	X	-	-	-	-		
392	25.08.2003	MAK-15-2.TI	TI	X	X	-	-	-	-		
393	25.08.2003	MAK-15-3.TI	TI	X	X	-	-	-	-		
394	25.08.2003	MAK-15-4.TI	TI	X	X	-	-	-	-		
395	25.08.2003	MAK-15-5.TI	TI	X	X	-	-	-	-		
396	25.08.2003	MAK-15-6.TI	TI	X	X	-	-	-	-		
397	25.08.2003	MAK-16-1.TI	TI	X	X	-	-	-	-		
398	25.08.2003	MAK-16-2.TI	TI	X	X	-	-	-	-		
399	25.08.2003	MAK-16-3.TI	TI	X	X	-	-	-	-		
400	25.08.2003	MAK-16-4.TI	TI	X	X	-	-	-	-		
401	25.08.2003	MAK-16-5.TI	TI	X	X	-	-	-	-		
402	25.08.2003	MAK-16-6.TI	TI	X	X	-	-	-	-		
403	25.08.2003	MAK-17-1.TI	TI	X	X	-	-	-	-		
404	25.08.2003	MAK-17-2.TI	TI	X	X	-	-	-	-		
405	25.08.2003	MAK-17-3.TI	TI	X	X	-	-	-	-		
406	25.08.2003	MAK-17-4.TI	TI	X	X	-	-	-	-		
407	25.08.2003	MAK-17-5.TI	TI	X	X	-	-	-	-		
408	25.08.2003	MAK-17-6.TI	TI	X	X	-	-	-	-		
409	25.08.2003	MAK-17-7.TI	TI	X	X	-	-	-	-		
410	25.08.2003	MAK-18-1.TI	TI	X	X	-	-	-	-		
411	25.08.2003	MAK-18-2.TI	TI	X	X	-	-	-	-		
412	25.08.2003	MAK-18-3.TI	TI	X	X	-	-	-	-		
413	25.08.2003	MAK-18-4.TI	TI	X	X	-	-	-	-		
414	25.08.2003	MAK-18-5.TI	TI	X	X	-	-	-	-		
415	25.08.2003	MAK-19-1.TI	TI	X	X	-	-	-	-		
416	25.08.2003	MAK-19-2.TI	TI	X	X	-	-	-	-		
417	25.08.2003	MAK-19-3.TI	TI	X	X	-	-	-	-		

Appendix 4-6. Continuation

Nr.	date	sample	type	Isotopes			Chemistry		LF μS/cm	pH	REMARKS
				¹⁸ O	² H	³ H	anion/ cation	HCO ₃			
418	25.08.2003	MAK-19-4.TI	TI	X	X	-	-	-	-	-	
419	25.08.2003	MAK-19-5.TI	TI	X	X	-	-	-	-	-	
420	25.08.2003	MAK-19-6.TI	TI	X	X	-	-	-	-	-	
421	25.08.2003	MAK-19-7.TI	TI	X	X	-	-	-	-	-	
422	25.08.2003	MAK-19-8.TI	TI	X	X	-	-	-	-	-	

Abbreviations : SP = snow patch; RW = rain water; IW = ice wedge ice; RIW = recent ice wedge ice ;
 SW = surface water; GW = ground water; TI = segregated ice; AL = active layer ice; CI = cavity ice,
 PO = Polosatic ice, SI = sea ice; ORG = organic matter.

Appendix 4-7. Collection of bone samples

No.	N samples	Taxon	Skeleton element	Preservation	Loc. type	Locality	Notes
	1	3	4	5	6	7	8
1	MaK-O 1	Ovibos sp.	cranium with horn cores	fragment	d	shore, right side under the "Mamontov Klyk" mark	
2	MaK-O 2	Mammuthus primigenius	tooth	fragment	d	shore, right side under the "Mamontov Klyk" mark	
3	MaK-O 3	Equus sp.	cervical vertebra		d	shore, right side under the "Mamontov Klyk" mark	
4	MaK-O 4	Rangifer tarandus	calcaneus		d	shore, right side under the "Mamontov Klyk" mark	
5	MaK-O 5	Rangifer tarandus	femur	distal fragment	d	shore, right side under the "Mamontov Klyk" mark	juv.
6	MaK-O 6	Rangifer tarandus	femur	distal fragment	d	shore, right side under the "Mamontov Klyk" mark	juv.
7	MaK-O 7	Rangifer tarandus	scapula	joint fragment	d	shore, right side under the "Mamontov Klyk" mark	
8	MaK-O 8	Rangifer tarandus	astrogalus		d	shore, right side under the "Mamontov Klyk" mark	
9	MaK-O 9	Rangifer tarandus	antebrachium	distal fragment	d	shore, right side under the "Mamontov Klyk" mark	
10	MaK-O 10	Rangifer tarandus	tibia	distal fragment	d	shore, right side under the "Mamontov Klyk" mark	
11	MaK-O 11	Rangifer tarandus	antebrachium	distal fragment	d	shore, right side under the "Mamontov Klyk" mark	
12	MaK-O 12	Rangifer tarandus	lumbar vertebra	damaged	d	shore, right side under the "Mamontov Klyk" mark	
13	MaK-O 13	Equus sp.	ph II	damaged	d	shore, right side under the "Mamontov Klyk" mark	
14	MaK-O 14	Equus sp.	tibia	? with marrow	d	shore, right side under the "Mamontov Klyk" mark	
15	MaK-O 15	Bison priscus	ph II		d	shore, right side under the "Mamontov Klyk" mark	
16	MaK-O 16	Phoca sp.	humerus	fragment	d	shore, right side under the "Mamontov Klyk" mark	? recent
17	MaK-O 17	Phoca sp.	humerus	damaged	d	shore, right side under the "Mamontov Klyk" mark	? recent, juv.
18	MaK-O 18	Equus sp.	lumbar vertebra	damaged	d	shore, right side under the "Mamontov Klyk" mark	
19	MaK-O 19	Equus sp.	ph II		d	shore, right side under the "Mamontov Klyk" mark	juv.
20	MaK-O 20	Equus sp.	thorax vertebra	damaged	d	shore, right side under the "Mamontov Klyk" mark	
21	MaK-O 21	Rangifer tarandus	thorax vertebra		d	shore, right side under the "Mamontov Klyk" mark	
22	MaK-O 22	Equus sp.	femur	fragment	d	shore, right side under the "Mamontov Klyk" mark	
23	MaK-O 23	Equus sp.	cervical vertebra	damaged	d	shore, right side under the "Mamontov Klyk" mark	
24	MaK-O 24	Equus sp.	atlas	fragment	d	shore, right side under the "Mamontov Klyk" mark	
25	MaK-O 25	Equus sp. ?	femur	proximal fragment	d	shore, right side under the "Mamontov Klyk" mark	

Appendix 4-7. Continuation

No.	N samples	Taxon	Skeleton element	Preservation	Loc. type	Locality	Notes
26	MaK-O 26	Bison priscus	femur	proximal fragment	d	shore, right side under the "Mamontov Klyk" mark	
27	MaK-O 27	Rangifer tarandus	atlas	damaged	d	shore, right side under the "Mamontov Klyk" mark	
28	MaK-O 28	Rangifer tarandus	cervical vertebra	damaged	d	shore, right side under the "Mamontov Klyk" mark	
29	MaK-O 29	Bison priscus	thorax vertebra	damaged	d	shore, right side under the "Mamontov Klyk" mark	
30	MaK-O 30	Mammuthus primigenius	metapodia	damaged	d	shore, right side under the "Mamontov Klyk" mark	
31	MaK-O 31	Mammuthus primigenius	tooth	fragment	d	shore, right side under the "Mamontov Klyk" mark	C 14
32	MaK-O 32	Lepus sp.	cranium		d	shore, right side under the "Mamontov Klyk" mark	
33	MaK-O 33	Rangifer tarandus	tooth		d	shore, right side under the "Mamontov Klyk" mark	? recent
34	MaK-O 34	Equus caballus	cranium (ocipitale)	fragment	d	shore, right side under the "Mamontov Klyk" mark	
35	MaK-O 35	Large herbivorous mammal	costa	fragment	d	shore, right side under the "Mamontov Klyk" mark	trashed
36	MaK-O 36	Large herbivorous mammal	cranium	fragment	d	shore, right side under the "Mamontov Klyk" mark	trashed
37	MaK-O 37	Rangifer tarandus	humerus	fragment	e	shore, mouth of Nuchcha-Dzhiele river	
38	MaK-O 38	Equus sp.	pelvis	fragment	e	shore, mouth of Nuchcha-Dzhiele river	
39	MaK-O 39	Equus sp.	ph I		e	shore, mouth of Nuchcha-Dzhiele river	
40	MaK-O 40	Equus sp.	ph I		e	shore, mouth of Nuchcha-Dzhiele river	
41	MaK-O 41	Equus sp.	ph I		e	shore, mouth of Nuchcha-Dzhiele river	
42	MaK-O 42	Equus sp.	ph I		e	shore, mouth of Nuchcha-Dzhiele river	
43	MaK-O 43	Equus sp.	mandibula	simphis fragment	e	shore, mouth of Nuchcha-Dzhiele river	
44	MaK-O 44	Equus sp.	ph I	fragment	e	shore, mouth of Nuchcha-Dzhiele river	
45	MaK-O 45	Rangifer tarandus	ph III	damaged	e	shore, mouth of Nuchcha-Dzhiele river	
46	MaK-O 46	Mammuthus primigenius	tooth, heavily worn	fragment	e	shore, mouth of Nuchcha-Dzhiele river	
47	MaK-O 47	Rangifer tarandus	astrogalus		e	shore, mouth of Nuchcha-Dzhiele river	
48	MaK-O 48	Canis sp.?	thorax vertebra	damaged	e	shore, mouth of Nuchcha-Dzhiele river	
49	MaK-O 49	Bison priscus	scapula	fragment	e	shore, mouth of Nuchcha-Dzhiele river	
50	MaK-O 50	Bison priscus ?	humerus ?	fragment	e	shore, mouth of Nuchcha-Dzhiele river	
51	MaK-O 51	Large herbivorous mammal	costa	fragment	e	shore, mouth of Nuchcha-Dzhiele river	trashed

Appendix 4-7. Continuation

No.	N samples	Taxon	Skeleton element	Preservation	Loc. type	Locality	Notes
52	MaK-O 52	Large herbivorus mammal	costa	fragment	e	shore, mouth of Nuchcha-Dzhiele river	trashed
53	MaK-O 53	Large herbivorus mammal	limb bone	fragment	e	shore, mouth of Nuchcha-Dzhiele river	trashed
54	MaK-O 54	Large herbivorus mammal	limb bone	fragment	e	shore, mouth of Nuchcha-Dzhiele river	trashed
55	MaK-O 55	Large herbivorus mammal	limb bone	fragment	e	shore, mouth of Nuchcha-Dzhiele river	trashed
56	MaK-O 56	Large herbivorus mammal	limb bone	fragment	e	shore, mouth of Nuchcha-Dzhiele river	trashed
57	MaK-O 57	Large herbivorus mammal	limb bone	fragment	e	shore, mouth of Nuchcha-Dzhiele river	trashed
58	MaK-O 58	Large herbivorus mammal	cranium	fragment	e	shore, mouth of Nuchcha-Dzhiele river	trashed
59	MaK-O 59	Rangifer tarandus	vertebra	fragment	e	shore, mouth of Nuchcha-Dzhiele river	
60	MaK-O 60	Rangifer tarandus	cranium (bulla timpani)	fragment	e	shore, mouth of Nuchcha-Dzhiele river	
61	MaK-O 61	Equus sp.	radius		e	shore, mouth of Nuchcha-Dzhiele river	
62	MaK-O 62	Equus sp.	humerus	fragment	e	shore, mouth of Nuchcha-Dzhiele river	
63	MaK-O 63	Equus sp.	Mt III		e	shore, mouth of Nuchcha-Dzhiele river	
64	MaK-O 64	Equus sp.	tibia	distal fragment	e	shore, mouth of Nuchcha-Dzhiele river	
65	MaK-O 65	Equus sp.	astrogalus		e	shore, mouth of Nuchcha-Dzhiele river	
66	MaK-O 66	Bison priscus	thorax vertebra	damaged	e	shore, mouth of Nuchcha-Dzhiele river	
67	MaK-O 67	Equus sp.	ph II		e	shore, mouth of Nuchcha-Dzhiele river	
68	MaK-O 68	Equus sp.	ph I		e	shore, mouth of Nuchcha-Dzhiele river	
69	MaK-O 69	Mammuthus primigenius	bone of tarsale		e	shore, mouth of Nuchcha-Dzhiele river	small
70	MaK-O 70	Bison priscus	cervical vertebra	damaged	e	shore, mouth of Nuchcha-Dzhiele river	
71	MaK-O 71	Bison priscus	humerus	distal fragment	e	shore, mouth of Nuchcha-Dzhiele river	
72	MaK-O 72	Rangifer tarandus	cervical vertebra		e	shore, mouth of Nuchcha-Dzhiele river	
73	MaK-O 73	Equus sp.	pelvis	fragment	e	shore, mouth of Nuchcha-Dzhiele river	

Appendix 4-7. Continuation

No.	N samples	Taxon	Skeleton element	Preservation	Loc. type	Locality	Notes
74	MaK-O 74	Bison priscus ?	mandibula ?	fragment (diastema)	e	shore, mouth of Nuchcha-Dzhiele river	
75	MaK-O 75	Rangifer tarandus	atler	fragment	e	shore, mouth of Nuchcha-Dzhiele river	
76	MaK-O 76	Rangifer tarandus	tibia	proximal fragment (??????)	e	shore, mouth of Nuchcha-Dzhiele river	
77	MaK-O 77	Alopex lagopus	epistropheus		e	shore, mouth of Nuchcha-Dzhiele river	? recent
78	MaK-O 78	Rangifer tarandus	cranium (brain part)	fragment	e	shore, mouth of Nuchcha-Dzhiele river	? recent
79	MaK-O 79	Mammuthus primigenius	limb bone	fragment	e	shore, mouth of Nuchcha-Dzhiele river	trashed
80	MaK-O 80	Rangifer tarandus	astrogalus		e	shore, mouth of Nuchcha-Dzhiele river	
81	MaK-O 81	Equus sp.	Mt IV	damaged	e	shore, mouth of Nuchcha-Dzhiele river	
82	MaK-O 82	Canis sp.?	humerus	fragment	e	shore, mouth of Nuchcha-Dzhiele river	
83	MaK-O 83	Large herbivorus mammal	costa	fragment	e	shore, mouth of Nuchcha-Dzhiele river	
84	MaK-O 84	Large herbivorus mammal	palanx	fragment	e	shore, mouth of Nuchcha-Dzhiele river	trashed
85	MaK-O 85	Equus sp.	atlas	damaged	b	exposure, 2-nd termo-erosional cirques, Ice Complex, altitude 3 m a.s.l.	
86	MaK-O 86	Bison priscus	atlas		c	exposure	
87	MaK-O 87	Mammuthus primigenius	humerus ?	fragment (4 pieces)	b	exposure, 2-nd termo-erosional cirques, Ice Complex, altitude 3 m a.s.l.	?14, trashed, 2pieces
88	MaK-O 88	Rangifer tarandus	mandibula	fragment	c	exposure, Ice Complex	? recent
89	MaK-O 89	Large herbivorus mammal	limb bone	fragment	a	in situ, exposure, send deposits, altitude 8 m a.s.l.	from Guido, AMS
90	MaK-O 90	Large herbivorus mammal	limb bone	fragment	a	in situ, exposure, send deposits, altitude 8 m a.s.l.	from Guido, AMS

No.	N samples	Taxon	Skeleton element	Preservation	Loc. type	Locality	Notes
91	MaK-O 91	Mammuthus primigenius	femur	damaged (4 pieces)	a	in situ, exposure, Ice Complex, altitude 10-12 m a.s.l.	juv., C 14
92	MaK-O 92	Rangifer tarandus	cervical vertebra		c	exposure	
93	MaK-O 93	Rangifer tarandus	humerus	fragment	c	exposure	
94	MaK-O 94	Equus sp.	cranium (maxillaria with left I 2-3; both C; right P2-P3; left M1), male	damaged	e	shore, mouth of Nuchcha-Dzhiele river	
95	MaK-O 95	Equus sp.	mandibula (left stem) with ? 2-? 3	fragment	e	shore, mouth of Nuchcha-Dzhiele river	
96	MaK-O 96	Rangifer tarandus	shed antler	fragment	e	shore, mouth of Nuchcha-Dzhiele river	
97	MaK-O 97	Mammuthus primigenius	scapula	fragment	e	shore, mouth of Nuchcha-Dzhiele river	C 14
98	MaK-O 98	Equus sp.	maxillaria (right stem) with dP1-M2	fragment	b	exposure, right side, send deposit, altitude 4,5 ? a.s.l.	samples 98, 99, 100 from the same specimen
99	MaK-O 99	Equus sp.	maxillaria	fragment	b	exposure, right side, send deposit, altitude 4,5 ? a.s.l.	
100	MaK-O 100	Equus sp.	left upper ?4 unerupted		b	exposure, right side, send deposit, altitude 4,5 ? a.s.l.	
101	MaK-O 101	Mammuthus primigenius	tibia ?	fragment	b	exposure, right side, send deposit, altitude 4,5 ? a.s.l.	cut C 14
102	MaK-O 102	Equus sp.	Mt III		b	exposure, right side, send deposit, 6,5 ? below the tundra surface	samples 102, 103 - from the same specimen
103	MaK-O 103	Equus sp.	Mt IV		b	exposure, right side, send deposit, 6,5 ? below the tundra surface	
104	MaK-O 104	Rangifer tarandus	atlas		c	exposure, right side, send deposit	
105	MaK-O 105	Equus sp.	tibia	fragment	c	exposure, right side, send deposit	juv.
106	MaK-O 106	Rangifer tarandus	calcaneus	fragment	c	exposure, right side, send deposit	
107	MaK-O 107	Rangifer tarandus	shed antler	fragment	c	exposure, right side, send deposit	

Appendix 4-7. Continuation

No.	N samples	Taxon	Skeleton element	Preservation	Loc. type	Locality	Notes
108	MaK-O 108	Rangifer tarandus ?	cranium	fragment	b	exposure, right side, sand deposit, altitude 4,5 ? a.s.l.	
109	MaK-O 109	Rangifer tarandus	femur		e	shore, mouth of Nuchcha-Dzhiele river	
110	MaK-O 110	Mammuthus primigenius ?	tibia	fragment	d	shore, right side under the 1-st and 2-nd thermo-erosional cirqueses	juv.
111	MaK-O 111	Rangifer tarandus	femur	distal fragment	d	shore, right side under the 1-st and 2-nd thermo-erosional cirqueses	
112	MaK-O 112	Equus sp.	scapula	fragment	d	shore, right side under the 1-st and 2-nd thermo-erosional cirqueses	
113	MaK-O 113	Rangifer tarandus	femur	distal fragment	d	shore, right side under the 1-st and 2-nd thermo-erosional cirqueses	
114	MaK-O 114	Rangifer tarandus	femur	distal fragment	d	shore, right side under the 1-st and 2-nd thermo-erosional cirqueses	
115	MaK-O 115	Rangifer tarandus	Mt	????? ???	d	shore, right side under the 1-st and 2-nd thermo-erosional cirqueses	
116	MaK-O 116	Rangifer tarandus	metapodia	distal fragment	d	shore, right side under the 1-st and 2-nd thermo-erosional cirqueses	
117	MaK-O 117	Rangifer tarandus	ph I		d	shore, right side under the 1-st and 2-nd thermo-erosional cirqueses	
118	MaK-O 118	Phoca sp.	humerus		d	shore, right side under the 1-st and 2-nd thermo-erosional cirqueses	? recent
119	MaK-O 119	Phoca sp.	radius		d	shore, right side under the 1-st and 2-nd thermo-erosional cirqueses	? recent
120	MaK-O 120	Large herbivorus mammal	thorax vertebra?	fragment	d	shore, right side under the 1-st and 2-nd thermo-erosional cirqueses	
121	MaK-O 121	Large herbivorus mammal	scapula	fragment	d	shore, right side under the 1-st and 2-nd thermo-erosional cirqueses	
122	MaK-O 122	Large herbivorus mammal	limb bone	fragment	d	shore, right side under the 1-st and 2-nd thermo-erosional cirqueses	trashed

No.	N samples	Taxon	Skeleton element	Preservation	Loc. type	Locality	Notes
123	MaK-O 123	Mammuthus primigenius ?	costa	fragment	d	shore, right side under the 1-st and 2-nd thermo-erosional cirqueses	trashed
124	MaK-O 124	Rangifer tarandus	cranium	fragment	e	shore, mouth of Nuchcha-Dzhiele river	? recent
125	MaK-O 125	Rangifer tarandus	Mc	fragment	e	shore, mouth of Nuchcha-Dzhiele river	
126	MaK-O 126	Equus sp.	scapula	fragment	e	shore, mouth of Nuchcha-Dzhiele river	
127	MaK-O 127	Equus sp.	humerus	fragment	e	shore, mouth of Nuchcha-Dzhiele river	
128	MaK-O 128	Equus sp.	humerus	distal fragment	e	shore, mouth of Nuchcha-Dzhiele river	
129	MaK-O 129	Equus sp.	ph II		e	shore, mouth of Nuchcha-Dzhiele river	
130	MaK-O 130	Rangifer tarandus	astrogalus	damaged	e	shore, mouth of Nuchcha-Dzhiele river	
131	MaK-O 131	Rangifer tarandus	???????????	damaged	e	shore, mouth of Nuchcha-Dzhiele river	
132	MaK-O 132	Bison priscus	tibia		e	shore, mouth of Nuchcha-Dzhiele river	
133	MaK-O 133	Equus sp.	radius	fragment	e	shore, mouth of Nuchcha-Dzhiele river	
134	MaK-O 134	Rangifer tarandus	antler	fragment	e	shore, mouth of Nuchcha-Dzhiele river	
135	MaK-O 135	Equus sp. ?	femur	fragment	e	shore, mouth of Nuchcha-Dzhiele river	
136	MaK-O 136	Rangifer tarandus	femur	distal fragment	e	shore, mouth of Nuchcha-Dzhiele river	
137	MaK-O 137	Mammuthus primigenius	tibia	fragment	e	shore, mouth of Nuchcha-Dzhiele river	C 14
138	MaK-O 138	Large herbivorus mammal	limb bone	fragment	a	in situ, exposure, Ice Complex, altitude ?? m a.s.l.	from Lutz, AMS
139	MaK-O 139	Lepus sp.	mandibula with teeth	fragment	a	in situ, exposure, sand deposits, altitude ?? m a.s.l.	
140	MaK-O 140	Lepus sp.	cranium	fragment	c	exposure	? recent
141	MaK-O 141	Mammuthus primigenius	2 lumbar vertebrae in natural conjunction	damaged	e	shore, mouth of Nuchcha-Dzhiele river	
142	MaK-O 142	Bison priscus ?	cranium with horn cores	fragment	e	shore, mouth of Nuchcha-Dzhiele river	juv.
143	MaK-O 143	Rangifer tarandus	cranium	fragment	e	shore, mouth of Nuchcha-Dzhiele river	juv.
144	MaK-O 144	Rangifer tarandus	scapula	fragment	e	shore, mouth of Nuchcha-Dzhiele river	
145	MaK-O 145	Rangifer tarandus	Mt	fragment	e	shore, mouth of Nuchcha-Dzhiele river	

Appendix 4-7. Continuation

No.	N samples	Taxon	Skeleton element	Preservation	Loc. type	Locality	Notes
146	MaK-O 146	Equus sp.	humerus	distal fragment	e	shore, mouth of Nuchcha-Dzhiele river	
147	MaK-O 147	Equus sp.	humerus	distal fragment	e	shore, mouth of Nuchcha-Dzhiele river	
148	MaK-O 148	Rangifer tarandus	lumbar vertebra	damaged	e	shore, mouth of Nuchcha-Dzhiele river	
149	MaK-O 149	Rangifer tarandus	epistropheus	damaged	e	shore, mouth of Nuchcha-Dzhiele river	
150	MaK-O 150	Rangifer tarandus	thorax vertebra	damaged	e	shore, mouth of Nuchcha-Dzhiele river	
151	MaK-O 151	Rangifer tarandus ?	vertebra	fragment	e	shore, mouth of Nuchcha-Dzhiele river	
152	MaK-O 152	Rangifer tarandus	humerus	distal fragment	e	shore, mouth of Nuchcha-Dzhiele river	
153	MaK-O 153	Mammuthus primigenius	pelvis	fragment	e	shore, mouth of Nuchcha-Dzhiele river	juv.
154	MaK-O 154	Equus sp.	ph I		e	shore, mouth of Nuchcha-Dzhiele river	
155	MaK-O 155	Equus sp.	thorax vertebra	damaged	e	shore, mouth of Nuchcha-Dzhiele river	juv.
156	MaK-O 156	Equus sp.	femur	fragment	e	shore, mouth of Nuchcha-Dzhiele river	
157	MaK-O 157	Rangifer tarandus	pelvis (right part)	fragment	e	shore, mouth of Nuchcha-Dzhiele river	
158	MaK-O 158	Rangifer tarandus	lower M	fragment	e	shore, mouth of Nuchcha-Dzhiele river	
159	MaK-O 159	Large herbivorous mammal	limb bone	fragment	e	shore, mouth of Nuchcha-Dzhiele river	trashed
160	MaK-O 160	Lepus sp.	cranium	fragment	e	shore, mouth of Nuchcha-Dzhiele river	? recent, trashed
161	MaK-O 161	Equus sp.	cervical vertebra	damaged	g	middle current Urasalakh river, shore under the sand deposit; latitude - 73 32,789' n., altitude - 116 23,382' e. from Bol'shiyanov D., samples 161, 162, 163 - from the same specimen probably	
162	MaK-O 162	Equus sp.	cervical vertebra	damaged	g		
163	MaK-O 163	Equus sp.	cervical vertebra	damaged	g		
164	MaK-O 164	Equus sp.	ph I		g	shore under the Ice Complex outcrop	from Kunit-sky V. V.
165	MaK-O 165	Rangifer tarandus	atlas	fragment	g	shore under the Ice Complex outcrop	

Appendix 4-7. Continuation

No.	N samples	Taxon	Skeleton element	Preservation	Loc. type	Locality	Notes
166	MaK-O 166	Rangifer tarandus	humerus	fragment	g	shore under the Ice Complex outcrop	from Kunit-sky V. V.
167	MaK-O 167	Rangifer tarandus	ph I		g	shore under the Ice Complex outcrop	
168	MaK-O 168	Large herbivorous mammal	costa	fragment	e	shore, mouth of Nuchcha-Dzhiele river	
169	MaK-O 169	Equus sp.	humerus	distal fragment	e	shore, mouth of Nuchcha-Dzhiele river	
170	MaK-O 170	Rangifer tarandus	tibia	distal fragment	e	shore, mouth of Nuchcha-Dzhiele river	
171	MaK-O 171	Large herbivorous mammal	limb bone	fragment	e	shore, mouth of Nuchcha-Dzhiele river	
172	MaK-O 172	Rangifer tarandus	antebrachium		e	shore, mouth of Nuchcha-Dzhiele river	
173	MaK-O 173	Mammuthus primigenius	tooth	fragment	e	shore, mouth of Nuchcha-Dzhiele river	
174	MaK-O 174	Rangifer tarandus	mandibula	fragment	e	shore, mouth of Nuchcha-Dzhiele river	
175	MaK-O 175	Rangifer tarandus	antebrachium	fragment	e	shore, mouth of Nuchcha-Dzhiele river	
176	MaK-O 176	Equus sp.	cervical vertebra	damaged	e	shore, mouth of Nuchcha-Dzhiele river	
177	MaK-O 177	Equus sp.	Mt III	proximal fragment	e	shore, mouth of Nuchcha-Dzhiele river	
178	MaK-O 178	Equus sp.	ph I		e	shore, mouth of Nuchcha-Dzhiele river	
179	MaK-O 179	Equus sp.	ph I		e	shore, mouth of Nuchcha-Dzhiele river	
180	MaK-O 180	Equus sp.	ph II		e	shore, mouth of Nuchcha-Dzhiele river	
181	MaK-O 181	Equus sp.	astrogalus		e	shore, mouth of Nuchcha-Dzhiele river	
182	MaK-O 182	Equus sp.	mandibula (simphis) with I2-I3, C		e	shore, mouth of Nuchcha-Dzhiele river	
183	MaK-O 183	Rangifer tarandus	antebrachium	proximal fragment	e	shore, mouth of Nuchcha-Dzhiele river	
184	MaK-O 184	Mammuthus primigenius	tusk	fragment	e	shore, mouth of Nuchcha-Dzhiele river	juv.
185	MaK-O 185	Rangifer tarandus	calcaneus	damaged	e	shore, mouth of Nuchcha-Dzhiele river	
186	MaK-O 186	Phoca sp.?	epistropheus		e	shore, mouth of Nuchcha-Dzhiele river	
187	MaK-O 187	Rangifer tarandus	shed antler	fragment	e	shore, mouth of Nuchcha-Dzhiele river	

Appendix 4-7. Continuation

No.	N samples	Taxon	Skeleton element	Preservation	Loc. type	Locality	Notes
188	MaK-O 188	Large herbivorous mammal	limb bone	fragment	e	shore, mouth of Nuchcha-Dzhiele river	
189	MaK-O 189	Rangifer tarandus	femur	distal fragment (articulation)	e	shore, mouth of Nuchcha-Dzhiele river	juv.
190	MaK-O 190	Equus sp.	os naviculare		e	shore, mouth of Nuchcha-Dzhiele river	
191	MaK-O 191	Phoca sp.	humerus	damaged	e	shore, mouth of Nuchcha-Dzhiele river	
192	MaK-O 192	Rangifer tarandus	thorax vertebra	fragment	e	shore, mouth of Nuchcha-Dzhiele river	
193	MaK-O 193	Rangifer tarandus	cervical vertebra	damaged	d	shore, right side under the Ice Complex outcrop	
194	MaK-O 194	Equus sp.	cervical vertebra	damaged	d	shore, right side under the Ice Complex outcrop	
195	MaK-O 195	Rangifer tarandus	thorax vertebra	damaged	d	shore, right side under the Ice Complex outcrop	
196	MaK-O 196	Rangifer tarandus	epistropheus	damaged	d	shore, right side under the Ice Complex outcrop	
197	MaK-O 197	Mammuthus primigenius	humerus	fragment	d	shore, right side under the Ice Complex outcrop	juv.
198	MaK-O 198	Rangifer tarandus	atler	fragment	d	shore, right side under the Ice Complex outcrop	
199	MaK-O 199	Rangifer tarandus	tibia	distal fragment	d	shore, right side under the Ice Complex outcrop	
200	MaK-O 200	Large herbivorous mammal	costa	fragment	d	shore, right side under the Ice Complex outcrop	trashed
201	MaK-O 201		pelvis	fragment	d	shore, right side under the Ice Complex outcrop	trashed
202	MaK-O 202		limb bone	fragment	e	shore, mouth of Nuchcha-Dzhiele river	trashed
203	MaK-O 203		limb bone	fragment	e	shore, mouth of Nuchcha-Dzhiele river	trashed
204	MaK-O 204		Equus sp.	crania (ocipitale)	fragment	e	shore, mouth of Nuchcha-Dzhiele river
205	MaK-O 205	Equus sp.	atlas	damaged	e	shore, mouth of Nuchcha-Dzhiele river	
206	MaK-O 206	Mammuthus primigenius	limb bone	fragment	e	shore, mouth of Nuchcha-Dzhiele river	C 14
207	MaK-O 207	Ovibos sp.	humerus	distal fragment	e	shore, mouth of Nuchcha-Dzhiele river	
208	MaK-O 208	Equus sp.	ph I		e	shore, mouth of Nuchcha-Dzhiele river	
209	MaK-O 209	Ovibos sp.	atlas	fragment	e	shore, mouth of Nuchcha-Dzhiele river	
210	MaK-O 210	Rangifer tarandus	scapula	fragment	e	shore, mouth of Nuchcha-Dzhiele river	
211	MaK-O 211	Mammuthus primigenius	cervical vertebra	fragment	e	shore, mouth of Nuchcha-Dzhiele river	trashed
212	MaK-O 212	Equus sp.	pelvis	fragment	e	shore, mouth of Nuchcha-Dzhiele river	

No.	N samples	Taxon	Skeleton element	Preservation	Loc. type	Locality	Notes
213	MaK-O 213	Equus sp.	pelvis	fragment	e	shore, mouth of Nuchcha-Dzhiele river	
214	MaK-O 214	Equus sp.	humerus	fragment	e	shore, mouth of Nuchcha-Dzhiele river	
215	MaK-O 215	Equus sp.	cervical vertebra	damaged	e	shore, mouth of Nuchcha-Dzhiele river	
216	MaK-O 216	Equus sp.	humerus	distal fragment	e	shore, mouth of Nuchcha-Dzhiele river	
217	MaK-O 217	Rangifer tarandus	Mt	fragment	e	shore, mouth of Nuchcha-Dzhiele river	juv.
218	MaK-O 218	Rangifer tarandus	Mc	distal fragment	e	shore, mouth of Nuchcha-Dzhiele river	
219	MaK-O 219	Rangifer tarandus	atler	fragment	e	shore, mouth of Nuchcha-Dzhiele river	
220	MaK-O 220	Rangifer tarandus	sacrum	fragment	e	shore, mouth of Nuchcha-Dzhiele river	
221	MaK-O 221	Large herbivorous mammal	limb bone	fragment	e	shore, mouth of Nuchcha-Dzhiele river	
222	MaK-O 222	Equus sp.	tibia	fragment	e	shore, mouth of Nuchcha-Dzhiele river	juv.
223	MaK-O 223	Bison priscus	cervical vertebra	damaged	e	shore, mouth of Nuchcha-Dzhiele river	
224	MaK-O 224	Equus sp.	cervical vertebra	damaged	e	shore, mouth of Nuchcha-Dzhiele river	
225	MaK-O 225	Equus sp.	humerus	fragment	e	shore, mouth of Nuchcha-Dzhiele river	
226	MaK-O 226	Rangifer tarandus	Mc	fragment	e	shore, mouth of Nuchcha-Dzhiele river	juv.
227	MaK-O 227	Bison priscus	ulna	fragment	e	shore, mouth of Nuchcha-Dzhiele river	
228	MaK-O 228	Rangifer tarandus ?	atler ?	fragment	e	shore, mouth of Nuchcha-Dzhiele river	
229	MaK-O 229	Equus sp.	astrogalus	fragment	e	shore, mouth of Nuchcha-Dzhiele river	
230	MaK-O 230	Rangifer tarandus	tibia	fragment	e	shore, mouth of Nuchcha-Dzhiele river	juv.
231	MaK-O 231	Rangifer tarandus	lumbar vertebra	fragment	e	shore, mouth of Nuchcha-Dzhiele river	
232	MaK-O 232	Rangifer tarandus	scapula	fragment	e	shore, mouth of Nuchcha-Dzhiele river	
233	MaK-O 233	Rangifer tarandus	scapula	fragment	e	shore, mouth of Nuchcha-Dzhiele river	
234	MaK-O 234	Rangifer tarandus	humerus	distal fragment	e	shore, mouth of Nuchcha-Dzhiele river	
235	MaK-O 235	Mammuthus primigenius	metapodia	fragment	e	shore, mouth of Nuchcha-Dzhiele river	C 14
236	MaK-O 236	Mammuthus primigenius	fibula	distal fragment	e	shore, mouth of Nuchcha-Dzhiele river	C 14
237	MaK-O 237	Bison priscus ?	pelvis	fragment	e	shore, mouth of Nuchcha-Dzhiele river	
238	MaK-O 238	Rangifer tarandus	calcaneus	damaged	e	shore, mouth of Nuchcha-Dzhiele river	
239	MaK-O 239	Ovibos sp.	cervical vertebra	damaged	e	shore, mouth of Nuchcha-Dzhiele river	

Appendix 4-7. Continuation

No.	N samples	Taxon	Skeleton element	Preservation	Loc. type	Locality	Notes
240	MaK-O 240	Rangifer tarandus	atler	fragment	e	shore, mouth of Nuchcha-Dzhiele river	trashed
241	MaK-O 241	Rangifer tarandus	atler	fragment	e	shore, mouth of Nuchcha-Dzhiele river	trashed
242	MaK-O 242	Rangifer tarandus	shed antler	fragment	e	shore, mouth of Nuchcha-Dzhiele river	trashed
243	MaK-O 243	Rangifer tarandus	lumbar vertebra		e	shore, mouth of Nuchcha-Dzhiele river	
244	MaK-O 244	Rangifer tarandus	ph I	damaged	e	shore, mouth of Nuchcha-Dzhiele river	juv.
245	MaK-O 245	Rangifer tarandus	limb bone	fragment	e	shore, mouth of Nuchcha-Dzhiele river	
246	MaK-O 246	Rangifer tarandus	Mt III		e	shore, mouth of Nuchcha-Dzhiele river	
247	MaK-O 247	Rangifer tarandus	ph I		e	shore, mouth of Nuchcha-Dzhiele river	
248	MaK-O 248	Mammuthus primigenius	bone of tarsus	fragment	e	shore, mouth of Nuchcha-Dzhiele river	
249	MaK-O 249	Bison priscus	patella	damaged	e	shore, mouth of Nuchcha-Dzhiele river	
250	MaK-O 250	Rangifer tarandus	sacrum	fragment	e	shore, mouth of Nuchcha-Dzhiele river	
251	MaK-O 251	Rangifer tarandus	Mc	distal fragment	e	shore, mouth of Nuchcha-Dzhiele river	
252	MaK-O 252	Rangifer tarandus	scapula	fragment	e	shore, mouth of Nuchcha-Dzhiele river	
253	MaK-O 253	Equus sp.	humerus	fragment	e	shore, mouth of Nuchcha-Dzhiele river	
254	MaK-O 254	Equus sp.	cervical vertebra	fragment	e	shore, mouth of Nuchcha-Dzhiele river	
255	MaK-O 255	Equus sp.	ph I	fragment	e	shore, mouth of Nuchcha-Dzhiele river	
256	MaK-O 256	Rangifer tarandus	scapula	fragment	e	shore, mouth of Nuchcha-Dzhiele river	trashed
257	MaK-O 257	Rangifer tarandus	Mc	fragment	e	shore, mouth of Nuchcha-Dzhiele river	
258	MaK-O 258	Rangifer tarandus	thorax vertebra	fragment	e	shore, mouth of Nuchcha-Dzhiele river	
259	MaK-O 259	Mammuthus primigenius	vertebra ?	fragment	e	shore, mouth of Nuchcha-Dzhiele river	? 14
260	MaK-O 260	Rangifer tarandus	calcaneus	damaged	e	shore, mouth of Nuchcha-Dzhiele river	
261	MaK-O 261	Rangifer tarandus	cranium (ocipitale)	fragment	e	shore, mouth of Nuchcha-Dzhiele river	
262	MaK-O 262	Rangifer tarandus	shed antler	fragment	e	shore, mouth of Nuchcha-Dzhiele river	trashed
263	MaK-O 263	Large herbivorous mammal	limb bone	fragment	e	shore, mouth of Nuchcha-Dzhiele river	trashed
264	MaK-O 264	Large herbivorous mammal	humerus	fragment	e	shore, mouth of Nuchcha-Dzhiele river	
265	MaK-O 265	Rangifer tarandus	humerus	fragment	e	shore, mouth of Nuchcha-Dzhiele river	trashed
266	MaK-O 266	Rangifer tarandus	limb bone	fragment	e	shore, mouth of Nuchcha-Dzhiele river	trashed

Appendix 4-7. Continuation

No.	N samples	Taxon	Skeleton element	Preservation	Loc. type	Locality	Notes
267	MaK-O 267	Large herbivorous mammal	limb bone	fragment	e	shore, mouth of Nuchcha-Dzhiele river	trashed
268	MaK-O 268	Equus sp.	ph III		e	shore, mouth of Nuchcha-Dzhiele river	
269	MaK-O 269	Equus sp.	ph I		e	shore, mouth of Nuchcha-Dzhiele river	
270	MaK-O 270	Equus sp.	ph II		e	shore, mouth of Nuchcha-Dzhiele river	
271	MaK-O 271	Equus sp.	ph I		e	shore, mouth of Nuchcha-Dzhiele river	
272	MaK-O 272	Equus sp.	ph II		e	shore, mouth of Nuchcha-Dzhiele river	
273	MaK-O 273	Rangifer tarandus	ph I		e	shore, mouth of Nuchcha-Dzhiele river	
274	MaK-O 274	Large herbivorous mammal	limb bone	fragment	e	shore, mouth of Nuchcha-Dzhiele river	
275	MaK-O 275	Large herbivorous mammal	limb bone	fragment	e	shore, mouth of Nuchcha-Dzhiele river	
276	MaK-O 276	Rangifer tarandus	shed antler	fragment	e	shore, mouth of Nuchcha-Dzhiele river	trashed
277	MaK-O 277	Rangifer tarandus	calcaneus	damaged	e	shore, mouth of Nuchcha-Dzhiele river	
278	MaK-O 278	Bison priscus	astrogalus		e	shore, mouth of Nuchcha-Dzhiele river	
279	MaK-O 279	Equus sp.	astrogalus		e	shore, mouth of Nuchcha-Dzhiele river	
280	MaK-O 280	Equus sp.	ulna		e	shore, mouth of Nuchcha-Dzhiele river	
281	MaK-O 281	Equus sp.	astrogalus	damaged	e	shore, mouth of Nuchcha-Dzhiele river	
282	MaK-O 282	Equus sp.	calcaneus	damaged	e	shore, mouth of Nuchcha-Dzhiele river	
283	MaK-O 283	Equus sp.	astrogalus	damaged	e	shore, mouth of Nuchcha-Dzhiele river	
284	MaK-O 284	Equus sp.	astrogalus		e	shore, mouth of Nuchcha-Dzhiele river	
285	MaK-O 285	Equus sp.	ph III	damaged	e	shore, mouth of Nuchcha-Dzhiele river	
286	MaK-O 286	Equus sp.	ph I		e	shore, mouth of Nuchcha-Dzhiele river	
287	MaK-O 287	Equus sp. ?	lumbar vertebra	damaged	e	shore, mouth of Nuchcha-Dzhiele river	
288	MaK-O 288	Rangifer tarandus	cervical vertebra	damaged	e	shore, mouth of Nuchcha-Dzhiele river	
289	MaK-O 289	Rangifer tarandus	vertebra	fragment	e	shore, mouth of Nuchcha-Dzhiele river	
290	MaK-O 290	Equus sp.	ph I		e	shore, mouth of Nuchcha-Dzhiele river	
291	MaK-O 291	Equus sp.	ph III	damaged	e	shore, mouth of Nuchcha-Dzhiele river	
292	MaK-O 292	Equus sp.	vertebra	fragment	e	shore, mouth of Nuchcha-Dzhiele river	

Appendix 4-7. Continuation

No.	N samples	Taxon	Skeleton element	Preservation	Loc. type	Locality	Notes
293	MaK-O 293	Rangifer tarandus	lumbar vertebra	damaged	e	shore, mouth of Nuchcha-Dzhiele river	
294	MaK-O 294	Rangifer tarandus	astrogalus		e	shore, mouth of Nuchcha-Dzhiele river	
295	MaK-O 295	Equus sp.	pelvis	fragment	e	shore, mouth of Nuchcha-Dzhiele river	
296	MaK-O 296	Rangifer tarandus	scapula	fragment	e	shore, mouth of Nuchcha-Dzhiele river	
297	MaK-O 297	Rangifer tarandus	scapula	fragment	e	shore, mouth of Nuchcha-Dzhiele river	
298	MaK-O 298	Equus sp.	ph III		e	shore, mouth of Nuchcha-Dzhiele river	
299	MaK-O 299	Equus sp.	calcaneus	damaged	e	shore, mouth of Nuchcha-Dzhiele river	
300	MaK-O 300	Equus sp.	ph II		e	shore, mouth of Nuchcha-Dzhiele river	
301	MaK-O 301	Rangifer tarandus	lumbar vertebra	damaged	e	shore, mouth of Nuchcha-Dzhiele river	
302	MaK-O 302	Rangifer tarandus	astrogalus	damaged	e	shore, mouth of Nuchcha-Dzhiele river	
303	MaK-O 303	Bison priscus	bone of tarsus	fragment	e	shore, mouth of Nuchcha-Dzhiele river	
304	MaK-O 304	Bison priscus	astrogalus		e	shore, mouth of Nuchcha-Dzhiele river	
305	MaK-O 305	Rangifer tarandus	calcaneus	fragment	e	shore, mouth of Nuchcha-Dzhiele river	
306	MaK-O 306	Rangifer tarandus	ph I		e	shore, mouth of Nuchcha-Dzhiele river	
307	MaK-O 307	Rangifer tarandus ?	cranium (palatina)	fragment	e	shore, mouth of Nuchcha-Dzhiele river	
308	MaK-O 308	Large herbivorous mammal	femur	fragment	e	shore, mouth of Nuchcha-Dzhiele river	juv., trashed
309	MaK-O 309	Rangifer tarandus	ph I	damaged	e	shore, mouth of Nuchcha-Dzhiele river	
310	MaK-O 310	Equus sp.	ph I	distal fragment	e	shore, mouth of Nuchcha-Dzhiele river	
311	MaK-O 311	Rangifer tarandus	ph I		e	shore, mouth of Nuchcha-Dzhiele river	
312	MaK-O 312	Rangifer tarandus	sacrum	fragment	e	shore, mouth of Nuchcha-Dzhiele river	
313	MaK-O 313	Equus sp.	patella	damaged	e	shore, mouth of Nuchcha-Dzhiele river	
314	MaK-O 314	Rangifer tarandus ?	vertebra	fragment	e	shore, mouth of Nuchcha-Dzhiele river	trashed
315	MaK-O 315	Bison priscus ?	limb bone	fragment	e	shore, mouth of Nuchcha-Dzhiele river	
316	MaK-O 316	Rangifer tarandus	metapodia	distal fragment	e	shore, mouth of Nuchcha-Dzhiele river	
317	MaK-O 317	Large herbivorous mammal	pelvis	fragment	e	shore, mouth of Nuchcha-Dzhiele river	trashed
318	MaK-O 318	Bison priscus	bone of tarsus		e	shore, mouth of Nuchcha-Dzhiele river	
319	MaK-O 319	Rangifer tarandus	ph II		e	shore, mouth of Nuchcha-Dzhiele river	
320	MaK-O 320	Rangifer tarandus	astrogalus	fragment	e	shore, mouth of Nuchcha-Dzhiele river	

No.	N samples	Taxon	Skeleton element	Preservation	Loc. type	Locality	Notes
321	MaK-O 321	Rangifer tarandus	thorax vertebra	fragment	e	shore, mouth of Nuchcha-Dzhiele river	trashed
322	MaK-O 322	Rangifer tarandus	vertabra	fragment	e	shore, mouth of Nuchcha-Dzhiele river	trashed
323	MaK-O 323	Mammuthus primigenius ?	limb bone	fragment	e	shore, mouth of Nuchcha-Dzhiele river	trashed
324	MaK-O 324	Large herbivorus mammal	limb bone	fragment	e	shore, mouth of Nuchcha-Dzhiele river	
325	MaK-O 325	Rangifer tarandus	astrogalus	fragment	e	shore, mouth of Nuchcha-Dzhiele river	
326	MaK-O 326	Phoca sp.?	lumbar vertebra	fragment	e	shore, mouth of Nuchcha-Dzhiele river	
327	MaK-O 327	Rangifer tarandus	shed antler	fragment	e	shore, mouth of Nuchcha-Dzhiele river	trashed
328	MaK-O 328	Rangifer tarandus	ph II	fragment	e	shore, mouth of Nuchcha-Dzhiele river	
329	MaK-O 329	Ovibos sp.	cervical vertebra	damaged	e	shore, mouth of Nuchcha-Dzhiele river	
330	MaK-O 330	Large herbivorus mammal	limb bone	fragment	e	shore, mouth of Nuchcha-Dzhiele river	
331	MaK-O 331	Rangifer tarandus	lumbar vertebra	damaged	e	shore, mouth of Nuchcha-Dzhiele river	
332	MaK-O 332	Lepus sp.?	femur	distal fragment	e	shore, mouth of Nuchcha-Dzhiele river	
333	MaK-O 333	Rangifer tarandus	bone of carsus		e	shore, mouth of Nuchcha-Dzhiele river	
334	MaK-O 334	Rangifer tarandus	upper tooth (?)		e	shore, mouth of Nuchcha-Dzhiele river	
335	MaK-O 335	Rangifer tarandus	bone of carsus	fragment	e	shore, mouth of Nuchcha-Dzhiele river	
336	MaK-O 336	Rangifer tarandus	cranium (bulla timpani)	fragment	e	shore, mouth of Nuchcha-Dzhiele river	
337	MaK-O 337	Large herbivorus mammal	limb bone	fragment	e	shore, mouth of Nuchcha-Dzhiele river	
338	MaK-O 338	Equus sp.	ph II ?	fragment	e	shore, mouth of Nuchcha-Dzhiele river	
339	MaK-O 339	Rangifer tarandus	bone of carsus ?	fragment	e	shore, mouth of Nuchcha-Dzhiele river	
340	MaK-O 340	Rangifer tarandus	bone of carsus	fragment	e	shore, mouth of Nuchcha-Dzhiele river	
341	MaK-O 341	Rangifer tarandus	bone of carsus	fragment	e	shore, mouth of Nuchcha-Dzhiele river	
342	MaK-O 342	Large herbivorus mammal	limb bone	fragment	e	shore, mouth of Nuchcha-Dzhiele river	
343	MaK-O 343	Rangifer tarandus	bone of carsus	fragment	e	shore, mouth of Nuchcha-Dzhiele river	
344	MaK-O 344	Large herbivorus mammal	limb bone	fragment	e	shore, mouth of Nuchcha-Dzhiele river	

No.	N samples	Taxon	Skeleton element	Preservation	Loc. type	Locality	Notes
345	MaK-O 345	Mammuthus primigenius	metapodia	fragment	e	shore, mouth of Nuchcha-Dzhiele river	
346	MaK-O 346	Rangifer tarandus	antler	fragment	e	shore, mouth of Nuchcha-Dzhiele river	trashed
347	MaK-O 347	Rangifer tarandus	metapodia	fragment	e	shore, mouth of Nuchcha-Dzhiele river	trashed
348	MaK-O 348	Rangifer tarandus	cervical vertebra	fragment	e	shore, mouth of Nuchcha-Dzhiele river	trashed
349	MaK-O 349	Rangifer tarandus	shed antler	fragment	e	shore, mouth of Nuchcha-Dzhiele river	trashed
350	MaK-O 350	Equus sp.	pelvis	fragment	e	shore, mouth of Nuchcha-Dzhiele river	
351	MaK-O 351	????? ?	thorax vertebra	fragment	e	shore, mouth of Nuchcha-Dzhiele river	
352	MaK-O 352	Rangifer tarandus	tibia	distal fragment (articulation)	e	shore, mouth of Nuchcha-Dzhiele river	
353	MaK-O 353	Large herbivorous mammal	limb bone	fragment	e	shore, mouth of Nuchcha-Dzhiele river	trashed
354	MaK-O 354	Mammuthus primigenius	lumbar vertebra	fragment	e	shore, mouth of Nuchcha-Dzhiele river	
355	MaK-O 355	Equus sp.	tibia	damaged	e	shore, mouth of Nuchcha-Dzhiele river	
356	MaK-O 356	Canis sp.?	metapodia	fragment	e	shore, mouth of Nuchcha-Dzhiele river	
357	MaK-O 357	Bison priscus	humerus	distal fragment	e	shore, mouth of Nuchcha-Dzhiele river	
358	MaK-O 358	Equus sp.	ph II	fragment	e	shore, mouth of Nuchcha-Dzhiele river	
359	MaK-O 359	Equus sp.	tibia	proximal fragment	e	shore, mouth of Nuchcha-Dzhiele river	
360	MaK-O 360	Equus sp.	cervical vertebra	damaged	e	shore, mouth of Nuchcha-Dzhiele river	
361	MaK-O 361	Rangifer tarandus	cervical vertebra	damaged	e	shore, mouth of Nuchcha-Dzhiele river	
362	MaK-O 362	Rangifer tarandus ?	cranium	fragment	e	shore, mouth of Nuchcha-Dzhiele river	
363	MaK-O 363	Rangifer tarandus	cranium	fragment	e	shore, mouth of Nuchcha-Dzhiele river	
364	MaK-O 364	Mammuthus primigenius	radius	fragment	e	shore, mouth of Nuchcha-Dzhiele river	juv.
365	MaK-O 365	Equus sp.	astrogalus	fragment	e	shore, mouth of Nuchcha-Dzhiele river	
366	MaK-O 366	Mammuthus primigenius	tibia	fragment	e	shore, mouth of Nuchcha-Dzhiele river	juv.
367	MaK-O 367	Equus sp.	tibia	fragment	e	shore, mouth of Nuchcha-Dzhiele river	trashed
368	MaK-O 368	Equus sp.	cervical vertebra	damaged	e	shore, mouth of Nuchcha-Dzhiele river	
369	MaK-O 369	Phoca sp.	femur		e	shore, mouth of Nuchcha-Dzhiele river	
370	MaK-O 370	Large herbivorous mammal	limb bone	fragment	e	shore, mouth of Nuchcha-Dzhiele river	

No.	N samples	Taxon	Skeleton element	Preservation	Loc. type	Locality	Notes
371	MaK-O 371	Bison priscus	bone of tarsus		e	shore, mouth of Nuchcha-Dzhiele river	
372	MaK-O 372	Bison priscus	horn sheet	fragment	e	shore, mouth of Nuchcha-Dzhiele river	
373	MaK-O 373	Rangifer tarandus	astrogalus		e	shore, mouth of Nuchcha-Dzhiele river	
374	MaK-O 374	Rangifer tarandus	astrogalus		d	shore, right side under the Ice Complex outcrop	
375	MaK-O 375	Equus sp.	tibia	distal fragment (articulation)	e	shore of Nuchcha-Dzhiele river under the Ice Complex outcrop	juv.
376	MaK-O 376	Equus sp.	Mc III		d	shore, right side under the Ice Complex outcrop	
377	MaK-O 377	Equus sp.	ph I		d	shore, right side under the Ice Complex outcrop	
378	MaK-O 378	Equus sp.	ph I	fragment	d	shore, right side under the Ice Complex outcrop	
379	MaK-O 379	Rangifer tarandus	ph I	fragment	d	shore, right side under the Ice Complex outcrop	
380	MaK-O 380	Lepus sp.?	metapodia		d	shore, right side under the Ice Complex outcrop	
381	MaK-O 381	Lepus sp.?	mandibula	fragment	e	shore, mouth of Nuchcha-Dzhiele river	
382	MaK-O 382	Equus sp.	radius	fragment	d	shore, right side under the Ice Complex outcrop	
383	MaK-O 383	Rangifer tarandus ?	pelvis	fragment	e	shore, mouth of Nuchcha-Dzhiele river	
384	MaK-O 384	Rangifer tarandus	ph I	fragment	e	shore, mouth of Nuchcha-Dzhiele river	
385	MaK-O 385	Mammuthus primigenius	tooth, heavily worn	fragment	e	shore, mouth of Nuchcha-Dzhiele river	
386	MaK-O 386	Mammuthus primigenius	tooth, heavily worn	fragment	e	shore, mouth of Nuchcha-Dzhiele river	
387	MaK-O 387	Rangifer tarandus	ph III	fragment	e	shore, mouth of Nuchcha-Dzhiele river	
388	MaK-O 388	Lepus sp.	metapodia		e	shore, mouth of Nuchcha-Dzhiele river	
389	MaK-O 389	Equus sp.	bone of tarsus	fragment	e	shore, mouth of Nuchcha-Dzhiele river	
390	MaK-O 390	Lepus sp. ?	limb bone	fragment	e	shore, mouth of Nuchcha-Dzhiele river	
391	MaK-O 391	Lepus sp.	ph I		e	shore, mouth of Nuchcha-Dzhiele river	
392	MaK-O 392	Phoca sp.?	cranium (bulla timpani)	fragment	e	shore, mouth of Nuchcha-Dzhiele river	
393	MaK-O 393	Equus sp.	tooth	fragment	e	shore, mouth of Nuchcha-Dzhiele river	
394	MaK-O 394	Rangifer tarandus	ph II	fragment	e	shore, mouth of Nuchcha-Dzhiele river	
395	MaK-O 395	Rangifer tarandus	shed antler	fragment	e	shore, right side under the Ice Complex outcrop	trashed
396	MaK-O 396	Rangifer tarandus	shed antler	fragment	e	shore, mouth of Nuchcha-Dzhiele river	trashed
397	MaK-O 397	Rangifer tarandus	shed antler	fragment	e	shore, mouth of Nuchcha-Dzhiele river	trashed
398	MaK-O 398	Rangifer tarandus	shed antler	fragment	e	shore, mouth of Nuchcha-Dzhiele river	trashed

No.	N samples	Taxon	Skeleton element	Preservation	Loc. type	Locality	Notes
399	MaK-O 399	Rangifer tarandus	shed antler	fragment	e	shore, mouth of Nuchcha-Dzhiele river	trashed
400	MaK-O 400	Rangifer tarandus	antler	fragment	f	shore, left side	trashed
401	MaK-O 401	Large herbivorous mammal	cranium	fragment	e	shore, mouth of Nuchcha-Dzhiele river	trashed
402	MaK-O 402	Mammuthus primigenius	tooth	fragment	e	shore, mouth of Nuchcha-Dzhiele river	trashed
403	MaK-O 403	Large herbivorous mammal	limb bone	fragment	e	shore, mouth of Nuchcha-Dzhiele river	trashed
404	MaK-O 404	Large herbivorous mammal	limb bone	fragment	e	shore, mouth of Nuchcha-Dzhiele river	trashed
405	MaK-O 405	Large herbivorous mammal	metapodia	fragment	e	shore, mouth of Nuchcha-Dzhiele river	trashed
406	MaK-O 406	Rangifer tarandus	vertebra	fragment	e	shore, mouth of Nuchcha-Dzhiele river	trashed
407	MaK-O 407	Large herbivorous mammal	phalax	fragment	e	shore, mouth of Nuchcha-Dzhiele river	trashed
408	MaK-O 408	Rangifer tarandus	tooth	fragment	e	shore, mouth of Nuchcha-Dzhiele river	trashed
409	MaK-O 409	Rangifer tarandus	shed antler		b	exposure, right side, sand deposit, altitude 4,5 ? a.s.l.	cut
410	MaK-O 410	Rangifer tarandus	shed antler	fragment	e	shore, mouth of Nuchcha-Dzhiele river	trashed
411	MaK-O 411	Rangifer tarandus	shed antler	damaged	d	shore, right side under the Ice Complex outcrop	trashed
412	MaK-O 412	Rangifer tarandus	?????????	fragment	e	shore, mouth of Nuchcha-Dzhiele river	
413	MaK-O 413	Lerus sp.?	limb bone	fragment	e	shore, mouth of Nuchcha-Dzhiele river	
414	MaK-O 414	Rangifer tarandus	bone of tarsus	fragment	e	shore, mouth of Nuchcha-Dzhiele river	
415	MaK-O 415	Rangifer tarandus	bone of tarsus		e	shore, mouth of Nuchcha-Dzhiele river	
416	MaK-O 416	Rangifer tarandus	cranium	fragment	e	shore, mouth of Nuchcha-Dzhiele river	
417	MaK-O 417	Large herbivorous mammal	limb bone	fragment	e	shore, mouth of Nuchcha-Dzhiele river	
418	MaK-O 418	Rangifer tarandus	ph II		e	shore, mouth of Nuchcha-Dzhiele river	
419	MaK-O 419	Alopex lagopus	calcaneus		e	shore, mouth of Nuchcha-Dzhiele river	
420	MaK-O 420	Alopex lagopus	ulna		e	shore, mouth of Nuchcha-Dzhiele river	
421	MaK-O 421	Rangifer tarandus	bone of tarsus		e	shore, mouth of Nuchcha-Dzhiele river	
422	MaK-O 422	Rangifer tarandus	ph III	fragment	e	shore, mouth of Nuchcha-Dzhiele river	

Appendix 4-7. Continuation

No.	N samples	Taxon	Skeleton element	Preservation	Loc. type	Locality	Notes
423	MaK-O 423	Rangifer tarandus	humerus	fragment	e	shore, mouth of Nuchcha-Dzhiele river	
424	MaK-O 424	Rangifer tarandus	humerus	fragment	e	shore, mouth of Nuchcha-Dzhiele river	
425	MaK-O 425	Rangifer tarandus	Mt	fragment	e	shore, mouth of Nuchcha-Dzhiele river	
426	MaK-O 426	Rangifer tarandus	ph I		e	shore, mouth of Nuchcha-Dzhiele river	
427	MaK-O 427	Bison priscus	bone of tarsus		e	shore, mouth of Nuchcha-Dzhiele river	
428	MaK-O 428	Bison priscus	limb bone	fragment	e	shore, mouth of Nuchcha-Dzhiele river	trashed
429	MaK-O 429	Alopex lagopus	molar tooth		e	shore, mouth of Nuchcha-Dzhiele river	
430	MaK-O 430	Equus sp.	phalax	fragment	e	shore, mouth of Nuchcha-Dzhiele river	trashed
431	MaK-O 431	Rangifer tarandus ?	vertebra	fragment	e	shore, mouth of Nuchcha-Dzhiele river	trashed
432	MaK-O 432	Rangifer tarandus	shed antler	fragment	e	shore, mouth of Nuchcha-Dzhiele river	trashed
433	MaK-O 433	Large herbivorous mammal	femur	distal fragment	e	shore, mouth of Nuchcha-Dzhiele river	
434	MaK-O 434	Mammuthus primigenius	tooth	fragment	e	shore, mouth of Nuchcha-Dzhiele river	trashed
435	MaK-O 435	Mammuthus primigenius	fibula ?	distal fragment	e	shore, mouth of Nuchcha-Dzhiele river	juv.
436	MaK-O 436	Rangifer tarandus	antler	distal fragment	e	shore, mouth of Nuchcha-Dzhiele river	
437	MaK-O 437	Rangifer tarandus	radius		e	shore, mouth of Nuchcha-Dzhiele river	
438	MaK-O 438	Rangifer tarandus	femur	distal fragment	e	shore, mouth of Nuchcha-Dzhiele river	
439	MaK-O 439	Rangifer tarandus	thorax vertebra	damaged	e	shore, mouth of Nuchcha-Dzhiele river	
440	MaK-O 440	Rangifer tarandus	atlas	fragment	e	shore, mouth of Nuchcha-Dzhiele river	
441	MaK-O 441	Mammuthus primigenius ?	pelvis	fragment	e	shore, mouth of Nuchcha-Dzhiele river	juv.
442	MaK-O 442	Mammuthus primigenius	vertebra	fragment	e	shore, mouth of Nuchcha-Dzhiele river	
443	MaK-O 443	Equus sp.	humerus	distal fragment	e	shore, mouth of Nuchcha-Dzhiele river	
444	MaK-O 444	Rangifer tarandus	scapula	fragment	e	shore, mouth of Nuchcha-Dzhiele river	
445	MaK-O 445	Rangifer tarandus	atlas	fragment	d	shore, right side under the Ice Complex outcrop	
446	MaK-O 446	Rangifer tarandus	epistropheum	fragment	e	shore, mouth of Nuchcha-Dzhiele river	
447	MaK-O 447	Rangifer tarandus	cranium with antler	fragment	e	shore, mouth of Nuchcha-Dzhiele river	
448	MaK-O 448	Rangifer tarandus	cranium with antler	fragment	e	shore, mouth of Nuchcha-Dzhiele river	
449	MaK-O 449	Bison priscus ?	tibia ?	proximal fragment	e	shore, mouth of Nuchcha-Dzhiele river	

Appendix 4-7. Continuation

No.	N samples	Taxon	Skeleton element	Preservation	Loc. type	Locality	Notes
450	MaK-O 450	Equus sp.	ph I		e	shore, mouth of Nuchcha-Dzhiele river	
451	MaK-O 451	Rangifer tarandus	scapula	fragment	e	shore, mouth of Nuchcha-Dzhiele river	
452	MaK-O 452	Rangifer tarandus	cranium (ocipitale)	fragment	e	shore, mouth of Nuchcha-Dzhiele river	
453	MaK-O 453	Rangifer tarandus	metapodia	fragment	e	shore, mouth of Nuchcha-Dzhiele river	
454	MaK-O 454	Rangifer tarandus	radius	proximal fragment	e	shore, mouth of Nuchcha-Dzhiele river	
455	MaK-O 455	Equus sp.	ph I		e	shore, mouth of Nuchcha-Dzhiele river	
456	MaK-O 456	Equus sp.	astrogalus		e	shore, mouth of Nuchcha-Dzhiele river	
457	MaK-O 457	Equus sp.	metapodia	fragment	e	shore, mouth of Nuchcha-Dzhiele river	
458	MaK-O 458	Rangifer tarandus	metapodia	distal fragment	e	shore, mouth of Nuchcha-Dzhiele river	
459	MaK-O 459	Rangifer tarandus ?	radius ?	fragment	e	shore, mouth of Nuchcha-Dzhiele river	juv.
460	MaK-O 460	Bison priscus	femur	fragment	e	shore, mouth of Nuchcha-Dzhiele river	
461	MaK-O 461	Large herbivorus mammal	limb bone	fragment	e	shore, mouth of Nuchcha-Dzhiele river	
462	MaK-O 462	Rangifer tarandus	ph I		e	shore, mouth of Nuchcha-Dzhiele river	
463	MaK-O 463	Rangifer tarandus	ph I		e	shore, mouth of Nuchcha-Dzhiele river	
464	MaK-O 464	Equus sp.	os sesamoidea		e	shore, mouth of Nuchcha-Dzhiele river	
465	MaK-O 465	Rangifer tarandus	bone of tarsus		e	shore, mouth of Nuchcha-Dzhiele river	
466	MaK-O 466	Rangifer tarandus	ph III ?	fragment	e	shore, mouth of Nuchcha-Dzhiele river	
467	MaK-O 467	Large herbivorus mammal	limb bone	fragment	e	shore, mouth of Nuchcha-Dzhiele river	
468	MaK-O 468	Bison priscus	limb bone		e	shore, mouth of Nuchcha-Dzhiele river	
469	MaK-O 469	Canis sp.?	metapodia ?	proximal fragment	e	shore, mouth of Nuchcha-Dzhiele river	
470	MaK-O 470	Rangifer tarandus	cranium (frontale)	fragment	e	shore, mouth of Nuchcha-Dzhiele river	
471	MaK-O 471	Rangifer tarandus	ph I	distal fragment	e	shore, mouth of Nuchcha-Dzhiele river	
472	MaK-O 472	Rangifer tarandus	bone of tarsus		e	shore, mouth of Nuchcha-Dzhiele river	
473	MaK-O 473	Lepus sp.	metapodia	distal fragment	e	shore, mouth of Nuchcha-Dzhiele river	
474	MaK-O 474	Rangifer tarandus	tooth, unerupted	fragment	e	shore, mouth of Nuchcha-Dzhiele river	
475	MaK-O 475	Large herbivorus mammal	pelvis	fragment	e	shore, mouth of Nuchcha-Dzhiele river	trashed

Appendix 4-7. Continuation

No.	N samples	Taxon	Skeleton element	Preservation	Loc. type	Locality	Notes
476	MaK-O 476	Mammuthus primigenius	femur	fragment,3pieces	a	in situ, exposure, lower part of Ice Complex (2-nd peat layer), altitude 10 m a.s.l. samples 476, 477, 478 - from the same specimen probably	C14,
477	MaK-O 477	Mammuthus primigenius	???????? ????????	damaged	a		
478	MaK-O 478	Mammuthus primigenius	tusk	fragment,3pieces	a		
479	MaK-O 479	Mammuthus primigenius	tusk	fragment (4 pieces)	f	shore	C14, from Kunitsky V.V.
480	MaK-O 480	Mammuthus primigenius	tusk	fragment	f	shore	
481	MaK-O 481	Mammuthus primigenius	tibia	fragment	e	shore, mouth of Nuchcha-Dzhiele river	juv.
482	MaK-O 482	Mammuthus primigenius	bone of tarsus		e	shore, mouth of Nuchcha-Dzhiele river	
483	MaK-O 483	Equus sp.	ph II		e	shore, mouth of Nuchcha-Dzhiele river	juv.
484	MaK-O 484	Equus sp.	ph I		e	shore, mouth of Nuchcha-Dzhiele river	
485	MaK-O 485	Equus sp.	ph II	fragment	e	shore, mouth of Nuchcha-Dzhiele river	
486	MaK-O 486	Equus sp.	pelvis	fragment	e	shore, mouth of Nuchcha-Dzhiele river	
487	MaK-O 487	Mammuthus primigenius ?	pelvis ?	fragment	e	shore, mouth of Nuchcha-Dzhiele river	C 14
488	MaK-O 488	Mammuthus primigenius	bone of tarsus	damaged	d	shore, right side under the Ice Complex outcrop	
489	MaK-O 489	Bison priscus	vertebra	fragment	e	shore, mouth of Nuchcha-Dzhiele river	
490	MaK-O 490	Mammuthus primigenius	vertebra	fragment	e	shore, mouth of Nuchcha-Dzhiele river	
491	MaK-O 491	Mammuthus primigenius	metapodia	fragment	e	shore, mouth of Nuchcha-Dzhiele river	
492	MaK-O 492	Rangifer tarandus	thorax vertebra	damaged	e	shore, mouth of Nuchcha-Dzhiele river	
493	MaK-O 493	Rangifer tarandus	sacrum	fragment	e	shore, mouth of Nuchcha-Dzhiele river	trashed
494	MaK-O 494	Mammuthus primigenius	metapodia	fragment	e	shore, mouth of Nuchcha-Dzhiele river	juv.
495	MaK-O 495	Mammuthus primigenius	pelvis	fragment	e	shore, mouth of Nuchcha-Dzhiele river	
496	MaK-O 496	Rangifer tarandus	ph II	damaged	e	shore, mouth of Nuchcha-Dzhiele river	
497	MaK-O 497	Rangifer tarandus	ph I		e	shore, mouth of Nuchcha-Dzhiele river	
498	MaK-O 498	Rangifer tarandus	ph I		e	shore, mouth of Nuchcha-Dzhiele river	
499	MaK-O 499	Lepus sp.	metapodia	distal fragment	e	shore, mouth of Nuchcha-Dzhiele river	
500	MaK-O 500	Rangifer tarandus	bone of tarsus		e	shore, mouth of Nuchcha-Dzhiele river	
501	MaK-O 501	Rangifer tarandus	bone of tarsus		e	shore, mouth of Nuchcha-Dzhiele river	

The Russian-German TRANSDRIFT IX Expedition 2003: Cruise Report and First Results

Carolyn Wegner, Jens Hölemann, Vladimir Churun, and Mashal Alawi



Content

1.	Process Studies on Permafrost Dynamics in the Laptev Sea – An Introduction.....	212
2.	The TRANSDRIFT IX Expedition: Process studies on submarine permafrost dynamics in the Laptev Sea.....	214
3.	Motivation: Deployment of two seafloor observatories.....	216
4.	Recent stability factors of submarine permafrost.....	218
4.1	Working program.....	218
4.2	Preliminary results.....	219
5.	Hydrochemical structure of the water column.....	221
5.1	Working program.....	221
6.	Diversity of nitrifying bacteria in submarine permafrost	222
6.1	Working program.....	222
6.2	Preliminary Results.....	224
7.	Appendix: Station list of the TRANSDRIFT IX (IK03) expedition.....	226
8.	References.....	231

1. Process Studies on Permafrost Dynamics in the Laptev Sea

– An Introduction

Permafrost of a thickness of up to 1000 m is an important feature of the seafloor of the Laptev Sea and of the landscape of the adjoining central part of Northern Siberia. By way of numerous studies carried out in the hinterland of the Laptev Sea, terrestrial permafrost, its distribution and its stability boundaries have been thoroughly investigated. Our knowledge of the submarine permafrost of the Laptev Sea, however, is only based on the results of Russian exploratory drillings off the Novosibirskiye Islands (NSI) during the 1960s and 1970s and of the scientific Russian-German expedition TRANSDRIFT VIII (2000), during which pilot drilling was carried out in the central Laptev Sea.

The submarine permafrost was formed under subaerial conditions during the last glacial and subsequently underwent submersion due to the postglacial sea-level rise and nowadays due to shoreline erosion. Therefore its present state is highly transient. The submarine permafrost regime is largely determined by heat and mass transport processes that control the response rate to the new warm and salty boundary conditions. A considerable amount of organic carbon is stored in the upper permafrost layer and gas hydrates are expected to be found within and beneath the submarine permafrost. Large increases of CO₂ and CH₄ emissions are associated with degradation of permafrost. Thawing of permafrost could release large quantities of greenhouse gases into the atmosphere, thus further increasing global warming. Even though the submarine permafrost is of importance for the global climate system, the knowledge on its recent dynamics is still limited.

During the past decade a large-scale change in the arctic atmospheric circulation took place causing different oceanographic boundary conditions, indicated by, e.g., decrease in ice coverage, increase in riverine input and in air temperatures and increased inflow of Atlantic water masses into the Arctic Ocean and the Laptev Sea. These changing boundary conditions probably influence the stability of the submarine permafrost. Since in permafrost regions geochemical processes are largely governed by microbiological processes, the role of micro-organisms is of major interest in studying the dynamics of biogeochemical cycles in permafrost regions. In particular methane formation/oxidation and formation of carbon dioxide are regarded as microbial key processes in frozen sediments.

The aim of the joint Russian-German project “Process Studies of Permafrost Dynamics in the Laptev Sea” is to investigate by way of an interdisciplinary approach to which extent exchange processes and interaction between atmosphere, hydrosphere and seafloor cause the degradation of submarine permafrost. On the basis of the scientific results of the predecessor Russian-German projects carried out in the Laptev Sea this joint project focuses on the processes taking place during the submersion of terrestrial permafrost, on

recent processes under "stable conditions" as well as on aggradation/degradation processes and their causes.

The Russian-German project "Process Studies of Permafrost Dynamics in the Laptev Sea" is funded by the German Federal Ministry of Education and Research (FKZ 03G0589A) and the Ministry of Industry, Science and Technology of the Russian Federation. The TRANSDRIFT IX expedition was the first marine expedition within the framework of the project mainly focusing on the investigations of the recent factors affecting the stability of submarine permafrost in the Laptev Sea and of the quantification of microbial processes and of their impact on the regulation of biogeochemical cycles in submarine permafrost. It started in Tiksi on August 29 and ended in Tiksi harbor on September 4 2003. The expedition was financially supported by the Alfred Wegener Institute for Polar and Marine Research.

The expedition would not have been possible without the support of numerous colleagues, authorities, and institutions in Russia and Germany. We would especially like to thank for the support and advice of Prof. L. Timokhov (AARI, Russia), Dr. S. Priamikov (AARI, Russia), Dr. H. Kassens (GEOMAR, Germany) and Dr. K. Volkmann-Lark (GEOMAR, Germany) as well as the directors of the hydrographic bases in Arkhangelsk and Tiksi. The expedition was financially supported by the Alfred Wegener Institute for Polar and Marine Research.

We wish to thank the ship's master, Captain Yuri Lekarev, and his crew of RV "IVAN KIREYEV" for their extraordinary contribution to the success of our work. The quick deployment of the two seafloor observatories within 3 days after leaving the harbor of Tiksi was only possible due to the professional and dedicated help of this team.

2. The TRANSDRIFT IX Expedition: Process studies on submarine permafrost dynamics in the Laptev Sea

The TRANSDRIFT IX expedition was carried out aboard RV “IVAN KIREYEV” within the framework of the Russian-German project “Laptev Sea System” and was funded by the German Federal Ministry of Education and Research and the Alfred Wegener Institute for Polar and Marine Research (AWI, Germany). The cruise took place at the same time as the expeditions “Mamontovy Klyk 2003” and “Samoylov 2003”. The research program during the expedition focused on recent processes influencing the stability of the submarine permafrost and on bacterially influenced processes of its biogeochemical cycles. Multidisciplinary experiments were performed comprising:

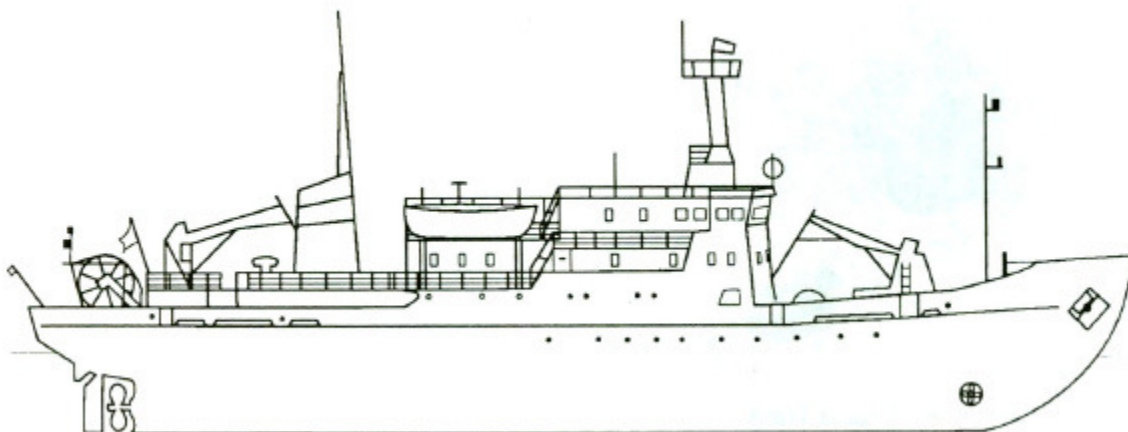
measurements of physical and chemical parameters of the water column and of sediments

sedimentological investigations of sediments and suspended particulate matter

micro-biological studies in the water column and on sediments

One of the major tasks was the investigation of the complex interaction between atmosphere, water column and seafloor/submarine permafrost. Therefore two seafloor observatories were deployed for a period of one year to monitor seasonal variability in surface-sediment temperature and in oceanographic parameters within the water column. They will be recovered during the TRANSDRIFT X expedition in 2004. This somewhat extensive working program for this comparably short period of ship time could be carried out due to fairly calm weather conditions. South-easterly to south-westerly winds prevailed with an average wind speed of 6.1 m/s. The air temperature varied from 2 to 6°C with a mean of 4°C.

RV “IVAN KIREYEV” was constructed in Finland in 1977 and belongs to the Hydrographic Department of Arkhangelsk (Figure 1). It is especially equipped for carrying out oceanographic investigations at high latitudes (class 3 ice capability).



Characteristics	Value
Year of construction	1977
Length over all (max.), m	68
Breadth (max), m	12.4
Draft at load, m	5
Register tons, tons; gross net	1267 380
Displacement at load, tons	1639
Cruising speed, knots	10
Power of main engine, kW	1470
Total crew (max.), persons	55
Tonnage, tons	609

Figure 1: General view and major technical characteristics of RV “IVAN KIREYEV”.

3. Motivation: Deployment of two seafloor observatories

The main task during the TRANDRIFT IX expedition was to deploy two seafloor observatories to study the seasonal variability in temperature and salinity distribution within the water column, interacting processes in the transition zone water column/sediment and in the current system, and the transport processes for the period of one year. One of the seafloor observatories was deployed in the nearshore area north of the Lena Delta to characterize processes in an onshore/offshore environment and within the frontal zone of the Lena River (LENA 03; Figure 2).

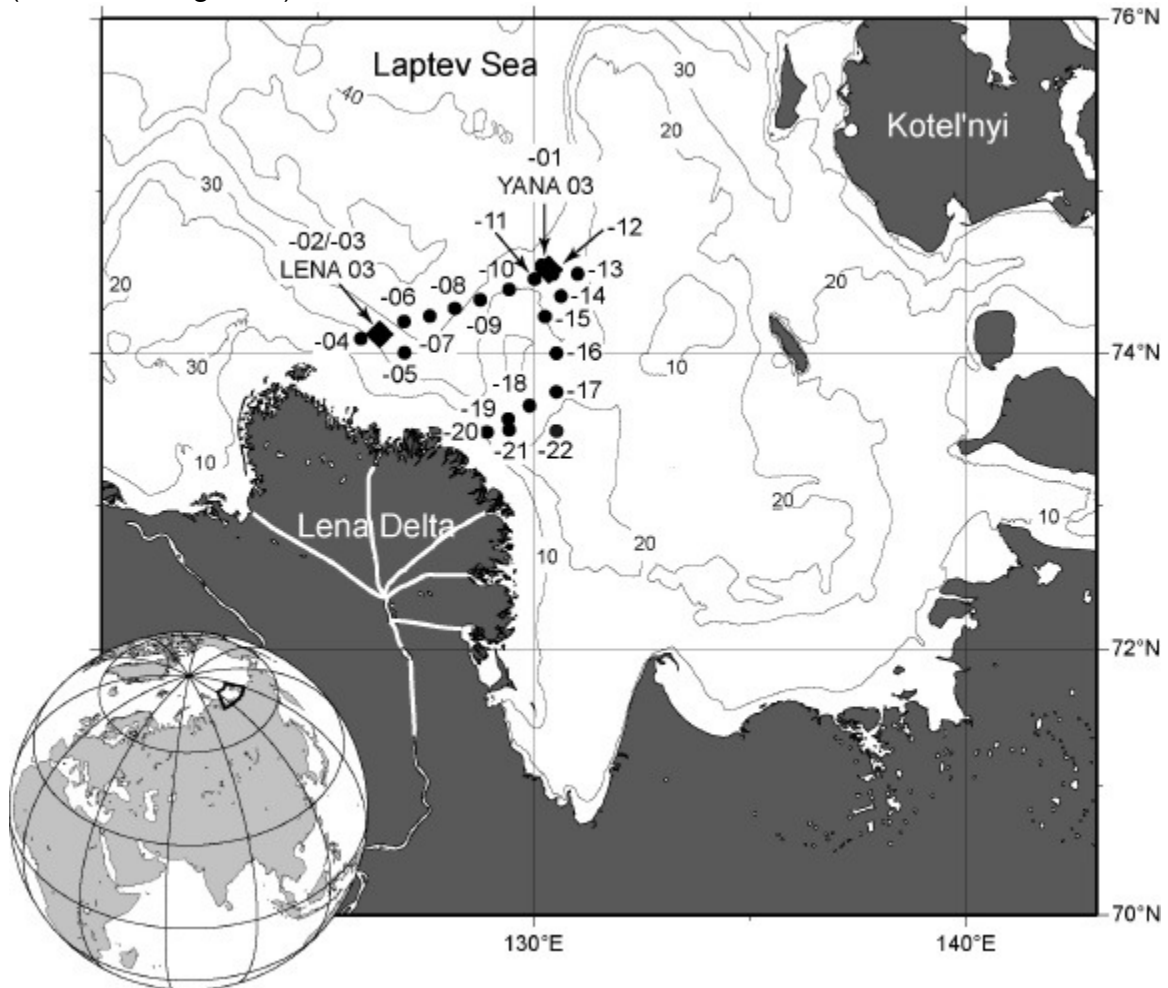


Figure 2: Bathymetric map of the eastern Laptev Sea shelf and the locations of the stations during the TRANSDRIFT IX expedition (IK03). Solid circles indicate short-term, solid squares long-term stations.

To study changes in the hydrodynamic system and its interaction with the seafloor, the second seafloor observatory was deployed in the mid-shelf area (YANA 03; Figure 2).

The seafloor observatories (Figure 3) are each equipped with 4 sediment thermometers (ANTARES, Germany), 1 Acoustic Doppler Current Profiler (ADCP, WH-Sentinel 300 kHz, RD-Instruments, USA), 2 Conductivity

Temperature Depth meters (CTDs, XR-420 CTD+2, RBR, Canada) in combination with turbidity meters (SEAPOINT), and 1 Conductivity Temperature meter (CT, XR-420 CT, RBR; FIGURE; observatories). Conductivity and temperature meters are deployed at defined water depths (LENA 03: 2, 10, and 15 m above seafloor; YANA 03: 2, 10, and 20 m above seafloor) along a sensor string to detect fluctuations in temperature and salinity within the water column. The sediment thermometers record the temperature from the sediment surface up to a depth of 70 cm to determine the heat flux between the water column and the seafloor. The bottom-moored upwards-looking broadband ADCPs monitor the current speed and direction of the entire water column to reconstruct the origin of warmer bottom waters. ADCP measurements at both stations will be carried out at intervals of 1 minute and averaged over 30 minutes in different depth cells.

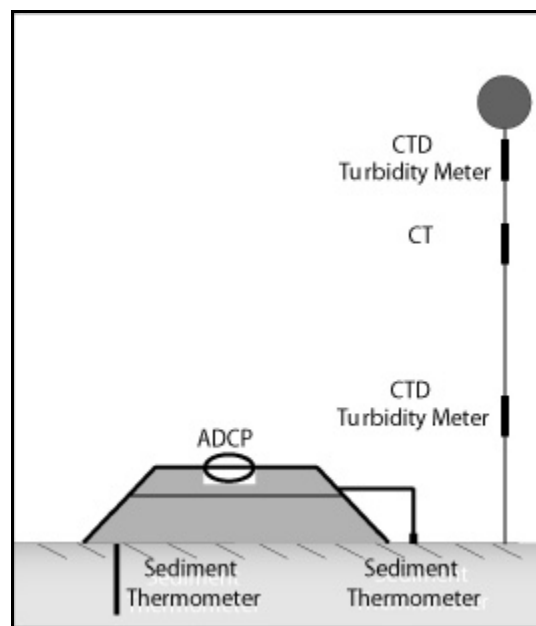


Figure 3: Seafloor observatories to monitor seasonal variability in salinity, temperature, turbidity, ice coverage, currents, and in bottom-sediment temperature.

4. Recent stability factors of submarine permafrost

After submergence submarine permafrost degrades, thawing from the seabed downwards by the influx of salt and heat as a result of the new oceanographic boundary conditions, even in the presence of negative mean seafloor temperatures (e.g. Osterkamp et al., 1989; Gosink & Baker, 1990). Both the transport of heat and the transport of salt are important for the dynamics of the submarine permafrost and, depending upon conditions, either or both may control the response rate to the oceanographic boundary conditions. Changes in temperature and salinity distribution within the water column are of major importance as they directly influence the energetic balance of the submarine permafrost (Vigdorchik, 1980; Gosink & Baker, 1990; Hutter & Straughan, 1999). Therefore process studies on the interaction between atmosphere, water column and seafloor/submarine permafrost were and still are carried out to characterize the stability factors of the submarine permafrost.

4.1 Working program

To investigate the influence of interactions between seafloor, water column, and atmosphere on the stability of the submarine permafrost, relevant parameters in the water column and of surface bottom sediments were determined along a grid of 22 long and short-term stations on the eastern Laptev Sea shelf (Figure 2). 3 long-term stations (at least 18 hours) were located in the adjacency of the seafloor observatories to calibrate the one-year records after recovering them during TRANSDRIFT X expedition in 2004. Measurements with a Conductivity Temperature Depth meter (CTD; SBE 19, Sea-Bird) in combination with a turbidity meter (SEAPOINT) have been carried out to obtain data on the distribution of temperature, salinity, and suspended particulate matter (SPM) within the water column. Water samples of about two liters each were collected with Niskin bottles from defined water depths. These water samples have been filtered through pre-weighed HVLP filters by MILLIPORE (0.45 microns) to obtain SPM concentration. All turbidity meter measurements were correlated with corresponding filtered water samples. A strong correlation was observed ($r= 0.801$; $p= 0.01$; $n=84$). Due to the linear relation between turbidity meter measurements and filtered water samples optical backscatter signals could be translated into SPM concentrations ($SPM_{optical}$). Complementary surface bottom-sediments were sampled with a small sediment grab to determine surface temperatures (depth: 0 – 10 cm), pore-water salinity, and grain size parameters. The long-term stations and the seafloor observatories were connected by a SW-NE transect of short-term stations for a better spatial representation. Additionally two transects of short-term stations crossing the river front of the River Lena have been carried out.

4.2 Preliminary results

A total of 52 CTD casts and 113 water samples were obtained during the expedition. Along the SW-NE transect a stratified water column was observed with the pycnocline situated in a depth between 5 and 10 m (Figure 4). The surface waters were characterized by temperatures of $>5^{\circ}\text{C}$ and salinities <10 , influenced by the freshwater input of the Lena River. Near the seafloor the temperature were $<-1^{\circ}\text{C}$ and salinities >30 . Highest SPM concentrations were mainly observed nearest to the Lena Delta with the maxima close to the seafloor. This maximum represents the bottom-nepheloid layer, a layer of increased SPM concentration. The material discharged by the Lena River settles quickly and forms the bottom nepheloid layer. Crossing the hydrological front of the Lena River a layer of increased temperature can be observed in a depth between 7 and 12 m showing the temperature signal of the surface water but with significantly increased salinity (Figure 4). This distribution might be explained by sinking of the surface water along isohalines.

The temperature of bottom surface sediments varied between -1.47°C and -0.53°C in water depths of 21 to 33 m. The temperature measurements were in the lower range of measurements carried out during TRANSDRIFT I-V expeditions (Kassens & Karpiy, 1994; Kassens & Dmitrenko, 1995; Kassens et al., 1997). Temperature measurements were limited to silty/clayey sediments due to the sampling technique. Even though the surface temperature of the bottom surface sediments is below 0°C and partly close to the freezing point of the surrounding seawater the sediments are not frozen. This can probably be explained by its pore water salinity which will be determined at the Otto Schmidt Laboratory in St. Petersburg.

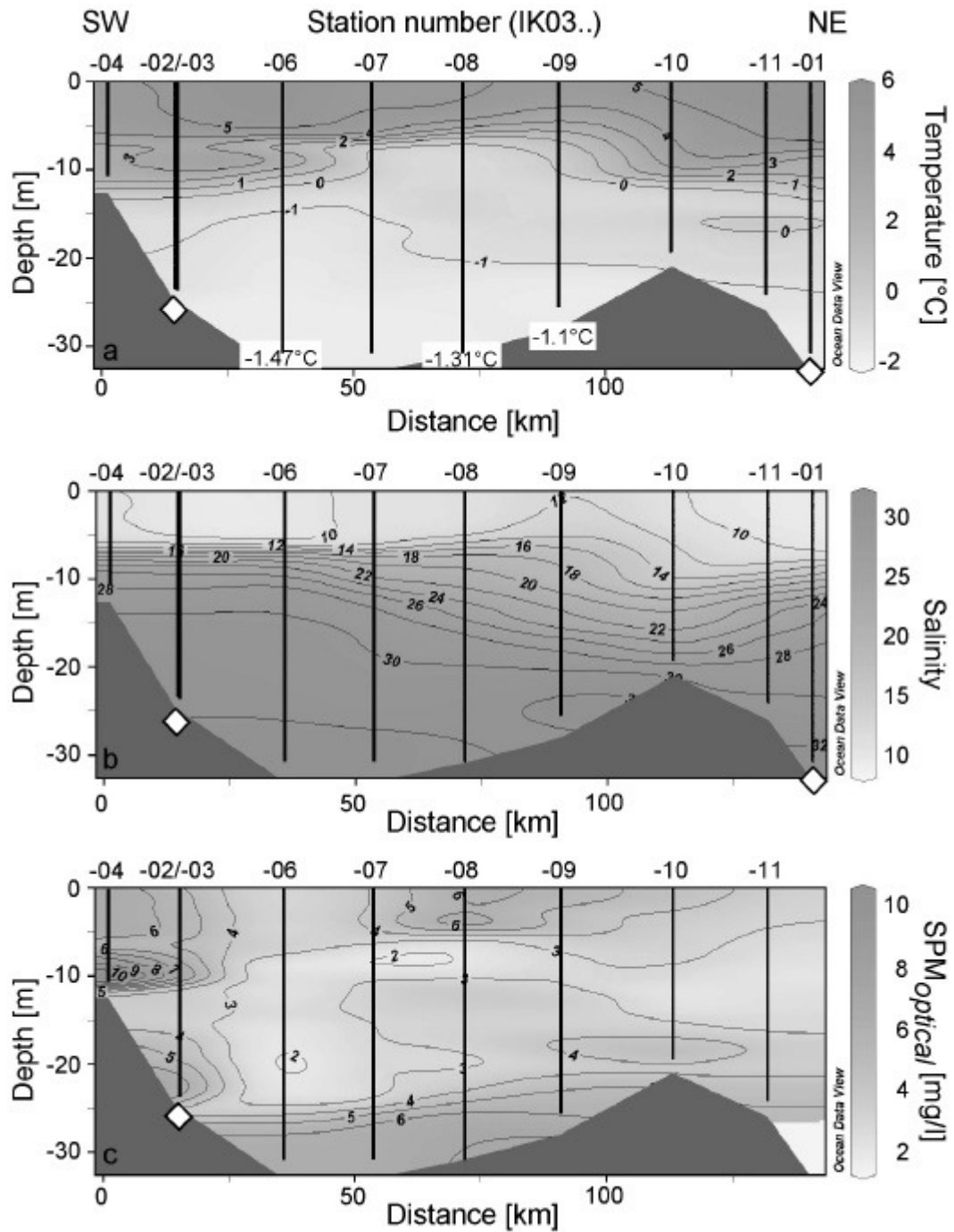


Figure 4: (a) Water and surface bottom sediment temperature [°C], (b) salinity, and (c) SPM [mg/l] distribution along a SW-NE transect. SPM has been derived from turbidity meter measurements. White squares indicate the position of the seafloor observatories.

5. Hydrochemical structure of the water column

In the Laptev Sea the strong variability of meteorological, oceanographical, and biological conditions, results in a complex water column structure (Pivovarov et al., accepted). During the different seasons water masses with different properties are formed in the same region. A small spatial distribution and a short life span are characteristic for these shallow water masses. In general, the water column can be subdivided vertically into surface, intermediate and bottom structural zones. Transport processes and biogeochemical cycling of dissolved and particulate matter differ from each other in these structural zones.

The surface structural zone (SSZ) is the most active area, where energy and material is transformed by interactions between sea, ice, and atmosphere. The thickness of the SSZ in the well-stratified seas is usually 5-10 m and changes seasonally. In the Laptev Sea two different regions can be distinguished due to their physical and chemical properties: i.) river plumes, which occupy the southern and eastern regions of the Laptev Sea and ii.) arctic basin surface waters, which influence the northwestern part of the sea. Especially the silicate concentration of surface waters is considered to be a good chemical tracer of the river plume. The $10 \mu\text{mol l}^{-1}$ silicate isoline is accepted to be a boundary of the river plume that is also characterized by low salinity (less than 25), low oxygen saturation (95 – 100 %), and high concentrations of suspended matter ($0.5\text{-}0.8 \text{ mg l}^{-1}$ at the outer shelf and up to 70 mg l^{-1} near the Lena River Delta).

The intermediate structural zone (ISZ) in the shallow arctic seas consists of the halocline, a layer up to 20 m of thickness with strong salinity gradients. It has a multi-layered structure itself and consists of water masses of various origins. Data of summer oceanographic surveys have shown that the water masses of the ISZ, formed in winter, in spring, and in summer can be distinguished by their chemical properties and temperature.

Low temperatures ($-1.2 \div -1.5 \text{ }^\circ\text{C}$), extremely low oxygen saturation (30-50%), and high nutrient concentrations are characteristic for the bottom structural zone. The intensive influx of riverine organic matter and limited ventilation are the reasons for the oxygen deficit. In winter the fast ice prevents gas exchange with the atmosphere, in summer the halocline insulates the bottom water masses from the surface waters.

5.1 Working program

To investigate the structure of the water column and to track dynamic processes in the coastal Arctic Ocean, the chlorinity and the distribution of silicon, phosphorus, and inorganic nitrogen compounds will be determined. Vertical profiles (5 m sampling interval) from the surface down to the seafloor were taken along a grid of 22 stations (Figure 2). Water samples were taken with a 2-liter plastic water sampler (PWS). From the PWS about 130 sub-samples were taken and stored frozen in high-density polyethylene bottles. Analysis will be

carried out in the Otto Schmidt Laboratory for Polar and Marine Sciences (OSL) in St. Petersburg. Chlorinity will be determined by means of ion chromatography (Metrohm 761 Compact IC). The determination of nutrients is based on automated continuous flow-analysis (Skalar San plus).

6. Diversity of nitrifying bacteria in submarine permafrost

The main scientific objectives of this study are the quantification and understanding of bacterially influenced processes of the biogeochemical cycles in permafrost. This extreme habitat causes highly specific adaptations of bacterial life and shows a high diversity. Knowledge of bacteria from permafrost is important for the ecological understanding because of their extreme adaptations to low temperatures and varying salinities. The enrichment and cultivation of bacteria from low temperatures is also of interest for biotechnology, such as waste-water treatment.

The comparison of submarine and terrestrial permafrost habitats and their dynamics in the case of a possible climate change are of particular interest. Therefore samples will be taken from various environments (nearshore and mid-shelf area) and shall be analyzed using physiological and molecular microbiological techniques.

6.1 Working program

During the TRANSDRIFT IX expedition the major task was the sterile sampling of submarine permafrost to determine the microbial nitrogen cycle. Sampling was focused on the diversity of nitrifying bacteria, which will be examined with several microbiological techniques (Figure 5). 11 sterile sediment samples were taken from aerobic habitats and prepared for transport at *in situ* temperatures. Various samples were taken from the water column at various depths and filtered (0,2 µm cellulose/acetate; Schleicher & Schüll, Germany). In addition, specialized polycarbonate filters (Nuclepore-edge, Whatman) were used for microscopy and FISH (Fluorescence *In Situ* Hybridisation).

In order to get an idea of the cell quantity, MPN (Most-Propable-Number) technique was used. Physiological and molecular-biological characterization of the cultures will be performed at the Department for Microbiology (University of Hamburg).

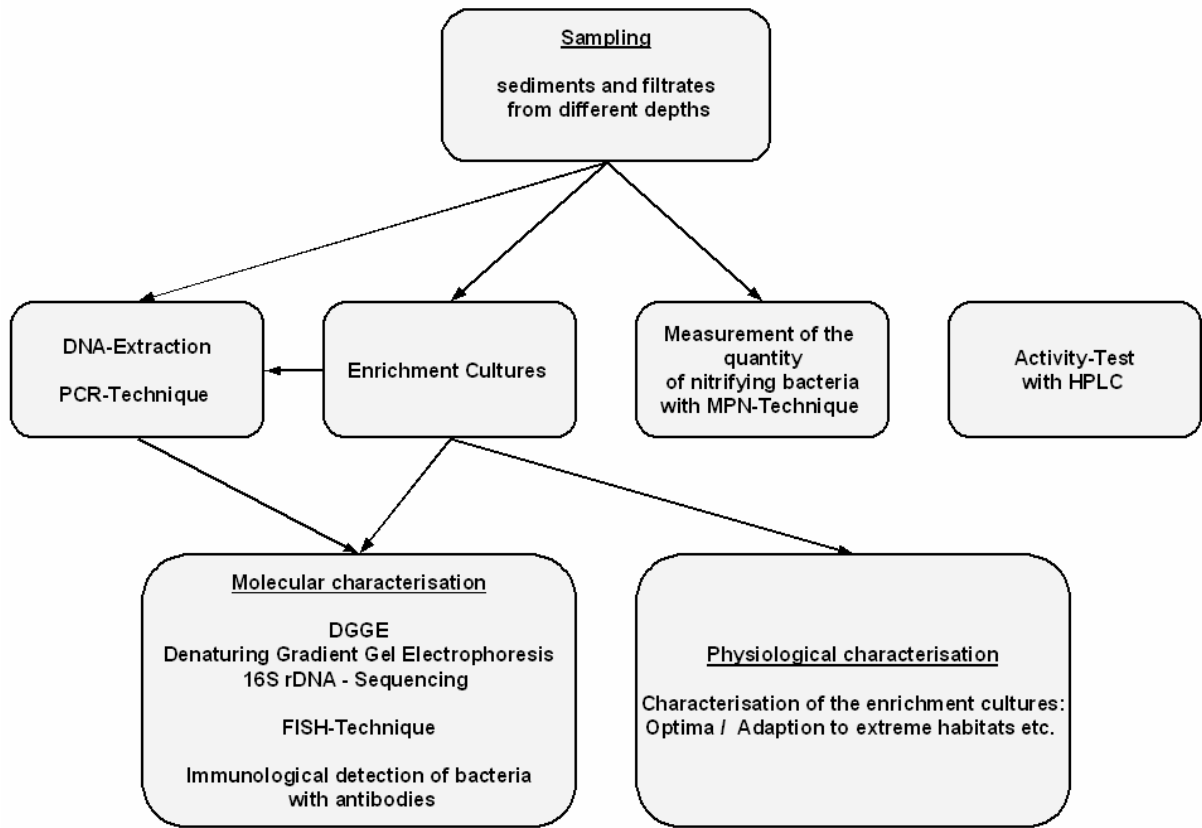


Figure 5: Flow-chart of planned sample treatment.

6.2 Preliminary Results

Due to the adapted transport conditions at *in situ* temperatures, several enrichment cultures and plates could be obtained (Table 1). Ammonia and nitrite oxidizing cultures obviously are psychrophilic (temperatures beneath 5°C). So there are hints for high diversity and adaption potentials for nitrifiers, revealed by various growth optima.

DNA extraction and amplification of 16S rDNA fragments from the hypervariable V3 region were performed successfully for all samples and several enrichment cultures. Molecular-biological techniques like TGGE (Temperature Gradient Gel Electrophoresis) will provide the means for a detailed phylogenetic analysis. With these approaches interesting and new bacteria could be detected at the beginning of the enrichment process.

Activity tests and further physiological examinations like electron microscopy and methods for enrichment etc. will be performed.

The amount of ammonia, nitrite and nitrate in the sediments will be quantified by HPLC (High Performance Liquid Chromatography) and IC (Ion Chromatography). Furthermore the detection of the nitrifiers will be performed by FISH (Fluorescence *in-situ* Hybridization) and immunological techniques based on specific binding of antibodies to key enzymes.

Table 1: Enrichment cultures from sediment (NIOX Nitrite oxidizing bacteria/ AMOX Ammonia oxidizing bacteria, + = culture grows)

	Station	Sample N.	Cultures at [°C]	DNA Extraction	NIOX 70% Sea water	NIOX 100% Sea water	AMOX 70% Sea water	AMOX 100% Sea water
IK-03	01	1S	4, 10, 17	+		+		
	01	2S	4, 10, 17	+		+		+
	04	3S	4, 10, 17	+	+			
	06	4S	4, 10, 17	+		+		
	11	5S	4, 10, 17	+	+		+	
	09	6S	4, 10, 17	+		+		+
	02	7S	4, 10, 17	+	+		+	
	04	8S	4, 10, 17	+		+	+	+
	18	9S	4, 10, 17	+		+		+
	01	10S	4, 10, 17	+		+	+	+
	09	11S	4, 10, 17	+		+		+

Shipboard scientific party

Name	Institute	Profession	Nationality
Alawi, Mashal	University of Hamburg	Biologist	German
Churun, Vladimir	AARI	Oceanographer	Russian
Gukov, Aleksandr	LDR	Geographer	Russian
Hölemann, Jens	AWI	Marine Geologist	German
Novikhin, Andrey	AARI	Hydrochemist	Russian
Wegner, Carolyn	GEOMAR	Geologist	German

Participating institutions

AARI	State Research Center – Arctic and Antarctic Research Institute, 199397 St. Petersburg, Ul. Beringa, 38, Russia
AWI	Alfred Wegener Institute for Polar and Marine Research, Columbusstr., 27568 Bremerhaven, Germany
GEOMAR	GEOMAR Research Center for Marine Geosciences, Wischhofstr. 1-3, 24148 Kiel, Germany
LDR	Lena Delta Reserve, 678400 Tiksi, Ul. Akademika Federova, 28, Russia
University of Hamburg	University of Hamburg, Faculty of Biology, Biocenter Klein Flottbek Ohnhorststr. 18, 22609 Hamburg, Germany

Appendix: Station list of the TRANSDRIFT IX (IK03) expedition

Station	Date	Time (GMT)	Latitude [°N]	Longitude [°E]	Water depth [m]	activity
IK03-01	08/29/2003	12:00	74° 33.03'	130° 10.19'	33	Begin of station
IK03-01-A	08/29/2003	12:30-12:40	74° 33.03'	130° 10.19'	33	CTD TM
IK03-01-A	08/29/2003	12:45-13:35	74° 33.03'	130° 10.19'	Surface, 5, 10, 15, 20, 25, 30	WS HCh MB
IK03-01-B	08/29/2003	13:45-13:55	74° 33.03'	130° 10.19'	33	CTD TM
IK03-01-P1	08/29/2003	14:00-14:30	74° 33.03'	130° 10.19'	5-0, 10-0, 20-0	PN
IK03-01-VV1	08/29/2003	14:30-15:00	74° 33.03'	130° 10.19'	33	VV
IK03-01-P2	08/29/2003	23:30-00:00	74° 33.03'	130° 10.19'	5-0, 10-0, 20-0	PN
IK03-01-C	08/30/2003	00:00-00:15	74° 33.03'	130° 10.19'	33	CTD TM
IK03-01-C	08/30/2003	00:15-00:55	74° 33.03'	130° 10.19'	Surface, 5, 10, 15, 20, 25, 30	WS HCh MB
IK03-01-D	08/30/2003	01:00-01:15	74° 33.03'	130° 10.19'	33	CTD TM
IK03-01-VV2	08/30/2003	01:15-01:45	74° 33.03'	130° 10.19'	33	VV
IK03-01-E	08/30/2003	03:15-03:25	74° 33.03'	130° 10.19'	33	CTD TM
IK03-01-VV3	08/30/2003	03:30-04:00	74° 33.03'	130° 10.19'	33	VV
YANA 03	08/30/2003	05:33-05:46	74° 31.6'	130° 19.1'	28.5	Deployment of seafloor observatory
IK03-02	08/30/2003	12:00	74° 07.03'	126° 25.4'	25	Begin of station
IK03-02-A	08/30/2003	12:30-12:45	74° 07.03'	126° 25.4'	25	CTD TM
IK03-02-P1	08/30/2003	23:15-23:45	74° 07.03'	126° 25.4'	5-0, 10-0, 20-0	PN
IK03-02-B	08/30/2003	23:45-00:20	74° 07.03'	126° 25.4'	Surface, 5, 10, 15, 20	WS HCh MB
IK03-02-B	08/31/2003	00:30-00:45	74° 07.03'	126° 25.4'	25	CTD TM
IK03-02-VV1	08/31/2003	00:45-01:10	74° 07.03'	126° 25.4'	25	VV
IK03-02-C	08/31/2003	01:15-01:30	74° 07.03'	126° 25.4'	25	CTD TM
IK03-02-D	08/31/2003	03:30-03:45	74° 07.03'	126° 25.4'	25	CTD TM
IK03-02-D	08/31/2003	03:45-04:15	74° 07.03'	126° 25.4'	Surface, 5, 10, 15, 20	WS HCh MB
IK03-02-E	08/31/2003	04:15-04:30	74° 07.03'	126° 25.4'	25	CTD TM

Appendix: Continuation

Station	Date	Time (GMT)	Latitude [°N]	Longitude [°E]	Water depth [m]	activity
IK03-02-F	08/31/2003	05:15-05:30	74° 07.03'	126° 25.4'	25	CTD TM
IK03-02-G	08/31/2003	06:15-06:30	74° 07.03'	126° 25.4'	25	CTD TM
LENA 03	08/31/2003	07:30-07:34	74° 07.2'	126° 25.3'	25.4	Deployment of seafloor observatory
IK03-03	08/31/2003	08:00	74° 06.91'	126° 27.04'	25	Begin of station
IK03-03-A	08/31/2003	08:00-08:15	74° 06.91'	126° 27.04'	25	CTD TM
IK03-03-A	08/31/2003	08:15-08:50	74° 06.91'	126° 27.04'	Surface, 5, 10, 15, 20, 22	WS HCh MB
IK03-03-B	08/31/2003	09:00-09:10	74° 06.91'	126° 27.04'	25	CTD TM
IK03-03-C	08/31/2003	10:00-10:10	74° 06.91'	126° 27.04'	25	CTD TM
IK03-03-VV1	08/31/2003	10:10-10:40	74° 06.91'	126° 27.04'	25	VV
IK03-03-D	08/31/2003	11:00-11:10	74° 06.91'	126° 27.04'	25	CTD TM
IK03-03-E	08/31/2003	12:00-12:10	74° 06.91'	126° 27.04'	25	CTD TM
IK03-03-F	08/31/2003	13:00-13:10	74° 06.91'	126° 27.04'	25	CTD TM
IK03-03-G	08/31/2003	14:00-14:09	74° 06.91'	126° 27.04'	25	CTD TM
IK03-03-H	08/31/2003	15:09-15:14	74° 06.91'	126° 27.04'	25	CTD TM
IK03-03-I	08/31/2003	16:00-16:06	74° 06.91'	126° 27.04'	25	CTD TM
IK03-03-J	08/31/2003	22:00-22:10	74° 06.91'	126° 27.04'	25	CTD TM
IK03-04	08/31/2003	23:45	74° 05.55'	125° 59.53'	12.6	Begin of station
IK03-04-A	08/31/2003	23:50-00:00	74° 05.55'	125° 59.53'	12.6	CTD TM
IK03-04-A	09/01/2003	00:00-00:20	74° 05.55'	125° 59.53'	Surface, 5, 8, 10	WS HCh MB
IK03-04-P1	09/01/2003	00:00-00:20	74° 05.55'	125° 59.53'	5-0,10-0	PN
IK03-04-VV1	09/01/2003	00:30-01:00	74° 06.05'	125° 56.85'	13	VV
IK03-04-B	09/01/2003	01:25-01:35	74° 06.72'	125° 53.7'	13	CTD TM
IK03-05	09/01/2003	03:55	74° 00.06'	127° 00.13'	25	Begin of station
IK03-05-A	09/01/2003	04:15-04:25	74° 00.06'	127° 00.13'	25	CTD TM
IK03-05-P1	09/01/2003	04:15-04:25	74° 00.06'	127° 00.13'	5-0, 10-0, 20-0	PN

Appendix: Continuation

Station	Date	Time (GMT)	Latitude [°N]	Longitude [°E]	Water depth [m]	activity
IK03-05-A	09/01/2003	04:30-04:50	74° 00.06'	127° 00.13'	Surface, 5, 10, 15, 20, 24	WS HCh MB
IK03-05-VV1	09/01/2003	04:50-05:05	74° 01.08'	127° 02.16'	26	VV
IK03-05-B	09/01/2003	05:05-05:15	74° 01.08'	127° 02.16'	26	CTD TM
IK03-06	09/01/2003	06:35	74° 11.97'	127° 00.06'	33	Begin of station
IK03-06-A	09/01/2003	06:40-06:50	74° 11.97'	127° 00.06'	34	CTD TM
IK03-06-A	09/01/2003	06:55-07:35	74° 11.97'	127° 00.06'	Surface, 5, 10, 15, 20, 25, 30	WS HCh MB
IK03-06-VV1	09/01/2003	07:40-08:00	74° 11.97'	127° 00.06'	34	VV
IK03-06-B	09/01/2003	08:00-08:10	74° 11.96'	127° 02.05'	34	CTD TM
IK03-07	09/01/2003	09:10	74° 14.10'	127° 35.18'	33	Begin of station
IK03-07-A	09/01/2003	09:15-09:25	74° 14.10'	127° 35.18'	33	CTD TM
IK03-07-P1	09/01/2003	09:15-09:25	74° 14.10'	127° 35.18'	5-0, 10-0, 20-0	PN
IK03-07-A	09/01/2003	09:25-09:50	74° 14.10'	127° 35.18'	Surface, 5, 10, 15, 20, 25, 30, 35	WS HCh MB
IK03-07-VV1	09/01/2003	09:50-10:10	74° 14.17'	127° 34.95'	33	VV
IK03-07-B	09/01/2003	10:10-10:20	74° 14.21'	127° 34.00'	33	CTD TM
IK03-08	09/01/2003	11:20	74° 17.00'	128° 09.75'	29	Begin of station
IK03-08-A	09/01/2003	11:25-11:35	74° 17.00'	128° 09.75'	29	CTD TM
IK03-08-P1	09/01/2003	11:25-11:40	74° 17.00'	128° 09.75'	5-0, 10-0, 20-0	PN
IK03-08-A	09/01/2003	11:45-12:15	74° 17.09'	128° 09.28'	Surface, 5, 10, 15, 20, 25	WS HCh MB
IK03-08-VV1	09/01/2003	12:15-12:30	74° 17.09'	128° 09.28'	29	VV
IK03-08-B	09/01/2003	12:30-12:40	74° 17.09'	128° 09.28'	29	CTD TM
IK03-09	09/01/2003	14:05	74° 20.13'	128° 45.15'	28	Begin of station
IK03-09-A	09/01/2003	14:10-14:20	74° 20.13'	128° 45.15'	28	CTD TM
IK03-09-P1	09/01/2003	14:10-14:20	74° 20.13'	128° 45.15'	5-0, 10-0, 20-0	PN
IK03-09-A	09/01/2003	14:20-14:40	74° 20.13'	128° 45.15'	Surface, 5, 10, 15, 20, 25, 28	WS HCh MB

Appendix: Continuation

Station	Date	Time (GMT)	Latitude [°N]	Longitude [°E]	Water depth [m]	activity
IK03-09-VV1	09/01/2003	14:40-15:10	74° 21.13'	128° 47.26'	28	VV
IK03-09-B	09/01/2003	15:15-15:30	74° 22.03'	128° 49.67'	28	CTD TM
IK03-10	09/01/2003	16:40	74° 24.03'	129° 25.2'	21	Begin of station
IK03-10-A	09/01/2003	16:45-16:55	74° 24.03'	129° 25.2'	21	CTD TM
IK03-10-P1	09/01/2003	16:45-16:55	74° 24.03'	129° 25.2'	5-0, 10-0	PN
IK03-10-A	09/01/2003	16:55-17:15	74° 24.03'	129° 25.2'	Surface, 5, 10, 15, 18	WS HCh MB
IK03-10-B	09/01/2003	17:15-17:25	74° 24.35'	129° 27.22'	21	CTD TM
IK03-11	09/01/2003	18:45	74° 28'	130°	26	Begin of station
IK03-11-A	09/01/2003	18:50-19:00	74° 28'	130°	26	CTD TM
IK03-11-P1	09/01/2003	18:55-19:05	74° 28'	130°	5-0, 10-0, 20-0	PN
IK03-11-A	09/01/2003	19:10-19:30	74° 28'	130°	Surface, 5, 10, 15, 20, 25	WS HCh MB
IK03-11-VV1	09/01/2003	19:30-19:40	74° 28'	130°	26	VV
IK03-11-B	09/01/2003	19:40-20:00	74° 28'	130°	26	CTD TM
IK03-12	09/01/2003	20:45	74° 29.9'	130° 25.3'	26	Begin of station
IK03-12-A	09/01/2003	20:45-20:55	74° 29.9'	130° 25.3'	26	CTD TM
IK03-12-A	09/01/2003	21:00-21:20	74° 29.9'	130° 25.3'	Surface, 5, 10, 15, 20, 25	WS HCh MB
IK03-12-B	09/01/2003	21:20-21:30	74° 29.9'	130° 25.3'	26	CTD TM
IK03-13	09/01/2003	22:30	74° 3'	131°	30	Begin of station
IK03-13-A	09/01/2003	22:30-22:40	74° 3'	131°	30	CTD TM
IK03-13-P1	09/01/2003	23:00-23:10	74° 3'	131°	5-0, 10-0, 20-0	PN
IK03-13-A	09/01/2003	23:00-23:10	74° 3'	131°	Surface, 5, 10, 15, 20, 28	WS HCh MB
IK03-13-VV1	09/01/2003	23:15-23:40	74° 3'	131°	30	VV
IK03-13-B	09/01/2003	23:40-23:50	74° 3'	131°	30	CTD TM
IK03-14	09/02/2003	01:05	74° 21.5'	130° 36.5'	23	Begin of station
IK03-14-A	09/02/2003	01:10-01:20	74° 21.5'	130° 36.5'	23	CTD TM
IK03-14-P1	09/02/2003	01:15-01:25	74° 21.5'	130° 36.5'	5-0, 10-0, 20-0	PN
IK03-14-A	09/02/2003	01:30-01:50	74° 21.5'	130° 36.5'	Surface, 5, 10, 15, 20	WS HCh MB

Appendix: Continuation

Station	Date	Time (GMT)	Latitude [°N]	Longitude [°E]	Water depth [m]	activity
IK03-14-B	09/02/2003	01:50-02:00	74° 21.5'	130° 36.5'	23	CTD TM
IK03-14-VV1	09/02/2003	02:00-02:20	74° 21.5'	130° 36.5'	23	VV
IK03-15	09/02/2003	03:25	74° 14'	130° 15'	21	Begin of station
IK03-15	09/02/2003	03:30-03:40	74° 14'	130° 15'	21	CTD TM
IK03-15	09/02/2003	03:40-03:45	74° 14'	130° 15'	Surface, 5, 10, 15, 20	WS HCh MB
IK03-16	09/02/2003	05:30	74°	130° 30'	26	Begin of station
IK03-16	09/02/2003	05:30-05:40	74°	130° 30'	26	CTD TM
IK03-16	09/02/2003	05:45-06:05	74°	130° 30'	Surface, 5, 10, 15, 20, 25	WS HCh MB
IK03-16-VV1	09/02/2003	06:05-06:25	74°	130° 30'	26	VV
IK03-17	09/02/2003	07:45	74° 44.99'	130° 29.95'	25	Begin of station
IK03-17	09/02/2003	07:50-08:00	74° 44.99'	130° 29.95'	25	CTD TM
IK03-17	09/02/2003	08:00-08:20	74° 44.99'	130° 29.95'	Surface, 5, 10, 15, 20, 22	WS HCh MB
IK03-17-VV1	09/02/2003	08:25-08:50	74° 44.99'	130° 29.95'	25	VV
IK03-18	09/02/2003	10:50	73° 39.58'	129° 52.78'	15	Begin of station
IK03-18	09/02/2003	10:55-11:00	73° 39.58'	129° 52.78'	15	CTD TM
IK03-18	09/02/2003	11:00-11:20	73° 39.58'	129° 52.78'	Surface, 5, 10, 12	WS HCh MB
IK03-18-VV1	09/02/2003	11:20-11:40	73° 39.58'	129° 52.78'	15	VV
IK03-19	09/02/2003	13:00	73° 34.53'	129° 24.83'	21	Begin of station
IK03-19	09/02/2003	13:05-13:15	73° 34.53'	129° 24.83'	21	CTD TM
IK03-19	09/02/2003	13:15-13:30	73° 34.53'	129° 24.83'	Surface, 5, 10, 15, 18	WS HCh MB
IK03-19-VV1	09/02/2003	13:30-13:40	73° 34.53'	129° 24.83'	21	VV
IK03-20	09/02/2003	14:55	73° 29.6'	128° 54.9'	12.5	Begin of station
IK03-20	09/02/2003	14:55-15:05	73° 29.6'	128° 54.9'	12.5	WS HCh MB
IK03-20-P1	09/02/2003	15:00-15:15	73° 29.6'	128° 54.9'	5-0, 10-0	PN
IK03-20-VV1	09/02/2003	15:15-15:35	73° 29.6'	128° 54.9'	12.5	VV

Appendix: Continuation

Station	Date	Time (GMT)	Latitude [°N]	Longitude [°E]	Water depth [m]	activity
IK03-21	09/02/2003	16:45	73° 30.05'	129° 25.4'	15.5	Begin of station
IK03-21	09/02/2003	16:50-17:00	73° 30.05'	129° 25.4'	15.5	CTD TM
IK03-21-P1	09/02/2003	16:50-17:00	73° 30.05'	129° 25.4'	5-0, 10-0	PN
IK03-21	09/02/2003	17:00-17:15	73° 30.05'	129° 25.4'	Surface, 5, 10, 14	WS HCh MB
IK03-21-VV1	09/02/2003	17:15-17:45	73° 30.05'	129° 25.4'	15.5	VV
IK03-22	09/02/2003	19:55	73° 30'	130° 30.2'	26	Begin of station
IK03-22	09/02/2003	19:55-20:05	73° 30'	130° 30.2'	26	CTD TM
IK03-22-P1	09/02/2003	19:55-20:05	73° 30'	130° 30.2'	5-0, 10-0, 20-0	PN
IK03-22	09/02/2003	20:10-20:35	73° 30'	130° 30.2'	Surface, 5, 10, 15, 20, 22	WS HCh MB
IK03-22-VV1	09/02/2003	20:35-20:55	73° 30'	130° 30.2'	26	VV

Abbreviations

CTD	C onductivity T emperature D epth Meter
HCh	H ydro ch emical sampling (Silicate, Phosphate, Nitrate, Nitrite, Ammonia, Chlorinity)
MB	M icrobiological measurements
PN	P hytoplankton n et
TM	T urbidity M eter
WS	W ater s amples for determination of suspended particulate matter concentration
VV	V an V een Greifer/Snapper

8. References

- Gosink, J.P. & Baker, G.C. 1990 Salt fingering in subsea permafrost: some stability and energy considerations. *Journal of Geophysical Research*, **95**, C6, 9,575-9,583.
- Hutter, K. & Straughan, B. 1999 Models of convection in thawing porous media in support for the subsea permafrost equations. *Journal of Geophysical Research*, **102**, 29,249-29,260.
- Kassens, H. & Kariy, V.Y. 1994 Russian-German Cooperation: The Transdrift I Expedition to the Laptev Sea. *Reports on Polar Research*, **151**, 168 pp.
- Kassens, H. & Dmitrenko, I. 1995 The TRANDRIFT II Expedition to the Laptev Sea. *Reports on Polar Research*, **182**, 1-180.
- Kassens, H., Dmitrenko, I., Timokhov, L. & Thiede, J. 1997 The TRANSDRIFT III Expedition: Freeze-up Studies in the Laptev Sea. *Reports on Polar Research*, **248**, 1-192.
- Osterkamp, T.E., Baker, G.C., Harrison, W.D. & Matava, T. 1989 Characteristics of the active layer and shallow subsea permafrost. *Journal of Geophysical Research*, **94**, C11, 16,227-16,236
- Pivovarov S., Hölemann J., Kassens H., Piepenburg D., and Schmid M. (accepted) Laptev and East Siberian seas. In: *The Sea*
- Vigdorichik, E. 1980 Arctic Pleistocene history and the development of submarine permafrost. Westview Press: Boulder Co., 250 pp.